ANALYSIS OF THE IMPACT OF A FACTS-BASED POWER FLOW CONTROLLER ON SUBSYNCHRONOUS RESONANCE

by

Rudiren Pillay Carpanen

MScEng

Submitted in the fulfillment of the academic requirements for the degree of Doctor of Philosophy in Engineering, in the School of Electrical, Electronic and Computer Engineering, University of KwaZulu-Natal, Durban, South Africa.

December 2012

I hereby declare that all the material incorporated into this thesis is my own original and unaided work except where a specific reference is made by name or in the form of a numbered reference. The work contained herein has not been submitted for a degree at any other university.

Signed: _____

R Pillay Carpanen

for my family

ABSTRACT

Electric power utilities are faced with the challenge of meeting increasing demand for electric power whilst many factors prevent traditional remedies such as the expansion of transmission networks and the construction of new generating facilities. Due to issues of environment, health and rights-of-way, the construction of new generating plants and transmission lines were either excessively delayed or prevented in many parts of the world in past years. An alternative resides in loading the existing transmission network beyond its present operating region but below its thermal limit, which would ensure no degradation of the system.

This alternative approach has been possible with the emergence of Flexible AC Transmission Systems (FACTS) technology. The FACTS concept involves the incorporation of power-electronic controlled devices into AC power transmission systems in order to safely extend the power-transfer capability closer of these systems to their stability limits. One member of the family of FACTS series compensators is the Static Synchronous Series Compensator (SSSC), and this thesis considers the use of the SSSC to carry out closed-loop control of AC power flow in a transmission system.

Although the SSSC has the potential to enhance the operation of power systems, the introduction of such a device can cause adverse interactions with other power system equipment or existing network resonances. This thesis examines the interaction between high-level power flow controllers implemented around the SSSC and a particular form of system resonance, namely subsynchronous resonance (SSR) between a generator turbine shaft and the electrical transmission network.

The thesis initially presents a review of the background theory on SSR and then presents a review of the theory and operation of two categories of SSSC, namely the reactance-controlled SSSC and the quadrature voltage-controlled SSSC. The two categories of SSSC are known to have different SSR characteristics, and hence this thesis considers the impact on the damping of subsynchronous torsional modes of additional controllers introduced around both categories of SSSC to implement AC power flow control.

The thesis presents the development of the mathematical models of a representative study system, which is an adaptation of the IEEE First Benchmark system for the study of SSR to allow it to be used to analyse the effect of closed-loop power flow control on SSR stability. The mathematical models of the study system are benchmarked against proven and accepted dynamic models of the study system.

The investigations begin by examining the effect of a reactance-controlled SSSC-based power flow controller on the damping of torsional modes with an initial approach to the design of the control gains of the power flow controller which had been proposed by others. The results show how the nature and extent of the effects on the damping of the electromechanical modes depend on both the mode in which the power flow controller is operated and its controller response times, even for the relatively-slow responding controllers that are obtained using the initial controller design approach. The thesis then examines the impact of a reactance-controlled SSSC-based power flow

controller on the damping of torsional modes when an improved approach is used to design the gains of the power flow controller, an approach which allows much faster controller bandwidths to be realised (comparable to those considered by others). The results demonstrate that for both of the modes in which the power flow controller can be operated, there is a change in the nature and extent of the power flow controller's impact on the damping of some the torsional modes when very fast controller response times are used.

Finally, the thesis investigates the impact of a quadrature voltage-controlled SSSC-based power flow controller on the damping of torsional modes in order to compare the influence of the design of both V_{SSSC}-controlled and X_{SSSC}-controlled SSSC-based power flow controllers on torsional mode damping for different power flow controller response times. The results obtained indicate that a V_{SSSC}-controlled SSSC-based power flow controller allows a larger range of SSR stable operating points as compared to a X_{SSSC}-controlled SSSC-based power flow controller.

ACKNOWLEDGEMENTS

The work presented in this thesis was carried out under the supervision of Professor Bruce S. Rigby of the Real Time Power System Studies Centre, Durban University of Technology, Durban. I wish to thank Professor Rigby for his support, guidance throughout the course of this thesis, and for his commendable efforts during the correction of this thesis. I would also wish to thank Professor Rigby for arranging much needed financial support.

In addition, I would like to thank:

my family for their support, patience and their best wishes;

my friends for their support and encouragement;

the University of KwaZulu–Natal for providing financial support;

the staff and postgraduate students of the School of Electrical, Electronic and Computer Engineering, unfortunately too many to mention by name, who have together contributed towards a friendly and stimulating work environment over the years.

TABLE OF CONTENTS

CHAPTER FOUR: INVESTIGATING THE IMPACT OF A REACTANCE-CONTROLLED SSSC-BASED POWER FLOW CONTROLLER ON TORSIONAL INTERACTION

CHAPTER FIVE: AN IMPROVED SSSC-BASED POWER FLOW CONTROLLER DESIGN APPROACH AND ITS IMPACT ON TORSIONAL INTERACTION

CHAPTER SIX: INVESTIGATING THE IMPACT OF A QUADRATURE VOLTAGE-CONTROLLED SSSC-BASED POWER FLOW CONTROLLER ON TORSIONAL INTERACTION

LIST OF SYMBOLS

The commonly used symbols and notations adopted in this thesis are listed below. Other symbols used the text are explained where there first occur.

Acronyms

AC	Alternating Current
DC	Direct Current
FACTS	Flexible AC Transmission Systems
IPFC	Interline Power Flow Controller
PSCAD	Power System Computer Aided Design
SMIB	Single Machine Infinite Bus
SSSC	Static Synchronous Series Compensator
SSR	Subsynchronous Resonance
STATCOM	Static Synchronous Compensator
SVC	Static Var Compensator
TCSC	Thyristor Controlled Series Capacitor
UPFC	Unified Power Flow Controller

Synchronous generator symbols

b_g	voltage source for generator equivalent circuit
$[D]$	diagonal matrix of damping coefficients
$[J]$	diagonal matrix of physical moments of inertia
$[K]$	symmetric matrix of shaft stiffness
L_g^*	inductance in generator equivalent circuit
P_m	total power output to the shaft from all turbine stages
R_a	stator phase resistance
$\underline{T_e}$	electrical torque vector
$\underline{T_m}$	mechanical torque vector
_	vector of rotor angle

System and SSSC symbols

C	capacitance
f_0	fundamental (synchronous) frequency in Hertz
f_{er}	subsynchronous natural frequency of a conventionally compensated transmission line
K_P	proportional gain
K_I	integral gain
L	inductance
P_i	instantaneous power at the AC terminals of the SSSC
P_L	active power transfer in the transmission line
P_{Lset}	set-point value of active power in the transmission line
P_t	active power transfer at the generator terminals
R	resistance
R_L	transmission line resistance
V_b	infinite bus voltage
V_{dc}	inverter DC voltage
V_R	receiving bus voltage
V_S	sending bus voltage
V_{SSSC}	denotes the magnitude of quadrature voltage injected by an SSSC
V_t	generator terminal voltage
X_C	denotes the capacitive reactance of a conventional series capacitor
X_L	transmission line reactance
X_{SSSC}	denotes the capacitive compensating reactance provided by an SSSC
X_T	transformer reactance
$_{PL}$	error in active line power transfer
$_0$	fundamental (synchronous) frequency in radians per second

General

p	signifies the derivative operator d/dt
pu.	per unit
$[X]$	signifies a matrix of X
$[X]^{-1}$	signifies the inverse of a matrix X
$[X]^{T}$	signifies the transpose of matrix X
x_d, x_q	siginifies the d and q axis components of variable x
x	signifies the desired value of x
x_0	signifies the set-point value of x
$\dot{x}$	signifies the time differential of x
$\underline{0}$	null vector

CHAPTER ONE

INTRODUCTION

1.1 General Background

In the past century, the world population has increased by nearly four times from 1.6 billion to 6 billion and the estimates show that by the year 2150, the world population will reach around 10 billion [1]. Such a continuous increase in human population is reflected in the rise of the global energy demand for the purposes of farming, manufacturing, transportation and other economic sectors. Further, this rise in the global energy demand particularly impacts on the continuous increase in the demand for electric power. For example, for a fast emerging country like China the installed generation capacity has increased from 517 GW in 2006 [2] to 900 GW in 2010 [3] in order to satisfy the demand required for high economic growth as well as the population growth.

In developed countries, the power utilities are however faced with the challenge of meeting the ever increasing demand for electric power while there are many other factors that prevent the traditional remedies such as the expansion of transmission networks and the construction of new generating facilities. Due to issues of environment, health and rights-of-way, the construction of new generating plants and transmission lines were either excessively delayed or prevented in many parts of the world in past years [4]. Nevertheless, the steep rise in the demand for electrical energy cannot be ignored: severe blackouts in different parts of the world [5] affected 140 million customers worldwide and the blackouts in the Western Cape, South Africa in 2006 served as the most recent reminder of this.

Historically, power systems have been controlled mechanically and even today there are major parts of the electric utility grid that are still being operated and controlled using such traditional methods. Although there is widespread use of computerised systems such as Supervisory Control and Data Acquisition (SCADA) and high-speed communications for protection and control of present transmission systems, when the operating signals are sent to the power circuits where the power control action is taken, the switching devices are mechanical and there is little high-speed control [6]. In addition to this, repeated control actions cannot be initiated frequently with such mechanical devices because they tend to wear out very quickly as opposed to static devices. Hence, these mechanical switching devices have been primarily used for steady-state control and are not practical for repeated fast dynamic control applications. These circumstances have necessitated transmission lines to be operated well below their theoretical maximum power transfer capabilities in order to keep a safe transient stability margin so that the power system can recover from severe transient contingencies. Consequently, transmission systems have historically been considerably under-utilised in part because of that limited capability to control transmission systems under dynamic conditions.

The power flow in an AC transmission line is a function of the line impedance, the magnitude of the sending- and receiving-end voltages, and the phase angle between these two end voltages. Kimbark [7] in the mid 1960s first recognised that the dynamic switching of series compensating

reactance in a transmission line could improve the stability margins of the power system by altering the power transfer characteristic of the line. However, at that time such conventional series capacitor switching could only be carried out using mechanical circuit breakers, which are impractical for achieving fast control of the amount of compensation. Furthermore, the traditional use of mechanically switched conventional series capacitors for enhancing the power transfer capability of transmission lines brought in further complications by interacting with the mechanical turbine-shaft system of turbogenerators, a phenomenon known as Subsynchronous Resonance (SSR) [8,9].

With the major advances made in high power semiconductor devices, the idea of improved dynamic control of AC power systems could finally be implemented to allow better utilisation of these systems without the limitations that were imposed by mechanical devices. The emergence of solid-state switching devices has allowed fast and efficient control over the four parameters that affect power flow in a transmission system. In 1988, Hingorani [10] introduced the idea of high-speed control over the factors that affect power flow in an AC transmission system, in order to increase availability, operating flexibility and system stability. Since Hingorani's first proposal, the concept of Flexible AC Transmission Systems (FACTS) has been launched and a long-term research initiative has been driven by the Electric Power Research Institute [6]. Fig. 1.1 is an illustration of a few cycles of voltage at the power system frequency. This figure shows that the speed of operation of mechanical switches (primarily circuit breakers) for conventional transmission line switching can be as fast as a couple of cycles of 50 Hz. Many power system constraints can be solved with this speed of operation. In addition to the considerable improvement in switching speed from mechanical to power-electronic based switching devices (Fig. 1.1 shows that the speed of power electronic switches is a fraction of a cycle), the main benefit that is provided by FACTS devices is the repeatability and smooth control [11]. In other words, solutions based on mechanical switches (which tend to wear out very quickly and cannot be operated too often) usually have "one and done" impact on system stability. By contrast, solutions that are based on power electronics can provide either a smooth and continuous, or a rapidly repeatable option for power system control.

The high-speed response of FACTS devices provides fast and efficient control of the power transmitted through transmission lines, and dynamic control applications using these devices have

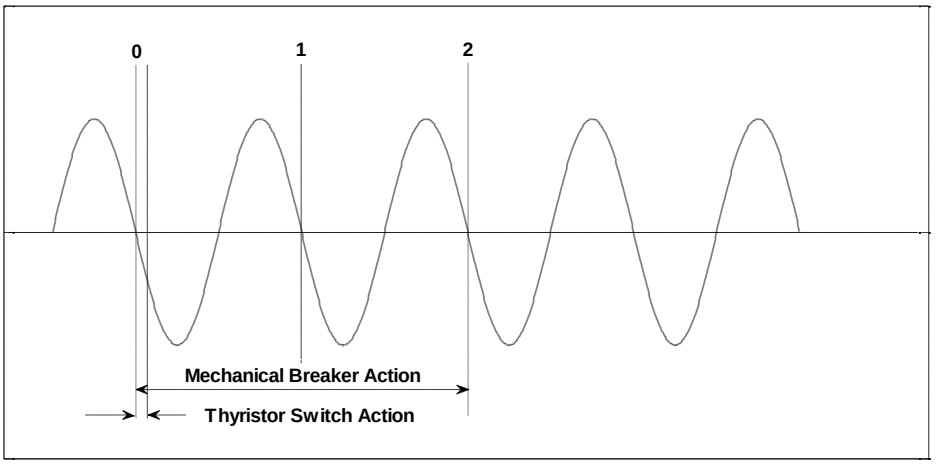

Fig. 1.1: Illustration of speed of power system control [11].

become practically feasible. As a consequence, a number of FACTS technologies have emerged with which to improve power system stability, thus allowing the system to be operated closer to its stability limits. FACTS devices have even been mentioned as one of the modern countermeasures for blackouts due to their ability to enhance the dynamic performance of the power system following major disturbances and hence mitigate the risks of potential cascading outages and islanding of the system [12]. The emergence of FACTS devices also promised several benefits with regards to the problem of SSR due to the difference in their impedance characteristics as compared to conventional series capacitors. This thesis aims to study the influence of FACTS-based closed-loop power flow control on SSR.

1.2 Thesis Objectives

Power system stability can be classified into large-signal (or transient) stability and small-signal stability phenomena. Power system operation can often be limited by small-signal stability concerns, in particular by lack of damping in the system oscillations. There are different types of small-signal oscillations: local modes, interarea modes, control modes and torsional modes [13]. Torsional modes, which are related to the turbine-generator mechanical shaft system's rotational components, are susceptible to interaction with transmission networks that are series compensated and this phenomenon is known as Subsynchronous Resonance (SSR). The IEEE SSR Working Group defines SSR as follows [14]:

"*Subsynchronous resonance is an electric power system condition where the electric network exchanges energy with a turbine generator at one or more of the natural frequencies of the combined system below the synchronous frequency of the system*".

The above definition thus encompasses any system condition that causes an exchange of energy at a given subsynchronous frequency. Hence, both the *natural* modes of oscillation that are due to the inherent system characteristics and the *forced* modes of oscillation that are driven by a particular device or control system are included.

Generally in power systems where the power transfer is limited as a result of stability issues, the inclusion of FACTS devices can prove to be a cost effective approach to utilise the transmission system more effectively. It is for this reason that the use of the dynamic ability of FACTS devices to control the power transfer in a transmission line has become an attractive option to enforce desired steady state power flow along parallel transmission paths.

This thesis considers the use of one of the family of FACTS series compensators in particular, namely the Static Synchronous Series Compensator (SSSC), to carry out closed-loop control of AC power flow in a transmission system. This SSSC-based closed-loop power flow controller is used to implement two different strategies for transmission line power flow control that have been proposed in literature: constant power control and constant angle control [15,16]. Since these two control strategies were proposed, it has been shown [17] that a closed-loop power flow controller can affect the small-signal damping characteristics of the inertial swing modes of generators feeding a power system, and in particular that the nature and extent of these effects on the system's stability depend on both the mode in which the power flow controller is operated (constant power or constant angle control) as well as its controller response time. Given the findings in [17], a logical concern that arises is whether the action of a fast-responding power flow controller implemented around an SSSC

could also impact on the SSR stability of any generators with multi-inertia turbines that are susceptible to torsional interaction. Hence, this thesis aims to investigate the effect of each power flow control strategy proposed in the literature on SSR and furthermore for each strategy, an investigation is carried out into the influence of the design of the SSSC-based power flow controller's response time on the damping of the torsional modes. It has also previously been shown that although the two main categories of SSSC that exist (namely reactance-controlled or quadrature voltage-controlled SSSCs) each have different SSR characteristics [18,19], both of these two types of SSSC have the potential of exciting SSR. Hence, this thesis considers both the reactance-controlled type of SSSC and the quadrature voltage-controlled type of SSSC in the studies carried out to examine the impact of power flow controls on SSR. Finally, since FACTS series compensation is relatively expensive, it is often proposed that, in practice, a carefully considered mix of FACTS and conventional series compensation could provide the best comprise between cost effective and flexible compensation of AC transmission networks. This thesis therefore examines the influence of reactance-controlled SSSC- and quadrature voltage-controlled SSSC-based power flow controls on the damping of torsional modes in the presence of conventional series capacitors in an adjacent transmission line of the studied system.

1.3 Thesis Layout

This thesis consists of eight subsequent chapters, which present the development of the mathematical models used in the analyses, and the results and findings of the various studies conducted. The subject matter has been arranged as follows.

At the outset, a literature review of the technical aspects regarding the SSR characteristics of FACTS series compensators as stand-alone devices and the use of FACTS devices for the application of power flow control had to be addressed. Chapter Two, in particular, provides the background theory on subsynchronous resonance, FACTS series compensation and power flow control using controllable series compensators. This chapter also reviews the SSR characteristics of one particular FACTS series compensator, the Static Synchronous Series Compensator (SSSC) and the impact of FACTS-based closed-loop control of AC power on the stability of the system.

Chapter Three presents the detailed mathematical models used for the simulation studies and analyses in the thesis: the generator model, the turbine-shaft model, the electrical transmission network model, the reactance-controlled (X_{SSSC}-controlled) SSSC model, the quadrature voltage-controlled (V_{SSSC}-controlled) SSSC model, the power flow controller model for the X_{SSSC}-controlled SSSC and the power flow controller model for the V_{SSSC}-controlled SSSC, all of which are required for the subsequent subsynchronous resonance studies of the chosen study system, which is an adaptation of the IEEE First Benchmark System for the study of SSR [20]. The time-domain responses obtained from the mathematical models of this study system written for this thesis in Matlab [21] were compared against the results obtained for the same study system modelled by the author in PSCAD [22] in order to verify the correctness the mathematical models. The Matlab-coded models, once benchmarked in this manner were then used to calculate eigenvalues of the study system using numerical linearisation tools available in the Matlab environment in order to gain further insight during the studies in the subsequent chapters.

Chapter Four initially examines the responses of an X_{SSSC}-controlled SSSC-based power flow controller to system disturbances by means of time-domain simulations to verify that the constant power and constant angle strategies for power flow control have been implemented correctly using the mathematical models developed in Chapter Three. The influence of this X_{SSSC}-controlled SSSC-based power flow controller on SSR is then investigated by means of eigenvalue analysis in a systematic manner. The SSR characteristics of a stand-alone X_{SSSC}-controlled SSSC are first considered, as a reference point, prior to the introduction of the power flow controller around the SSSC. The design of the power flow controller for different dynamic response times is then presented. Finally, Chapter Four investigates the influence of the design of the X_{SSSC}-controlled SSSC-based power flow controller for different dynamic response times on torsional mode damping at different operating points in the AC transmission system.

Chapter Five then presents an improved method of designing the gains of the X_{SSSC}-controlled SSSC-based power flow controller that enables a much higher bandwidth of the power flow controls to be realised. By using frequency-domain linearised transfer function analysis, the influence of the design of the power flow controller gains (and hence its speed of response) on the resonant characteristics of this X_{SSSC}-controlled SSSC-based power flow controller is investigated for both cases: the initial controller design method of Chapter Four and the improved design method presented in Chapter Five. It has been found that a much higher bandwidth of the power flow controller can be achieved with the improved method of designing the control gains over the initial controller design method of Chapter Four. This improved method of designing control gains of the power flow controller for fast response times is then verified by using time-domain simulations. Chapter Five then compares the influence of the relatively slow-responding and the faster-responding X_{SSSC}-controlled SSSC-based power flow controllers on torsional mode damping.

The investigations in Chapter Five are then extended to consider the effect of having conventional series capacitors in the adjacent transmission line of the study system. The SSR-stable ranges of conventional series compensation in the adjacent line are first identified by means of eigenvalue scans, and two specific values of conventional series compensation are then selected for further investigations. The SSR characteristics of the X_{SSSC}-controlled SSSC are then presented for the two selected cases of conventional series compensation in the adjacent line. A single SSR-stable operating point for the X_{SSSC}-controlled SSSC is initially identified for each of the two selected cases of conventional series compensation in the adjacent line. For each of these selected cases of combined conventional and X_{SSSC}-controlled SSSC compensation the influence of the fast-responding power flow controllers on torsional mode damping is examined for the improved controller design approach presented earlier in the chapter. Finally, the studies consider the degree to which the damping added by a high-bandwidth X_{SSSC}-based power flow controller allows the SSR-stable range of set-point values of the X_{SSSC} in the FACTS device to be extended beyond that possible in a stand-alone X_{SSSC}-type SSSC.

In Chapters Four and Five of the thesis, the studies consider the X_{SSSC}-controlled SSSC as the FACTS device used for power flow control applications. However, as discussed in the previous section, a V_{SSSC}-controlled SSSC is known to have different SSR characteristics in comparison with a X_{SSSC}-controlled SSSC [18,19]. Hence, Chapter Six considers the V_{SSSC}-controlled SSSC as the FACTS device for power flow controls in order to investigate whether the aforementioned difference in the FACTS device's own SSR characteristics also affects the way the power flow controller around the device

interacts with the damping of the torsional modes. This chapter first verifies the correctness of the constant power and constant angle modes of operation of the V_{SSSC}-controlled SSSC-based power flow controller using time-domain simulations to confirm that the control strategies have been implemented correctly using the mathematical models developed in Chapter Three. The influence of this V_{SSSC}-controlled SSSC-based power flow controller on torsional mode damping is then investigated by means of eigenvalue analysis in a systematic manner. As a reference point, the SSR characteristics of a stand-alone V_{SSSC}-controlled SSSC are considered first, prior to the introduction of the power flow controller around the SSSC. The design of the power flow controller for different dynamic response times is then presented, following which the chapter compares the influence of the design of both V_{SSSC}-controlled and X_{SSSC}-controlled SSSC-based power flow controllers on torsional mode damping for different power flow controller bandwidth designs.

The investigations of Chapter Six also consider the effect of having conventional series capacitors in the adjacent transmission line of the study system. The SSR-stable ranges of conventional series compensation in the adjacent line are again identified by means of eigenvalue scans and two specific values of conventional series compensation are then selected for further investigations. The SSR characteristics of the V_{SSSC}-controlled SSSC are then examined for the two selected cases of conventional series compensation in the adjacent line and a single SSR-stable operating point of the V_{SSSC}-controlled SSSC is initially identified for each of the two selected cases of conventional series compensation in the adjacent line. Chapter Six then compares the influence of the design of both V_{SSSC}-controlled and X_{SSSC}-controlled SSSC-based power flow controllers on torsional mode damping for each of the two selected cases of conventional series compensation in the adjacent line at different power flow controller bandwidth designs. Finally, the studies consider the degree to which the damping added by a high-bandwidth V_{SSSC}-based power flow controller allows the SSR-stable range of set-point values of the V_{SSSC} in the FACTS device to be extended beyond that possible in a stand-alone V_{SSSC}-type SSSC.

Finally, Chapter Seven presents the overall conclusions of the thesis and author's suggestions for further work.

1.4 Main Findings and Contributions of the Thesis

The main findings and contributions of the thesis are summarised as follows:

1. Detailed mathematical models of the studied power system, including a transmission network that is suitable for power flow control studies, have been developed in Matlab and validated against a detailed simulation model of the IEEE First Benchmark Model for SSR analysis in PSCAD. This Matlab-coded model of the study system provides the functionality to conduct both non-linear, time-domain simulations as well as numerical linearisation of the model equations required for eigenvalue analysis. This mathematical model, adapted from the IEEE First Benchmark Model for the study of SSR, furthermore provides the flexibility of allowing FACTS series compensation or conventional series capacitors in either of the transmission lines of the study system. (Chapter Three)
2. Re-confirmation, using the detailed mathematical model of the studied power system, that the SSR characteristics of the two categories of the SSSC, namely the X_{SSSC}-controlled and V_{SSSC}-controlled categories, are quite different. (Chapter Four and Chapter Six)

3. An initial design of an X_{SSSC}-controlled SSSC-based power flow controller that has a relatively slow response time is presented. Frequency-domain linearised transfer function analysis is used to investigate the influence of the design of the power flow controller gains (and hence its speed of response) on the resonant characteristics of the X_{SSSC}-controlled SSSC. A detailed study using the full mathematical model of the power system investigates the impact of the X_{SSSC}-controlled SSSC-based power flow controller's mode of operation and its response time on the damping of the torsional modes over a range of operating points. (Chapter Four)
4. An improved method of designing a SSSC-based power flow controller is presented that enables much faster response times for the power flow control to be obtained. A detailed study compares the impact of the relatively slow responding and fast responding X_{SSSC}-controlled SSSC-based power flow controllers on torsional mode damping. A detailed study then investigates the impact of such fast-responding X_{SSSC}-controlled SSSC-based power flow controllers on torsional mode damping in the presence of conventional series capacitors in an adjacent transmission line. (Chapter Five)
5. Detailed studies compare the impact of the influence of the design of both V_{SSSC}-controlled and X_{SSSC}-controlled SSSC-based power flow controllers on torsional mode damping both with, and without, additional conventional series capacitors present in adjacent transmission lines. (Chapter Five and Chapter Six)

1.5 Research Publications

Some of the findings of this thesis have been presented at national [23,24] and international [25-27] conferences.

Some of the work in the thesis has been published in peer-reviewed journals [28,29].

CHAPTER TWO

LITERATURE REVIEW

2.1 Introduction

The previous chapter has described the problems that power utilities are facing and explained the role of FACTS devices in alleviating these problems by allowing power systems to be operated closer to their stability limits without risking the security of the system. FACTS series compensators can potentially have a large impact on system stability but research has shown that, just like conventional series compensation, care has to be taken with regard to SSR.

Hence, this chapter starts by reviewing the mechanism of SSR, FACTS series compensation and how this form of series compensation can be used to influence the power transfer capability of an AC power system. The chapter then reviews the SSR characteristics of FACTS series compensators, and in particular the SSR characteristics of the SSSC. Finally, the chapter reviews the applications of FACTS series compensators that have been proposed in literature for closed-loop power flow control.

2.2 Background Theory on SSR, FACTS and Power Flow Control

2.2.1 Mechanism of SSR

When conventional series capacitors are connected in series with an RL transmission line to reduce its series impedance, a resonant RLC circuit is formed whose natural frequency f_{er} is given by [32]:

$$f_{er} = \frac{1}{2\pi\sqrt{LC}} = f_o\sqrt{\frac{X_C}{X_L}} \qquad (2.1)$$

where

f_o is the synchronous frequency of the system,

$X_L = 2\pi f_o L$ is the line inductive reactance at the synchronous frequency,

$X_C = \frac{1}{2\pi f_0 C}$ is the capacitive compensating reactance at the synchronous frequency.

Fig. 2.1 shows the behaviour of the magnitude of the series impedance of this capacitive compensated line as a function of frequency. It can be observed that with increasing frequency the inductive reactance X_L increases linearly whereas the capacitive reactance X_C decreases. Hence, there is always a point where these two reactances are equal and cancel each other out such that $\left(X_{TOTAL} = X_L - X_C\right)$ leaving a small resistance in the transmission line to limit the resonant-frequency current flow. This particular point occurs at the natural frequency f_{er} given in Eqn. 2.1

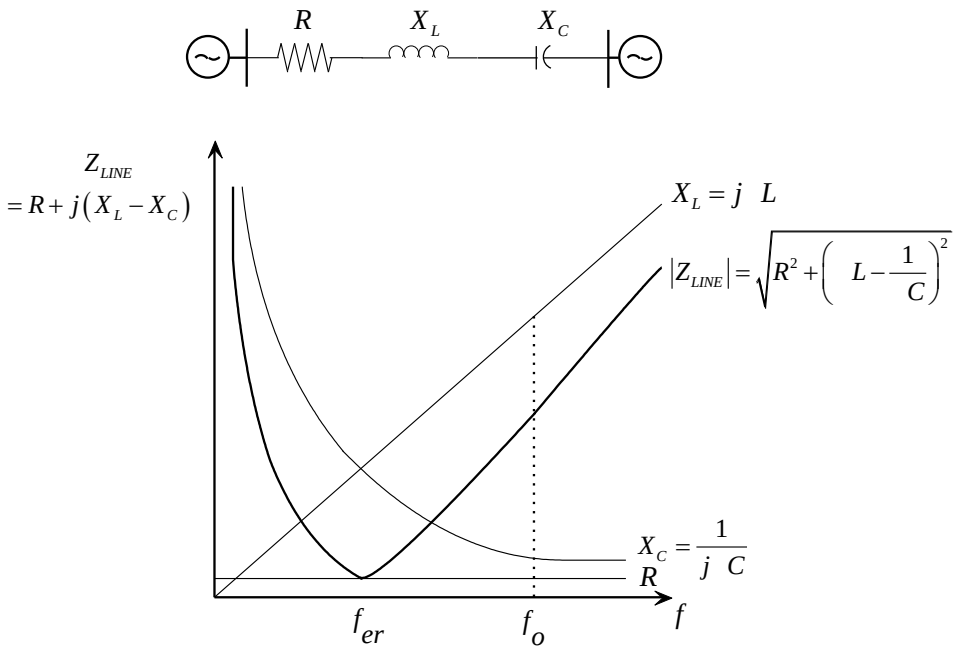

Fig. 2.1 Conventional RLC line impedance elements as a function of frequency [33].

where the series impedance of the line exhibits a resonant minimum as shown in Fig. 2.1. In practice, because the compensation ratio X_C/X_L is always less than unity (i.e. $X_C < X_L$) the natural frequency f_{er} is lower than the system frequency f_o (i.e. f_{er} is subsynchronous).

Following any system disturbance, the above characteristics of an RLC line thus cause the transient currents in the line to flow at the subsynchronous frequency f_{er} with large amplitude and they are poorly damped. These transient currents produce rotor currents and torques at complementary frequencies $f_o \pm f_{er}$ and it is the subsynchronous component $(f_o - f_{er})$ of these currents and torques that gives rise to the phenomenon of SSR. The SSR phenomenon manifests itself in different forms [14,32-36]:

The induction generator effect

This form of self excitation is purely an electrical phenomenon that is not dependent on the shaft torsional characteristics, and it can be explained as follows. Since the rotating magnetic field produced by the subsynchronous armature currents are moving slower than the speed of the rotor circuits, the rotor presents a *negative* resistance to these currents when viewed from the stator terminals. As explained previously in Fig. 2.1, the series compensated line presents a small but positive resistance to currents at its natural frequency f_{er}. However, if the negative resistance of the generator rotor exceeds the positive resistance of the transmission line at the natural frequency, then the flow of subsynchronous currents becomes self excited. This phenomenon is referred to as the induction generation effect.

Torsional Interaction

This form of self excitation involves both the rotor electrical dynamics and mechanical shaft dynamics of the generator. The multi-inertia system of a turbine generator has several natural torsional frequencies of oscillation f_n that lie in the subsynchronous frequency range. Generator rotor oscillations at one of these mechanical natural frequencies f_n induce armature voltage components at frequencies $f_{en} = f_o \pm f_n$. If the subsynchronous component $(f_o - f_n)$ of these armature voltages is close to the resonant frequency of the electrical system f_{er}, the resulting subsynchronous currents are large and produce an oscillatory component of rotor torque whose phase is such that it enhances the generator rotor oscillations. This can result in self-sustained oscillations and this phenomenon is referred to as torsional interaction.

Torque Amplification

As explained earlier, system disturbances in a series capacitor compensated line produce transient electromagnetic torques on the generator rotor at complementary frequencies $f_o \pm f_{er}$. If the subsynchronous component of these transient torques at frequency $(f_o - f_{er})$ is close to one of the mechanical natural torsional frequencies f_n, the resulting shaft torques can have large amplitudes immediately following the disturbance, although they may decay eventually. This phenomenon is referred to as shaft torque amplification.

In all these forms of SSR, the existence of conventional series capacitors is instrumental in introducing an electrical resonance in the transmission line for these different types of interactions to take place. The SSR phenomenon has attracted the focus of a lot of researchers and much has been written in this subject area [37-41] since the two shaft failures that occurred at the Mohave Generating Station in Southern Nevada, U.S.A where the cost of each those accidents was estimated to be a hundred million US dollars [42]. The emergence of FACTS series compensators has led to a renewed interest in determining the SSR characteristics of these more advanced forms of series compensation, in particular the SSSC [18,19,43].

2.2.1.1 SSR Analysis

Since the SSR phenomenon is a complex interaction that involves the electrical and mechanical dynamics of the turbine generator, it is required to represent all these elements of the generator in sufficient detail within the mathematical model of the power system in order to predict SSR in an affected machine. In addition to these modelling requirements there are several analytical tools that can be used in the study of SSR [13,32,44,45].

Frequency Scanning

Each generator in the system is represented by a voltage source behind an impedance in the frequency scanning method. The equivalent resistance and impedance of the electrical network are then computed, as a function of frequency, as seen looking into the network

from a point behind the stator winding of that particular machine. This approach is an approximate method particularly suited for preliminary SSR studies in large networks.

Eigenvalue Analysis

The eigenvalue analysis method is considered more accurate than frequency scanning for identifying SSR conditions but is computationally more intensive. In this method, the mathematical model is more complex consisting of linear differential equations that represent the dynamics of the full turbine-generator shaft mechanical and electrical system coupled with the dynamics of the electrical transmission networks. The eigenvalue results show both the frequencies of oscillation and the damping of each dynamic mode of the system in a single calculation [32]. Due to the complexity of the mathematical model, this approach is limited to relatively small systems where fundamental SSR interactions are the focus of study.

Time Domain Simulations

In this method, the non-linear differential equations representing the dynamics of the full turbine-generator shaft mechanical and electrical systems coupled with the dynamics of the electrical transmission networks are solved by iterative step-by-step numerical integration. This approach may be used to confirm the results obtained from linearised eigenvalue calculations as well as to study the transient interactions of SSR [13].

In this thesis, since the SSR interactions between a new SSSC-based power flow controller and the turbine-generator are studied, the focus is on a study system which is relatively small, but which is still sufficiently detailed so as to be representative of those dynamics of the power system needed in order to understand fundamental issues. Hence, the eigenvalue analysis method has been used for the majority of the studies considered in this thesis. In addition, time domain simulations have also been used to confirm certain results obtained from the eigenvalue calculations. However, during the initial designs of the SSSC-based power flow controller for different dynamic response times, an approach similar to the frequency scanning method has been employed to study the frequency-domain characteristics of the power flow controller's transfer function in isolation from the generator shaft torsional dynamics, and in so doing to determine the maximum bandwidth that can be used in the power flow controller. However, in all cases, once this simplified analysis method has been used to arrive at designs of the power flow controller's gains, the full system model (including the full representation of the generator electrical and mechanical system dynamics) is used to carry out the actual SSR studies, both via eigenvalue analysis and time domain simulations.

2.2.2 Flexible AC transmission Systems (FACTS)

In the previous chapter, the role of FACTS devices as a countermeasure to the problems faced by power utilities was discussed. FACTS devices can be categorised in two different groups [4]:

Thyristor-based FACTS devices

This category of FACTS devices comprises the Static Var Compensator (SVC), the Thyristor Controlled Series capacitor (TCSC) and the phase-shifter.

Inverter-based FACTS devices

This category of FACTS devices comprises the Static Synchronous Series Compensator (SSSC), the Unified Power Flow Controller (UPFC), the Static Synchronous Compensator (STATCOM) and the Interline Power Flow Controller (IPFC).

Across the above two different categories of FACTS devices, the TCSC and SSSC are also classified as FACTS *series* compensators whereas the SVC and STATCOM are classified as FACTS shunt compensators [6,46]. The UPFC combines a STATCOM and a SSSC that are connected via a dc link. The IPFC combines two SSSCs that are connected via a dc link. Since this thesis considers the SSSC as the FACTS device to be used for power flow controls, the remainder of the review focuses primarily on the SSSC and its characteristics.

2.2.2.1 The SSSC

The inverter-based FACTS series compensator, now termed the SSSC, was first proposed by Gyugyi in 1989 [47]. The SSSC shown in Fig. 2.2 is used to insert, in series into the transmission line, an AC voltage v_{SSSC} at the synchronous frequency via a series injection transformer to influence the power flow on the line. The mode of operation of the SSSC determines the magnitude and phase of this injected voltage v_{SSSC}. When the SSSC operates as a stand-alone FACTS series compensator, the device is restricted to the reactive power domain, where the injected voltage v_{SSSC} must be in quadrature with the line current.

There are two possible modes of operation of the SSSC that give rise to two categories of SSSC implementation [18,19,48,49]:

Reactance-Controlled SSSC

The SSSC is referred to as a reactance-controlled SSSC when it operates in the line impedance emulation mode, where the SSSC injects an AC voltage that emulates capacitive reactance. Various researchers have given this mode of operation different names in the literature. It is sometimes referred to as the "constant reactance mode" [48], or the "X_q-controlled SSSC" [19]. In this mode, the voltage injected into the line is in lagging quadrature

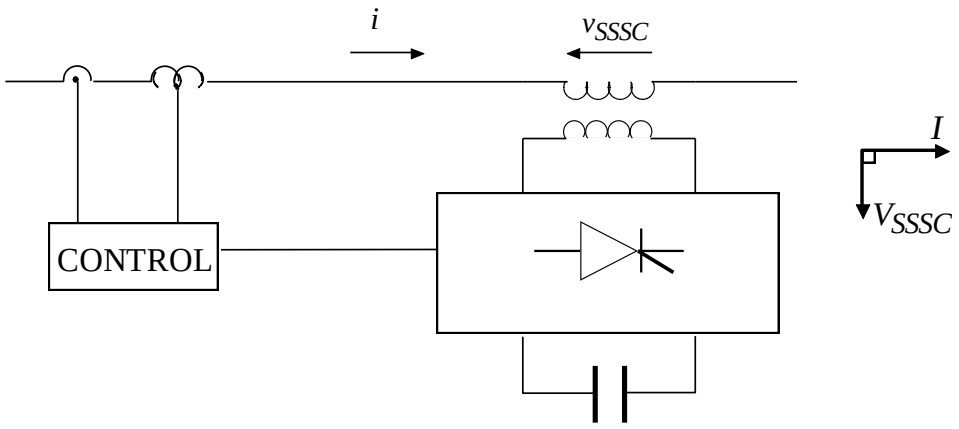

Fig. 2.2 Schematic diagram of the SSSC.

with the line current i, thus emulating a capacitive reactive voltage drop in series with the transmission line. The mathematical relationship between the current phasor $\boldsymbol{I}$ and the injected voltage phasor $\boldsymbol{V_{SSSC}}$ can be described by the phasor equation:

$$\boldsymbol{V_{SSSC}} = k\boldsymbol{I}e^{-j\frac{\pi}{2}} \tag{2.2}$$

where the term k determines the degree of series compensation [49]. Hence, by controlling k, the degree of series compensation can be continuously varied within the rating of the inverter from zero compensation $(k = 0)$ to some maximum value $(k = k_{max})$. Also, by controlling the term k, the reactive compensation is specified in a similar manner to a conventional series capacitive reactance [50], where

$$k = \frac{|\boldsymbol{V_{SSSC}}|}{|\boldsymbol{I}|} = X_{SSSC} \tag{2.3}$$

The term k in Eqn (2.3) becomes analogous to the ohmic magnitude of a series capacitive reactance emulated by the reactance-controlled SSSC [33]. Thus, in this mode of operation, the SSSC effectively replaces a conventional series capacitor with $X_{SSSC} = k$ being, in effect, equivalent to the fundamental-frequency reactance X_C of the traditional series capacitor bank. However, in the case of the reactance-controlled SSSC, the magnitude of the compensating reactance is rapidly controllable because the amplitude $|V_{SSSC}|$ of the inverter output voltage can be adjusted very rapidly. Note, although the SSSC is intended to emulate a conventional capacitive reactance at the fundamental frequency, throughout this thesis the variables V_{SSSC} and X_{SSSC} are used to describe the inserted voltage and emulated capacitive reactance of the SSSC, whereas the variables V_C and X_C are used to describe the voltage across, and reactance of, a conventional series capacitor bank.

Quadrature Voltage-Controlled SSSC

When the SSSC operates in the direct voltage injection mode [51], it is referred to as a quadrature voltage-controlled SSSC, where the controllable series compensating voltage is independent of the magnitude of the line current. This mode of operation is also referred to as "constant quadrature voltage mode" [48] or the "V_q-controlled SSSC" [19]. In this mode, the injected voltage v_{SSSC} is typically capacitive in nature, but has no direct enforced magnitude relationship with the line current i. For example, the magnitude of this compensating voltage can be used as part of a closed-loop control scheme to schedule the active power the transmission line to follow a desired reference value. However, in this mode of operation the SSSC does not emulate any *specific value* of capacitive reactance as it does in the case of the previous category of SSSC.

The literature has shown that the SSR characteristics of these two types of SSSC have important differences as stand-alone devices [18,19], that is, even prior to adding closed-loop power flow control around such compensators. Hence, this thesis considers both categories of the SSSC and revisits the SSR characteristics of each of these two types of SSSC to confirm the validity of the mathematical models being used prior to considering the application of power flow controls around these two categories of SSSC. In both types of SSSC the VA rating of the device itself is determined simply by the product of the maximum value of the injected series compensating voltage and the

maximum value of the transmission line current at which compensation is still desired [6], that is $VA_{SSSC} = I_{max}V_{SSSC_{max}}$. Thus, in both types of SSSC, higher degrees of series compensation provided by the device would require a larger rating of the SSSC. However, although in practical applications the degree of compensation achievable from an SSSC might therefore have to be limited, such practical rating limitations of the SSSC in any one application lie outside of the scope of this thesis. Therefore in the studies to be carried out in the thesis the ranges of the SSSC compensation considered are chosen to ensure that the SSR characteristics of the device, both with and without power flow controls, are fully understood prior to any practical operating constraints that may arise for particular installations.

2.2.3 Basic Concepts of Power Flow Control

This subsection will now address the concept of power flow control using FACTS series compensators, in particular the SSSC. Fig. 2.3 shows a single machine infinite bus (SMIB) study system consisting of a synchronous generator that is connected to a transmission network via a step up transformer. The transmission network consists of two transmission lines in parallel, where line 1 is compensated by the SSSC and line 2 is left uncompensated (at least at this stage of the discussion).

In Fig. 2.3 the active power transfer in transmission line 1 is given by

$$P_{L1} \approx \frac{|V_S||V_R|}{X_{L1}-X_{SSSC}} \sin\theta_{SR} \qquad (2.4)$$

where $|V_R|$ and $|V_S|$ are the magnitudes of the voltages at the sending and receiving buses and θ_{SR} is the transmission angle between these bus voltages.

Equation 2.4 highlights the principle by which the reactance emulation type of series compensation can be used to manipulate the net impedance of the transmission line and hence influence its power transfer. When the SSSC's compensating reactance X_{SSSC} is increased for a given transmission angle θ_{SR}, the net reactance $X_{L1} - X_{SSSC}$ of the compensated line 1 is reduced, thereby increasing the active power transfer. Hence, the magnitude of the active power transfer in the compensated line can be increased for a given transmission angle by increasing the amount of controllable compensation. Alternatively, an increase in the amount of controllable compensation can be used to reduce the transmission angle required for a given active power transfer in the compensated line. Although the quadrature voltage-controlled type of SSSC does not emulate a specific ohmic reactance in the line, it has the same effect, that is an increase in the magnitude of the quadrature voltage V_{SSSC} increases the flow of power down the line for a given θ_{SR}. A more detailed treatment of the two forms of compensation and their interchangeability can be found in [48].

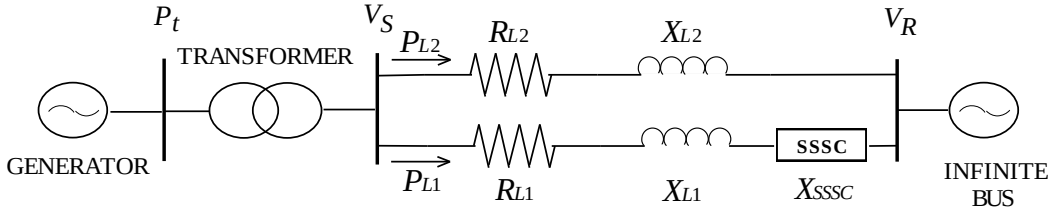

Fig. 2.3 Single-line diagram of the SMIB study system.

These two observations underlie two distinct strategies that have been proposed for closed-loop control of line power flow [15,16]: the "constant power strategy" which keeps the power flow in the compensated line constant, and the "constant angle strategy" which ensures that the compensated line transfers any increase in dispatched power. Each of these strategies will be now be explained in more detail.

2.2.3.1 Constant Power Strategy

Consider the system shown in Fig. 2.3 initially operating at steady state, and then subjected to an increase in the active power output from the generator. This increase in the generator dispatched power P_t causes the common transmission angle θ_{SR} between the sending and receiving buses to increase, and hence the active power transfer by both parallel lines 1 and 2 initially increases. However, in the constant power strategy the power flow in line 1 is to be kept constant at some desired set point value. Using the relationship in Eqn. 2.4, following an increase in the generator dispatched power the power flow controller will respond so as to decrease the SSSC's reactance X_{SSSC} so that the power transfer in line 1 remains unchanged from the desired set point value. Consequently, in this mode of power flow control, all the increase in dispatched power from the generator is then forced to flow through line 2. In this mode of operation of the power flow controller, for the case of the quadrature voltage-controlled type SSSC, following an increase in the generator power dispatch, the power flow controller will respond by decreasing the magnitude of the quadrature voltage V_{SSSC} so that the power transfer in line 1 remains constant.

2.2.3.2 Constant Angle Strategy

Consider, once again, the situation when the generator output power in Fig. 2.3 is increased, but now with the SSSC-based power flow controller used to maintain a constant transmission angle θ_{SR} across both lines. From Eqn. 2.4, following an increase in generator dispatched power, the power flow controller will respond so as to increase the SSSC's reactance X_{SSSC} in order that transmission line 1 is made to transfer all the additional dispatched power. This ensures that the transmission angle across the line 1 and 2 is kept constant and that the power transfer in the uncompensated line 2 remains unchanged. In this power flow control strategy, for the case of the quadrature voltage-controlled type SSSC, following an increase in the generator power dispatch, the power flow controller will respond by increasing the magnitude of the quadrature voltage V_{SSSC} so that all the additional power dispatched is transferred by line 1, hence keeping the angle across both lines 1 and 2 unchanged.

In [17] it has already been shown that each of these two power flow control strategies influences the damping of the inertial swing mode of a generator differently; furthermore, the findings in [17] indicate that the response times of the power flow controller also have an impact on a generator's inertial swing mode damping. Hence, this thesis now considers the impact of each of these two power flow control strategies, around the two categories of SSSC presented in the previous subsection, on the damping of the *torsional* modes of a generator shaft. Furthermore, this thesis also considers the impact of the response times of the power flow controller on generator torsional mode damping.

2.3 Literature Review on more-specific SSR related issues

In the previous sections the background theory of SSR, FACTS series compensation and the application of FACTS series compensators for power flow controls was reviewed but this section reviews more specific issues in the subject area of SSR.

The SSR problems associated with conventional series capacitor compensation have been summarised in the previous section. The root cause of the SSR phenomenon in conventionally series compensated transmission systems is the presence of a resonant minimum in the impedance of the compensated line at a subsynchronous frequency, which in turn is caused by the fact that the series capacitors themselves present a compensating reactance not just at the system (synchronous) frequency but also at subsynchronous frequencies [32]. The emergence of a new generation of modern, FACTS series compensators (thyristor-based FACTS series compensators such as the TCSC [52-71] and inverter-based FACTS series compensators such as the SSSC [49-51]) promised several advantages over traditional series capacitor compensation, including the possibility of mitigating, or even avoiding SSR. However, since this thesis considers the SSSC as the FACTS device for its particular application as a power flow controller in an AC transmission system, more attention will be paid to the SSSC in the following review of the literature on more specific SSR related issues.

When the SSSC was first proposed it was originally thought [49] that the series compensation provided by a switching converter could not cause SSR because the converter would simply inject the required quadrature compensating voltage in series with the line at the fundamental frequency, and would therefore exhibit a theoretically-zero impedance in the line at all other frequencies. A subsequent discussion of the SSSC by its proposer Gyugyi [50] sounded a more cautious note in regard to SSR, explaining that the *aim* of this form of compensation is to inject a compensating voltage containing only the fundamental frequency; Gyugyi [50] explained that series compensation by a voltage source that can be restricted to the fundamental frequency is superior to conventional compensation because it cannot therefore cause SSR, but noted that such a scheme would require proper implementation. The SSSC implementation proposed in [50] is one in which the magnitude of the injected compensating voltage is controlled to maintain a specified proportionality with the magnitude of the transmission line current so as to emulate an ohmic magnitude of compensating reactance. As discussed in the previous section, this particular approach to implementing an SSSC is commonly referred to as a reactance-controlled type of SSSC.

More recently Gyugyi et al [51] described an alternative implementation of the SSSC in which the magnitude of the compensating voltage injected in series with the line is independent of the magnitude of the transmission line current, such that the injected voltage could relatively easily be restricted to the fundamental frequency of the transmission system. As discussed in the previous section, this alternative approach to implementing an SSSC is commonly referred to as a quadrature voltage-controlled type of SSSC. Although it was claimed in [51] that this form of SSSC cannot cause SSR, at the time that these claims were made they had yet to be supported either by analytical studies or by numerical simulations that made use of detailed dynamic models of the SSSC and its controls. Although the claims regarding SSR immunity of the SSSC made in [51] were the subject of supporting simulation studies by others in [72,73], these studies in [72,73] used an ideal series voltage source that was intentionally restricted to the fundamental frequency as the mathematical model representing the SSSC, and not a full dynamic model of the SSSC and its controls. In other

words, the studies described in [72,73] appear to have assumed, *a priori* in the properties of the simplified model used to represent the SSSC, the very conditions posited in [50] as being necessary for SSR immunity of the device.

However, it has subsequently been shown in [18], through detailed numerical simulation studies of the SSSC over a range of frequencies (using a full dynamic model of the device), that in the case of both the reactance–controlled and quadrature voltage–controlled SSSC implementations, the voltages injected by an SSSC are not inherently restricted to the fundamental frequency. It was shown in [18] that in both these types of SSSC, the impedance of the compensated line exhibits a resonant minimum at a subsynchronous frequency, albeit at distinct frequencies from conventional series compensation, and that these resonant characteristics also depend to a significant extent on the design of the SSSC's controller. Subsequently, the conclusions reached in [18] have been confirmed by Pradhan and Lehn in [19] by means of exhaustive and detailed analytical modelling of the SSSC, in both the X_{SSSC}– and V_{SSSC}–control modes (again using a full dynamic model of the SSSC and its internal controls). References [18] and [19] have shown that the SSR characteristics of the SSSC can be (depending on the SSSC mode of operation, i.e. X_{SSSC} or V_{SSSC} – controlled) dependent on either transmission line operating point, SSSC controller design, or both of these factors, but that neither type of SSSC implementation is inherently SSR immune. Thus while it may be quite possible, with careful design, to achieve an SSR-stable system as reported in other SSSC studies such as [74-77] this does not imply that the SSSC is SSR stable inherently, or under all operating conditions.

An alternative approach that has been considered theoretically in the literature [78-86] is to exploit the flexibility of the SSSC in such a way as to employ supplementary control around this form of controllable compensation, specifically designed to damp SSR caused either by itself or by other, conventional series compensators in the same transmission system or even in the same line: that is to use an SSSC with supplementary control as an explicit SSR countermeasure. However, despite the success of such schemes it should be recognised that the SSR stability demonstrated in such implementations is the result of careful supplementary controller design in the studied system, rather than due to inherent SSR immunity of the SSSC as is clear from close analysis of the results presented in studies such as [83].

In light of the above historical experience and the growing understanding of the SSSC, it is evident that the SSR characteristics of the device itself, and of any supplementary controls employed around it, need careful attention when considering the use of this device in future system-control strategies. As presented in the previous section, one such control strategy that is widely being considered for the SSSC in the literature is its use for closed-loop control of the flow of power down a particular line in an interconnected transmission network [15,16]. Such closed-loop control of power flow in an AC system can provide a number of possible benefits: preventing unwanted loop flows in an interconnected system; allowing power to be directed along a "contract" path in a transmission system; preventing inadvertent overloading of lines already near their thermal limits [15]. However, more recently it has been shown [17] that a closed-loop power flow controller can affect the small-signal damping characteristics of the inertial swing modes of generators feeding a power system, and in particular that the nature and extent of these effects on the system's stability depend on both the mode in which the power flow controller is operated and its controller response time. The literature has also shown that other forms of line power scheduling such as HVDC implementations in [87,88] and fast-responding power flow controllers implemented around other types of FACTS

devices such as the TCSC in [65], are both known to have had an influence on the damping of generator torsional modes. Given the findings in [17,65,87,88], a logical concern that arises is whether the action of a fast-responding power flow controller implemented around an SSSC could also impact on the SSR stability of any generators with multi-inertia turbines that are susceptible to torsional interaction.

2.4 Summary

This thesis aims to investigate the effect of closed-loop power flow controls on the damping of any subsynchronous torsional modes in the shafts of turbine-generators that feed the power system. The SSR characteristics of the two categories of SSSC ($X_{SSSC}-$ and $V_{SSSC}-$ controlled devices) are revisited in order to validate the mathematical models of the SSSC used in the thesis before the addition of an external closed-loop power flow controller around the SSSC is considered. The design of the power flow controller around the two types of SSSCs is presented, and, furthermore, an improved method is proposed for designing the controller in order to achieve controller response times that are comparable to those reported in literature. The effects on torsional interaction of both the constant power and constant angle control strategies around each of the two types of SSSC are considered. Finally, the impact of both the power flow control strategies and both types of SSSC on torsional mode damping is also considered in the presence of conventional series capacitor compensation in an adjacent transmission line in the study system.

CHAPTER THREE

MATHEMATICAL MODELLING

3.1 Introduction

Chapter One has described the problems that power utilities are facing and explained the role of FACTS devices in alleviating these problems by allowing power systems to be operated closer to their stability limits without risking the security of the system. The previous chapter has shown that FACTS series compensators can potentially have a large impact on system stability but research has shown that, just like conventional series compensation, care has to be taken with regard to SSR. Furthermore, Chapter Two also highlighted the concern of whether FACTS-based closed-loop control of AC power can influence the damping of the torsional modes of a turbine-generator.

This chapter now focuses on the detailed mathematical models of the various system components that are required in order to study the impact of FACTS-based power flow controls on torsional interaction. The chapter describes the development of mathematical models of a representative study system, which is an adaptation of the IEEE First Benchmark system for the study of SSR to allow it to be used to analyse the effect of closed-loop power flow control on SSR stability. In addition, this chapter discusses the various components of the study system and describes how they are represented in the mathematical models of the system as a whole. Finally, in order to verify the correctness of the mathematical models of the study system written in Matlab, the time-domain responses of this study system were then compared with the results obtained for the same study system modelled using a different power system simulation package PSCAD.

3.2 The Study System

The study system considered in this thesis is a modification of the IEEE First Benchmark Model (FBM) [20] for SSR analysis, altered to include two transmission lines in parallel (as opposed to a single transmission line in the original benchmark model) as shown in Fig. 3.1. This modification of the IEEE First Benchmark Model to include a second parallel path in the transmission network was needed in order to allow specific types of power flow controller proposed in the literature [15,16] to be studied. However throughout the studies conducted in the thesis, the parameters of the individual lines in this modified transmission system have been adjusted (to twice the original series resistance and inductance) such that the impedance of the combined new parallel-line transmission system prior to compensation remains the same as that of the single transmission line of the original IEEE First Benchmark Model. The study system consists of a 892.4MVA cross-compound steam turbine generator connected to a 500kV transmission network via a step-up transformer, where X_T denotes the transformer reactance. The transmission network consists of the aforementioned two lines in parallel, where R_L denotes the resistance and X_L the inductive reactance of the respective line. Line 1 is equipped with series compensation provided by an SSSC, where X_{SSSC} denotes the effective capacitive reactance provided by the SSSC at the fundamental frequency if used in reactance-controlled mode, whereas V_{SSSC} represents the injected voltage if the SSSC is used quadrature voltage-controlled mode. The model of this study system also allows for the inclusion of

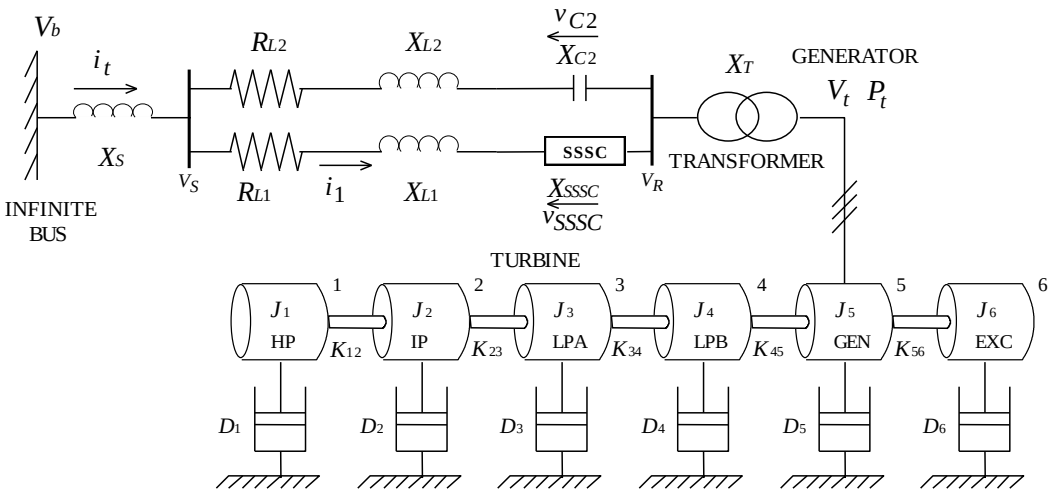

Fig. 3.1 Single line diagram of the electrical and mechanical parts of the study system.

series compensation in line 2 in the form of conventional series capacitors, where X_{C2} denotes the capacitive reactance provided by the series capacitors at the fundamental frequency. The transmission network is connected to an infinite bus via X_S, the system reactance between the end of the transmission lines and the infinite busbar. The mechanical system comprises six lumped masses: a high pressure turbine (HP), an intermediate pressure turbine (IP), two low pressure turbines (LPA, LPB), the generator (GEN) and the exciter (EXC), which are mechanically coupled by shaft sections of known torsional elasticity.

3.3 Power Flow Controllers

The previous chapter has already discussed the theory of power flow control in general, and in particular the constant power and constant angle control strategies have been presented. A feedback control system has been developed in order to implement closed-loop control of transmission line power flow in the benchmark system of Fig. 3.1 for the studies in this thesis. The structure of this control system has been devised in such a way that the power flow controller can be operated in either the constant power mode or the constant angle mode proposed in [15,16] simply by adjusting a user-selectable switch setting within the simulation model. Fig. 3.2 and Fig. 3.3 show a simplified, conceptual layout of the structure of this feedback control system which is supplied at its inputs with both the desired and measured values of active power in a particular line as well as the change in generator dispatch.

The structure of the controller shown in Fig. 3.2 is specifically intended for the case when the FACTS-based series compensator is implemented using a reactance-controlled SSSC, for which the input control signal is the commanded magnitude of compensating reactance X_{SSSC}, whereas the structure of the controller shown in Fig. 3.3 is intended for the voltage quadrature-controlled SSSC, for which the input control signal is the commanded magnitude of the injected voltage V_{SSSC}.

Specifically, in either constant power mode (mode select switch set to position A in Fig. 3.2 and 3.3) or constant angle mode (switch set to position B) a feedback loop compares a signal P_{L1}^{*}, representing the commanded value of power transfer in line 1, to the actual (measured) value of power transfer in line 1 (P_{L1}) in order to generate an error signal $\varepsilon_{P_{L1}}$; this error signal $\varepsilon_{P_{L1}}$ is used to

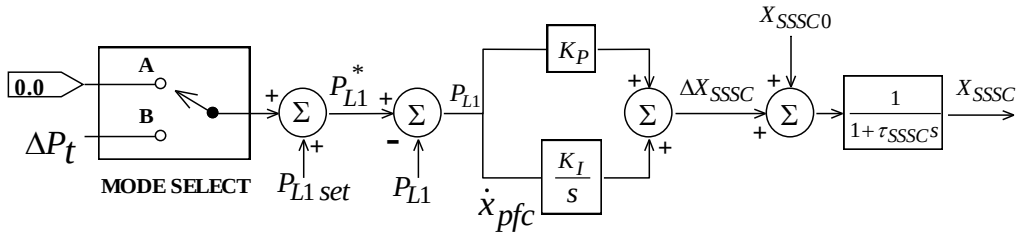

Fig. 3.2 Reactance-controlled SSSC-based power flow controller as it appears in the constant power mode of control.

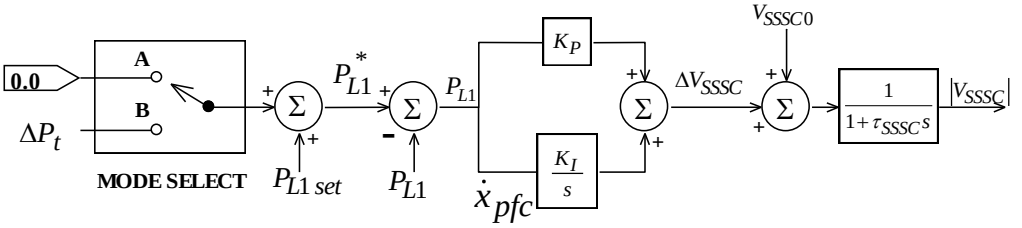

Fig. 3.3 Quadrature Voltage-controlled SSSC-based power flow controller as it appears in the constant power mode of control.

drive a proportional-integral (PI) controller which adjusts the amount of compensation demanded from the SSSC (X_{SSSC}-controlled or V_{SSSC}-controlled) around some set-point value (X_{SSSC0} or V_{SSSC0}) in order to force P_{L1} to follow the commanded value P_{L1}^*. For the case of constant power mode $P_{L1}^* = P_{L1set}$ where P_{L1set} represents the set-point value for the power transfer in line 1. For the case of constant angle mode, $P_{L1}^* = P_{L1set} + \Delta P_t$ where ΔP_t represents any change in generator dispatch.

3.4 The SSSC

In Chapter Two, the two categories of SSSC (reactance-controlled and quadrature voltage-controlled) have been reviewed and discussed in detail, and in this section the schematic block diagram of the two types of SSSC is presented. Figs. 3.4 and 3.5 show, respectively, the schematic block diagram of a reactance-controlled SSSC and a quadrature voltage-controlled SSSC [18,19,48,49] and their main controls. Both categories of SSSC comprise a voltage-sourced inverter and a coupling transformer that is used to insert the AC output voltage of the inverter in series with the transmission line. In this thesis, the internal control scheme used to make the inverter function as both a reactance-controlled SSSC and as a quadrature voltage-controlled SSSC is based on that described in [89]. The theory of operation of this scheme and its design for dynamic performance have been treated in detail in [89], but the main features of its controls are shown in Fig. 3.4. For the reactance-controlled mode of the SSSC operation, these internal controls comprise two distinct parts that supply the required *magnitude* and *phase angle* of the AC compensating voltage to the inverter's switching controls. The required magnitude of the compensating voltage to be supplied by the inverter is determined by calculating the amplitude $|I|$ of the line current and multiplying this by the magnitude of the compensating reactance value X_{SSSC} commanded at the control input to the SSSC. The required angle of the compensating voltage is maintained by a two-loop regulator within the angle control block that acts on the inverter DC voltage and the active

power at the inverter AC terminals. This phase angle controller steers the phase of the injected voltages to be in quadrature with the line currents to ensure no active power is exchanged at the AC terminals of the inverter at steady state, and in so doing regulates the inverter's DC voltage to a desired value [89].

In the quadrature voltage-controlled SSSC shown in Fig. 3.5, as is the case with the reactance-controlled SSSC in Fig. 3.4, the voltage source inverter is used to inject an ac voltage in series with the transmission line, and the device's internal angle controls ensure that this injected voltage lags the transmission line current by 90°. However, in the quadrature voltage-controlled approach to SSSC implementation, the magnitude of the AC voltage injected by the inverter is no longer a function of the magnitude of the transmission line current, but rather the magnitude V_{SSSC} of this compensating voltage is determined directly by an external control input according to the real or reactive power flow required in the transmission line [18,19,51].

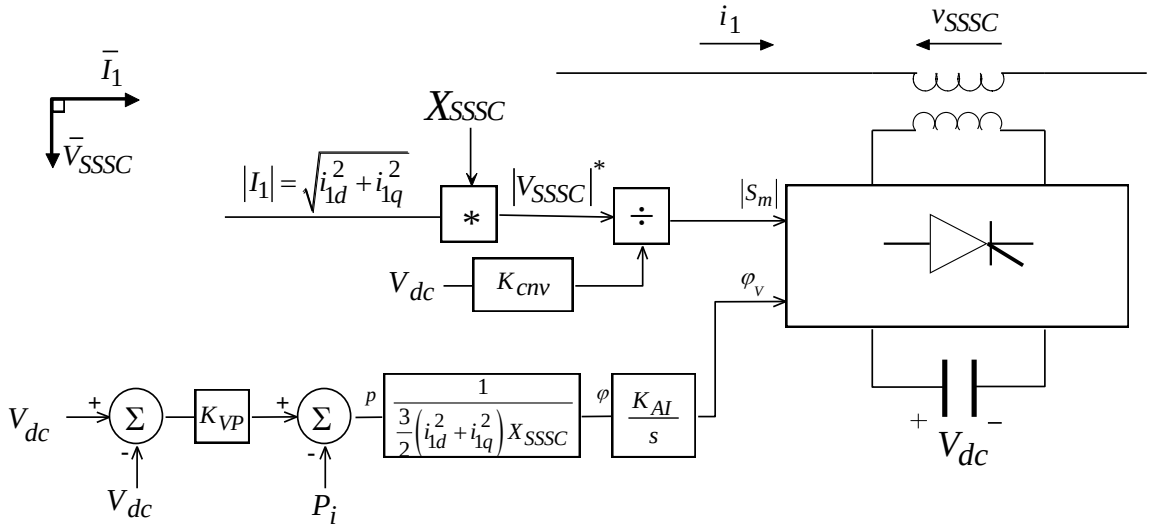

Fig. 3.4 Schematic block diagram of a reactance-controlled SSSC and its controls.

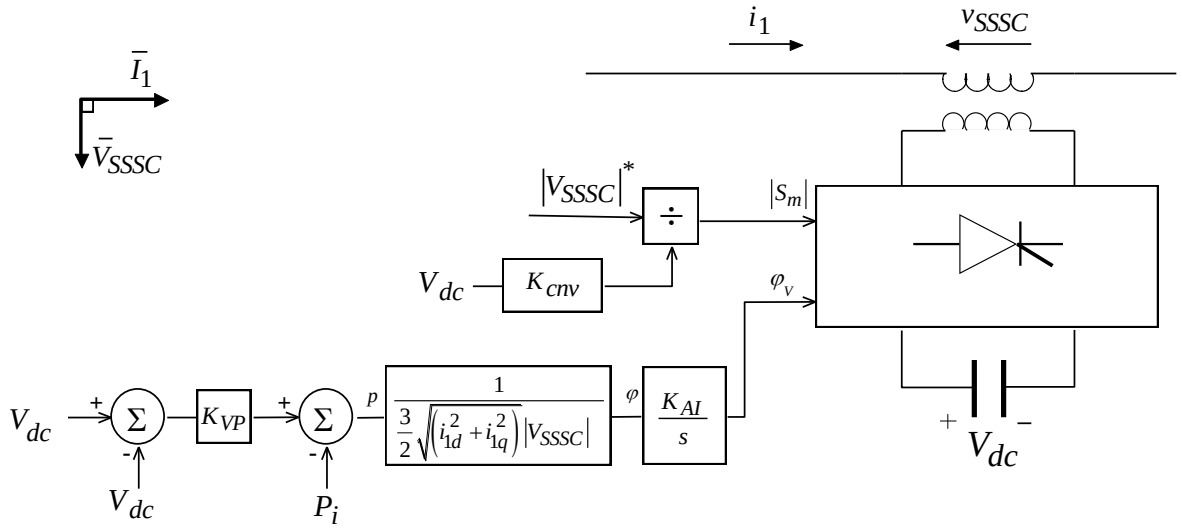

Fig. 3.5 Schematic block diagram of a quadrature voltage-controlled SSSC and its controls.

3.5 Mathematical Modelling

In order to analyse the SSR characteristics of the study system of Fig. 3.1 it is necessary to introduce a comprehensive mathematical model describing each system element.

3.5.1 Generator Electrical Model

Based on the usual assumptions [90] relevant to the two-axis theory, the mathematical model of a synchronous generator, expressed in terms of currents and a rotor reference frame, takes the following state-space form:

$$p\underline{i} = [L]^{-1}\{\underline{v} - ([R] + \omega[G])\underline{i}\} \tag{3.1}$$

where ω is the rotor speed, $[G]$ is the rotational voltage inductance inductance matrix, and $[R]$ is the machine resistance matrix. The vector of the dq axes winding currents is given by:

$$\underline{i} = \left[i_d, i_{fd}, i_{kd}, i_q, i_{kq1}, i_{kq2}\right]^T \tag{3.2}$$

and that of the dq axes voltages by:

$$\underline{v} = \left[v_d, v_{fd}, 0, v_q, 0, 0\right]^T \tag{3.3}$$

The above model consists of one damper circuit on the d-axis and two damper circuits on the q-axis to represent the effects of the damper windings in the synchronous machine of the IEEE FBM model [20].

The axis currents from Eqn. 3.2 are used to calculate the electrical torque T_e as follows:

$$T_e = -\underline{i}^T[G]\underline{i}\omega_0 \,/\, 2 \tag{3.4}$$

The mechanical torque T_m is related to P_m (the total output power onto the shaft by all the turbine stages) by the following relation:

$$T_m = P_m\omega_0 \,/\, \omega \tag{3.5}$$

In the simulation model of the study system developed in this thesis, the above Eqns. 3.1 to 3.5 are recast in a synchronously-rotating two-axis reference frame in order to integrate them with the dynamic model of the transmission network. In this new reference frame, the generator stator is represented by an equivalent non-linear voltage source b_g which does not neglect transformer voltage terms, in series with the stator phase resistance R_a and an equivalent inductance L_g^* (as shown in Fig. 3.6) as part of an AC equivalent circuit of the transmission network [91].

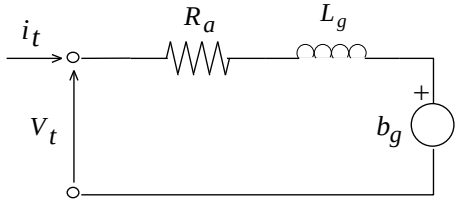

Fig. 3.6 Equivalent-circuit of the synchronously-rotating reference frame dynamic model of a generator stator suitable for inclusion in the transmission network.

This alternative format of the generator model nevertheless remains mathematically identical to the generator model in the more familiar format of Eqns. 3.1 to 3.5.

3.5.2 Mechanical System

The mechanical system of the steam turbine and generator in the study system consists of a four-stage turbine, a generator and an exciter. This system is represented in Fig. 3.7 as six inertias interconnected by five torsional springs (the connecting shafts), and can be described by a set of second order differential equations of the form:

$$[J]p^2\underline{\delta} + [D]p\underline{\delta} + [K]\underline{\delta} + \underline{T_e} + \underline{T_m} = \underline{0} \tag{3.6}$$

where $[J]$ is a diagonal matrix of inertias, $[D]$ is a diagonal matrix of damping coefficients, $[K]$ is a symmetric matrix of shaft stiffnesses, $\underline{T_e}$ is the electrical torque vector, $\underline{T_m}$ is the mechanical input torque vector and $\underline{\delta}$ is an angular position vector. Equation 3.6 consists of six, second order differential equations; each of these second order differential equations is decomposed into two, first order differential equations by change of variable so that the mechanical model of the turbine-generator shaft becomes

$$p\dot{\delta}_1 = -\frac{D_1}{J_1}\dot{\delta}_1 - \frac{K_{12}}{J_1}(\delta_1 - \delta_2) - \frac{T_{e1}}{J_1} - \frac{T_{m1}}{J_1}$$

$$p\delta_1 = \dot{\delta}_1$$

.

.

$$p\dot{\delta}_6 = -\frac{D_6}{J_6}\dot{\delta}_6 - \frac{K_{56}}{J_6}(\delta_6 - \delta_5) - \frac{T_{e6}}{J_6} - \frac{T_{m6}}{J_6}$$

$$p\delta_6 = \dot{\delta}_6$$

(3.7)

Equation 3.7 is shown in its full form in Appendix A.

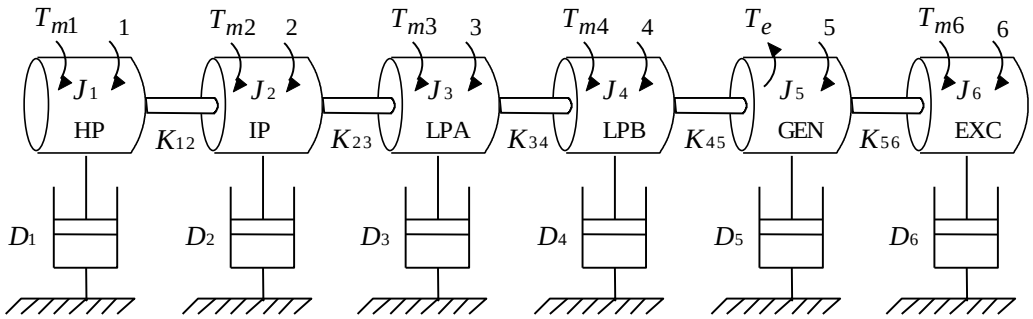

Fig. 3.7 Spring-mass model of the turbine shaft in [20].

3.5.3 Transmission Line Model

By using the synchronously rotating reference frame equivalent circuit form of the generator stator circuits shown in Fig. 3.6, the electrical dynamics of the transmission system and the generator stator in the study system of this thesis can be represented in ABC variables by the combined AC equivalent circuit of Fig. 3.8. Each of the transmission lines in Fig. 3.8 is assumed to consist of a lumped series resistance R_L and inductance L_L. The model allows for Line 1 to be compensated by either an SSSC or a conventional series capacitor whereas Line 2 can be compensated by only conventional series capacitors. In the following transmission line model, both transmission lines are initially considered to be compensated by conventional series capacitors. However, when Line 1 is compensated by an SSSC instead of a conventional series capacitor, the mathematical model describing the dynamics of the series capacitor in Line 1 is replaced by the mathematical model representing the dynamics of the SSSC which will be considered in the next subsection.

The equations describing the dynamic behaviour of the two three-phase RLC transmission lines can be written by inspection of Fig. 3.8 as

$$v_b - b_g = (L_s + L_t)pi_t + (R_s + R_t)i_t + R_1 i_1 + L_1 pi_1 + v_{C1} \tag{3.8}$$

$$v_b - b_g = (L_s + L_t)pi_t + (R_s + R_t)i_t + R_2 i_2 + L_2 pi_2 + v_{C2} \tag{3.9}$$

where

$$i_2 = i_t - i_1 \tag{3.10}$$

and

$$pv_{C1} = \frac{1}{C_1} i_1 = \omega_0 X_{C1} i_1 \tag{3.11}$$

$$pv_{C2} = \frac{1}{C_2} i_2 = \omega_0 X_{C2} i_2 \tag{3.12}$$

By substituting Eqn. 3.10 into Eqns. 3.8 and 3.9, the differential equations describing the transmission system in the stationary (abc) reference frame can be written as

$$p[i_t]_{abc} = a_{11}[i_t]_{abc} + a_{12}[i_1]_{abc} + a_{13}[v_{C1}]_{abc} + a_{14}[v_{C2}]_{abc} + a_{15}[e_{sr}]_{abc} \tag{3.13}$$

$$p[i_1]_{abc} = a_{21}[i_t]_{abc} + a_{22}[i_1]_{abc} + a_{23}[v_{C1}]_{abc} + a_{24}[v_{C2}]_{abc} + a_{25}[e_{sr}]_{abc} \tag{3.14}$$

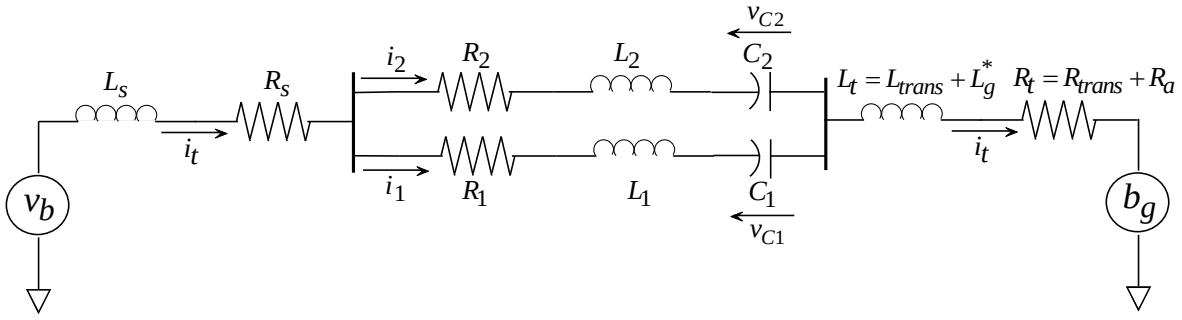

Fig. 3.8 Single line diagram of a parallel RLC transmission line system.

$$p[v_{C1}]_{abc} = \omega_0 X_{C1}[i_1]_{abc} \tag{3.15}$$

$$p[v_{C2}]_{abc} = \omega_0 X_{C2}[i_t]_{abc} - \omega_0 X_{C2}[i_1]_{abc} \tag{3.16}$$

where $e_{sr} = (v_b - b_g)$ is the voltage across the entire transmission network, and the coefficients a_{ij} in Eqns. 3.13 to 3.16 are made up of combinations of the individual parameters R_L, L_L, L_S, L_t of the two transmission lines in Fig. 3.8 as defined in Appendix A. The full derivation of Eqns. 3.13 to 3.16 from Eqns. 3.8 to 3.12 also appears in Appendix A.

By applying the appropriate Park Transform, Eqns. 3.13 to 3.16 which describe the dynamics of the transmission network in the stationary (abc) reference frame, may be transformed into the synchronously-rotating (dq) reference frame and written in shorthand notation as

$$p[i_t]_{dq} = a_{11}[i_t]_{dq} - \begin{bmatrix} 0 & \omega_0 \\ -\omega_0 & 0 \end{bmatrix}[i_t]_{dq} + a_{12}[i_1]_{dq} + a_{13}[v_{C1}]_{dq} + a_{14}[v_{C2}]_{dq} + a_{15}[e_{sr}]_{dq} \tag{3.17}$$

$$p[i_1]_{dq} = a_{21}[i_t]_{dq} + a_{22}[i_1]_{dq} - \begin{bmatrix} 0 & \omega_0 \\ -\omega_0 & 0 \end{bmatrix}[i_1]_{dq} + a_{23}[v_{C1}]_{dq} + a_{24}[v_{C2}]_{dq} + a_{25}[e_{sr}]_{dq} \tag{3.18}$$

$$p[v_{C1}]_{dq} = \omega_0 X_{C1}[i_1]_{dq} - \begin{bmatrix} 0 & \omega_0 \\ -\omega_0 & 0 \end{bmatrix}[v_{C1}]_{dq} \tag{3.19}$$

$$p[v_{C2}]_{dq} = \omega_0 X_{C2}[i_t]_{dq} - \omega_0 X_{C2}[i_1]_{dq} - \begin{bmatrix} 0 & \omega_0 \\ -\omega_0 & 0 \end{bmatrix}[v_{C2}]_{dq} \tag{3.20}$$

Equations 3.17 to 3.20 describe the dynamics of the of the transmission network of Fig. 3.8 in which both transmission lines are compensated by conventional series capacitors.

However, in the case of having line 1 compensated by an SSSC as shown in Fig. 3.1, the Eqn. 3.19 which describes the dynamics of the series capacitor is no longer considered and is replaced by the equations representing the dynamics of the SSSC which will be presented in the next subsection. In that case, the dynamics of this modified transmission system are represented in the synchronously-rotating (dq) reference frame as follows

$$p[i_t]_{dq} = a_{11}[i_t]_{dq} + a_{12}[i_1]_{dq} + a_{13}[v_{SSSC}]_{dq} + a_{14}[v_{C2}]_{dq} + a_{15}[v_b]_{dq} - a_{15}[b_g]_{dq} - \begin{bmatrix} 0 & \omega_0 \\ -\omega_0 & 0 \end{bmatrix}[i_t]_{dq} \tag{3.21}$$

$$p[i_1]_{dq} = a_{21}[i_t]_{dq} + a_{22}[i_1]_{dq} + a_{23}[v_{SSSC}]_{dq} + a_{24}[v_{C2}]_{dq} + a_{25}[v_b]_{dq} - a_{25}[b_g]_{dq} - \begin{bmatrix} 0 & \omega_0 \\ -\omega_0 & 0 \end{bmatrix}[i_1]_{dq} \tag{3.22}$$

$$p[v_{C2}]_{dq} = \omega_0 X_{C2}[i_t]_{dq} - \omega_0 X_{C2}[i_1]_{dq} - \begin{bmatrix} 0 & \omega_0 \\ -\omega_0 & 0 \end{bmatrix}[v_{C2}]_{dq} \tag{3.23}$$

where the term $[v_{C1}]_{dq}$ in Eqns. 3.17 and 3.18 is replaced by $[v_{SSSC}]_{dq}$ in Eqns. 3.21 and 3.22 which is a vector containing the d-axis and q-axis components of the AC voltage injected in series with Line 1 by the SSSC. Hence, Eqns. 3.21 to 3.23 describe the dynamics of the transmission network of Fig. 3.1 when Line 1 is compensated by an SSSC and Line 2 is compensated by a conventional series capacitor.

3.5.4 The SSSC Model

The mathematical model of the SSSC in this thesis makes use of a detailed dynamic model of the device previously developed for the work described in [89]. This model includes, without

simplification, all of the SSSC's internal synchronisation and control systems, and is hence able to represent the response of the SSSC's internal controls to both synchronous and non-synchronous frequency components present in the transmission system variables. The validity of this model of the SSSC and its internal controls under dynamic conditions has previously been established by direct comparison with practical measurements, both in the work presented in [89] and subsequently in the practical measurements presented in [92]; in this latter work in [92] the SSSC model was integrated into a detailed dynamic model of a transmission system fed from a multi-inertia turbine-generator, similar in nature to the study system now considered in this thesis.

In this model, the power electronic converter in the SSSC is represented in the synchronously-rotating dq reference frame as an ideal DC to AC converter whose AC output (compensating) voltages v_{SSSCd} and v_{SSSCq} are a function of the instantaneous value of the voltage V_{dc} on the converter's DC capacitor, the instantaneous values of the magnitude $|S_m|$ and angle φ_v of the modulating signals received from the low-level SSSC controls, and the DC to AC gain K_{cnv} of the converter. Although this model therefore does not represent the actual switching of the power semiconductor devices, the practical circuit topology of the power electronic converter in the SSSC assumed in this work is the same as that considered in the practical studies of [89] and [92], a diagram of which can be seen in Fig. 4 of reference [89].

For Reactance-Controlled SSSC:

Considering the block diagram of Fig. 3.4 for the reactance-controlled SSSC implementation, the output $|S_m|$ commanded from the SSSC's magnitude controls is given by

$$|S_m| = X_{SSSC}\sqrt{i_{1d}^2 + i_{1q}^2} \cdot \frac{1}{K_{cnv}V_{dc}} = X_{SSSC}\sqrt{i_{1d}^2 + i_{1q}^2} \cdot \frac{2\sqrt{2}}{V_{dc}} \tag{3.24}$$

Equation 3.24 shows that when the magnitude $|S_m|$ of the modulating signal is determined within the SSSC's controls it is pre-scaled by dividing by both the converter gain $K_{cnv} = 1 \,/\, 2\sqrt{2}$ and the instantaneous value of the converter DC voltage V_{dc}, such that the d- and q-axis components of compensating voltage at the AC output of the SSSC's converter are given by

$$v_{SSSCd} = |S_m| \sin(\varphi_v) \cdot K_{cnv}V_{dc} = \sqrt{i_{1d}^2 + i_{1q}^2}\, X_{SSSC} \sin(\varphi_v) \tag{3.25}$$

$$v_{SSSCq} = |S_m| \cos(\varphi_v) \cdot K_{cnv}V_{dc} = \sqrt{i_{1d}^2 + i_{1q}^2}\, X_{SSSC} \cos(\varphi_v) \tag{3.26}$$

where φ_v is the instantaneous phase angle of the compensating voltages commanded at the output of the SSSC's low-level controls. Thus, provided the value of φ_v is such that the correct quadrature relationship is maintained between the SSSC's voltages and the transmission line currents, the relationships in Eqns. 3.25 to 3.26 ensure that the magnitude of the SSSC voltage correctly emulates the volt drop across the commanded value of controllable compensating reactance X_{SSSC} as intended in a reactance-control type SSSC. As explained in more detail in [89], in this particular implementation of the SSSC the correct quadrature orientation (phase) of the SSSC's compensating voltages is maintained by a two-loop regulator whose outer loop regulates the SSSC's DC voltage V_{dc} and whose inner loop regulates the active power P_i exchanged at the AC terminals of the SSSC

converter. The differential equation describing the dynamics of this two-loop regulator in the SSSC model can be obtained by inspection of the diagram in Fig. 3.4 as

$$p\varphi_v = \frac{K_{AI}}{\frac{3}{2}(i_{1d}^2+i_{1q}^2)X_{SSSC}}\{K_{VP}(V_{dc}^* - V_{dc}) - P_i\} \quad (3.27)$$

where V_{dc}^* is the desired set-point value of the SSSC's DC voltage, V_{dc} is the actual value of this DC voltage, and P_i is the instantaneous active power measured at the terminals of the SSSC. The gain term $1 / \left[\frac{3}{2}\left(i_{1d}^2 + i_{1q}^2\right)X_{SSSC}\right]$ is included in the inner loop of the regulator to ensure that the control of the instantaneous active power P_i by steering the phase of the SSSC's AC compensating voltages is independent of operating point (power transfer) in the compensated transmission line [89]. The conversion from the commanded power error to an equivalent commanded angle error uses the approximate relationship: $\varepsilon_p^* = \frac{3}{2}|V_{SSSC}||I_1|\varepsilon_\theta^* = \frac{3}{2}|I_1|^2 X_{SSSC}\varepsilon_\theta^*$ where X_{SSSC} is the commanded input signal to the SSSC.

For Quadrature Voltage-Controlled SSSC:

Considering the block diagram of Fig. 3.5 for the quadrature voltage-control SSSC implementation, the output $|S_m|$ commanded from the SSSC's magnitude controls is given by

$$|S_m| = |V_{SSSC}|^* \cdot \frac{1}{K_{cnv}V_{dc}} = |V_{SSSC}|^* \cdot \frac{2\sqrt{2}}{V_{dc}} \quad (3.28)$$

Equation 3.28 shows that when the magnitude $|S_m|$ of the modulating signal is determined within the SSSC's controls it is again pre-scaled by dividing by both the converter gain $K_{cnv} = 1 / 2\sqrt{2}$ and the instantaneous value of the converter DC voltage V_{dc}, such that the d- and q-axis components of compensating voltage at the AC output of the SSSC's converter are given by

$$v_{SSSCd} = |S_m|\sin(\varphi_v) \cdot K_{cnv}V_{dc} = |V_{SSSC}|^* \sin(\varphi_v) \quad (3.29)$$

$$v_{SSSCq} = |S_m|\cos(\varphi_v) \cdot K_{cnv}V_{dc} = |V_{SSSC}|^* \cos(\varphi_v) \quad (3.30)$$

where φ_v is the instantaneous phase angle of the compensating voltages commanded at the output of the SSSC's low-level controls. The dynamics of the feedback regulator in Fig. 3.5 are described by the following equation

$$p\varphi_v = \frac{K_{AI}}{\frac{3}{2}\sqrt{\left(i_{1d}^2+i_{1q}^2\right)}\,|V_{SSSC}|^*}\{K_{VP}(V_{dc}^* - V_{dc}) - P_i\} \quad (3.31)$$

where V_{dc}^* is the desired set-point value of the SSSC's DC voltage, V_{dc} is the actual value of this DC voltage, and P_i is the instantaneous active power measured at the terminals of the SSSC. The gain term $1 / \frac{3}{2}\sqrt{\left(i_{1d}^2 + i_{1q}^2\right)}\,|V_{SSSC}|^*$ is included in the inner loop of the regulator to again ensure that the control of the instantaneous active power P_i by steering the phase of the SSSC's AC compensating voltages is independent of operating point in the compensated line. However, this gain term now takes a different form in the case of a V_{SSSC}-controlled SSSC because the conversion from the commanded power error to an equivalent commanded angle error uses the approximate relationship: $\varepsilon_p^* = \frac{3}{2}|V_{SSSC}|^*|I_1|\varepsilon_\theta^*$ where $|V_{SSSC}|^*$ is the commanded input signal to the SSSC.

The dynamic model of the AC-side voltages and the controllers of the SSSC are therefore described by either Eqns. 3.25 to 3.27 in the case of the reactance-controlled SSSC, or Eqns. 3.29 to 3.31 for the quadrature voltage-controlled SSSC.

The dynamic model of both types of SSSC (X_{SSSC}-controlled and V_{SSSC}-controlled) is then completed by describing the charging dynamics of its DC voltage V_{dc} in terms of the instantaneous power P_i at its AC terminals. In terms of the dq reference frame of the full study system model, the instantaneous active power at the AC terminals of the SSSC is given by

$$P_i = \frac{3[v_{SSSCd} i_{1d} + v_{SSSCq} i_{1q}]}{2} \tag{3.32}$$

From which the differential equation describing the dynamics of the SSSC's DC capacitor voltage is then given by

$$pV_{dc} = \frac{P_i}{C \cdot V_{dc}} \tag{3.33}$$

3.5.5 The Power Flow Controller Model

In the case of a reactance-controlled SSSC, the differential equations describing the dynamic model of the power flow controller can be derived by inspection of Fig. 3.2 as:

$$pX_{SSSC} = \frac{1}{\tau_{SSSC}}\{X_{SSSC0} + K_P(P_{L1}^* - P_{L1}) + x_{pfc} - X_{SSSC}\} \tag{3.34}$$

$$px_{pfc} = K_I(P_{L1}^* - P_{L1}) \tag{3.35}$$

where the output signal X_{SSSC} from the power flow controller is the input control signal to the reactance-controlled SSSC; the first order lag (time constant τ_{SSSC}) is included to approximate the transport lag across the DC/AC inverter, and in so doing to prevent an algebraic loop in the dynamics of the system model as a whole.

In the case of a quadrature voltage-controlled SSSC, the differential equations describing the power flow controller model can be derived by inspection of Fig. 3.3 as:

$$pV_{SSSC} = \frac{1}{\tau_{SSSC}}\{V_{SSSC0} + K_P(P_{L1}^* - P_{L1}) + x_{pfc} - |V_{SSSC}|^*\} \tag{3.36}$$

$$px_{pfc} = K_I(P_{L1}^* - P_{L1}) \tag{3.37}$$

where the output signal $|V_{SSSC}|^*$ from the power flow controller is the input control signal to the quadrature voltage-controlled SSSC.

3.5.6 Linearised Models for Eigenvalue and Transfer Function Analysis

In the previous section the mathematical models of the various components of the study system of Fig. 3.1 have been presented. Depending on the category of SSSC that is being employed in Line 1 of Fig. 3.1, a combination of the nonlinear differential equations presented in the previous section can be used to represent the dynamics of the full study system. For the case of having the power flow controller of Fig. 3.2 fitted around a reactance-controlled type SSSC (as shown in Fig. 3.4) as the FACTS device in Line 1, Eqns. (3.1 to 3.7), (3.21 to 3.27) and (3.32 to 3.35) represent the dynamics of

the full study system. For the case of having the power flow controller of Fig. 3.3 fitted around a quadrature voltage-controlled type SSSC (as shown in Fig. 3.5) as the FACTS device in Line 1, Eqns. (3.1 to 3.7), (3.21 to 3.23), (3.28 to 3.33) and (3.36 to 3.37) represent the dynamics of the full study system. For the time domain studies considered in this thesis, these nonlinear differential equations are solved by iterative step-by-step numerical integration.

For the eigenvalue and transfer function analysis considered in this thesis the nonlinear differential equations describing the dynamics of the full study system with the power flow controller implemented around either type of SSSC, are linearised into a 26th-order state space representation of the system. By using the Matlab-Simulink S-function tools [21], the nonlinear differential equations described in the previous section can be numerically linearised around a steady operating point to obtain a linearised state space approximation to the system model, which is valid for small-signal studies, of the following structure [93]:

$$p\Delta\bar{x} = [A]\Delta\bar{x} + [B]\Delta\bar{u} \tag{3.38}$$

$$\Delta\bar{y} = [C]\Delta\bar{x} + [D]\Delta\bar{u} \tag{3.39}$$

Chapter Two has reviewed the various small-signal (and other) study methods typically used in SSR analysis, and their particular suitabilities for different aspects of such analysis. Within the broad scope of the small-signal studies presented in this thesis, the eigenvalues of the $[A]$ matrix of the linearised study system model are used for those parts of the analysis where torsional interaction due to the SSSC itself, or due to the power flow controls around the SSSC, is the particular focus. For other parts of the analysis, where the gains of the power flow controller are designed, and the impact of these power flow controller designs on the resonant characteristics of the transmission line are considered, transfer functions of the form $\frac{\Delta\bar{y}}{\Delta\bar{u}}(s) = [C]\{s[I] - [A]\}^{-1}[B] + [D]$ between specific system inputs and outputs are calculated using additional Matlab tools applied to the numerically-linearised study system model.

3.6 Validation of the Mathematical Models of the Study System

The power system simulation package PSCAD is known to have a well-tested implementation of the IEEE FBM for SSR analysis. PSCAD also provides the advantage that the dynamic models of the individual components used to simulate power systems are proven and accepted [22]. However, while PSCAD would therefore be an ideal platform for the time domain aspects of the kinds of studies presented in this thesis, the disadvantage of this package is that it does not allow calculation of the linearised state space models required for some particular study methods (eigenvalues and transfer function analysis) used in SSR studies. Thus, for the purposes of this thesis the full non-linear differential equation models describing the study system have been written in Matlab which then allows both the time domain simulation and numerical linearisation methods of analysis as described previously. However, it is still important to validate such user-written models against known and proven dynamic models to the full extent possible.

For this reason, comparisons of the dynamic models of the generator electrical system, torsional spring mass model, and conventionally compensated parallel line transmission system developed for this thesis have been validated by direct comparison against PSCAD simulations (The dynamic models of the SSSC used in this thesis, as explained previously, have already been extensively

validated against measured results by others [92]; the validation of the power flow controller models derived for this thesis are validated using specific tests on the simulation model of the study system in Chapter Four and Chapter Six of the thesis).

As discussed in Section 3.2, the original IEEE FBM model has a single transmission line and hence the simulation model of the IEEE FBM provided by PSCAD had to be adapted by the author to include a second, parallel, transmission line; the parameters of the individual lines in this modified transmission system were again adjusted (to twice the original series resistance and inductance) such that the impedance of the combined new parallel-line transmission system matched that of the single transmission line of the original IEEE FBM model. In order to compare the time domain response of the author's Matlab-coded model of the study system with the time domain response of the PSCAD model, a second modification was required to the PSCAD model to allow a different type of test disturbance to that classically considered in the IEEE FBM model to be considered (a three-phase line-to-ground fault on the transmission line). Since the model of the study system has been derived in this thesis in the synchronously-rotating (dq) reference frame (to allow subsequent linearisation), this particular test disturbance cannot be applied in exactly the same manner to both models. Instead, a different type of disturbance was applied to the PSCAD model which can also be replicated exactly in the Matlab model of the same study system: the magnitude of the voltage at the infinite bus was dropped to zero for a short duration. The PSCAD simulation model is shown in Appendix B.

In the following time domain simulation study, which uses the full non-linear system model of Fig. 3.1, both transmission lines were initially equipped with conventional series capacitors. Hence, the mathematical model of the full study system of Fig. 3.1, incorporating two parallel conventionally compensated transmission lines coupled with the turbine-generator system, can be validated. The selected form of disturbance was applied to both simulation models at a specific degree of conventional series compensation in both transmission lines that is known to result in closely-tuned and unstable torsional interaction SSR in a particular mechanical shaft mode of the benchmark study system, and hence self-excited (negatively damped) oscillations are expected to arise following a disturbance to the system.

Fig. 3.9 shows the results of such a time domain comparison in which the magnitude of the voltage at the infinite bus V_b was dropped to zero for 75 ms with both conventional compensating series capacitors set at $X_{C1} \equiv X_{C2}$ = 0.757 pu. Following the disturbance, it can be observed that there are self-excited (negatively damped) oscillations at approximately 20 Hz (127.0 rad/s) in both the mechanical shaft system of the turbine (shaft torques GEN-EXC and LPA-LPB) as well as in the generator rotor's speed deviation. Fig. 3.9 thus confirms that a series compensation of $X_{C1} \equiv X_{C2}$ = 0.757 pu. (tuned to Mode 2) in both transmission lines, the study system is unstable when the mechanical damping of all the turbine stages is zero. The results also verify the correctness of the mathematical model developed for the study system as both Matlab and PSCAD results agree closely with each other.

The above study has thus established the validity of the mathematical models of the parts of the study system of Fig. 3.1 that include the turbine-generator system, coupled to the parallel line transmission network and conventional series capacitor compensation. Further studies will be considered to re-confirm the validity of the SSSC models in the study system by analysing the SSR

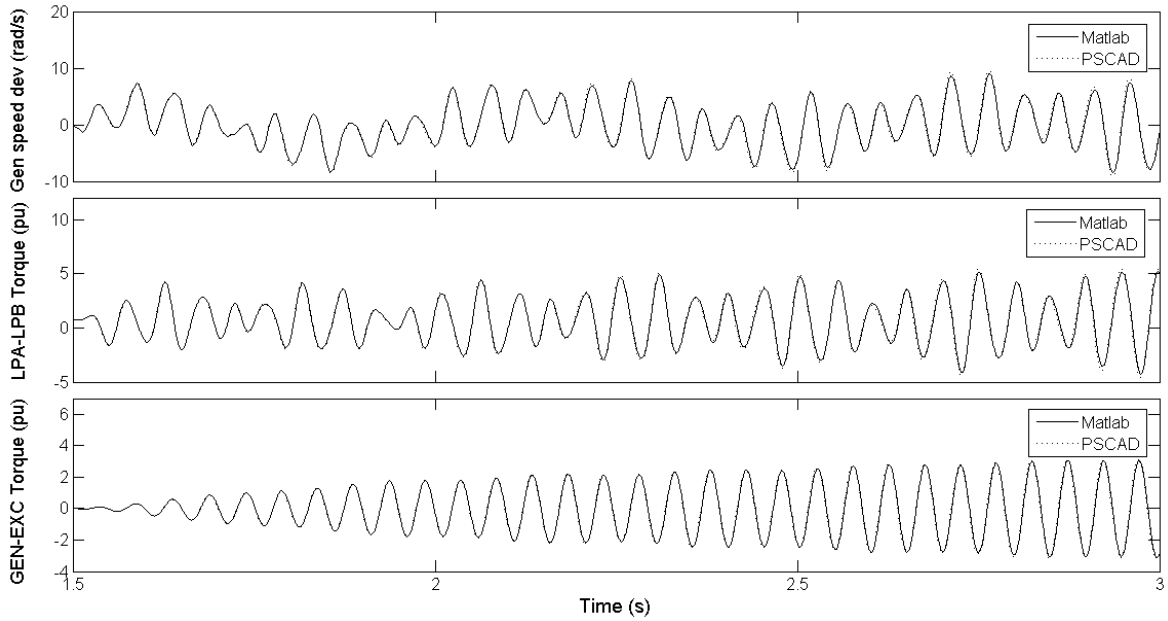

Fig. 3.9 Time-domain response of the study system following a disturbance at the infinite bus.

characteristics of both the X_{SSSC}-controlled SSSC and the V_{SSSC}-controlled SSSC. The above study has also not considered the power flow controller models and hence the verification of these models will also be considered in subsequent chapters of the thesis.

3.7 Conclusion

In this chapter, the mathematical models of the study system developed in Matlab for the simulation studies and analyses in subsequent chapters of the thesis have been presented. The dynamics of each element of the chosen study system have been represented in detail in order to predict SSR in an affected machine and its interaction with the system components. The mathematical model of the study system, which is an adaptation of the IEEE First Benchmark Model for SSR studies, provides the flexibility of allowing FACTS series compensation or conventional series capacitors in either of the transmission lines of the system. This Matlab-coded model of the study system provides the functionality to conduct both non-linear time domain simulations as well as numerical linearisation of the model equations required for eigenvalue and transfer function analysis. In order to verify the correctness of the mathematical models, time-domain responses from this Matlab-coded model were compared against the results obtained for the same study system modelled in PSCAD.

In the following chapter, the verification of the power flow controller model for a reactance-controlled SSSC, and the SSR characteristics of the reactance-controlled SSSC, will be revisited to further confirm the correctness of the mathematical models. After these mathematical models have been verified, the effect on torsional interaction of closed-loop power flow control around an X_{SSSC}-controlled SSSC will be investigated over a range of operating points.

CHAPTER FOUR

INVESTIGATING THE IMPACT OF A REACTANCE-CONTROLLED SSSC-BASED POWER FLOW CONTROLLER ON TORSIONAL INTERACTION

4.1 Introduction

The previous chapter presented the development of mathematical models of a representative study system which is an adaptation of the IEEE First Benchmark system for the study of SSR to allow it to be used to analyse the effect of closed-loop power flow control on SSR stability. In addition, the previous chapter has discussed the various components of the study system and described how they are represented in the mathematical models of the study system. Finally, in order to verify the correctness of parts of the mathematical models of the study system written in Matlab, the time-domain responses of this study system were then compared with the results obtained from a well established model of the same system in a different power system simulation package, PSCAD.

This chapter now investigates the impact of a reactance-controlled SSSC-based power flow controller on the damping of torsional modes in the shafts of the turbine-generators of this study system. However, the chapter begins by verifying the operation of the different modes of power flow control in order to confirm the correctness of the mathematical models of the power flow controller derived in Chapter Three. The chapter then examines the design of the controller parameters for a reactance-controlled SSSC-based power flow controller by using frequency-domain linearised transfer-function analysis. This chapter also uses the frequency-domain analysis approach to derive an understanding of how the design of the control gains of the power flow controller affects the resonant characteristics in the series impedance of a transmission network compensated by a reactance-controlled SSSC. An important characteristic of SSR in conventionally-compensated systems is that it is known to be operating-point dependant [32], and this has been shown to be an equally-important consideration in studies involving the SSSC [19]; thus, the investigations in this chapter consider not only the impact of the reactance-controlled SSSC at one operating point, but over a range of operating points. Finally, the chapter examines the impact of the power flow controller on a generator's torsional modes of oscillation, again over a range of operating conditions.

4.2 Verification of Control Modes

The mathematical model of the power flow controller for a reactance-controlled SSSC described in Chapter Three can be verified by means of two test studies using the study system shown in Fig. 4.1, where the transmission system incorporates a reactance-controlled SSSC that is fitted with a power flow controller in Line 1; Line 2 was left uncompensated for the purposes of the investigations considered in this chapter.

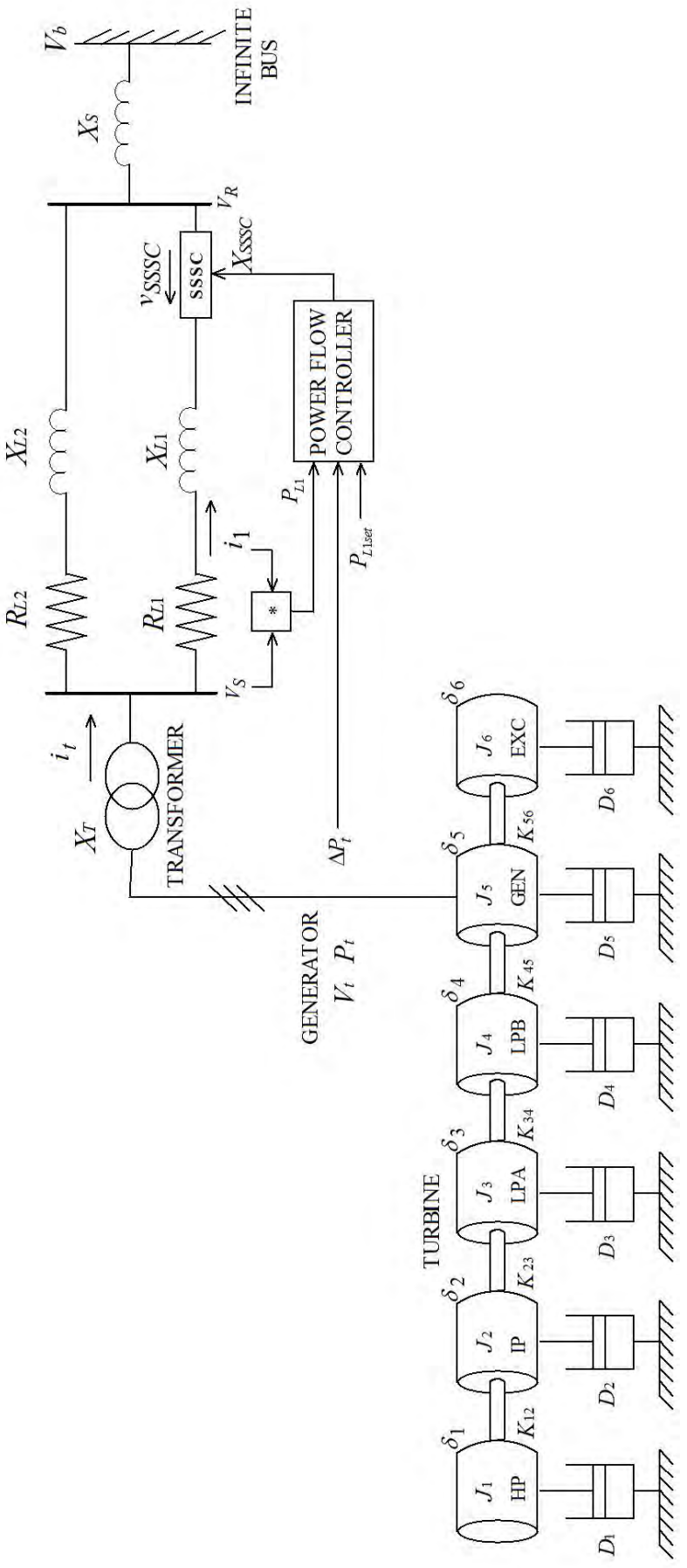

Fig. 4.1 Single line diagram of the study system.

To verify the implementation of the two control strategies presented in Chapter Two, in each case the simulation study was started from the same steady state condition in which the generator's active power output P_t = 0.5 pu., and with this active power being initially transferred by the lines 1 and 2 as follows: P_{L1} = 0.3 pu. and P_{L2} = 0.19 pu. Subsequently, the mechanical input power to the generator was increased by ΔP_m = 0.1 pu. such that the total active power P_t dispatched was increased to 0.6 pu. The response of the system to this small increase in generator dispatch was then studied for the system with the power flow control activated in each of the two possible control modes. Although a *step* change ΔP_m in the input to the turbine is not realistic in practice, it has been considered here as a theoretical test disturbance because it facilitates comparison of the dynamics of the two power flow controller modes.

Fig. 4.2 shows the response of the study system with the power controller active and set to the constant power mode. The results show that, following the increase in generator dispatch, initially the power transfer in Line 1 increases, which then results in the power flow controller reducing the degree of capacitive compensation provided by the reactance-controlled SSSC. By reducing the reactance X_{SSSC} provided by the SSSC, the power transfer in Line 1 is decreased accordingly and returns to its nominal operating point of 0.3 pu. All the additional power dispatched by the generator is thus forced to flow through Line 2, where the power transfer is increased to 0.29 pu. This response thus verifies the correct operation of this reactance-controlled SSSC-based power flow controller's mathematical model when in constant power mode.

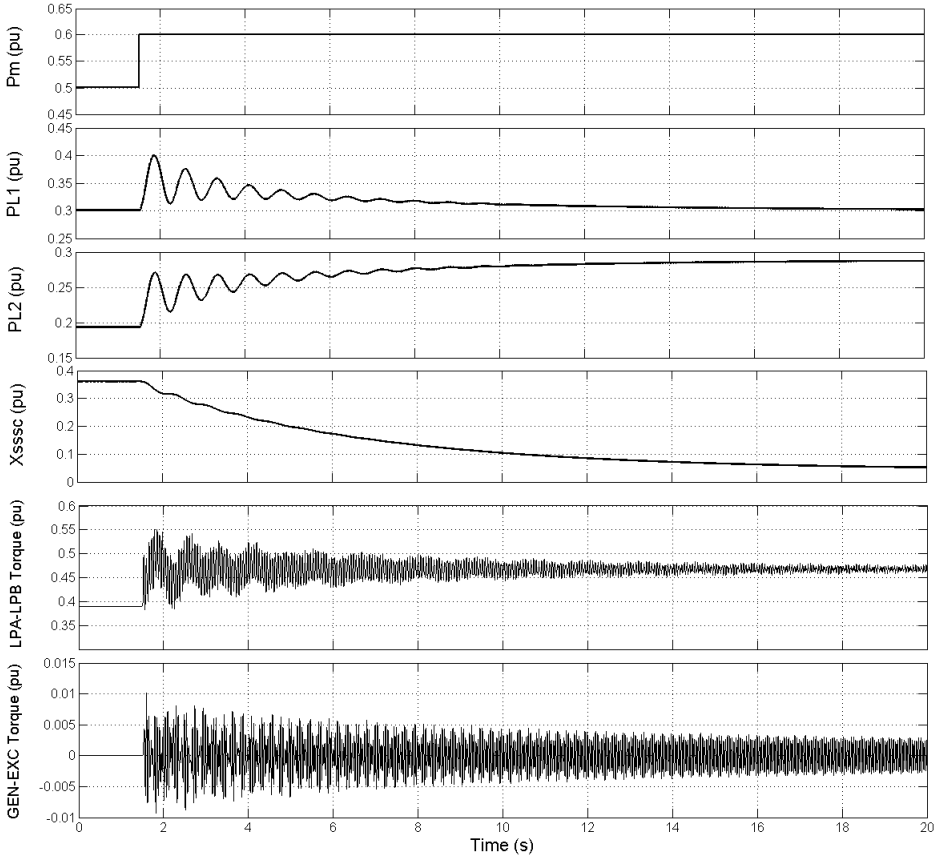

Fig. 4.2 Response of the study system to an increase in generator dispatch with the power flow controller in constant power mode.

Fig. 4.3 shows the response of the study system following the increase in generator dispatch with the power flow controller now set to operate in constant angle mode. According to [15,16] the constant angle strategy should ensure that the compensated line transfers all the additional output power of the generator. Fig. 4.3 shows that following the increase in generator dispatch, the power flow controller responds by increasing the degree of capacitive compensation provided by the series compensator such that the power transfer in Line 2 returns to its nominal operating point of 0.19 pu. and all the additional dispatch is transferred by Line 1 (P_{L1} increases to 0.4 pu.). Fig. 4.3 thus confirms that the constant angle controller is correctly implemented in the mathematical model of the study system of Fig. 4.1.

4.2.1 Influence of Power Flow Control on Turbine-Generator Torsional Oscillations

The time domain simulation results in Figs. 4.2 and 4.3 also show the influence of each power flow controller mode of operation on the torsional dynamics of the study system. Fig. 4.2 shows that in the constant power mode of control, the post-disturbance operating condition is SSR stable as the torsional oscillations are positively damped. Fig. 4.3 also shows that in the constant angle mode of control, the post-disturbance operating condition is likewise SSR stable for this operating condition as the torsional oscillations are positively damped. However, it can be observed that in this mode of operation of the power flow controller, the damping of the torsional oscillations is slightly reduced compared to the results shown in Fig. 4.2, particularly the damping of the oscillations between the LPA and LPB turbine stages. This effect on the torsional mode damping could be due to the mode of

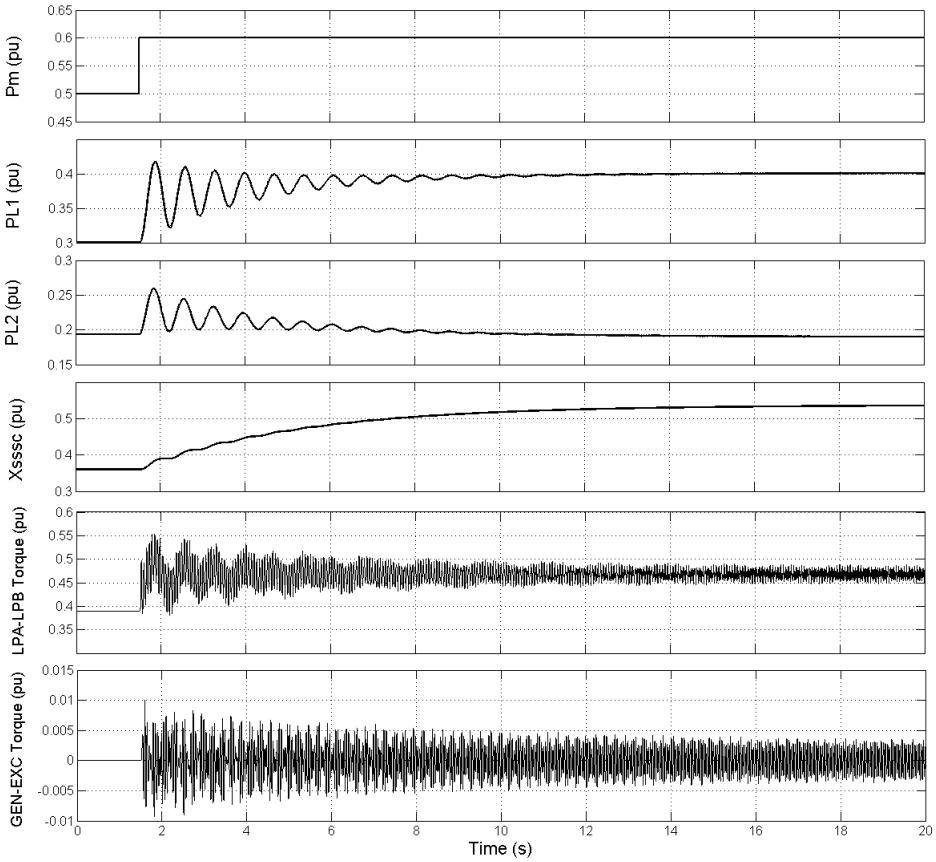

Fig. 4.3 Response of the study system to an increase in generator dispatch with the power flow controller in constant angle mode.

operation of the power flow controller, or due to the new value of series compensation in Line 1 as a result of the change in the set point of the power flow controller, or a combination of these two effects. In order to investigate these effects in more detail, eigenvalue analysis of the study system is considered in the following section.

4.3 SSR Characteristics of the Study System without Power Flow Control

This section initially investigates the SSR characteristics of the study system of Fig. 4.1 at different values of the series compensating reactance provided by the X_{SSSC}-controlled SSSC, with Line 2 uncompensated, using the mathematical model of the study system without the power flow controller enabled. In the first part of the analysis, the value of series compensation in Line 1 is varied from X_{SSSC} = 0.10 pu. to X_{SSSC} = 0.95 pu. corresponding to an increase in the percentage compensation of transmission Line 1 from 10% to 95%. Fig. 4.4 shows the loci of the eigenvalues of this study system as the compensation of Line 1 is varied in this way.

The loci of the individual eigenvalues of Fig. 4.4 are affected by different parts of the system in Fig. 4.1. Eigenvalues E2, E3 and E4 are related to the electrical transmission network (incorporating the SSSC, and generator stator circuits); in particular E2 represents the subsynchronous component of the generator air-gap flux; eigenvalues M0 to M5 represent the six torsional natural frequencies

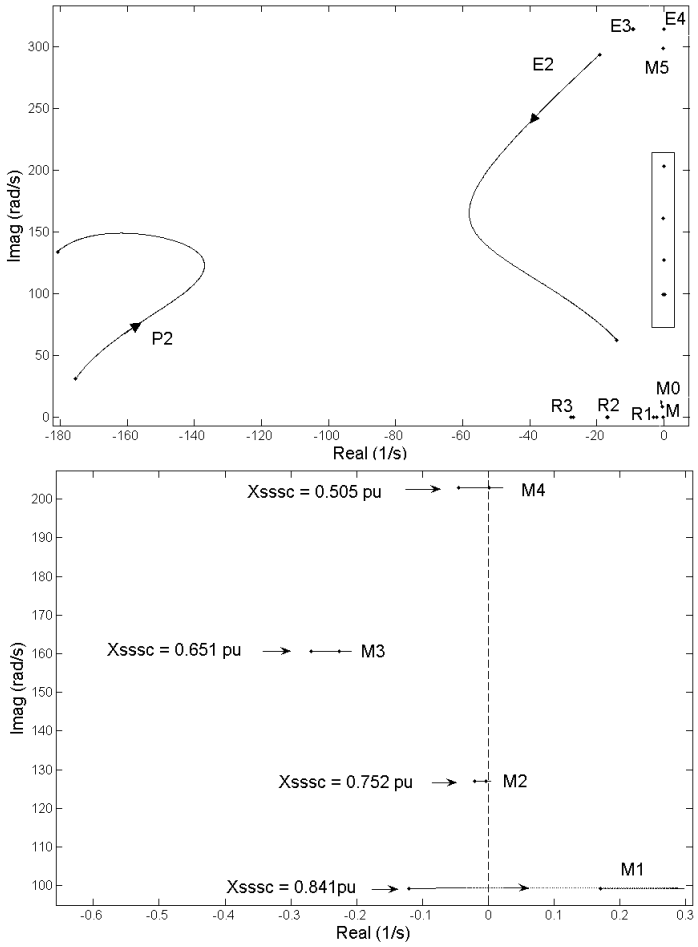

Fig. 4.4. Loci of eigenvalues of the study system as the series compensation X_{SSSC} in Line 1 is varied from 0.1 pu. to 0.95 pu.

of the turbine-generator's distributed–mass mechanical shaft; eigenvalue M is associated with the magnetic stability of the machine and it enters the right hand plane when the load angle of the generator exceeds 90 degrees; eigenvalues R1, R2 and R3 are associated with the rotor circuits of the machine.

The system of Fig. 4.4 has similar eigenvalues to a system compensated with conventional series capacitors, with the exception that eigenvalue E1 associated with the supersynchronous component of air-gap flux is replaced by the eigenvalue P2 associated with the feed-back regulator dynamics of the SSSC. Fig. 4.4 shows that, as is the case with conventional series capacitive compensation [26], the subsynchronous electrical frequency (eigenvalue E2) of the SSSC compensated system also decreases as the capacitive compensating reactance X_{SSSC} is increased.

Torsional interaction occurs when this subsynchronous electrical frequency approaches the natural frequencies of the turbine-generator's mechanical shaft system. Torsional interaction in this study system occurs in the small rectangular area of the eigenvalue plot which is enlarged in the bottom half of Fig. 4.4. It can be observed that as the subsynchronous frequency of the electrical system (E2) approaches each natural frequency of the mechanical system (M1 to M4), strong torsional interaction between the mechanical and electrical system occurs, forcing the eigenvalue associated with that torsional shaft mode towards the right hand plane. Fig. 4.4 shows that the destabilising effect of this torsional interaction is sufficient to cause the eigenvalues associated with modes 4, 2 and 1 of this study system to enter the right hand plane, with the exception of mode 3 which remains in the left plane at all the values of X_{SSSC}. Fig. 4.4 therefore indicates that as X_{SSSC} is increased, unstable mechanical oscillations in the turbine-generator shaft would be expected to occur in succession at the natural frequencies of modes 4, 2 and 1. The labels in Fig. 4.4 indicate the particular values of X_{SSSC} at which each torsional shaft mode reaches its most unstable condition. It should also be noted, again, that the eigenvalue study in Fig. 4.4 indicates the SSR characteristics of the reactance-controlled SSSC for a range of values of its compensating reactance without power flow control enabled around the SSSC. The following section considers the design of the power flow controller to be added around the X_{SSSC}-controlled SSSC.

4.4 Design of Reactance-Controlled SSSC-based Power Flow Controller

This section examines the design of the power flow controller to be added around the X_{SSSC}-controlled SSSC by using frequency domain linearised transfer function analysis. In particular, the study investigates the influence of the design of the gains of the power flow controller on the resonant characteristics of a transmission network compensated by the X_{SSSC}-controlled SSSC. The design of the gains K_P and K_I of the power flow controller to achieve specified response criteria is first carried out using a simplified model of the study system shown in Fig. 4.1 in which the generator is replaced by an ideal voltage source. The detailed SSR interaction studies are then carried out using the full system model once the range of power flow controller designs has been chosen. Each design of the power flow controller is carried out by adjusting its gains K_P and K_I to manipulate the positions of the first-order pole and zero in the transfer function $\Delta P_{L1} \,/\, \Delta P_{L1}^{*}(s)$ between the input and output of the controller in constant power mode (c.f. Fig. 3.2). The initial approach used to design the dynamic response characteristic of the power flow controller in this thesis follows the approach originally presented in [94], and can be summarised as follows. The proportional and integral gains K_P and K_I are adjusted together in order to meet two specifications:

(i) positioning the closed-loop pole in the transfer function $\Delta P_{L1} \,/\, \Delta P_{L1}^{*}(s)$ in the left-hand plane so as to meet the specific bandwidth (settling time) required in the dynamic response of the power flow controls; (ii) positioning the closed-loop zero in the same transfer function at -10s^{-1} in the left-hand plane, such that it always lies well to the left of the closed-loop pole, irrespective of what controller bandwidth has been chosen for study.

Fig. 4.5 shows the small-signal transfer function $\Delta P_{L1} \,/\, \Delta P_{L1}^{*}(s)$ of the power flow controller in the simplified model of the study system when the values of K_P and K_I are together adjusted to increase the power flow controller bandwidth from 0.13 rad/s to 1.82 rad/s. Fig. 4.5(a) shows the transfer function in the form of its pole and zero locations in the complex plane whilst Fig. 4.5(b) shows the transfer function in the form of its magnitude and phase as a function of frequency at four selected bandwidth designs. As expected, it can be observed that as the controller's bandwidth is increased, the real pole P0 associated with the closed-loop response of the controller moves further into the left-hand plane (Fig.4.5(a)). Fig. 4.5(a) also reveals that the design of the controller's bandwidth influences the resonant characteristics of the transmission network. As the response of the controller is made faster, the eigenvalue E2 associated with the resonant characteristics of the transmission network exhibits an increase in its frequency and it moves slightly closer to the right-hand plane. Fig. 4.5(b) also confirms that as the design of the controller is changed in order to

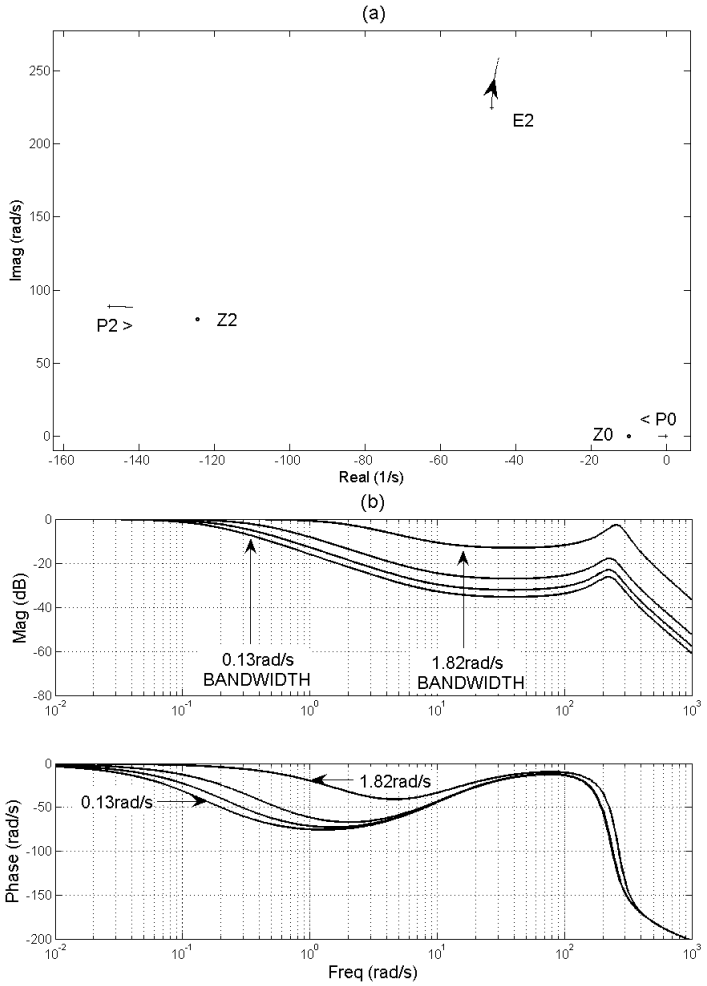

Fig. 4.5. Power flow controller transfer function $\Delta P_{L1}/\Delta P_{L1}^{*}(s)$with increasing controller bandwidth designs (sending end of the study system fed from ideal source).

increase its 0 to -3dB bandwidth, the underdamped resonant peak in the transfer function (associated with transmission line's resonant characteristics) increases slightly in frequency, but becomes significantly less damped. The above results demonstrate that when designing the power flow controller to achieve different controller bandwidths in this way (fixing the position of its transfer function zero, and moving the position of its pole) the choice of the controller bandwidth does in fact have an influence on the resonant characteristics of the transmission line, even at a single value of compensating reactance provided by the X_{SSSC}-controlled SSSC. The following section therefore investigates the influence of the bandwidth design of the power flow controller on the damping of the electromechanical modes.

4.5 Impact of Reactance-Controlled SSSC-based Power Flow Controller Design on the Damping of Electromechanical Modes

In order to investigate the influence of the power flow controller on the damping of the torsional modes of the study system of Fig. 4.1, the study in the previous section was repeated using the full mathematical model of the study system, that is with the transmission network now fed by a generator and multi-inertia turbine model at the sending end, and with the power flow controller enabled and set to operate in constant power mode.

Fig. 4.6 shows the loci of the eigenvalues of the study system as the gains K_P and K_I of the power flow controller are together adjusted to increase the power flow controller bandwidth from 0.13 rad/s to 1.82 rad/s. As expected, it can be observed that as the bandwidth of the power flow controller is increased, the real eigenvalue P0, corresponding to the closed-loop pole in the power flow controller transfer function, moves further into the left-hand plane. Fig. 4.6 also reveals that increasing the bandwidth of the power flow controller does influence the damping of the torsional modes of the study system. It can be observed that as the response time of the controller is made faster, the eigenvalues M1, M2, M3 and M4 associated with the torsional shaft modes, together with

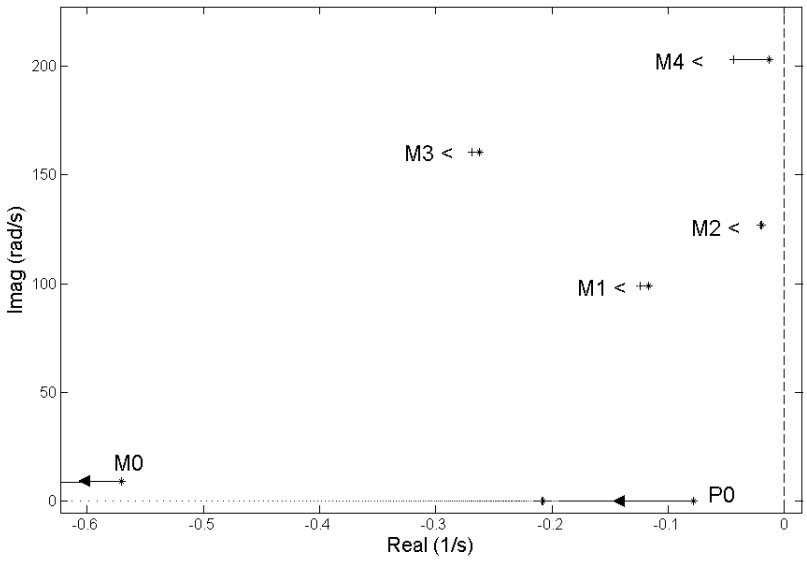

Fig. 4.6. Loci of the eigenvalues of the full study system as the power flow controller's bandwidth is varied from 0.13 rad/s to 1.82 rad/s with the controller set in constant power mode and X_{SSSC0} = 0.36 pu.

the eigenvalue M0 associated with the generator's inertial swing mode, all move to the left. The result in Fig. 4.6 thus shows that in the constant power mode of operation, the effect of the power flow controller is to increase the damping of the generator's inertial swing mode as well as the damping of its torsional modes; furthermore this positive influence on the electromechanical modes increases at increasing bandwidths of the controller.

The above eigenvalue analysis was then repeated with the power flow controller set to operate in constant angle mode, with the results shown in Fig. 4.7. As expected, the real eigenvalue P0 associated with the response of the closed-loop pole of the power flow controller moves towards the left as the controller's bandwidth is increased from 0.13 rad/s to 1.82 rad/s. Fig. 4.7 once again shows that in this mode of operation, the controller's bandwidth design also affects the damping of the electromechanical modes of the study system. However, it can be observed that while the eigenvalues M0 and M4 move towards the right, and hence closer to the imaginary axis, the eigenvalues M1, M2 and M3 move towards the left. The results thus show that in this mode of power flow controller operation, the influence of increased controller bandwidth is to decrease the damping associated with the generator's inertial swing mode as well as its torsional mode 4, whilst increasing the damping associated with torsional modes 1, 2 and 3, at least at this operating point.

The above studies on the impact of the power flow controller on torsional mode damping were carried out at a single operating point in the transmission system with the set-point value of the SSSC reactance X_{SSSC0} at 0.36 pu. in each case. In order to investigate the influence of the power flow controller on torsional mode damping at different operating points of the controller (and hence of the transmission line), the next section initially shows the SSR characteristics of the study system of Fig. 4.1 at different operating points of the controller by varying the set-point value of SSSC reactance X_{SSSC0} for a given mechanical input power to the generator of 0.5 pu.

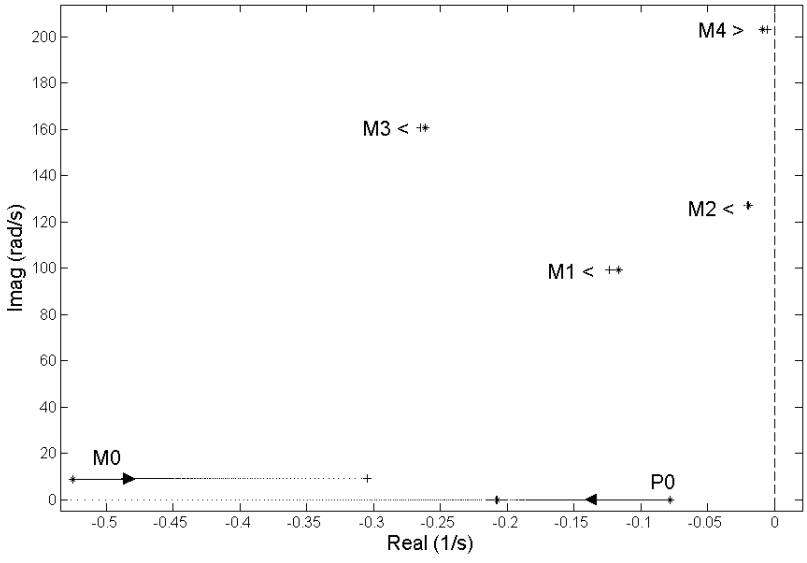

Fig. 4.7. Loci of the eigenvalues of the full study system as the power flow controller's bandwidth is varied from 0.13 rad/s to 1.82 rad/s with the controller set in constant angle mode and X_{SSSC0} = 0.36 pu.

4.6 SSR Characteristics of the Study System at different Operating Points of the Power Flow Controller

In order to investigate the SSR characteristics of the study system at different operating points of the power flow controller, Fig. 4.8 shows the loci of the eigenvalues of the study system as the SSSC's set-point value of compensation is increased from X_{SSSC0} = 0.36 pu. to X_{SSSC0} = 0.90 pu. with the power flow controller gains kept constant. Fig. 4.8 shows that the effect of increasing the set-point reactance of the SSSC when the power flow controller is enabled around it is similar to the effect seen when the SSSC reactance is increased with no power flow controls (c.f. Fig. 4.4): in both cases, the eigenvalue E2 associated with resonant frequency of the SSSC-compensated transmission network decreases as X_{SSSC0} increases, and in each case this results in successive torsional interaction with, and destabilisation of, the electromechanical modes M4 to M1. This comparison demonstrates that the presence of the electrical resonance in the transmission system has its origins in the characteristics of the SSSC compensating reactance itself (as also reported elsewhere in [18,19]). However, the studies shown in the previous two figures (Figs. 4.6 and 4.7) also now demonstrate that the addition of a power flow controller around the SSSC at a particular value of X_{SSSC0} influences the *characteristics* of this SSSC-created resonance, with both the mode of

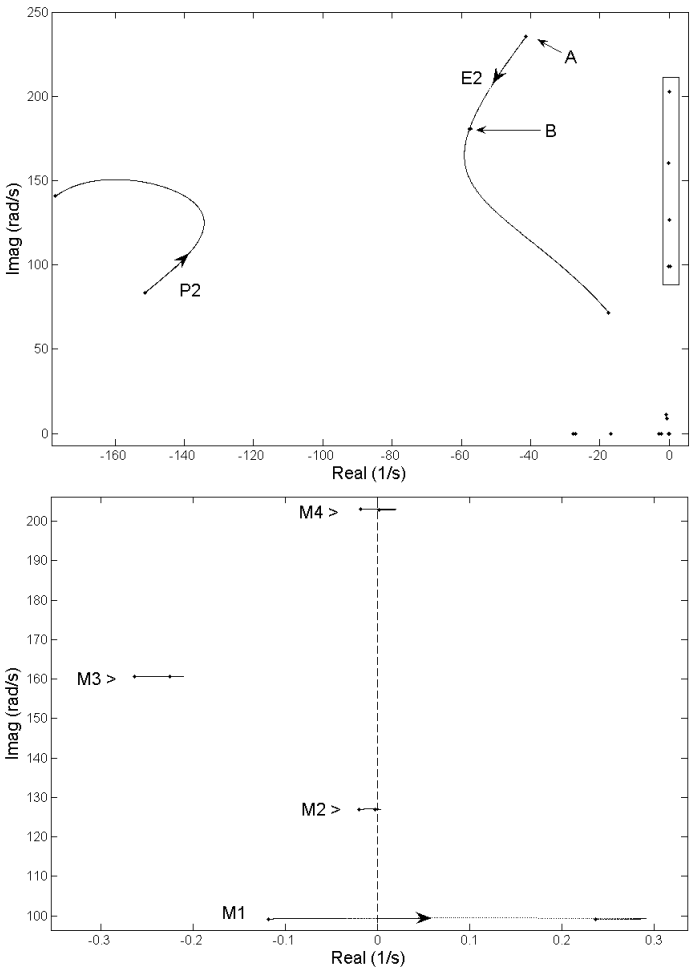

Fig. 4.8. Loci of the eigenvalues of the study system as the operating point of the power flow controller is varied by changing the set-point X_{SSSC0} from 0.36 pu to 0.90 pu.

operation of the controller, and its bandwidth, having important modifying effects. The following study therefore considers whether the influence of the power flow controller on these resonances is different at different set-point values of the SSSC.

4.7 Impact of Reactance-Controlled SSSC-based Power Flow Controller Design on the Damping of Electromechanical Modes at a different Operating Point of the Power Flow Controller

The studies shown in Figs. 4.6 and 4.7 have already considered the impact of varying the power flow controller bandwidth at one particular value of X_{SSSC0} , namely that corresponding to point A in Fig. 4.8. Each of these studies is now repeated at a different value of X_{SSSC0} = 0.5 pu., which corresponds to point B in Fig. 4.8, to investigate the impact of the power flow controller design on the damping of the electromechanical modes at a different operating point of the power flow controller. Fig. 4.9 shows the loci of the eigenvalues of the study system as the gains K_P and K_I of the power flow controller are together adjusted to increase the power flow controller bandwidth from 0.13 rad/s to 1.82 rad/s with the power flow controller set to operate in constant power mode with X_{SSSC0} now set to 0.5 pu. It can be observed that as the response of the power flow controller is made faster (as the real eigenvalue P0 is made to move towards the left) this causes the eigenvalues M1, M2, M3, M4 and M0 all to move to the left. The result shows that at this new value of X_{SSSC0}, the effect of a constant power mode power flow controller is once again to increase the damping of all the electromechanical modes as the bandwidth is increased, with the result that the torsional mode 4 actually becomes stable at a sufficiently high controller bandwidth.

In order to confirm the validity of the predictions obtained using the linearised system model and eigenvalue scans, the time-domain response of the system is now considered at two different values of controller bandwidth along the loci in Fig. 4.9. Fig. 4.10(a) shows the response of the system, determined using the full non-linear differential equation model, to a small increase in generator

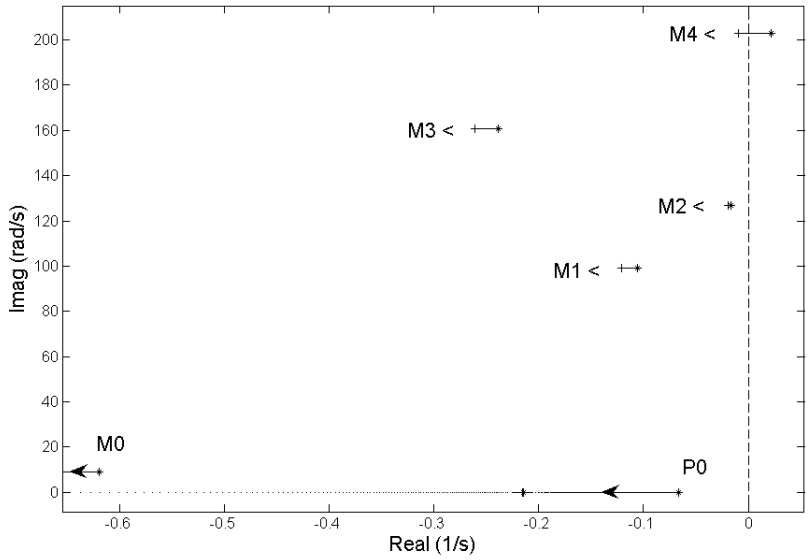

Fig. 4.9. Loci of the eigenvalues of the study system as the power flow controller's bandwidth is varied from 0.13 rad/s to 1.82 rad/s with the controller set in constant power mode and X_{SSSC0} = 0.5 pu.

dispatch when the power flow controller is in constant power mode at X_{SSSC0} = 0.5 pu. with a bandwidth of 0.13 rad/s. These conditions correspond to those at the start of the loci shown in Fig. 4.9, for which the eigenvalue locations predict that torsional mode 4 of the system is unstable and slightly negatively damped. The time-domain simulation results in Fig. 4.10(a) confirm this behaviour

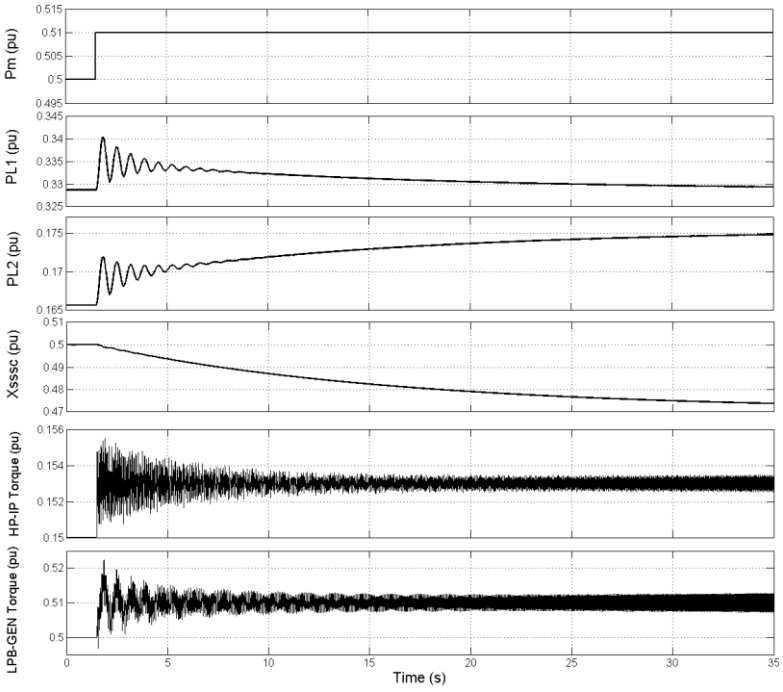

Fig. 4.10(a) Time-domain response of the system to an increase in generator dispatch in constant power mode with X_{SSSC0} = 0.5 pu. and a controller bandwidth of 0.13 rad/s.

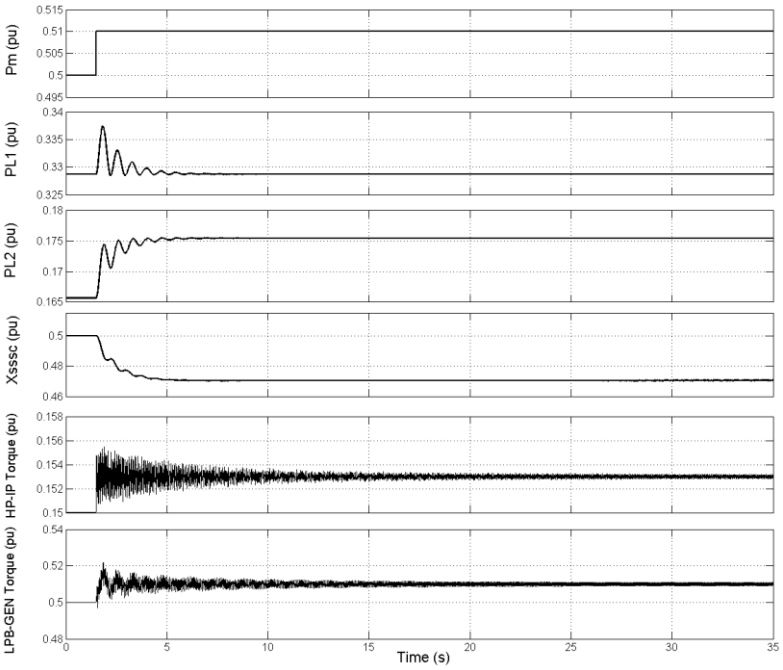

Fig. 4.10(b) Time-domain response of the system to an increase in generator dispatch in constant power mode with X_{SSSC0} = 0.5 pu. and a controller bandwidth of 1.82 rad/s.

predicted by the eigenvalues at the start of the loci in Fig. 4.9, with the post-disturbance HP-IP and LPB-GEN shaft section torques showing a slowly-increasing amplitude in the oscillations at the frequency of mode 4, after the oscillations of the lower-frequency and stable torsional modes have died away. The slow rate of increase in the amplitude of these mode 4 oscillations is consistent with the small positive value of the eigenvalue at the start of the mode 4 locus in Fig. 4.9.

Similarly, Fig. 4.10(b) shows the time-domain response of the system to the same disturbance with the power flow controller again in constant power mode at X_{SSSC0} = 0.5 pu, but with the controller bandwidth increased to 1.82 rad/s. These conditions correspond to those at the end of the loci shown in Fig. 4.9, for which the eigenvalue locations predict that torsional mode 4 of the system is stable and slightly positively damped. The time-domain simulation results in Fig. 4.10(b) confirm this behaviour predicted by the eigenvalues at the end of the loci in Fig. 4.9, with the post-disturbance HP-IP and LPB-GEN shaft section torques showing oscillations at the frequency of mode 4 that are now stable, decreasing slowly in amplitude with time. The noticeably shorter settling times in the active powers P_{L1} and P_{L2} in the transmission lines and the compensating reactance X_{SSSC} in response to the change in generator dispatch in Fig. 4.10 (b) also confirm the fast-acting nature of power flow controls at this increased bandwidth design.

The eigenvalue analysis considered in Fig. 4.9 was then repeated with the power flow controller now set to operate in the constant angle mode, with results shown in Fig. 4.11. As expected, the real eigenvalue P0 associated with the closed-loop pole of the power flow controller moves towards the left as the controller's bandwidth is increased. However, it can be observed that as the response time of the controller is made faster, the eigenvalues M0, M3 and M4 move towards the right, and hence closer to the imaginary axis, while the eigenvalues M1 and M2 move towards the left. The results thus show that in this mode of power flow controller operation, at this new value of X_{SSSC0} the influence of increased controller bandwidth is to decrease the damping associated with the

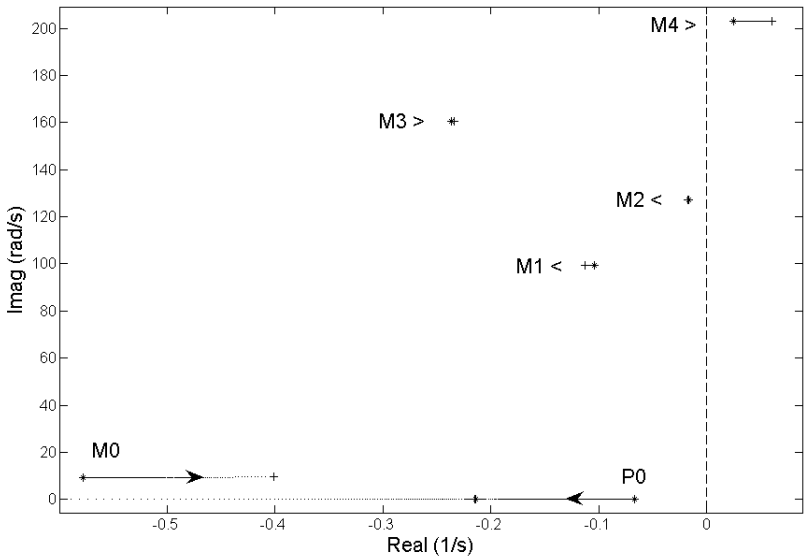

Fig. 4.11 Loci of the eigenvalues of the study system as the power flow controller's bandwidth is varied from 0.13 rad/s to 1.82 rad/s with the controller set in constant angle mode and X_{SSSC0} = 0.5 pu.

inertial swing mode as well as that of the torsional modes 4 and 3, while the damping associated with torsional modes 1 and 2 is increased.

Comparing the results in Fig. 4.11 with those in Fig. 4.7 shows that the influence of the power flow controller on the damping of particular torsional modes changes at different set-point values of X_{SSSC0} in the constant angle mode of operation. For example, the results in Fig. 4.7 show that at X_{SSSC0} = 0.36 pu., the influence of increased controller bandwidth has a beneficial impact on the damping of torsional mode 3 (M3); however Fig. 4.11 shows that at X_{SSSC0} = 0.5 pu., increasing the bandwidth is detrimental to the damping of mode 3.

The behaviour of the system in the constant angle mode of control predicted by the linearised eigenvalue scans can likewise be verified using time-domain simulations. Fig. 4.12(a) now shows the response of the system, determined using the full non-linear differential equation model, to a small increase in generator dispatch when the power flow controller is in constant angle mode at X_{SSSC0} = 0.5 pu. with a bandwidth of 0.13 rad/s. These conditions correspond to those at the start of the loci shown in Fig. 4.11, for which the eigenvalue locations predict that torsional mode 4 of the system is unstable and slightly negatively damped. The time-domain simulation results in Fig. 4.12(a) confirm this behaviour predicted by the eigenvalues at the start of the loci in Fig. 4.11, with the post-disturbance HP-IP and LPB-GEN shaft section torques showing a slowly-increasing amplitude in the oscillations at the frequency of mode 4, after the oscillations of the lower-frequency and stable torsional modes have died away. The slow rate of increase in the amplitude of these mode 4 oscillations is consistent with the small positive value of the eigenvalue at the start of the mode 4 locus in Fig. 4.11.

Similarly, Fig. 4.12(b) shows the time-domain response of the system to the same disturbance with the power flow controller again in constant angle mode at X_{SSSC0} = 0.5 pu, but with the controller bandwidth increased to 1.82 rad/s. These conditions correspond to those at the end of the loci shown in Fig. 4.11, for which the eigenvalue locations predict that torsional mode 4 of the system is even more unstable than at the lower-bandwidth controller design. The time-domain simulation results in Fig. 4.12(b) confirm this behaviour predicted by the eigenvalues at the end of the loci in Fig. 4.11, with the post-disturbance HP-IP and LPB-GEN shaft section torques exhibiting oscillations in the lower-frequency torsional modes that are stable, and negatively-damped oscillations at the higher-frequency mode 4 that grow more rapidly in amplitude with time than was the case with the lower-bandwidth controller design response in Fig. 4.12(a). (In particular, an analysis of the negatively-damped oscillations in the LPB-GEN shaft torque during the final 0.5 seconds of the plot shown in Fig. 4.12(b) in fact confirmed these to be at a frequency of 32.26 Hz: this corresponds closely to specific value of the damped natural frequency of mode 4 (32.3 Hz) predicted by the linearised eigenvalue study in Fig. 4.11, since the imaginary part of the eigenvalue at the end of the M4 locus in this figure was found to be 203.1 rads^{-1}, hence confirming the validity of the linearised model.)

4.8 Conclusion

Chapter Four has initially verified the correctness of the mathematical model of the power flow controller that has been implemented around the reactance-controlled SSSC in the study system in this thesis. The eigenvalue results of this chapter have shown that a closed-loop power flow

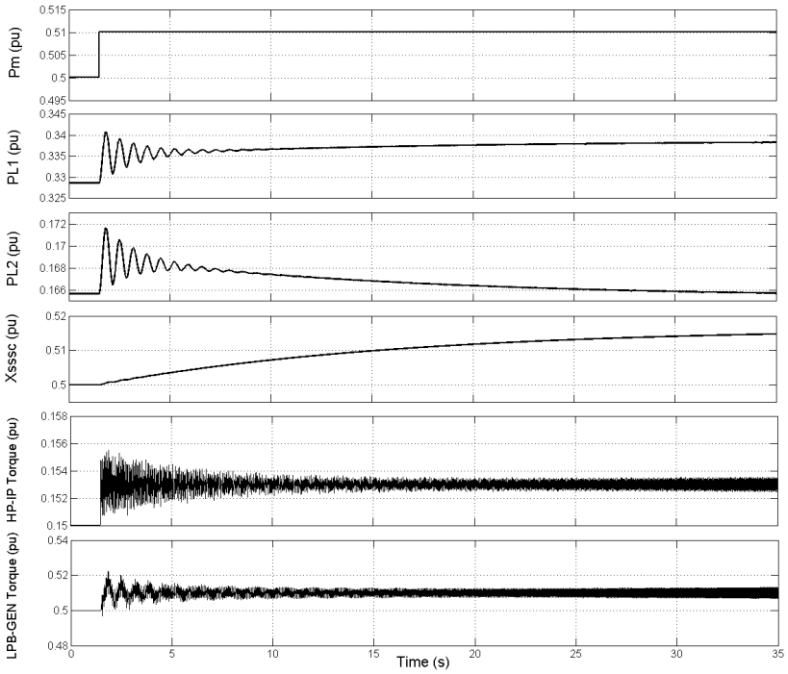

Fig. 4.12(a) Time-domain response of the system to an increase in generator dispatch in constant angle mode with X_{SSSC0} = 0.5 pu. and a controller bandwidth of 0.13 rad/s.

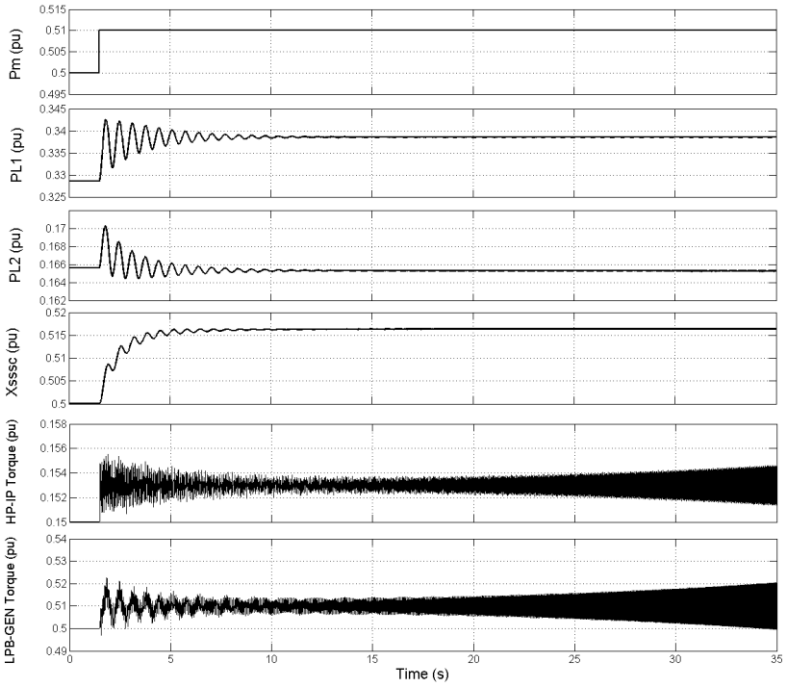

Fig. 4.12(b) Time-domain response of the system to an increase in generator dispatch in constant angle mode with X_{SSSC0} = 0.5 pu. and a controller bandwidth of 1.82 rad/s.

controller can affect the small-signal damping characteristics of the inertial swing modes of generators feeding a power system, and in particular that the nature and extent of these effects on the system's stability depend on both the mode in which the power flow controller is operated and its controller response time. The eigenvalue results in this chapter have therefore reinforced the findings previously reported in [17] which considered only the issue of generator inertial swing mode

characteristics and which relied solely on time-domain simulation results. However, based on the findings in [17,65,87,88] that were initially discussed in Chapter Two, a logical concern was raised as to whether a closed-loop power flow controller could also impact on the SSR stability of any generators with multi-inertia turbines that are susceptible to torsional interaction. Hence this chapter has presented the results of studies aimed at initially confirming whether one particular form of controllable series compensation, the reactance-controlled SSSC, as well as various forms of high-level system controls implemented around an X_{SSSC}-controlled SSSC, can influence the subsynchronous oscillations in neighbouring turbine-generators. In particular, this chapter has been able to show, using detailed mathematical models of the chosen study system, that the addition of a closed-loop power flow controller around an X_{SSSC}-controlled SSSC has a significant effect on the damping of generator torsional modes, and has shown how this effect on torsional mode damping is influenced by the speed at which the power flow controls are designed to respond and, importantly, by the mode of operation selected for the power flow controller.

In particular, the results have shown that in the constant power mode, a fast-responding power flow controller adds damping to both the generator inertial swing mode as well as to all of the turbine's torsional modes. Furthermore, it has been confirmed that this positive impact on torsional mode damping occurs over a range of different operating conditions, and not just at a single operating point; this is an important consideration because by its very nature a power flow controller is intended, in practice, to vary the degree of compensation provided by the X_{SSSC}-controlled SSSC over a range of values in response to the normal variations in transmission system loading levels. By contrast, in the constant angle mode, a fast-responding power flow controller design has been shown to significantly reduce the damping of the inertial swing mode. However, for this mode of operation, the influence of the power flow controls on torsional mode damping has been shown in this chapter to be operating point dependent: at certain operating points the influence of a fast-responding constant angle controller adds damping to a particular torsional mode, while it acts to reduce the damping of the same mode at other operating points.

Thus, not only have the results of these studies shown that a power flow controller influences the damping of shaft torsional modes but, importantly, as a result of these studies it can be concluded that when using X_{SSSC}-controlled SSSC-based power flow controllers in the presence of SSR-susceptible generators, it is clearly preferable to use such controls only in the constant power mode and not in the constant angle mode of control, so as to avoid destabilising either the inertial swing mode or any turbine shaft torsional modes. Furthermore, even though the studies have shown that the constant power mode of operation is preferable in SSR-susceptible systems because of its positive impact on torsional mode damping over a range of operating conditions, the results nevertheless show that careful SSR analysis is required when designing such controls so as to ensure torsional stability is maintained over the full range of compensation values envisaged for the particular torsional mode frequencies that are present in each particular system in which such schemes are to be deployed.

The designs of the reactance-controlled, SSSC-based power flow controller considered for study in this chapter (and thus far in this thesis) are relatively slow-responding when compared to the response times of power flow controllers reported in other work, such as [65,95]. Indeed, the results in [65,95] have shown that very fast-response power flow controllers not only can be achieved, but also have been seriously considered in the literature. Furthermore, the discussions reported in [65]

in particular also appear, at first glance, to suggest different conclusions to those that have been reached in this chapter regarding the influence of a constant power flow controller on the damping of the electromechanical modes. Specifically, it has been reported in [65] that a fast-responding constant power flow controller has a detrimental impact on the damping of both inertial and torsional modes, whereas with the initial design method considered in this chapter it has been observed that the constant power flow controller has a beneficial impact on the damping of both the inertial and torsional modes over a range of operating points.

The following chapter therefore presents an improved design of the control gains of the closed-loop AC power flow controller that enables much faster controller bandwidths to be realised (comparable to those considered in [65,95]). Once this improved design of the control gains of the power flow controller has been verified, the impact on torsional interaction of this improved reactance-controlled SSSC-based power flow controller is then investigated, in order to ascertain whether the conclusions reached in this chapter also hold true for much faster-responding controllers in light of the observations described in [65].

CHAPTER FIVE

AN IMPROVED SSSC-BASED POWER FLOW CONTROLLER DESIGN APPROACH AND ITS IMPACT ON TORSIONAL INTERACTION

5.1 Introduction

The previous chapter has shown that a closed-loop power flow controller can affect the SSR stability of generators with multi-inertia turbines that are susceptible to torsional interaction. In particular, it was shown in Chapter Four how the nature and extent of these effects on the damping of the electromechanical modes depend on both the mode in which the power flow controller is operated and its controller response times, even for relatively-slow responding controllers designed using the design approach proposed in [94]. In the constant power mode of operation, a faster-responding power flow controller adds damping to both the generator inertial swing mode as well as to all the torsional modes over a range of operating points. By contrast, in the constant angle mode, a faster-responding controller reduces the damping of the inertial swing mode. However, for this mode of operation, the influence of the power flow controller on torsional mode damping has been shown to be operating point dependent: at certain operating points the influence of a constant angle controller is to add damping to a particular torsional mode, while it acts to reduce the damping of the same mode at other operating points.

In Chapter Four, the designs of the reactance-controlled SSSC-based power flow controller considered for study are relatively slow-responding when compared to the response times of the power flow controllers reported in work such as [65,95]. This chapter now presents an improved approach to the design of the control gains of the closed-loop AC power flow controller, by using frequency-domain linearised transfer-function analysis, to enable a much faster controller bandwidth to be realised (comparable to those considered in [65,95]). The chapter then verifies this improved design approach for the control gains of the power flow controller by means of time domain simulation. Finally, the chapter examines the impact on torsional interaction of the resulting, significantly-faster, reactance-controlled SSSC-based power flow controller over a range of operating conditions.

5.2 An Improved Design of Reactance-Controlled SSSC-based Power Flow Controller

This section examines an improved approach to designing the power flow controller to be added around the X_{SSSC}-controlled SSSC using frequency domain linearised transfer function analysis. In particular, the study investigates the influence of this improved approach to designing the gains of the power flow controller on the resonant characteristics of a transmission network compensated by the X_{SSSC}-controlled SSSC. The design of the gains K_P and K_I of the power flow controller to achieve specified response criteria is again carried out using a simplified model of the study system shown in Fig. 4.1 in which the generator is replaced by an ideal voltage source. Then, detailed SSR interaction

studies are again carried out using the full system model once the range of power flow controller designs has been chosen. In the previous chapter, the approach adopted in designing the dynamic response characteristics of the power flow controller followed that originally presented in [94]: the controller gains K_P and K_I were adjusted together to set the position of the closed-loop pole in the transfer function $\Delta P_{L1} \,/\, \Delta P_{L1}^{*}(s)$ according to the specific bandwidth (settling time) required from the controller, whilst setting the position of the closed-loop zero in this transfer function at a fixed position −10 s^{-1} in the left hand plane, well to the left of the closed-loop pole for all bandwidths being considered. However, in the transfer functions obtained using this approach seen in the previous chapter (c.f. Fig. 4.5), it was found that if the controller's bandwidth was increased to a value above 1.82 rad/s, the magnitude of the underdamped resonant peak in the transfer function $\Delta P_{L1} \,/\, \Delta P_{L1}^{*}(s)$ increased above the 0 dB line, in effect forcing an upper limit of 1.82 rad/s on the controller's bandwidth when adopting this design approach.

Further investigations into this issue have shown that the position of the closed loop zero in the transfer function $\Delta P_{L1} \,/\, \Delta P_{L1}^{*}(s)$ also has a significant influence on the underdamped resonant peak in this transfer function when the controller's bandwidth is increased. In order, to examine the particular influence of the position of the closed loop zero in the power flow controller transfer function $\Delta P_{L1} \,/\, \Delta P_{L1}^{*}(s)$, the controller design studies in Fig. 4.5 were repeated, initially for the same range of desired controller bandwidths, but now fixing the location of the closed loop zero of the transfer function at a different position, significantly further to the left of the closed loop pole of the transfer function at −303 s^{-1} in the left-hand complex plane. The particular value (−303s^{-1}) chosen for the new location for the closed-loop zero was to ensure that it remains well to left of the closed-loop pole (by approximately an order of magnitude) for the entire range of higher controller bandwidths to be considered in subsequent parts of the chapter.

Fig. 5.1 shows the small-signal transfer function $\Delta P_{L1} \,/\, \Delta P_{L1}^{*}(s)$ of the simplified study system when the values of K_P and K_I are together adjusted to increase the power flow controller bandwidth from 0.13 rad/s to 1.82 rad/s with the closed loop zero of the transfer function now positioned at −303 s^{-1}. Fig. 5.1(a) shows the transfer function in the form of its pole and zero locations in the complex plane whilst Fig. 5.1(b) shows the transfer function in the form of its magnitude and phase as a function of frequency at four selected bandwidth designs.

By comparing the results in Fig. 5.1(a) to those in Fig. 4.5(a), it can be observed that the extent to which the design of the gains of the power flow controller influences the eigenvalue E2 (associated with the resonant characteristics of the transmission network) differs noticeably, even though the same controller bandwidth range has been considered in both cases. In Fig. 5.1(a), as the response of the controller is made faster, the eigenvalue E2 again moves slightly closer to the right-hand plane while also increasing in frequency: however, it can now be observed that the extent to which this change in the resonant characteristics occurs is markedly reduced when the zero of the power flow controller's transfer function is fixed at −303 s^{-1}. Hence, this alternative approach to designing the controller gains now potentially allows the use of a much larger range of controller bandwidths as compared to the initial design approach in which the controller's bandwidth had to be limited to 1.82 rad/s: at this particular bandwidth in the earlier Fig. 4.5, it can be observed that the magnitude of the resonant peak is already approaching 0 dB; by contrast, Fig. 5.1(b) shows that at a controller bandwidth of 1.82 rad/s, the magnitude of this resonant peak is now considerably reduced

(−29.2 dB) so that it should now only approach 0 dB for significantly larger power flow controller bandwidth values.

The results of Fig. 5.1 thus demonstrate that when designing the power flow controller at different bandwidths via this second approach (fixing the position of its transfer function zero much further into the left hand plane at −303 s^{-1}, and moving the position of its pole) the choice of the controller bandwidth still has an influence on the resonant characteristics of the transmission line, even at a single value of compensating reactance provided by the SSSC. However, the choice of the position of the zero in the power flow controller's transfer function influences the extent to which the change in the controller's bandwidth affects the resonant characteristics of the transmission line. By positioning the zero of the transfer function much further to the left along the real axis, the extent of the influence of controller bandwidth on the transmission line resonances is markedly reduced, thus allowing a much higher power flow controller bandwidth to be achieved.

In order to demonstrate the extent to which the bandwidth of the power flow controller can be made higher by using this improved approach to designing the power flow controller gains (fixing the position of its transfer function zero much further into the left hand plane at −303 s^{-1}, and

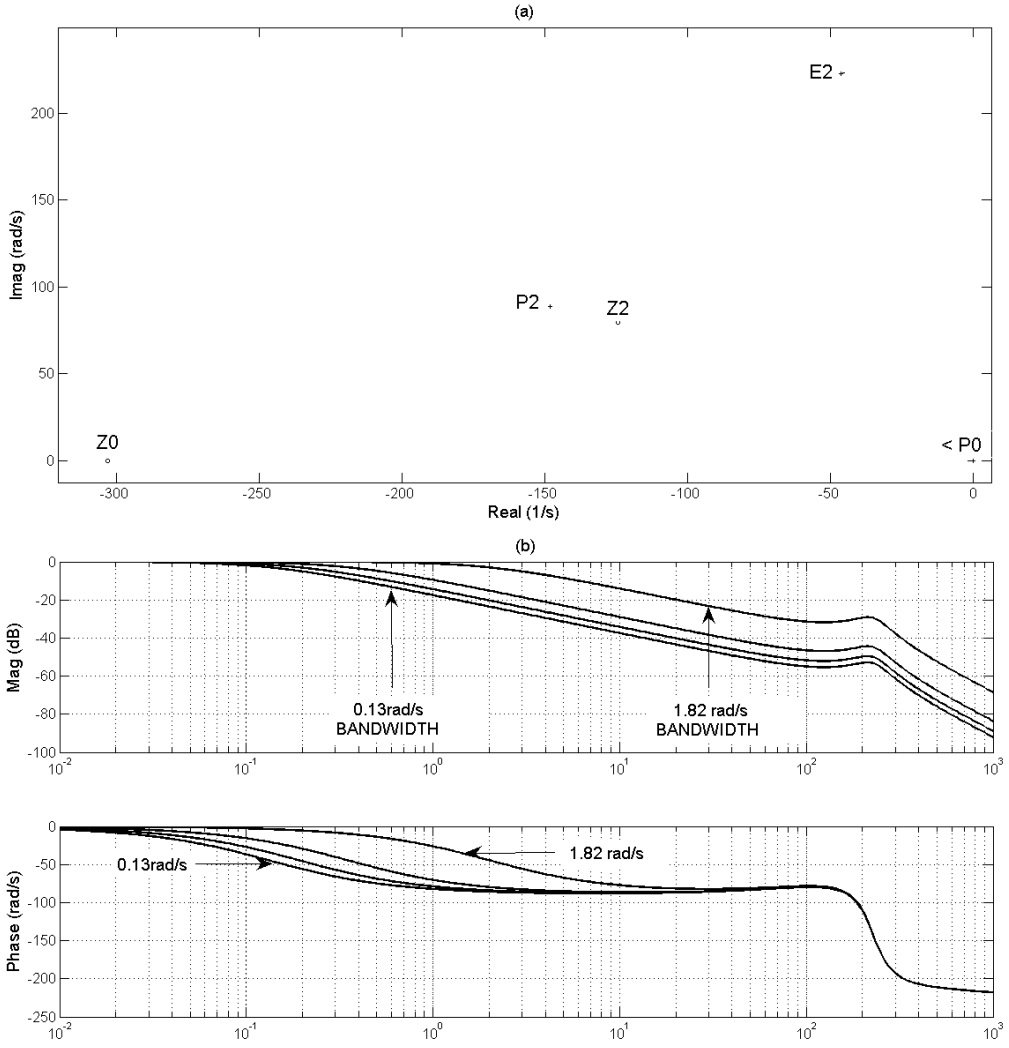

Fig. 5.1. Power flow controller transfer function ΔP_{L1} / $\Delta P_{L1}^{*}(s)$ with increasing controller bandwidth design with its zero fixed at −303 1/s (sending end of the study system fed from ideal source).

moving the position of its pole), the above controller design studies were repeated, but with the values of K_P and K_I now adjusted together so as to increase the power flow controller bandwidth from 0.13 rad/s up to 33.5 rad/s.

Fig. 5.2 shows the small-signal transfer function $\Delta P_{L1} \,/\, \Delta P_{L1}^{*}(s)$ of the simplified study system when the values of K_P and K_I are together adjusted to increase the power flow controller bandwidth from 0.13 rad/s to 33.5 rad/s with the closed loop zero of the transfer function positioned at −303 s^{-1}. Fig. 5.2(a) shows the transfer function in the form of its pole and zero locations in the complex plane whilst Fig. 5.2(b) shows the transfer function in the form of its magnitude and phase as a function of frequency at four selected bandwidth designs.

Fig. 5.2(a) reveals that the design of the controller's bandwidth influences the resonant characteristics of the transmission network to a larger extent in comparison to Fig. 5.1(a) now that a much larger range of controller bandwidths is being considered. As the response of the controller is

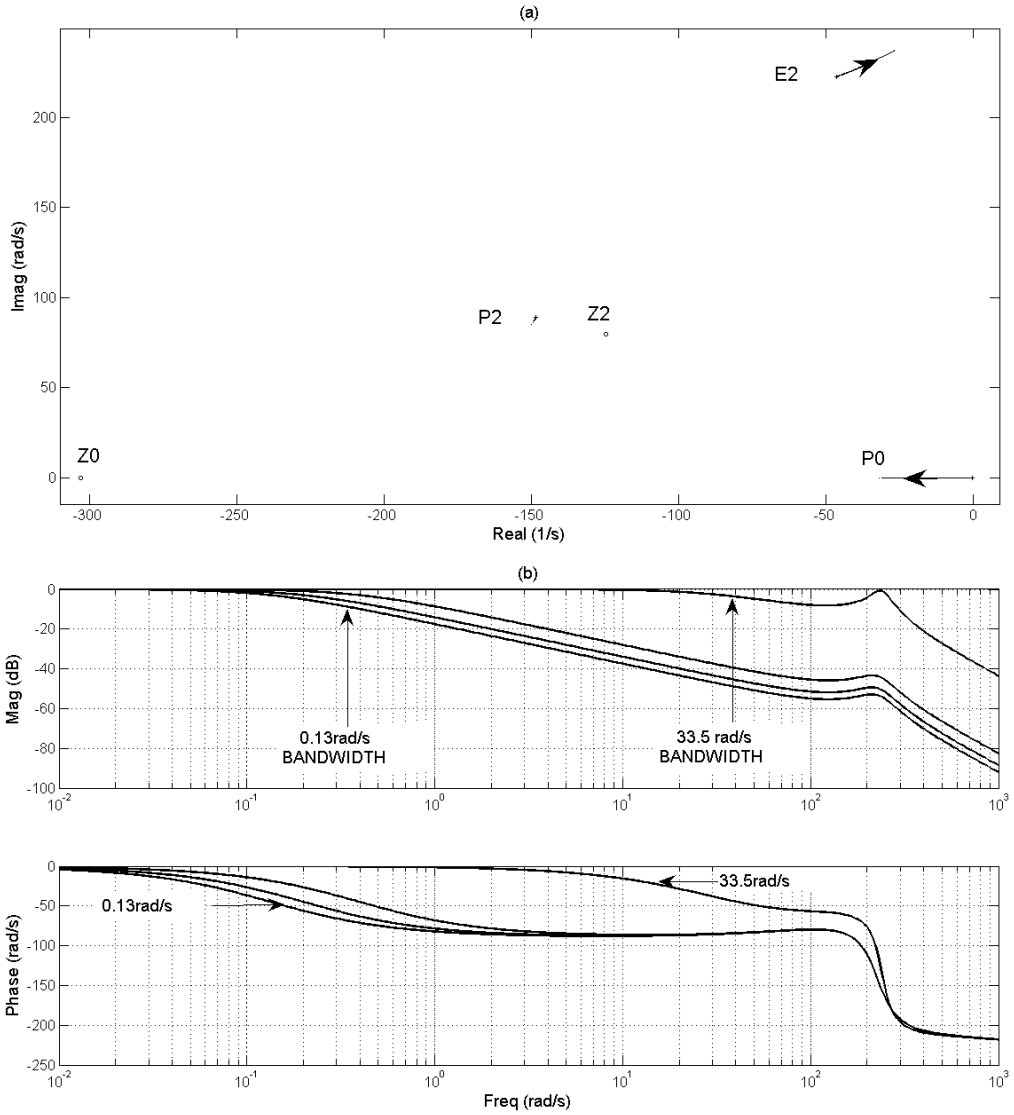

Fig. 5.2. Power flow controller transfer function $\Delta P_{L1} \,/\, \Delta P_{L1}^{*}(s)$ with increasing controller bandwidth design with its zero fixed at −303 1/s (sending end of the study system fed from ideal source).

made faster, the eigenvalue E2 associated with the resonant frequency of the transmission network moves closer to the right-hand plane while also increasing in frequency. However, the benefit of this alternative location of the power flow controller's zero is that it now allows the use of a much faster controller bandwidth of up to 33.5 rad/s as compared with the initial design approach shown in Fig. 4.5 (where the zero of the power flow controller's transfer function was fixed at −10 s^{-1} and the controller's bandwidth had to be limited to 1.82 rad/s). Fig. 5.1(b) has shown that at a controller bandwidth of 1.82 rad/s, the magnitude of the resonant peak is reduced considerably to −29.2 dB with this new design approach, and Fig. 5.2(b) shows that the magnitude of the resonant peak now approaches 0 dB only for the significantly larger controller bandwidth value of 33.5 rad/s. The results of Fig. 5.2 thus confirm that when designing the power flow controller at different bandwidths via this second approach (fixing the position of its transfer function zero much further into the left hand plane at −303 s^{-1}, and moving the position of its pole) the choice of the controller bandwidth still has an influence on the resonant characteristics of the transmission line, even at a single value of compensating reactance provided by the SSSC. The results of Fig. 5.2 also confirm that the choice of the position of the zero in the power flow controller's transfer function influences the extent to which the change in the controller's bandwidth affects the resonant characteristics of the transmission line. Hence, by positioning the zero of the transfer function much further to the left along the real axis, the extent of the influence of controller bandwidth on the transmission line resonances is markedly reduced, thus allowing a much faster power flow controller bandwidth to be achieved.

The results so far have shown how the power flow controller's design can be improved to achieve a relatively high controller bandwidth which is comparable to fast-responding power flow controllers with settling times of the order of 60 ms shown in [95] as well as within the range of power flow controller settling times reported in [65] (that is between 12 ms and 100ms). Prior to examining the impact of such fast-responding power flow controllers on the damping of the electromechanical modes of the study system, this improved approach to designing the power flow controller is first verified by means of time domain simulation studies.

5.3 Verification of the Improved Approach to the Design of the SSSC-based Power Flow Controller

The improved approach to the design of the gains of the power flow controller shown in the previous section was then verified by means of a time domain simulation study, still using the simplified version of the study system in Fig. 4.1 in which the synchronous machine is replaced by an ideal source. Fig. 5.3 shows the response of this simplified study system following a step increase of 0.1 pu in P_{L1}^{*}, the commanded value of power transfer in Line 1, with the gains K_P and K_I set to achieve a power flow controller bandwidth of 33.5 rad/s.

From an analysis of the time domain response in Fig. 5.3, it can be observed that following this step increase in P_{L1}^{*}, the power flow controller responds by adjusting the commanded value of the SSSC reactance X_{SSSC} to a new steady state value within 80 ms; this increase in the SSSC reactance X_{SSSC} increases the actual real power flow P_{L1} in Line 1 to the desired value of P_{L1}^{*} again within 80 ms. Fig. 5.3 therefore confirms that the improved method of designing the power flow controller has allowed the value of the real power transmitted by Line 1 to be adjusted to track a set point change within 4 AC cycles, and such a fast-responding controller is comparable to the speed of response of the power flow controllers reported in [65,95].

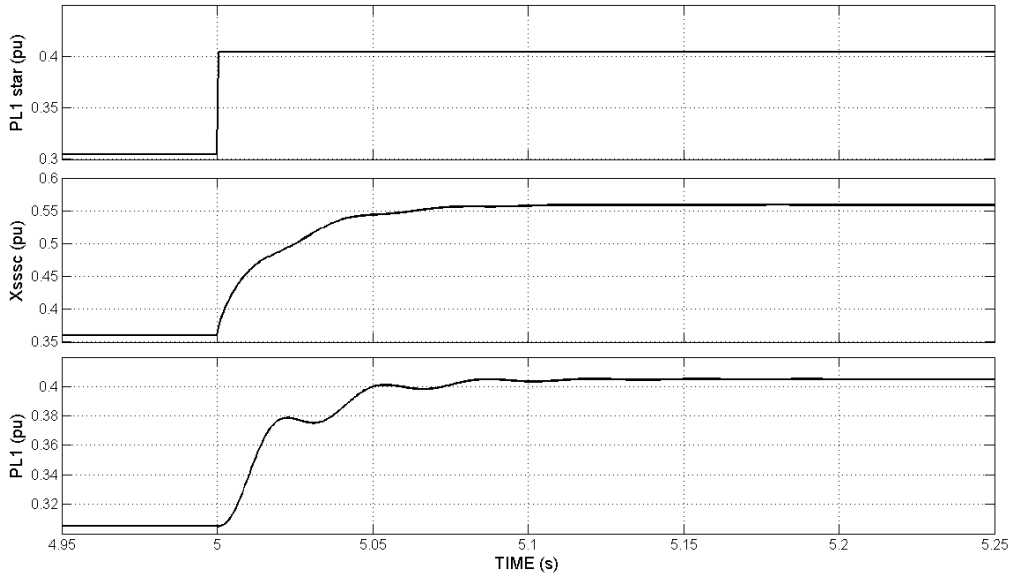

Fig. 5.3. Time domain response of the power flow controller to a step in P_{L1}^{*} for controller bandwidth design of 33.5 rad/s; study system with sending end fed from an ideal source.

5.4 Impact of Improved SSSC-based Power Flow Controller Design on Damping of the Electromechanical Modes

The previous chapter considered the impact on torsional interaction of relatively slow responding X_{SSSC}-controlled SSSC-based power flow controllers with bandwidths in the range between 0.13 rad/s and 1.82 rad/s. In the constant power mode of operation, it was shown (Fig. 4.6) that with the initial design approach for the power flow controller (closed-loop zero of the transfer function $\Delta P_{L1} \,/\, \Delta P_{L1}^{*}(s)$ fixed at $-10s^{-1}$) the effect of the power flow controller is to increase the damping of the generator's inertial swing mode as well as the damping of its torsional modes; furthermore this positive influence on the electromechanical modes increases at increasing bandwidths of the controller. By contrast, in the constant angle mode of operation, it was shown (Fig. 4.7) that with the initial design approach for the power flow controller the influence of increased controller bandwidth is to decrease the damping associated with the generator's inertial swing mode as well as its torsional mode 4, whilst increasing the damping associated with torsional modes 1, 2 and 3. In order to investigate the influence of the improved power flow controller design approach on the damping of the torsional modes of the study system of Fig. 4.1, as well as to be able to assess the findings of this work more fully against the observations described in [65], the studies in Figs. 4.6 and 4.7 were repeated with the power flow controller gains determined using the improved design approach shown in Fig. 5.2, thus allowing much higher controller bandwidths to be achieved.

Fig. 5.4 now shows the loci of the eigenvalues of the full study system model as the gains K_P and K_I of the power flow controller are together adjusted to increase the power flow controller bandwidth from 0.13 rad/s to 33.5 rad/s. As expected, it can be observed that as the bandwidth of the power flow controller is increased, the real eigenvalue P0, corresponding to the closed-loop pole in the power flow controller transfer function, moves further into the left-hand plane. Fig. 5.4 also reveals that increasing the bandwidth of the power flow controller does influence the damping of the

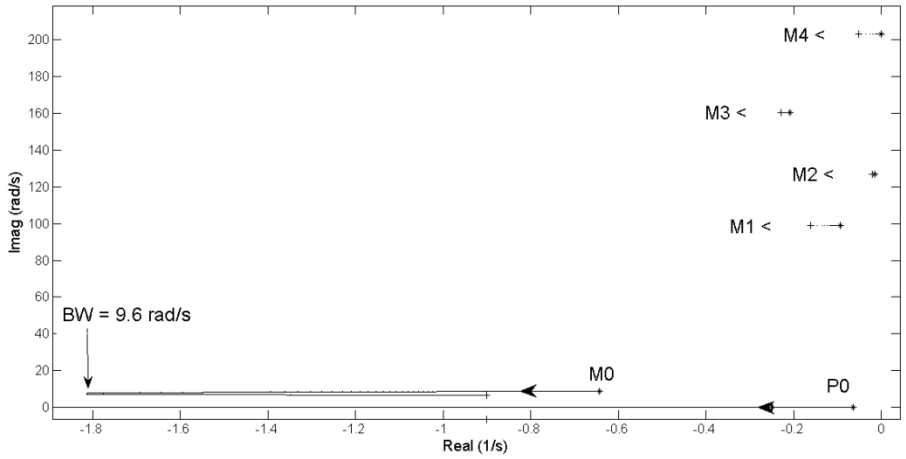

Fig. 5.4 Loci of the eigenvalues of the full study system as the power flow controller's bandwidth is varied from 0.13 rad/s to 33.5 rad/s with the controller set in constant power mode (improved design approach).

torsional modes of the study system. It can be observed that as the response time of the controller is made faster (up to a controller bandwidth of 9.6 rad/s), the eigenvalues M1, M2, M3 and M4 associated with the torsional shaft modes, together with the eigenvalue M0 associated with the generator's inertial swing mode, all move to the left. However, when the controller's bandwidth is increased beyond 9.6 rad/s, all the torsional mode eigenvalues M1, M2, M3 and M4 continue to move towards the left but the inertial mode eigenvalue M0 starts to move back towards the right-hand plane. The result in Fig. 5.4 thus shows that in the constant power mode of operation, the effect of the power flow controller designed in this manner is to increase the damping of the inertial swing mode as well as the damping of all of the torsional modes; furthermore this positive influence on the electromechanical modes increases at increasing bandwidths of the controller up to 9.6 rad/s. However, at bandwidths above 9.6 rad/s, there is still a net positive influence on the damping of all of the torsional modes, but there is less damping added to the inertial mode by the action of the power flow controller than is the case at lower controller bandwidths. It should be also pointed out that due to the much larger range of controller bandwidths considered in Fig. 5.4, as compared to the range considered in the study in Fig. 4.6, the extent of the movement of all eigenvalues is much larger in Fig. 5.4. For example, the movement of the eigenvalue M1 in Fig. 4.6 caused the real part of the eigenvalue M1 to change by 0.007 s^{-1} whereas the movement of the same eigenvalue M1 in Fig 5.4 causes the real part of the eigenvalue to change by 0.067 s^{-1}. Hence, this improved approach to designing the power flow controller also allows significant improvement in the stabilisation of all the generator torsional and inertial modes.

As discussed in the previous chapter, the findings of the work by others [65] have shown that very fast-responding closed-loop AC power flow controls implemented around another form of FACTS series compensation, namely the TCSC, in the constant power mode of operation have a detrimental impact on the damping of the inertial swing mode and the torsional mode 3 of their studied system. By contrast, in Chapter Four of this thesis, which considered the impact of a relatively slow-responding power flow controller in which the controller gains were designed using the initial design approach, it was shown that as the controller's bandwidth is increased in constant power mode both the inertial mode damping as well as the damping of all torsional modes of this study system were improved. In light of the results now shown in Fig. 5.4, in which a wider range of controller

bandwidths has been considered, the apparent disagreement between the findings in Chapter Four and the observations described in [65] can be better understood and explained. When, in the studies in Chapter Four, the controller bandwidth was restricted to low values and varied over a narrow range between 0.13 rad/s and 9.6 rad/s, it could be clearly observed that the impact of increased bandwidth in a constant power flow controller is to increase the damping of both the inertial swing mode as well as that of all the torsional modes. However, when the range of controller bandwidths considered is much larger, between 9.6 rad/s and 33.5 rad/s as in this chapter, increasing the bandwidth of a constant power flow controller is still seen to increase the damping of all the *torsional modes* of this system over the full range of bandwidths considered, but in the case of the system's inertial swing mode, above a certain bandwidth, any *further* increase in bandwidth is then indeed seen to decrease the damping of that mode as reported in [65]. Thus, the findings of a study such as that in [65], which only considered very high values of power flow controller bandwidth, are in fact consistent with the findings of the work in this thesis with respect to high values of controller bandwidth. However, the results of this work have allowed a fuller understanding of the impact of the controller bandwidth on inertial mode damping over a wider range of possible bandwidths so that the possible stabilising benefit of the constant power type of controller at more modest bandwidths can also be revealed.

It was also reported in [65] that fast-responding constant power flow controllers are detrimental to the damping of torsional mode 3 of their study system, whereas the results in Fig. 5.4 have shown that in this study the constant power flow controller is still adding damping to all the torsional modes even at the highest values of bandwidth considered in the study range. Although the findings by the authors of [65] may appear to be different with regards to the damping of torsional mode 3 in their study system, there are other factors that can affect the way in which the power flow controller interacts with the damping of this particular torsional mode. Firstly, the FACTS device used in [65] is a TCSC and it has very different SSR characteristics compared to the SSSC which is the FACTS device considered in the analysis of this thesis. Secondly, the range of controller settling times considered in [65] translates into a much higher upper limit of controller bandwidth when compared to the upper limit of the controller bandwidth range considered in this chapter, which is limited to 33.5 rad/s. Lastly, it can be observed that the study system in [65] although based on the IEEE FBM, does not have an additional line in the transmission network in parallel with the line whose power flow is being controlled. The second line was introduced as a modification to the IEEE FBM in this thesis specifically to allow constant angle power flow controllers to be studied, but the presence of an additional line in parallel could conceivably affect the torsional interaction between a constant power flow controller and the turbine generator. Any of the above factors could possibly contribute to this different observation described in [65] with regards to the influence of a constant power controller's design on the damping of torsional mode 3 in the IEEE FBM, and these factors could be considered for future study.

The analysis of the effect of the improved power flow controller design approach on torsional interaction was then repeated with the controller set to operate in constant angle mode, with the results shown in Fig. 5.5. As expected, the real eigenvalue P0 associated with the response of the closed-loop pole of the power flow controller moves towards the left as the controller's bandwidth is increased from 0.13 rad/s to 33.5 rad/s. Fig. 5.5 shows that in this mode of operation, the controller's bandwidth design once again affects the damping of the electromechanical modes of the study system. However, it can be observed that the eigenvalues M1, M2, M3 and M4, together with

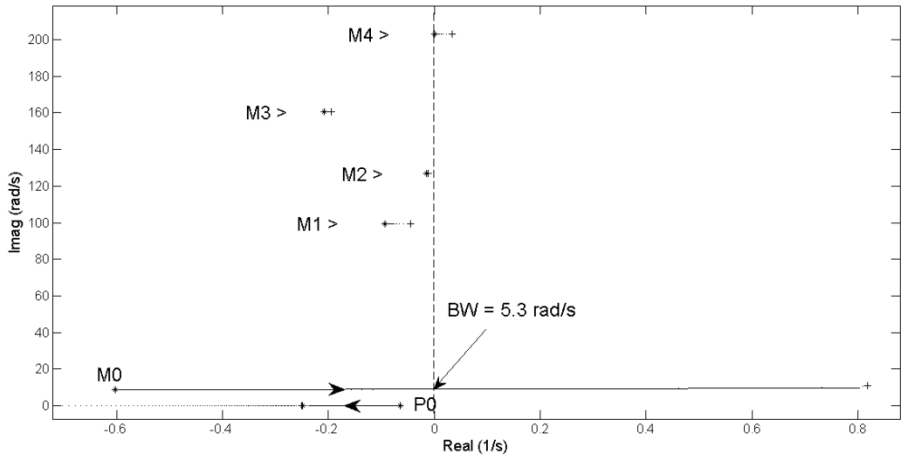

Fig. 5.5 Loci of the eigenvalues of the full study system as the power flow controller's bandwidth is varied from 0.13 rad/s to 33.5 rad/s with the controller set in constant angle mode (improved design).

the eigenvalue M0, all move towards the right, and hence closer to the imaginary axis. The results thus show that in this mode of power flow controller operation, the influence of increased controller bandwidth is to decrease the damping associated with both torsional and inertial modes. Furthermore, at controller bandwidths higher than 5.3 rad/s, both the inertial mode M0 and the torsional mode M4 are unstable.

The results in Figs. 5.4 and 5.5 show that although the design of the power flow controller's bandwidth can be made very fast, the mode of operation chosen for the power flow controller does impose some limitations on its controller bandwidth design. At this particular operating point of the power flow controller, it was observed that in the constant power mode of operation, for bandwidths above 9.6 rad/s, there is less damping added to the inertial mode than is the case for lower bandwidth designs, although the net impact of the power flow controller on damping remained positive at all bandwidths considered. The results thus show that if the aim is to optimise the damping of all the electromechanical modes, a bandwidth of 9.6 rad/s will be the best design of the controller for the constant power mode. However, if the aim is to achieve the fastest possible power flow controller response, a bandwidth of 33.5 rad/s can be used since all the electromechanical modes are still stable at this highest controller bandwidth. In the case of the constant angle mode of operation, it is not even possible to operate the power flow controller at bandwidths above 5.3 rad/s as some of the electromechanical modes become unstable. The results thus show that if the aim is to optimise the damping of all the modes, this mode of operation is not recommended at all since there is a detrimental impact on the damping of all the generator's electromechanical modes. The results also show that if the aim is to achieve the fastest power flow controller response, this mode of operation is also not recommended since a maximum bandwidth of 5.3 rad/s can be used.

The results presented in Chapter Four, and thus far in this chapter, have examined the influence of the power flow controller on torsional mode damping for the simplest case in which the only form of series compensation present in the system is the SSSC itself. Restricting the study, at first, to only series compensation by an SSSC, and examining the SSR characteristics of the system with and without power flow controllers of various designs was necessary to understand how the power flow

controller, its design, and mode of operation each influence the SSR characteristics of the SSSC in isolation from other complicating factors. Now that such fundamental studies have been conducted, the knowledge and understanding gained from this simplest case of having the SSSC as the only series compensator in the system can be extended to investigate further practical issues associated with SSR in actively-controlled compensators, specifically the issue of how the SSSC and its power flow controls interact with, and are affected by, other compensators in the transmission system that give rise to torsional interaction due to their own resonant characteristics.

In practice, in a real-world transmission system, due to the still relatively high cost of FACTS series compensators, most transmission lines would still employ conventional series compensating capacitors with only a few key lines likely to include FACTS series compensators such as the SSSC for specific applications such as line power scheduling (the focus of this thesis) or for other stability improvement issues. Hence, in a practical transmission network, it is likely to be the case that one line in the system incorporates an SSSC while an adjacent line might include a conventional series capacitor. As discussed in Chapter Two, the SSSC can be specifically designed to damp SSR caused by itself or by other conventional series capacitors in the same line by employing supplementary control around this form of controllable series compensation [78-86]. However, although the issue of having two potential sources of SSR in the same line (an SSSC combined with a fixed series capacitor) has received a lot of attention in the literature, the case of having an SSSC in one transmission line while an adjacent line incorporates a conventional series capacitor, that is, the issue of having potential sources of SSR in each of two adjacent lines, is also an important practical case to be investigated. Hence, the following sections of this chapter consider the influence of adding conventional capacitive series compensation in Line 2 as shown in Fig. 5.6.

5.5 SSR Characteristics of the Study System with Line 2 Compensated

The following eigenvalue studies aim to investigate the impact of the improved approach to designing the X_{SSSC}-controlled SSSC-based power flow controller on the damping of the electromechanical modes of the study system in the presence of conventional series capacitors in Line 2. However, in order to consider such a study, it is first necessary to identify a combination of values of X_{SSSC}-controlled SSSC-based compensation in Line 1 and conventional compensation in Line 2 for which the system is SSR-stable prior to the addition of the power flow controller in Line 1. In order to identify ranges of series compensation values over which all the electromechanical modes in a study system are stable, it is more useful to present the results of the eigenvalue scans in an alternative format in which the real parts of the eigenvalue loci are plotted as a function of the compensation value being varied; this format is adopted for the remainder of the eigenvalue results in this section of the chapter.

5.5.1 Locating SSR-stable Ranges of Line 2 Compensation

In order to identify SSR-stable ranges of the series compensation in Line 2, the following study initially considers the SSR characteristics of the study system of Fig. 5.6 at different values of conventional series compensating reactance in Line 2, while the series compensation provided by the X_{SSSC}-controlled SSSC in Line 1 is held fixed at X_{SSSC} = 0.1 pu., without the power flow controller enabled. The value of the conventional series compensating reactance in Line 2 is varied from X_{C2} = 0.10 pu. to X_{C2} = 0.95 pu. corresponding to an increase in the percentage compensation of

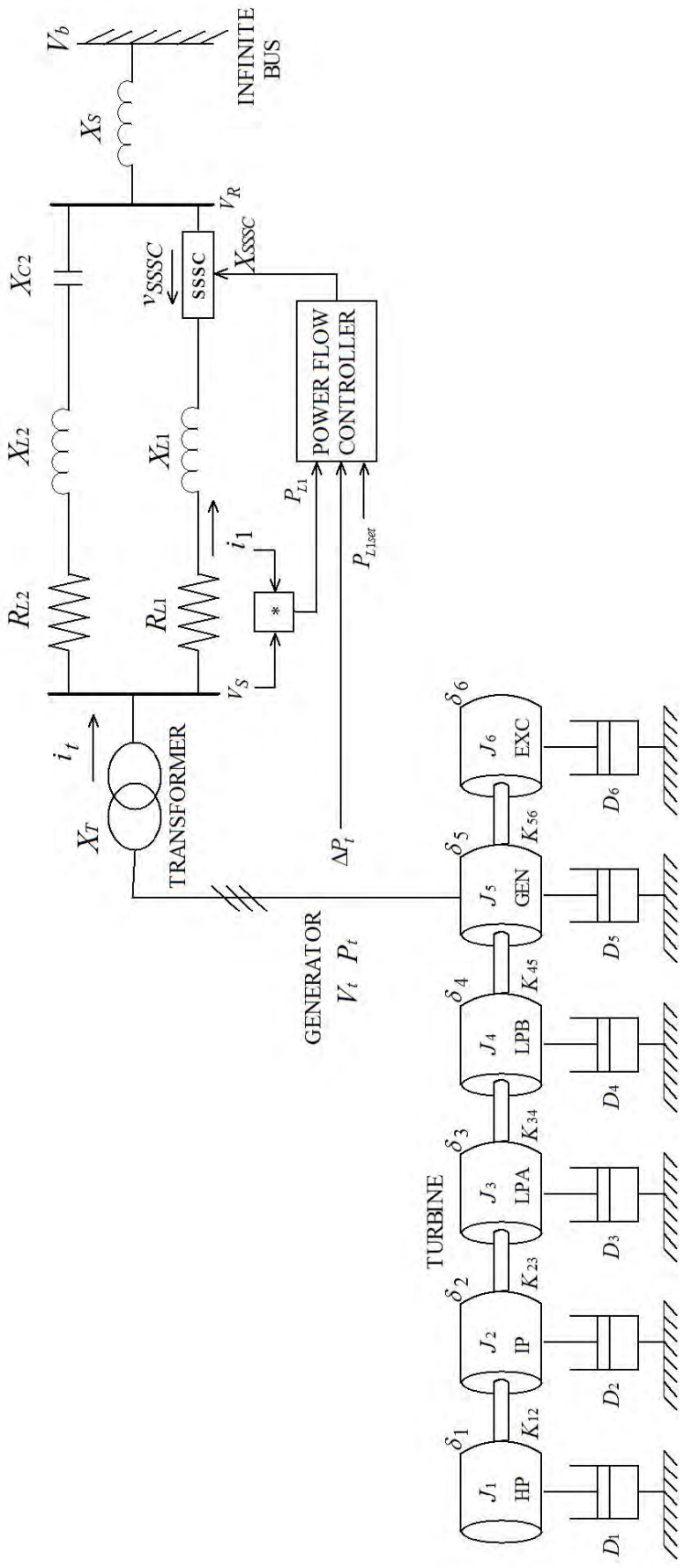

Fig. 5.6 Single line diagram of the study system with conventional series compensation in Line 2

transmission Line 2 from 10% to 95%. Fig. 5.7 shows the real parts of the eigenvalues associated with the torsional modes of this study system at each value of X_{C2} as the compensation in Line 2 is varied in this way.

It can be observed that as the conventional series compensation in Line 2 is increased, there is successive destabilisation of the mechanical torsional modes M4, M3, M2 and M1 as the real parts of the eigenvalues associated with each of these torsional modes move into the positive plane of Fig. 5.7. It can be observed that there are certain ranges of series capacitive compensation in Line 2 where the real parts of all the torsional mode eigenvalues M1, M2, M3 and M4 are in the negative plane of Fig. 5.7 (that is all four torsional modes are simultaneously SSR-stable). Within these stable ranges, two specific values of series compensating reactance were chosen for further study in the remaining eigenvalue scans, case A: X_{C2} = 0.23 pu. and case B: X_{C2} = 0.36 pu. At each of these values of conventional series compensation in Line 2, the SSR characteristics of the X_{SSSC}-controlled SSSC compensation in Line 1 were then considered for a range of its compensation values.

5.5.2 Locating an SSR-stable Operating Point for the X_{SSSC}-controlled SSSC in Line 1 in the presence of Conventional Series Capacitors for the two Selected Cases in adjacent Line 2

In order to identify the SSR-stable operating ranges of the SSSC in Line 1 for each of the above two values of series capacitive compensative compensation in Line 2, the eigenvalues of the study system were calculated as the series compensation X_{SSSC} provided by the X_{SSSC}-controlled SSSC is varied from 0.1 pu. to 0.95 pu, without power flow control enabled around the SSSC, with the series compensation X_{C2} in Line 2 fixed, in turn, at each of the values chosen in case A and case B. Fig. 5.8 shows the real parts of the eigenvalues associated with the torsional modes of this study system as the series compensation X_{SSSC} in Line 1 is varied in this way with the compensation in Line 2 fixed at the value for case A: X_{C2} = 0.23 pu. It can be observed that as the series compensation provided by the X_{SSSC}-controlled SSSC in Line 1 is increased there is successive destabilisation of the mechanical torsional modes M4 and M1 as the real parts of the eigenvalues associated with these two torsional modes move into the positive plane of Fig. 5.8. Fig. 5.8 shows that the SSR-stable operating range of

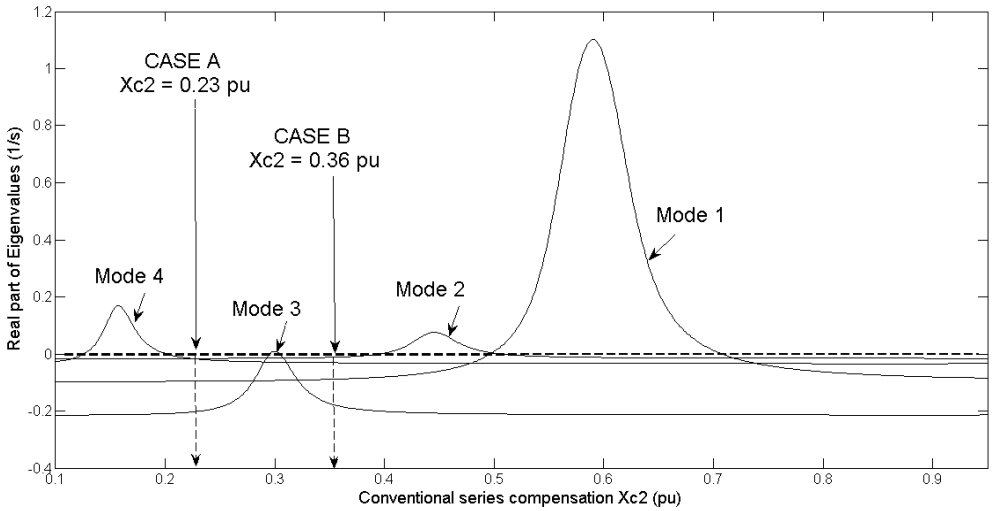

Fig. 5.7 Real parts of the eigenvalues of the study system as the conventional series compensation X_{C2} is varied from 0.1 pu. to 0.95 pu. with X_{SSSC} in Line 1 fixed at 0.1 pu.

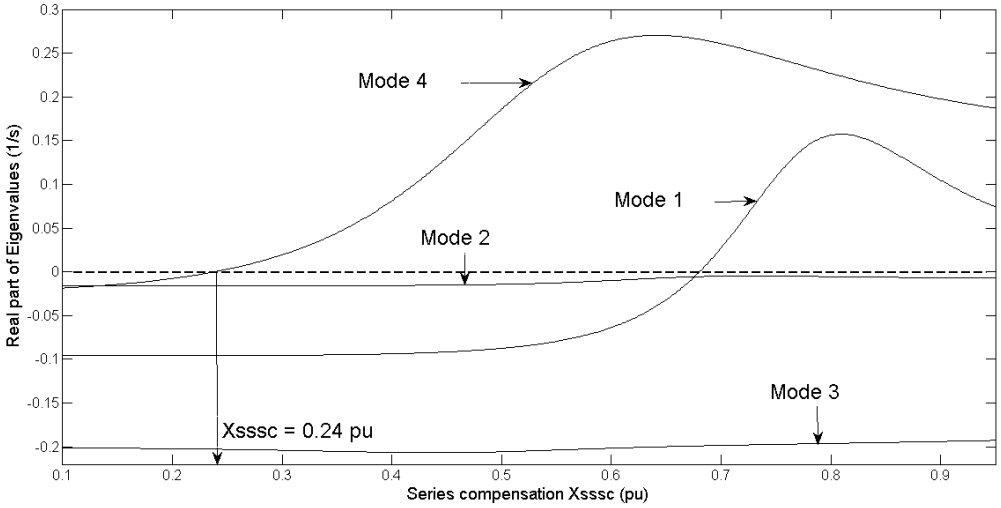

Fig. 5.8 Real parts of the eigenvalues of the study system as the series compensation provided by the SSSC, (X_{SSSC} in Line 1) is varied from 0.1 pu. to 0.95 pu. while the series capacitive reactance X_{C2} in Line 2 is fixed at 0.23 pu. (case A)

series compensation in Line 1 is from X_{SSSC} = 0.1 pu. to a maximum value of X_{SSSC} = 0.24 pu. for the case A value of conventional compensation in Line 2, since at all values of X_{SSSC} above 0.24 pu, torsional mode M4 remains unstable.

Fig. 5.9 shows the real parts of the eigenvalues associated with the torsional modes of this study system as the series compensation X_{SSSC} of Line 1 is again varied from 0.1 pu to 0.95 pu. with the series compensation X_{C2} in Line 2 fixed at the value for case B: X_{C2} = 0.36 pu. It can be observed that as the series compensation provided by the X_{SSSC}-controlled SSSC in Line 1 is increased there is successive destabilisation of the torsional modes M4, M1 and M3 as the real parts of the eigenvalues associated with these torsional modes move into the positive plane of Fig. 5.9. Fig. 5.9 shows that the SSR-stable operating range of series compensation of the X_{SSSC}-controlled SSSC in Line 1 for the

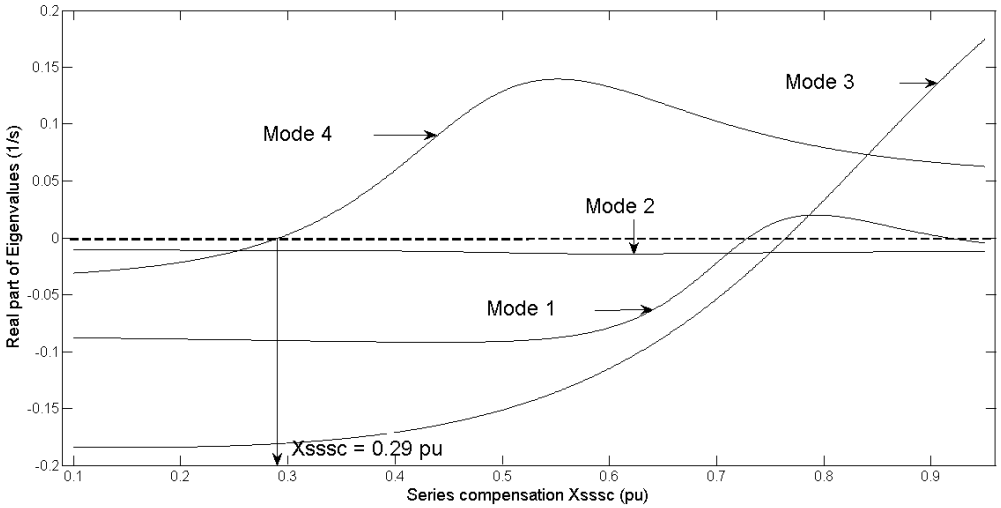

Fig. 5.9 Real parts of the eigenvalues of the study system as the series compensation provided by the SSSC, (X_{SSSC} in Line 1) is varied from 0.1 pu. to 0.95 pu. while the series capacitive reactance X_{C2} in Line 2 is fixed at 0.36 pu. (case B)

case B value of conventional series compensation in line 2 is from X_{SSSC} = 0.1 pu. up to a maximum value of X_{SSSC} = 0.29 pu. after which, torsional mode M4 remains unstable.

Figs. 5.8 and 5.9 have shown that the SSR-stable operating ranges of the series compensation X_{SSSC} in Line 1 at the two different values of capacitive reactance in Line 2 (case A and case B) are quite limited. In order to study the effect of the power flow controller on torsional mode damping at the two different values of conventional series compensation in Line 2 in these two cases, a common SSR-stable operating value for the X_{SSSC}-controlled SSSC's set-point reactance of X_{SSSC0} = 0.15 pu. was used for the following eigenvalue studies, which consider the impact of the improved approach to the design of the power flow controller added around the X_{SSSC}-controlled SSSC on the damping of the electromechanical modes.

5.6 Impact of the Improved Approach to Designing the SSSC-based Power Flow Controller on the Damping of Electromechanical Modes with Conventional Series Capacitors in Line 2

In order to investigate the influence of the power flow controller on the damping of the torsional modes of the study system of Fig. 5.6, Fig. 5.10 shows the loci of the eigenvalues of the study system as the gains K_P and K_I of the power flow controller are together adjusted to increase the power flow controller bandwidth from 0.13 rad/s to 33.5 rad/s using the improved approach to designing the controller gains presented in the first part of this chapter. In this particular study, the power flow controller is set to operate in constant power mode at a nominal value of X_{SSSC0} = 0.15 pu. and with X_{C2} fixed at 0.23 pu (case A).

From Fig. 5.10 it can be observed that as the bandwidth of the power flow controller is increased, the real eigenvalue P0, corresponding to the closed-loop pole in the power flow controller transfer function moves further into the left-hand plane. Fig. 5.10 also reveals that increasing the bandwidth of the power flow controller does influence the damping of the torsional modes of the study system. It can be observed that as the response time of the controller is made faster (up to a controller bandwidth of 4.6 rad/s), the eigenvalues M1, M2, M3 and M4 associated with the torsional shaft modes, together with the eigenvalue M0 associated with the generator's inertial swing mode, all

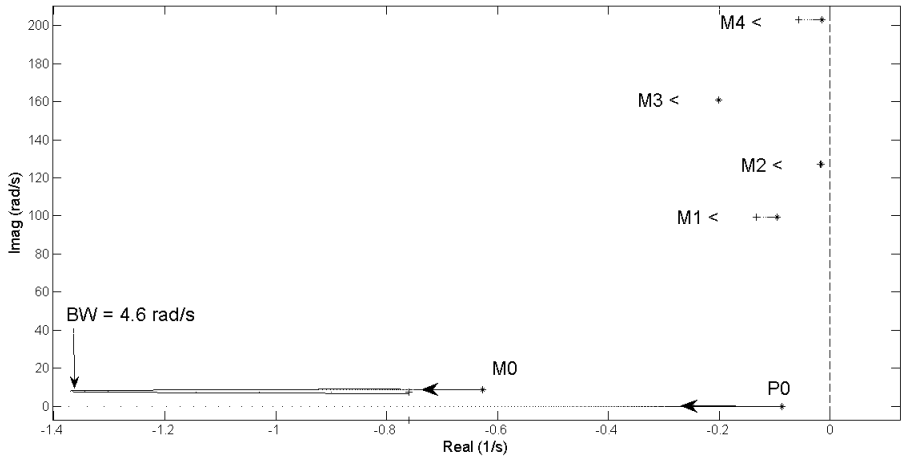

Fig. 5.10 Loci of the eigenvalues of the study system as the power flow controller's bandwidth is varied from 0.13 rad/s to 33.5 rad/s with the controller set in constant power mode, X_{SSSC0} = 0.15 pu. and X_{C2} = 0.23 pu (case A).

move to the left. However, when the controller's bandwidth is increased beyond 4.6 rad/s, all the torsional mode eigenvalues M1, M2, M3 and M4 continue to move towards the left, but the inertial mode eigenvalue M0 starts to move back towards the right hand plane. The result in Fig. 5.10 thus shows that in the constant power mode of operation, even with the presence of a fixed series capacitor in Line 2, the effect of the power flow controller is to increase the damping of the inertial swing mode as well as the damping of all of the torsional modes; furthermore this positive influence on the electromechanical modes increases at increasing bandwidths of the controller up to 4.6 rad/s. However, at controller bandwidths that are higher than 4.6 rad/s, while there is still an increasing positive influence on the damping of the torsional modes, the influence of the power flow controller on the inertial mode damping is less significant than is the case at lower bandwidths (although still net positive).

The above eigenvalue analysis was then repeated with the power flow controller set to operate in constant angle mode, with the results shown in Fig. 5.11. As expected, the real eigenvalue P0 associated with the response of the closed-loop pole of the power flow controller moves towards the left as the controller's bandwidth is increased from 0.13 rad/s to 33.5 rad/s. Fig. 5.11 shows that in this mode of operation the controller's bandwidth design also affects the damping of the electromechanical modes of the study system. However, it can be observed that the eigenvalues M1, M2, M3 and M0 all move towards the right, and hence closer to the imaginary axis, whilst eigenvalue M4 moves to the left as the controller bandwidth is increased. The results thus show that in this mode of power flow controller operation, the influence of increased controller bandwidth is to decrease the damping associated with all the electromechanical modes other than mode 4. Furthermore, at controller bandwidths higher than 2.3 rad/s, the inertial mode M0 is unstable.

The above study was repeated for the second, case B value of compensation in Line 2, in which the fixed series capacitive reactance X_{C2} was set at 0.36 pu. Fig. 5.12 shows the loci of the eigenvalues of the study system as the gains K_P and K_I of the power flow controller are together adjusted to increase the power flow controller bandwidth from 0.13 rad/s to 33.5 rad/s with the power flow controller set to operate in constant power mode at a nominal X_{SSSC0} value of 0.15 pu and X_{C2} fixed

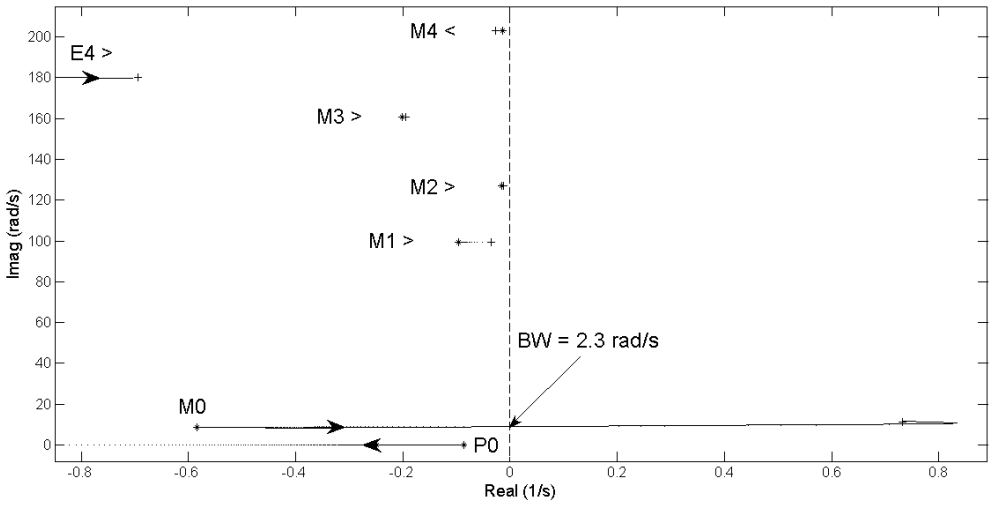

Fig. 5.11 Loci of the eigenvalues of the study system as the power flow controller's bandwidth is varied from 0.13 rad/s to 33.5 rad/s with the controller set in constant angle mode, X_{SSSC0} = 0.15 pu. and X_{C2} = 0.23 pu (case A).

at 0.36 pu (case B). It can be observed that as the bandwidth of the power flow controller is increased, the real eigenvalue P0, corresponding to the closed-loop pole in the power flow controller transfer function moves further into the left-hand plane.

Fig. 5.12 also reveals that increasing the bandwidth of the power flow controller does influence the damping of the torsional modes of the study system. It can be observed that as the response time of the controller is made faster (up to a controller bandwidth of 5.2 rad/s), the eigenvalues M1, M2, M3 and M4 associated with the torsional shaft modes, together with the eigenvalue M0 associated with the generator's inertial swing mode, all move to the left. However, when the controller bandwidth is increased beyond 5.2 rad/s, all the torsional mode eigenvalues M1, M2, M3 and M4 continue to move towards the left while the inertial mode eigenvalue M0 starts to move back towards the right.

The result in Fig. 5.12 thus shows that in the constant power mode of operation, even with the presence of a fixed series capacitor in Line 2 at a different value of conventional series compensation X_{C2} = 0.36 pu. in Line 2, the effect of the power flow controller is still to increase the damping of the inertial swing mode as well as the damping of all of the torsional modes; furthermore this positive influence on all of the electromechanical modes increases at increasing bandwidths of the controller up to 5.2 rad/s. However, at controller bandwidths that are higher than 5.2 rad/s, there is still a positive influence on the damping of all of the torsional modes, but there is less positive damping added to the inertial mode than at a bandwidth of 5.2 rad/s.

The above eigenvalue analysis was then repeated with the power flow controller set to operate in constant angle mode, with the results shown in Fig. 5.13. As expected, the real eigenvalue P0 associated with the response of the closed-loop pole of the power flow controller moves towards the left as the controller's bandwidth is increased from 0.13 rad/s to 33.5 rad/s. Fig. 5.13 once again shows that in this mode of operation, the controller bandwidth design also affects the damping of the electromechanical modes of the study system. However, it can be observed that the eigenvalues M1, M2, M4 and M0 all move towards the right, and hence closer to the imaginary axis, whilst

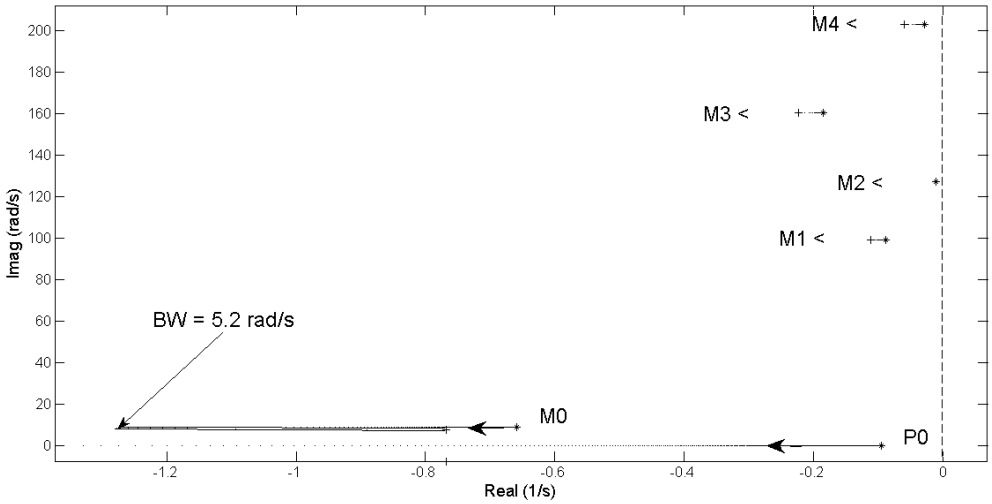

Fig. 5.12 Loci of the eigenvalues of the study system as the power flow controller's bandwidth is varied from 0.13 rad/s to 33.5 rad/s with the controller set in constant power mode, X_{SSSC0} = 0.15 pu. and X_{C2} = 0.36 pu (case B).

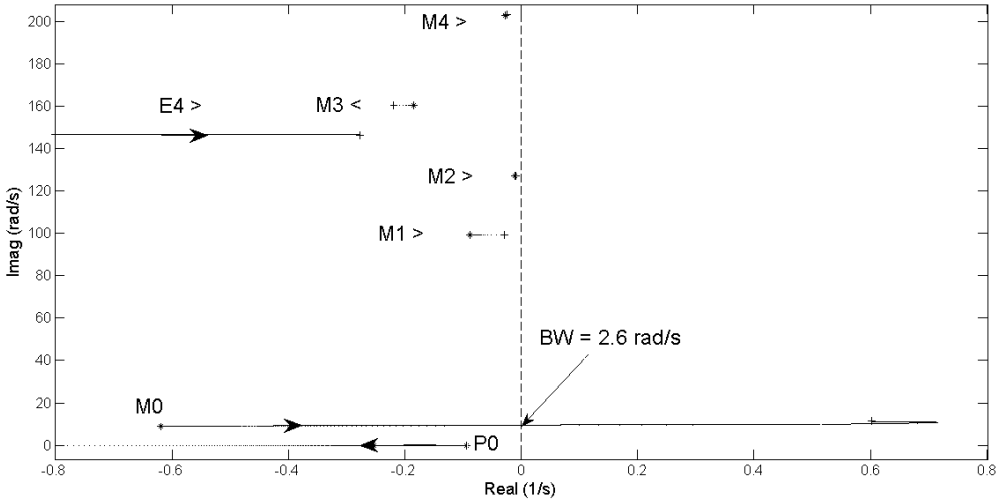

Fig. 5.13 Loci of the eigenvalues of the study system as the power flow controller's bandwidth is varied from 0.13 rad/s to 33.5 rad/s with the controller set in constant angle mode, X_{SSSC0} = 0.15 pu. and X_{C2} = 0.36 pu (case B).

eigenvalue M3 moves to the left as the controller bandwidth is increased. The results thus show that in this mode of power flow controller operation, the influence of increased controller bandwidth is to decrease the damping associated with all the electromechanical modes other than torsional mode M3. Furthermore, at controller bandwidths higher than 2.6 rad/s, the inertial mode M0 is unstable.

The results in this section have demonstrated that even in the presence of conventional series capacitors in an adjacent line, which is an additional source of torsional interaction in the transmission system, the influence of the design of this SSSC-based power flow controller on the damping of the inertial mode as well as all torsional modes is still similar to the previous, simpler case of having the SSSC as the only series compensator in the system when the power flow controller is operating in constant power mode. In this mode of operation of the power flow controller, and at different operating points of conventional series compensation in the adjacent line, the influence of increased controller bandwidth is still an increase in the damping of all the torsional modes, and initially in the damping of the inertial mode as well, although there is less positive damping added to the inertial mode beyond a certain critical controller bandwidth.

In the case of the constant angle controller, the results in this section have demonstrated that in the presence of conventional series capacitors in an adjacent line, the influence of increased controller bandwidth is still to reduce the damping of the inertial mode as was the case when there were no series capacitors in the adjacent line. Similarly, it has also been observed that beyond a certain critical controller bandwidth, the inertial mode is unstable. However, with regard to the torsional modes, the results have shown that in the presence of series capacitors in the adjacent line, the influence of increased controller bandwidth on torsional mode damping is dependent on the degree of conventional compensation. At one value of conventional series compensation in the adjacent line more damping is added to a particular torsional mode than is the case at another value of capacitive series compensation in the adjacent line.

The results in this chapter have thus demonstrated how fast-responding constant power flow controllers in particular can contribute positively to the damping of all the torsional modes of this

study system at any given set-point value X_{SSSC0} of the SSSC's compensating reactance. Since the impact of a constant-power mode controller is to improve the stability of all the electromechanical modes at any particular set-point value of X_{SSSC0} at which the SSSC is operating, a further benefit of this form of power flow control is that it should therefore make it possible to operate the SSSC, with its power flow controls, over a wider (i.e. more practical) range of compensating reactances X_{SSSC}, without risking SSR, as the bandwidth of the controller is increased. The following section of the chapter investigates this issue by considering the SSR characteristics of the study system at two different bandwidths of the constant-power mode controller (the highest and lowest bandwidth designs just considered in this section) as the set-point value X_{SSSC0} of the SSSC's compensating reactance is varied.

5.7 SSR-stable Ranges of the Study System with Power Flow Controller set to operate in Constant Power Mode at different Controller Bandwidth Designs

In order to further demonstrate the stabilising effect of constant power flow controllers on the SSR characteristics of the study system, the following studies consider the SSR characteristics of the study system over a range of values of the set-point reactance X_{SSSC0} of the SSSC for the lowest and highest controller bandwidth designs (0.13 rad/s and 33.5 rad/s) considered in the previous section. The investigations again start with the simpler case scenario of having the SSSC as the only form of series compensation in the study system (as shown in Fig. 4.1) and then go on to consider the more practical case of adding conventional capacitive compensation in Line 2 (as shown in Fig. 5.6).

5.7.1 Uncompensated Line 2

Fig. 5.14 shows the variation in the real parts of the eigenvalues associated with the torsional modes of the study system of Fig 4.1 (no series compensation in Line 2) as the set-point value of the SSSC's compensating reactance is increased from X_{SSSC0} = 0.1 pu. to X_{SSSC0} = 0.9 pu. for a fixed controller bandwidth value of 0.13 rad/s. Fig. 5.14 shows that as the set-point value of the SSSC's reactance is increased there is successive destabilisation of the mechanical torsional modes M4, M2 and M1 as the real parts of these torsional mode eigenvalues move into the positive plane. Fig. 5.14 shows that the SSR-stable operating range of the SSSC's set-point reactance for this particular value of controller bandwidth of 0.13 rad/s is from X_{SSSC0} = 0.1 pu. to X_{SSSC0} = 0.39 pu.; at values of X_{SSSC0} above 0.39 pu. one or more of modes M4, M2 or M1 are unstable.

By contrast, Fig. 5.15 shows the variation in the real parts of the eigenvalues associated with the torsional modes of the study system as the set-point value of the SSSC's compensating reactance is again increased from X_{SSSC0} = 0.1 pu. to X_{SSSC0} = 0.9 pu. for a fixed controller bandwidth value of 33.5 rad/s. It can be observed that as the set-point value of the SSSC's reactance is increased there is still successive destabilisation of the mechanical torsional modes M4, M2 and M1 as the real parts of these torsional mode eigenvalues move into the positive plane of Fig. 5.15. However, Fig. 5.15 shows that the SSR-stable operating range of the SSSC's set-point reactance for this highest controller bandwidth of 33.5 rad/s now extends from X_{SSSC0} = 0.1 pu. to X_{SSSC0} = 0.45 pu.

The SSR-stable ranges of the SSSC's set-point reactance for both of the controller bandwidth designs considered in Figs. 5.14 and 5.15 are quite limited. Nevertheless, Fig. 5.15 confirms that a fast-operating constant power flow controller does permit a wider operating range of SSR-stable values

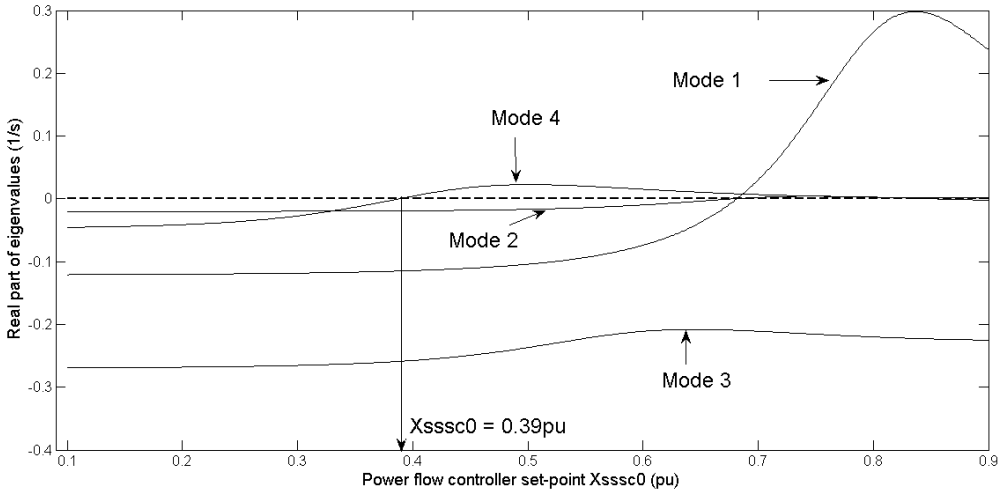

Fig. 5.14 Real parts of the eigenvalues of the study system as the set-point value of the SSSC's compensating reactance X_{SSSC0} is varied from 0.1 pu. to 0.9 pu. at a fixed controller bandwidth of 0.13 rad/s.

of SSSC compensation than is the case for a slow responding controller in Fig. 5.14 for the case when the parallel line in the system (Line 2) is uncompensated. The following subsection now examines the same issue for different values of conventional series compensation in Line 2.

5.7.2 Conventionally-Compensated Line 2

In section 5.6 the impact of the power flow controller bandwidth on SSR stability was examined for two specific values of fixed, conventional series compensation in Line 2: X_{C2} = 0.23 pu. (case A) and X_{C2} = 0.36 pu. (case B). This section now considers the SSR-stable ranges of the SSSC's compensating reactance in Line 1 for the lowest and highest bandwidth designs considered for a constant-power controller at each of these values of conventional compensation in Line 2.

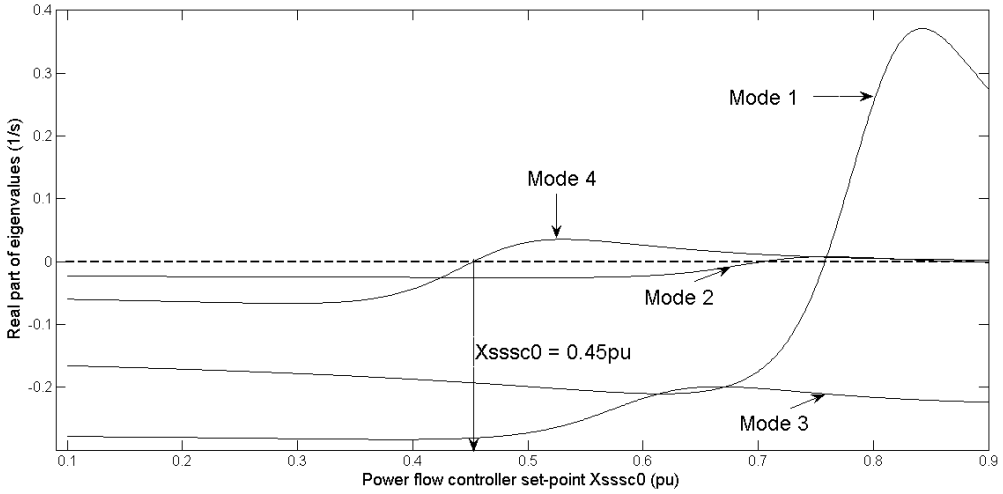

Fig. 5.15 Real parts of the eigenvalues of the study system as the set-point value of the SSSC's compensating reactance X_{SSSC0} is varied from 0.1 pu. to 0.9 pu. at a fixed controller bandwidth of 33.5 rad/s.

Fig. 5.16 shows the real parts of the eigenvalues associated with the torsional modes of the study system of Fig. 5.6 as the set-point value of the SSSC's compensating reactance is increased from X_{SSSC0} = 0.1 pu. to X_{SSSC0} = 0.9 pu for a fixed controller bandwidth value of 0.13 rad/s with the series compensation in Line 2 fixed at a value of X_{C2} = 0.23 pu. Fig. 5.16 shows that as the set-point value of the SSSC's reactance is increased there is successive destabilisation of the mechanical torsional modes M4 and M1 as the real parts of these torsional mode eigenvalues move into the positive plane of Fig. 5.16. Fig. 5.16 shows that the SSR-stable operating range of the SSSC's set-point reactance for this particular controller bandwidth of 0.13 rad/s is from X_{SSSC0} = 0.1 pu. to X_{SSSC0} = 0.27 pu.; at all values of X_{SSSC0} above 0.27 pu. one or both of the modes M4 and M1 are unstable.

Fig. 5.17 shows the real parts of the eigenvalues associated with the torsional modes of the study system as the set-point value of the SSSC's compensating reactance is again increased from X_{SSSC0} = 0.1 pu. to X_{SSSC0} = 0.9 pu for a fixed controller bandwidth value of 33.5 rad/s when the series compensation in Line 2 is fixed at a value of X_{C2} = 0.23 pu. It can be observed that as the set-point value of the SSSC's reactance is increased there is once again successive destabilisation of the mechanical torsional modes M4 and M1 as the real parts of these torsional mode eigenvalues move into the positive plane of Fig. 5.17. However, Fig. 5.17 shows that the SSR-stable operating range of the SSSC's set-point reactance for this highest controller bandwidth of 33.5 rad/s now extends from X_{SSSC0} = 0.1 pu. to X_{SSSC0} = 0.43 pu.

The above study was repeated for the second (case B) value of conventional compensation in Line 2, in which the fixed series capacitive reactance X_{C2} was set at 0.36 pu. Fig. 5.18 shows the real parts of the eigenvalues associated with the torsional modes of the study system as the set-point value of the SSSC's compensating reactance is increased from X_{SSSC0} = 0.1 pu. to X_{SSSC0} = 0.9 pu. for a fixed controller bandwidth value of 0.13 rad/s with the series compensation in Line 2 fixed at a value of X_{C2} = 0.36 pu. Fig. 5.18 shows that as the set-point value of the SSSC's reactance is increased there is successive destabilisation of the mechanical torsional modes M4 and M3 as the real parts of these

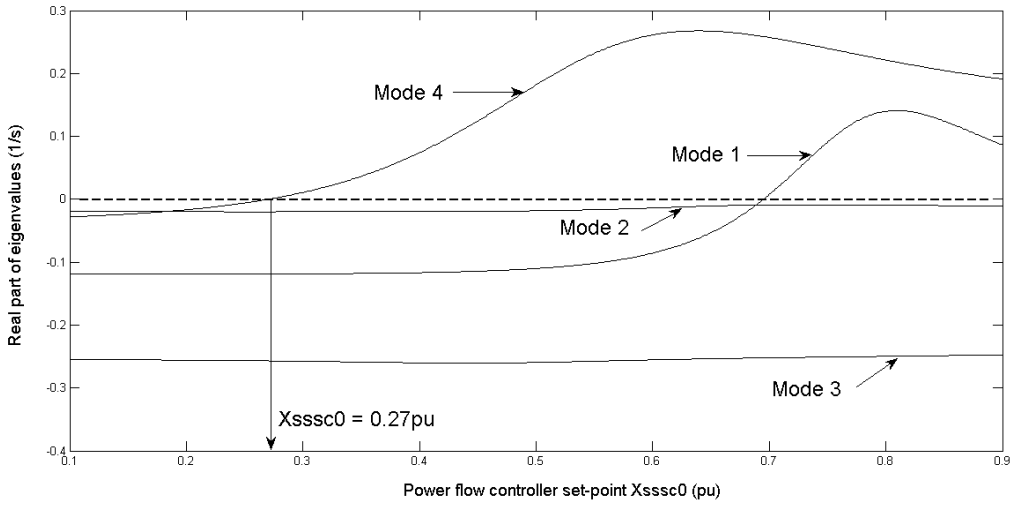

Fig. 5.16 Real parts of the eigenvalues of the study system as the set-point value of the SSSC's compensating reactance X_{SSSC0} is varied from 0.1 pu. to 0.9 pu. at a fixed controller bandwidth of 0.13 rad/s with the series capacitive reactance X_{C2} in Line 2 fixed at 0.23 pu.

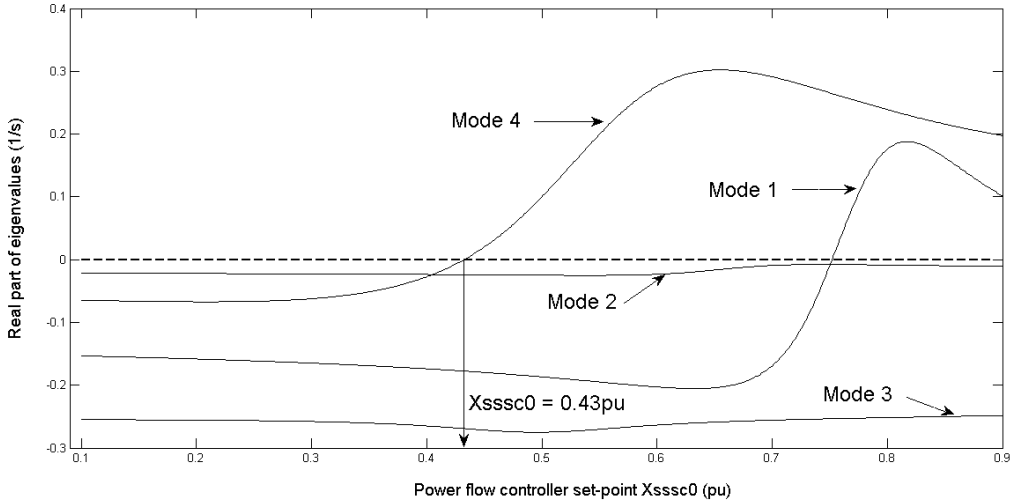

Fig. 5.17 Real parts of the eigenvalues of the study system as the set-point value of the SSSC's compensating reactance X_{SSSC0} is varied from 0.1 pu. to 0.9 pu. at a fixed controller bandwidth of 33.5 rad/s with the series capacitive reactance X_{C2} in Line 2 fixed at 0.23 pu.

torsional mode eigenvalues move into the positive plane of Fig. 5.18. Fig. 5.18 shows that the SSR-stable operating range of the SSSC's set-point reactance for this particular value of controller bandwidth of 0.13 rad/s is from X_{SSSC0} = 0.1 pu. to X_{SSSC0} = 0.32 pu.; at all values of X_{SSSC0} above 0.32 pu. one or both of the modes M4 and M3 are unstable.

Fig. 5.19 shows the real parts of the eigenvalues associated with the torsional modes of the study system as the set-point value of the SSSC's compensating reactance is again increased from X_{SSSC0} = 0.1 pu. to X_{SSSC0} = 0.9 pu for a fixed controller bandwidth value of 33.5 rad/s when the series compensation in Line 2 is fixed at X_{C2} = 0.36 pu. It can be observed that as the set-point value of the

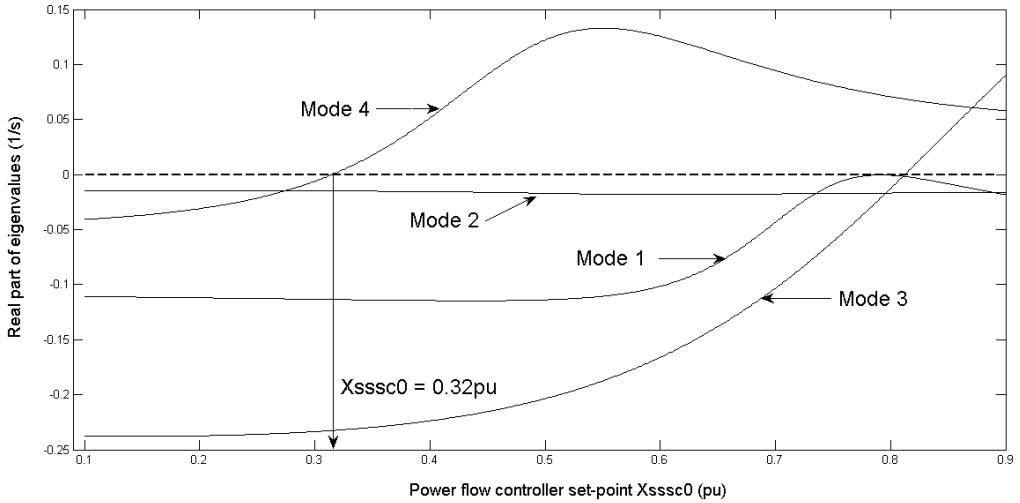

Fig. 5.18 Real parts of the eigenvalues of the study system as the set-point value of the SSSC's compensating reactance X_{SSSC0} is varied from 0.1 pu. to 0.9 pu. at a fixed controller bandwidth of 0.13 rad/s with the series capacitive reactance X_{C2} in Line 2 fixed at 0.36 pu.

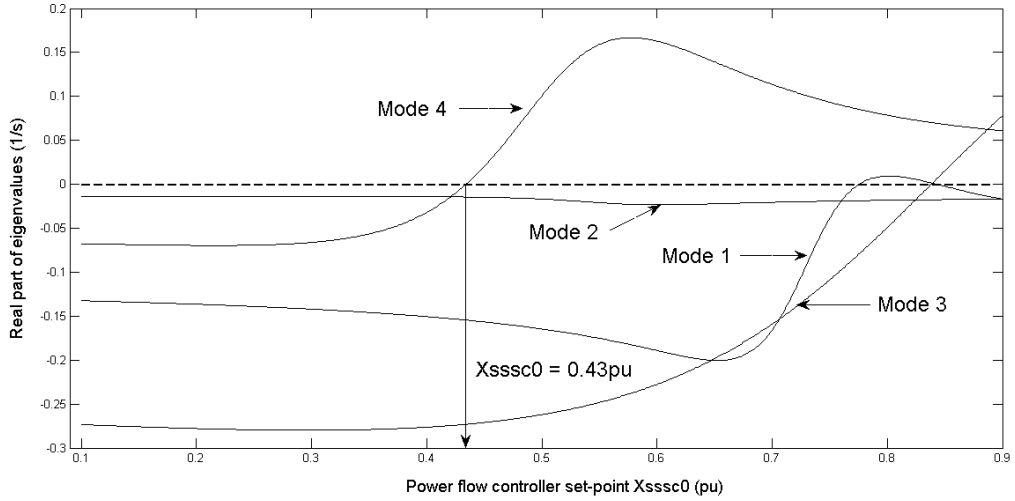

Fig. 5.19 Real parts of the eigenvalues of the study system as the set-point value of the SSSC's compensating reactance X_{SSSC0} is varied from 0.1 pu. to 0.9 pu. at a fixed controller bandwidth of 33.5 rad/s with the series capacitive reactance X_{C2} in Line 2 fixed at 0.36 pu.

SSSC's reactance is increased, there is successive destabilisation of the mechanical torsional modes M4, M1 and M3 as the real parts of these torsional mode eigenvalues move into the positive plane of Fig. 5.19. However, Fig. 5.19 shows that the SSR-stable operating range of the SSSC's set-point reactance for this highest controller bandwidth of 33.5 rad/s now extends from X_{SSSC0} = 0.1 pu. to X_{SSSC0} = 0.43 pu.

The two sets of results in this subsection (Figs. 5.16 and 5.17, followed by Figs. 5.18 and 5.19) have again showed that the SSR-stable ranges of the SSSC's set-point reactance are quite limited, for the range of controller bandwidth designs considered, in this more complex case with conventional series compensation in Line 2. However, both sets of results demonstrate that even in the presence of conventional series compensation in the adjacent line, a fast-operating constant power flow controller permits a wider operating range of SSR-stable values of SSSC compensation than is the case for a slow-responding controller.

Hence, the studies in this section demonstrate generally that a much faster power flow controller design further improves the SSR characteristics of the study system, such that a wider operating range of the power flow controller can then be employed. This positive influence of the power flow controller on the SSR characteristics of the study system has even been confirmed in the more practical cases of two selected values of conventional series compensation in the adjacent line of the study system, with the faster-responding controller again allowing a wider range of the power flow controller to be realised without the destabilisation of any particular torsional modes of this study system.

5.8 Conclusion

Chapter Four has shown the dependence of torsional mode damping (and hence SSR stability) on both the mode of operation and the speed of response of a power flow controller that was designed for relatively slow-responding control action in the adapted IEEE FBM study system. This chapter has now presented an improved design of the gains of the power flow controller in this study system

that allows much higher-bandwidth controllers to be achieved that are comparable to other fast-responding power flow controllers reported in the literature [65,95]. This chapter has therefore considered whether the findings reported in the previous chapter, with the initial design approach, also hold true for fast-responding controllers, particularly in light of the different observations described in [65]. In the process, it has been shown that the alternative approach to pole-zero placement used in this improved design not only allows greater controller bandwidths to be attained, but, in the case of constant-power type controllers, allows significantly improved stabilisation of all generator electromechanical modes (torsional and inertial) to be achieved. Detailed studies have been presented to confirm not only that a constant power mode controller adds stabilising damping to all torsional modes, and is able to do so even in the presence of conventional series compensation in an adjacent line, but that this stabilisation can be increased by a faster acting power flow controller. However, the results have also shown that although the design of the power flow controller's bandwidth can be made very fast, the mode of operation chosen for the power flow controller does impose some limitations on its controller bandwidth design. For the different operating conditions of the transmission network considered in this chapter, it was observed that in the constant power mode of operation, for controller bandwidths beyond certain critical values, damping begins to be removed from the inertial mode as the bandwidth increases, although the net impact of the power flow controller on damping remained positive at all bandwidths considered. Hence, by considering a wider range of controller bandwidths for study in this chapter compared to the range of controller bandwidths considered in [65], the results in this chapter are of wider scope than those in [65] and arguably extend the findings of that study, by demonstrating the change in the influence of the controller response times on damping beyond a critical value of bandwidth.

In other words, in light of the findings in this chapter of the thesis, the apparently different observations reported in [65] may well in fact be consistent with those of this thesis, and simply be valid over a narrower range of conditions than those considered here: that is, if the range of controller bandwidths considered for study in [65] lay above the critical controller bandwidth identified here, then within that narrower range of controller bandwidths considered in [65] the damping of the inertial mode would appear only to decrease at increasing controller bandwidths. By contrast, by also considering lower bandwidth designs the results in this chapter also demonstrate that the influence of increasing controller bandwidth in a range that lies below the critical bandwidth value is to add damping to the inertial mode.

As a result of considering a wider range of controller bandwidths for study, the results in this chapter have also shown that if the aim is to optimise the damping of all the electromechanical modes, a bandwidth equal to this critical value will be the best design of the controller for the constant power mode. However, if the aim is to achieve the fastest possible power flow controller response, the maximum achievable bandwidth can be used since all the electromechanical modes are still stable at this highest controller bandwidth. The observations described in [65], where a much higher upper limit was used in the range of controller bandwidths considered, further suggest that at very fast controller bandwidths, the effect of increasing controller bandwidths may also be to destabilise the torsional modes. However, it is difficult to comment in depth on the likely reasons for this conclusion since the studies in [65] employed a TCSC, which has distinct SSR characteristics to those of the SSSC.

CHAPTER FIVE

The results in this chapter add further weight to the findings in the previous chapter, which concluded that the alternative mode of operation of a power flow controller that has been proposed in the literature (constant angle mode) is not suitable for environments where SSR is a concern. In particular, this mode of control has been shown to destabilise a number of generator torsional modes in the study system, with the extent of the destabilisation of torsional mode 4 and the inertial swing mode being very sensitive to the system operating conditions and power flow controller design. In the case of the constant angle mode of operation, it is not even possible to operate the power flow controller at bandwidths above a certain critical value as some of the electromechanical modes become unstable. The results thus show that if the aim is to optimise the damping of all the modes, this mode of power flow control is not recommended at all since there is a detrimental impact on the damping of all the generator's electromechanical modes. Conversely, if the aim is to achieve the fastest power flow controller response, this mode of operation is still not recommended since the maximum controller bandwidth that can be achieved is limited to the critical controller bandwidth after which the inertial swing mode of the generator itself becomes unstable.

The results in this chapter have also demonstrated that in the constant power mode of operation of the power flow controller, due its stabilising influence on the torsional modes at all values of compensation, the SSR-stable operating range of the power flow controller increases as the bandwidth of the controller is increased even in the presence of conventional series compensation in the adjacent line of the study system.

The review presented in Chapter Two of the thesis highlighted the fact that the two main categories of SSSC (referred to in this thesis as X_{SSSC}-controlled and V_{SSSC}-controlled devices) have very important differences in their SSR characteristics [18,19]. Chapters Four and Five have so far considered only one of these categories of SSSC, that is the reactance-controlled SSSC, when considering closed-loop power flow controls and their additional impact on torsional interaction. The following chapter now considers the second category of SSSC, that is the quadrature voltage-controlled SSSC, and investigates the impact on torsional interaction of power flow controllers implemented around this category of SSSC.

CHAPTER SIX

INVESTIGATING THE IMPACT OF A QUADRATURE VOLTAGE-CONTROLLED SSSC-BASED POWER FLOW CONTROLLER ON TORSIONAL INTERACTION

6.1 Introduction

The review in Chapter Two of the thesis has shown that there are two main types of SSSC implementation, namely the reactance-controlled and the quadrature voltage-controlled types (also referred to in this thesis as X_{SSSC}-controlled and V_{SSSC}-controlled devices) and that although both of these types of SSSC have the potential to excite SSR, there are important differences in their SSR characteristics as stand-alone devices [18,19]. The V_{SSSC}-controlled category of SSSC is already known to be inherently more stable with regard to any torsional interaction than the X_{SSSC}-controlled type of SSSC due to the additional resistance inserted series with the line at subsynchronous frequencies by the V_{SSSC}-controlled device [18].

Chapter Four of this thesis has investigated the impact on torsional interaction of an initial design approach for an X_{SSSC}-controlled SSSC-based power flow controller. Subsequently, Chapter Five considered an improved approach to designing the control gains of the X_{SSSC}-controlled SSSC-based power flow controller that enables much faster controller bandwidths to be realised. In particular, it was shown in Chapter Five how the design of this significantly-faster SSSC-based power flow controller affects the SSR stability of generators with multi-inertia turbines. The results have shown that although the design of the power flow controller's bandwidth can be made very fast, the mode of operation chosen for the power flow controller does impose some limitations on its controller bandwidth design. For constant-power type controllers, the influence of increased controller bandwidth is an increase in the damping of all the torsional modes, and initially in the damping of the inertial mode as well, although there is less net positive damping added to the inertial mode beyond a certain critical value of controller bandwidth. In the case of the constant angle controller, the results have demonstrated that this alternative mode of operation is not suitable for environments where SSR is a concern. However, the results presented thus far in this thesis have examined the influence on torsional interaction of the design of power flow controllers around only one category of SSSC, that is the X_{SSSC}-controlled type of SSSC.

This chapter now aims to investigate whether the implementation of power flow controls around the second category of SSSC, namely the V_{SSSC}-controlled type, will also affect the damping of the torsional modes in the shafts of turbine-generators and in particular, how the different SSR characteristics of the V_{SSSC}-controlled SSSC impact on the way in which the design of the power flow controller affects the SSR stability of the study system. The investigations in the chapter follow a similar structure to those carried out in Chapter Four where the power flow controller was implemented around an X_{SSSC}-controlled SSSC. Hence, the chapter begins by verifying the operation of the different modes of power flow control in order to confirm the correctness of the

mathematical models of the power flow controller derived in Chapter Three for the V_{SSSC}-controlled SSSC. The chapter then examines the design of the controller gains for a quadrature voltage-controlled SSSC-based power flow controller by using frequency-domain linearised transfer-function analysis. However when doing so, this chapter will only consider the improved approach to designing the power flow controller as presented in Chapter Five, which has been shown to allow a much higher controller bandwidth to be realised. Finally, the chapter examines the impact on torsional interaction of the V_{SSSC}-controlled SSSC-based power flow controller over a range of operating conditions.

6.2 Verification of Control Modes

The mathematical model of the power flow controller for a quadrature voltage-controlled SSSC described in Chapter Three can be verified by means of two test studies using the study system shown in Fig. 6.1, where the transmission system incorporates a quadrature voltage-controlled SSSC that is fitted with a power flow controller in Line 1; Line 2 was initially left uncompensated for the purposes of the investigations considered in the first part of this chapter.

To verify the correct implementation of the two power flow control strategies considered in the previous chapters of this thesis, in each case the simulation study was started from the same steady state condition in which the generator's active power output P_t = 0.5 pu., and with this active power being initially transferred by the lines 1 and 2 as follows: P_{L1} = 0.32 pu. and P_{L2} = 0.18 pu. Subsequently, the mechanical input power to the generator was increased by ΔP_m = 0.1 pu. such that the total active power P_t dispatched was increased to 0.6 pu. The response of the system to this small increase in generator dispatch was then studied for the system with the power flow control activated in each of the two possible control modes. As discussed in Chapter Four, although a step change ΔP_m in the input to the turbine is not realistic in practice, it has been considered here as a theoretical test disturbance because it facilitates comparison of the dynamics of the two power flow controller modes.

Fig. 6.2 shows the response of the study system with the power flow controller active and set to the constant power mode. The results show that, following the increase in generator dispatch, initially the power transfer in Line 1 increases, which then results in the power flow controller reducing the magnitude of the injected voltage V_{SSSC} provided by the SSSC. By reducing the magnitude of the compensating voltage provided by the SSSC, the power transfer in Line 1 is decreased accordingly and returns to its nominal operating point of 0.32 pu. All the additional power dispatched by the generator is thus forced to flow through Line 2, where the power transfer is increased to 0.28 pu. This response thus verifies the correct operation of the power flow controller model when operating in constant power mode around a quadrature voltage-controlled SSSC.

Fig. 6.3 shows the response of the study system following the increase in generator dispatch with the power flow controller now set to operate in constant angle mode. According to [15,16] the constant angle strategy should ensure that the compensated line transfers all the additional output power of the generator. Fig. 6.3 shows that following the increase in generator dispatch, the power flow controller responds by increasing the magnitude of the injected voltage V_{SSSC} provided by the series compensator such that the power transfer in Line 2 returns to its nominal operating point of

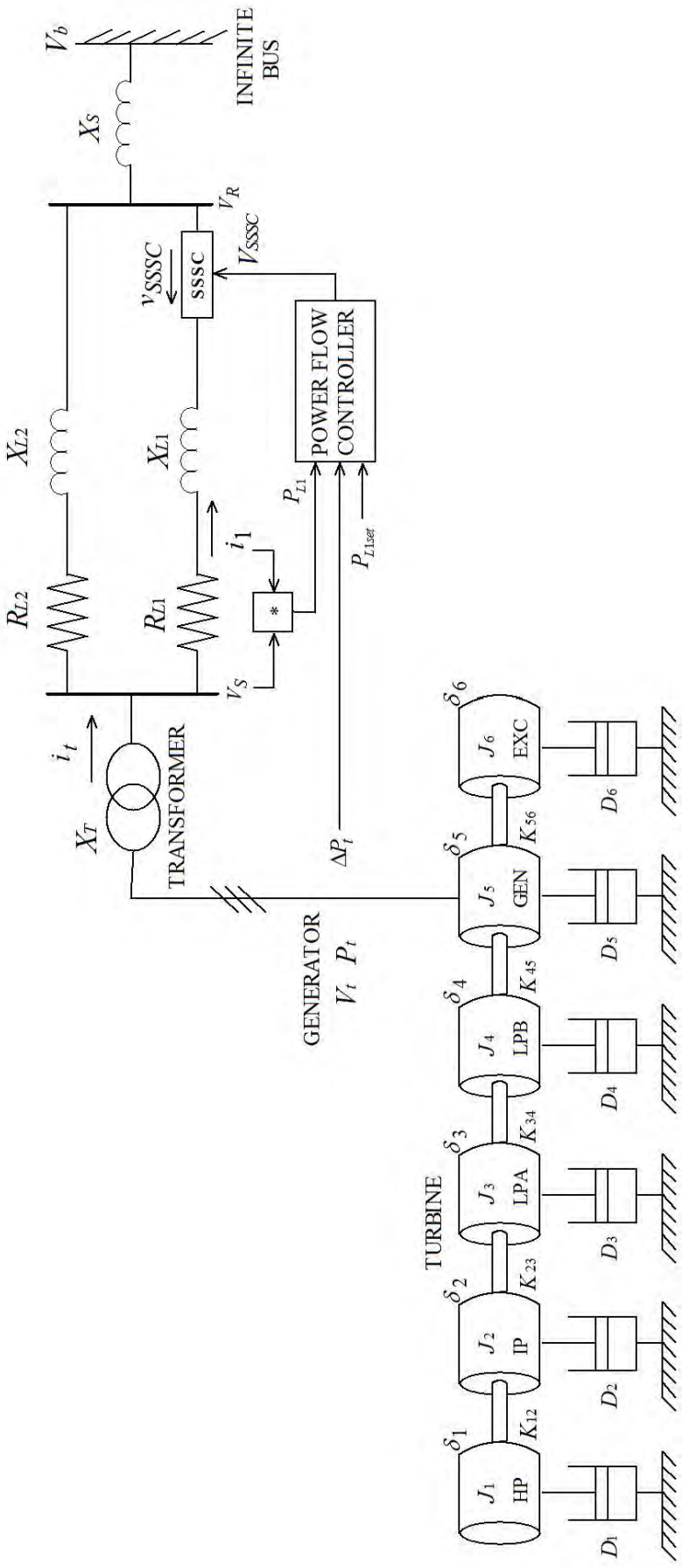

Fig. 6.1 Single line diagram of the study system.

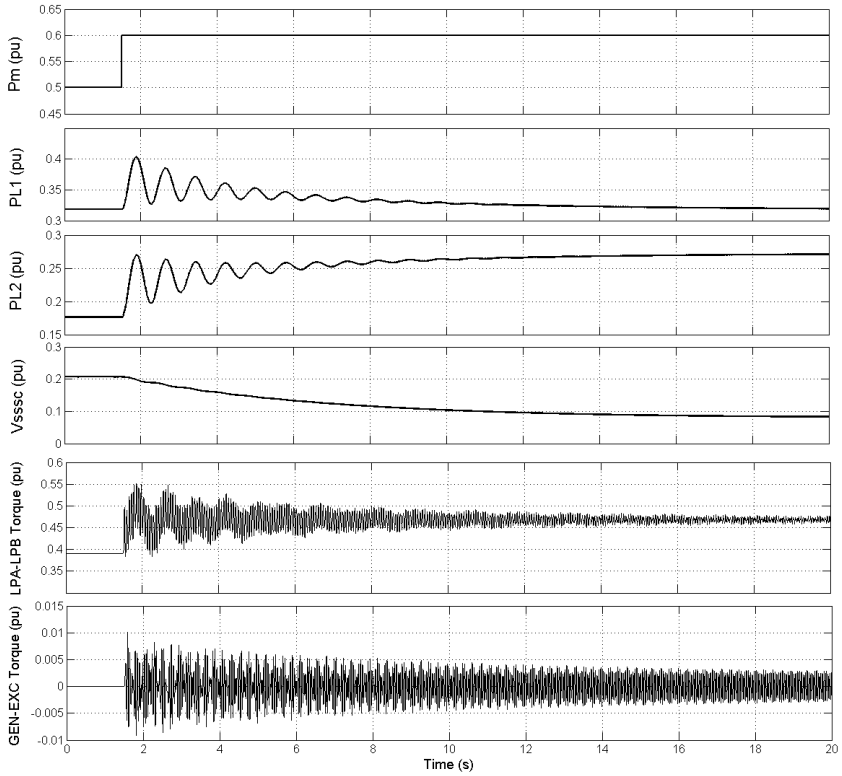

Fig. 6.2 Response of the study system to an increase in generator dispatch with the power flow controller in constant power mode; quadrature voltage-controlled SSSC.

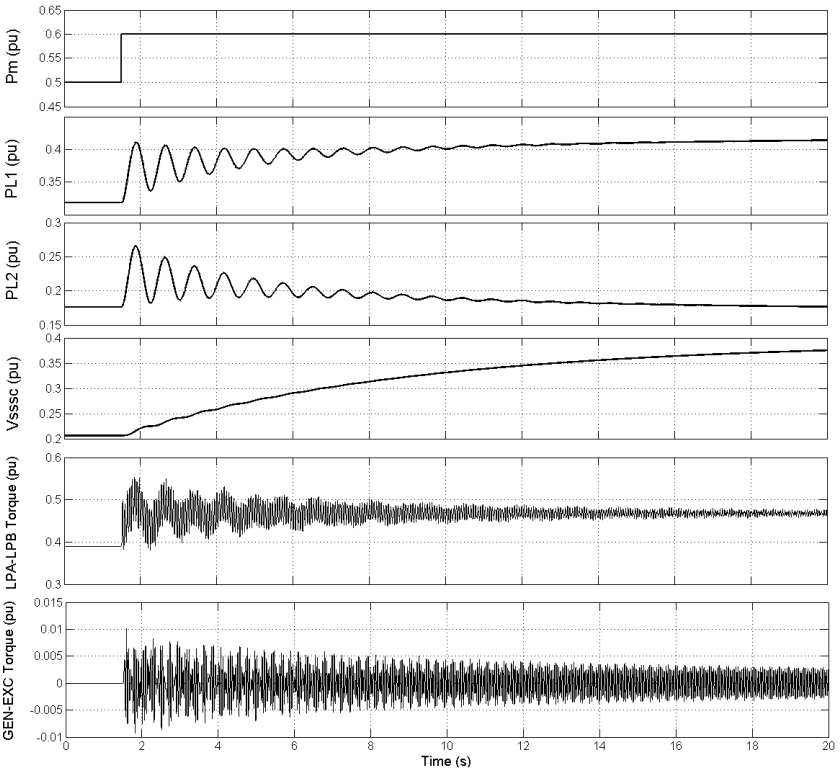

Fig. 6.3 Response of the study system to an increase in generator dispatch with the power flow controller in constant angle mode; quadrature voltage-controlled SSSC.

0.18 pu. and all the additional dispatch is transferred by Line 1 (P_{L1} increases to 0.42 pu.). Fig. 6.3 thus confirms that the constant angle controller is correctly implemented in the mathematical model of the study system of Fig. 6.1 which incorporates a quadrature voltage-controlled SSSC.

Although the mathematical model of the power flow controller has been verified for both the constant power and constant angle modes of operation, the remaining studies in this chapter will consider only the constant power mode of operation of the power flow controller, since in all previous chapters the constant angle mode has been shown to be consistently detrimental to the damping of the electromechanical modes of this study system. In fact, although the results are not included here, studies carried out as part of these investigations did show that even with the quadrature voltage-controlled SSSC, the constant angle mode of operation has a negative influence on the damping of the electromechanical modes of oscillation of this study system. This chapter therefore considers only the constant power mode of operation in order to investigate the influence of power flow controls around this second category of SSSC on the damping of the torsional modes of oscillation of the study system.

6.3 SSR Characteristics of the Study System without Power Flow Control

In Chapter Four, the SSR characteristics of the study system were initially examined for a range of different values of the series compensating reactance provided by an X_{SSSC}-controlled SSSC, with Line 2 uncompensated, and without the power flow controller enabled. Fig. 4.4 has shown that the destabilising effect of the torsional interaction caused by the reactance-controlled SSSC was sufficient to cause the eigenvalues associated with modes 4, 2 and 1 of this study system to enter the right hand plane, with the exception of mode 3 which remained in the left plane at all the values of X_{SSSC}. Fig. 4.4 therefore indicated that as the compensating reactance X_{SSSC} is increased, unstable mechanical oscillations in the turbine-generator shaft would be expected to occur in succession at the natural frequencies of modes 4, 2 and 1.

In order to investigate the SSR characteristics of the study system with the second category of SSSC, that is the quadrature voltage-controlled SSSC, the study of Fig. 4.4 was repeated, but with the X_{SSSC}-controlled SSSC in Line 1 replaced by a V_{SSSC}-controlled SSSC as shown in Fig. 6.1, and with the power flow controller initially disabled. In the following analysis, the magnitude of the injected voltage of the SSSC in Line 1 is varied from V_{SSSC} = 0.04 pu. to V_{SSSC} = 0.58 pu.; this magnitude range of the injected voltage corresponds to the same range of percentage series compensation that was used in the study of Fig. 4.4 when the X_{SSSC}-controlled SSSC was used in Line 1 instead of the V_{SSSC}-controlled SSSC. Fig. 6.4 shows the loci of the eigenvalues of this study system as the commanded compensating voltage injected by the SSSC is varied in this way.

The system of Fig. 6.4 has similar eigenvalues to a system compensated by a reactance-controlled SSSC as shown in Fig. 4.4. Fig. 6.4 shows that as is the case with reactance-controlled SSSC, the subsynchronous electrical frequency (eigenvalue E2) of the voltage quadrature-controlled SSSC compensated system also decreases as V_{SSSC} is increased. Torsional interaction in this study system again occurs in the small rectangular area of the eigenvalue plot which is enlarged in the bottom half of Fig. 6.4. It can be observed that as the subsynchronous frequency of the electrical system (E2) approaches each natural frequency of the mechanical system (M1 to M4), torsional interaction between the mechanical and electrical system occurs, forcing the eigenvalue associated with that

torsional shaft mode towards the right hand plane. However, Fig. 6.4 shows that the destabilising effect of this torsional interaction is not sufficient to cause the eigenvalues associated with modes 4, 3, 2 or 1 of this study system to enter the right hand plane, as all these eigenvalues remain in the left plane at all the values of V_{SSSC} considered. Fig. 6.4 therefore indicates that as the magnitude of the injected voltage V_{SSSC} is increased, the mechanical oscillations in the turbine-generator shaft would be expected to remain stable even when the subsynchronous electrical frequency of this voltage quadrature-controlled SSSC compensated system approaches the natural frequencies of modes 4, 2, 3 and 1. The above results thus confirm the findings reported in [18], where it was found that the quadrature voltage-controlled SSSC is more SSR-stable than the reactance-controlled SSSC as a result of its particular resonant characteristics in the frequency domain. The results also extend the findings of [18] to demonstrate that the V_{SSSC}-controlled SSSC is also more SSR-stable than the X_{SSSC}-controlled SSSC as a stand-alone device in a more complex transmission system that incorporates an additional transmission line in parallel. It should also be noted, again, that the eigenvalue study in Fig. 6.4 indicates the SSR characteristics of the quadrature voltage-controlled SSSC for a range of values of the magnitude of the commanded injected voltage V_{SSSC} without power flow control enabled around the SSSC. The following section considers the design of the power flow controller to be added around the V_{SSSC}-controlled SSSC.

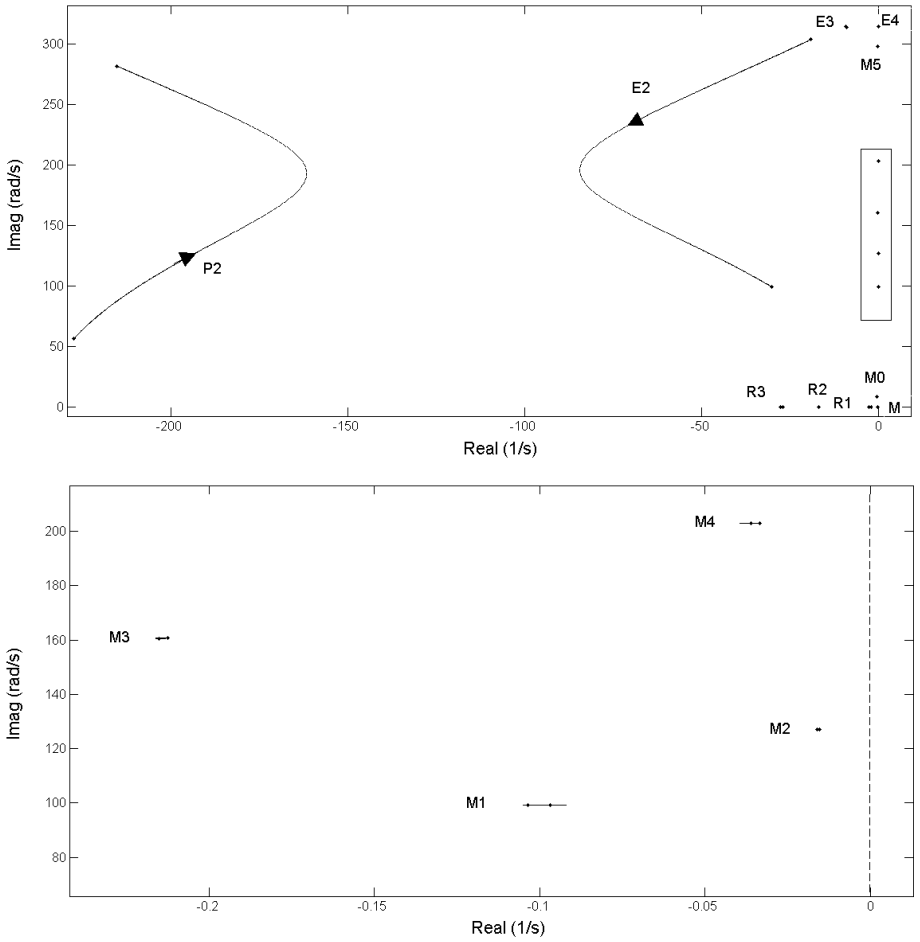

Fig. 6.4 Loci of eigenvalues of the study system as the magnitude of the injected voltage V_{SSSC} is varied from 0.04 pu. to 0.58 pu.; no power flow control.

6.4 Design of Quadrature Voltage-Controlled SSSC-based Power Flow Controller

In Chapter Five, the design of the power flow controller using the improved design approach around a reactance-controlled SSSC was presented in Fig. 5.2. The results of Fig. 5.2 confirmed that the improved design approach (positioning the zero of the power flow controller's transfer-function much further into the left had plane at -303 s^{-1}) allows a much higher power flow controller bandwidth to be achieved.

This section now examines the design of the power flow controller to be added around the V_{SSSC}-controlled SSSC by using frequency domain linearised transfer function analysis. In particular, the study investigates the influence of the design of the gains of the power flow controller on the resonant characteristics of a transmission network compensated by the V_{SSSC}-controlled SSSC. The design of the gains K_P and K_I of the power flow controller to achieve specified response criteria is first carried out using a simplified model of the study system shown in Fig. 6.1 in which the generator is replaced by an ideal voltage source. The detailed SSR interaction studies are then carried out using the full system model once the range of power flow controller designs has been chosen. Each design of the power flow controller is carried out by adjusting its gains K_P and K_I to manipulate the positions of the first-order pole and zero in the transfer function $\Delta P_{L1} \,/\, \Delta P_{L1}^{*}(s)$ between the input and output of the controller in constant power mode. The improved design approach used to design the dynamic response characteristic of the power flow controller in this chapter follows the approach presented in Chapter Five, and can be summarised as follows. The proportional and integral gains K_P and K_I are adjusted together in order to meet two specifications: (i) positioning the closed-loop pole in the transfer function $\Delta P_{L1} \,/\, \Delta P_{L1}^{*}(s)$ in the left-hand plane so as to meet the specific bandwidth (settling time) required in the dynamic response of the power flow controls; (ii) positioning the closed-loop zero in the same transfer function at -303s^{-1} in the left-hand plane, such that it always lies well to the left of the closed-loop pole, irrespective of what controller bandwidth has been chosen for study.

Fig. 6.5 shows the small-signal transfer function $\Delta P_{L1} \,/\, \Delta P_{L1}^{*}(s)$ of the power flow controller in the simplified model of the study system when the values of K_P and K_I are together adjusted to increase the power flow controller bandwidth from 0.13 rad/s to 33.5 rad/s. Fig. 6.5(a) shows the transfer function in the form of its pole and zero locations in the complex plane whilst Fig. 6.5(b) shows the transfer function in the form of its magnitude and phase as a function of frequency at four selected bandwidth designs. As expected, it can be observed (Fig.6.5(a)) that as the controller's bandwidth is increased, the real pole P0 associated with the closed-loop response of the controller moves further into the left-hand plane. Fig. 6.5(a) also reveals that the design of the controller's bandwidth influences the resonant characteristics of this quadrature voltage-controlled SSSC compensated transmission network. As the response of the controller is made faster, the eigenvalue E2 associated with the resonant characteristics of the transmission network exhibits an increase in its frequency and it moves slightly closer to the right-hand plane. Fig. 6.5(b) also confirms that as the design of the controller is changed in order to increase its 0 to -3dB bandwidth, the underdamped resonant peak in the transfer function (associated with transmission line's resonant characteristics) increases slightly in frequency, but becomes significantly less damped. The above results demonstrate that when designing the power flow controller to achieve different controller bandwidths in this way (fixing the position of its transfer function zero at -303s^{-1}, and moving the position of its pole) the choice of the controller bandwidth does in fact have an influence on the resonant characteristics of

the transmission line, even at a single value of injected voltage provided by the V_{SSSC}-controlled SSSC. Furthermore, the results also demonstrate that when designing power flow controls around the two categories of SSSC (reactance-controlled SSSC designs shown in Fig 5.2 or quadrature voltage-controlled SSSC designs shown in Fig. 6.5) the upper limit on the controller bandwidth that can be achieved when using the improved design approach is the same in each case. Thus, although the V_{SSSC}-controlled SSSC has been shown to be more SSR stable than the X_{SSSC}-controlled SSSC as a stand-alone device in this particular study system, the above results demonstrate that the design of power flow controller's bandwidth has a similar influence on the resonant characteristics of both the V_{SSSC}-controlled SSSC compensated transmission system as well as the X_{SSSC}-controlled SSSC compensated transmission system: the eigenvalue E2 moves by the same distance in Figs. 5.2(a) and 6.5(a). The following section now investigates the influence of the design of the power flow controller around the V_{SSSC}-controlled SSSC on the damping of the electromechanical modes in the full study system.

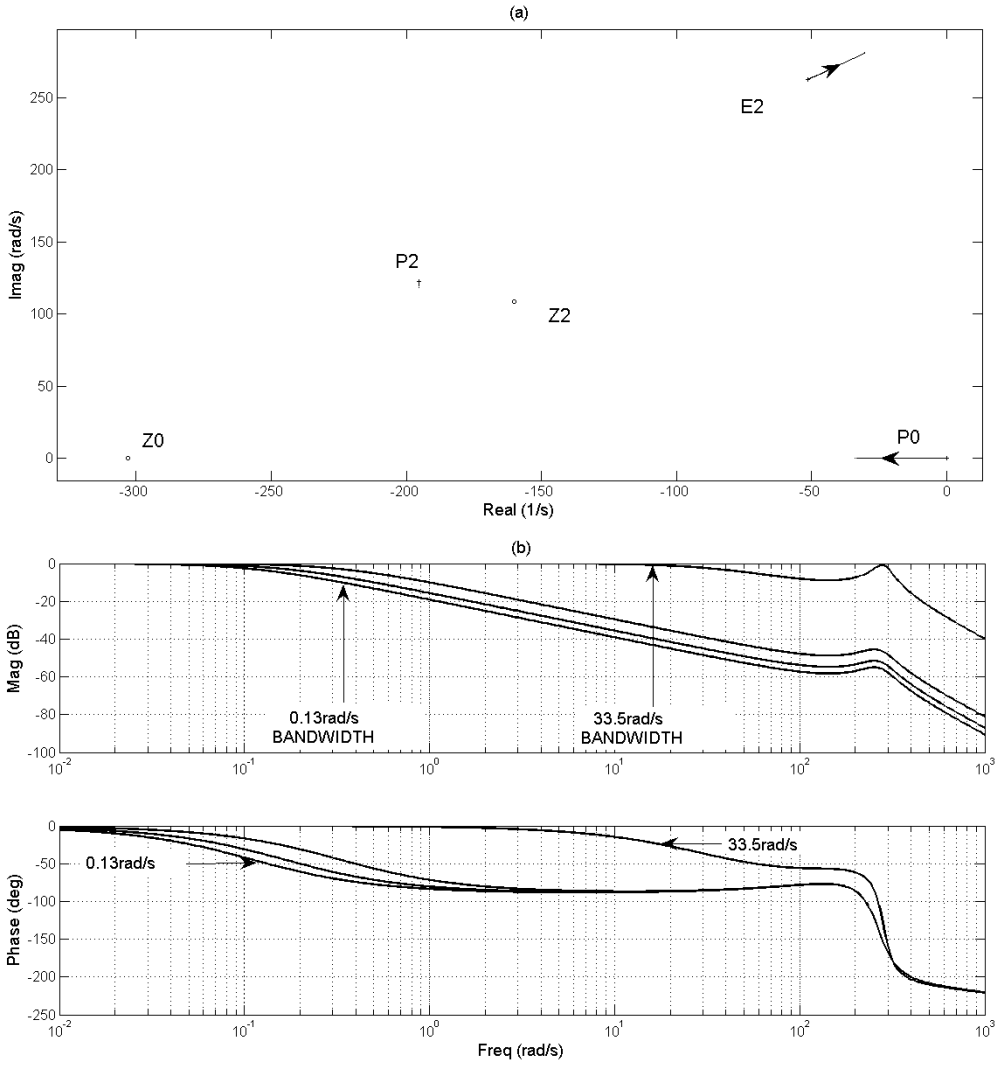

Fig. 6.5. Power flow controller transfer function $\Delta P_{L1}/\Delta P_{L1}^{*}(s)$with increasing controller bandwidth designs (sending end of the study system fed from ideal source).

6.5 Impact of Quadrature Voltage-Controlled SSSC Power Flow Controller Design on the Damping of Electromechanical Modes

In Chapter Five, the impact on torsional interaction of reactance-controlled SSSC-based power flow controllers was examined using the improved design approach which allows much higher controller bandwidths to be achieved. In particular, Fig. 5.4 has shown that in the constant power mode of operation, the effect of a power flow controller designed in this manner is to increase the damping of the inertial swing mode as well as the damping of all of the torsional modes; furthermore this positive influence on the electromechanical modes increases at increasing bandwidths of the controller up to 9.6 rad/s. However, at bandwidths above 9.6 rad/s, there is still a positive influence on the damping of all of the torsional modes, but there is less net damping added to the inertial mode by the action of the power flow controller than is the case at lower controller bandwidths. In order to investigate the influence of the design of a V_{SSSC}-controlled SSSC-based power flow controller on the damping of the torsional modes of the study system, the study in Fig. 5.4 was repeated using the full mathematical model of the study system of Fig. 6.1 which incorporates a quadrature voltage-controlled SSSC instead of a reactance-controlled SSSC.

Fig. 6.6 now shows the loci of the eigenvalues of the full study system model as the gains K_P and K_I of the power flow controller are together adjusted to increase the power flow controller bandwidth from 0.13 rad/s to 33.5 rad/s. As expected, it can be observed that as the bandwidth of the power flow controller is increased, the real eigenvalue P0, corresponding to the closed-loop pole in the power flow controller transfer function, moves further into the left-hand plane. Fig. 6.6 also reveals that increasing the bandwidth of the power flow controller does influence the damping of the torsional modes of the study system. It can be observed that as the response time of the controller is made faster (up to a controller bandwidth of 9.5 rad/s), the eigenvalues M1, M2, M3 and M4 associated with the torsional shaft modes, together with the eigenvalue M0 associated with the generator's inertial swing mode, all move to the left. However, when the controller's bandwidth is increased beyond 9.5 rad/s, all the torsional mode eigenvalues M1, M2, M3 and M4 continue to move towards the left but the inertial mode eigenvalue M0 starts to move back towards the right-hand plane. The result in Fig. 6.6 thus shows that even with a V_{SSSC}-controlled SSSC-based power flow controller in the constant power mode of operation, the effect of the power flow controller designed in this manner is to increase the damping of the inertial swing mode as well as the damping of all of the torsional modes; furthermore this positive influence on the electromechanical modes increases at increasing bandwidths of the controller up to 9.5 rad/s. However, at bandwidths above 9.5 rad/s, there is still a net positive influence on the damping of all of the torsional modes, but there is less damping added to the inertial mode by the action of the power flow controller than is the case at lower controller bandwidths.

The above results also demonstrate that the influence on torsional interaction of the design of the power flow controller in the constant power mode of operation is of the same nature for both categories of SSSCs. Figs. 5.4 and 6.6 demonstrate that with both types of SSSCs (X_{SSSC}-controlled SSSC and V_{SSSC}-controlled SSSC) the influence of an increasing bandwidth design of the power flow controller is still an increase in the damping of all the torsional modes, and initially in the damping of the inertial mode as well, although there is less positive damping added to the inertial mode beyond a certain critical controller bandwidth.

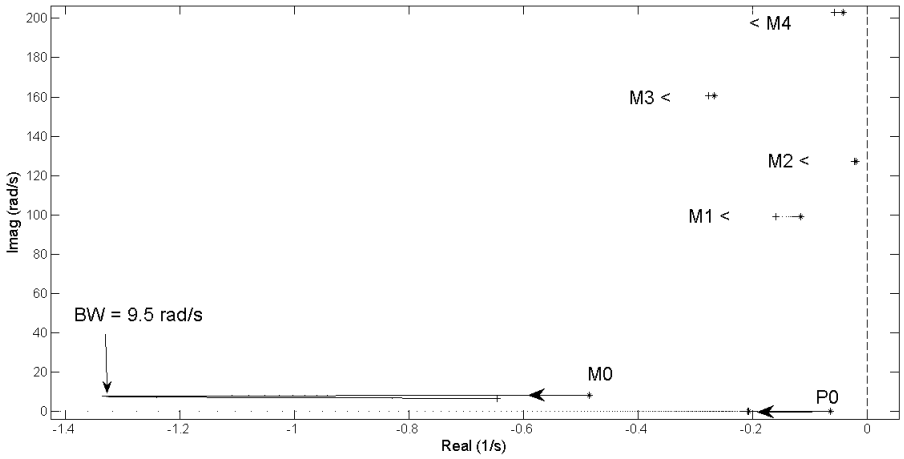

Fig. 6.6. Loci of the eigenvalues of the full study system as the V_{SSSC}-controlled SSSC-based power flow controller's bandwidth is varied from 0.13 rad/s to 33.5 rad/s.

The results presented thus far in this chapter have examined the influence of the V_{SSSC}-controlled SSSC-based power flow controller on torsional mode damping for the simplest case in which the only form of series compensation present in the system is the SSSC itself. As discussed in the previous chapter, it is necessary to understand the influence of the power flow controller design on the SSR characteristics of the SSSC in isolation from other complicating factors such as other sources of SSR in the transmission system. Hence, this chapter has initially examined the impact of the design of the power flow controller on the SSR characteristics of this V_{SSSC}-controlled SSSC compensated system without the presence of other series compensators in the adjacent transmission line. However, once such fundamental studies have been conducted, the knowledge and understanding gained from this simplest case of having the SSSC as the only series compensator in the system can be further extended to investigate how this V_{SSSC}-controlled SSSC and its power flow controls interact with other compensators in the transmission system that give rise to SSR as a result of their own resonant characteristics. Hence, the following sections of this chapter consider the influence of adding conventional capacitive series compensation in Line 2 as shown in Fig. 6.7.

6.6 SSR Characteristics of the Study System with Line 2 Compensated

The following eigenvalue studies aim to investigate the impact of the improved approach to designing the V_{SSSC}-controlled SSSC-based power flow controller on the damping of the electromechanical modes of the study system in the presence of conventional series capacitors in Line 2. However, in order to consider such a study, it is first necessary to identify a combination of values of V_{SSSC}-controlled SSSC-based compensation in Line 1 and conventional compensation in Line 2 for which the system is SSR-stable prior to the addition of the power flow controller in Line 1. In order to identify ranges of series compensation values over which all the electromechanical modes in a study system are stable, it is again useful to present the results of the eigenvalue scans in the alternative format in which the real parts of the eigenvalue loci are plotted as a function of the compensation value being varied; this format is adopted for the remainder of the eigenvalue results in this section of the chapter.

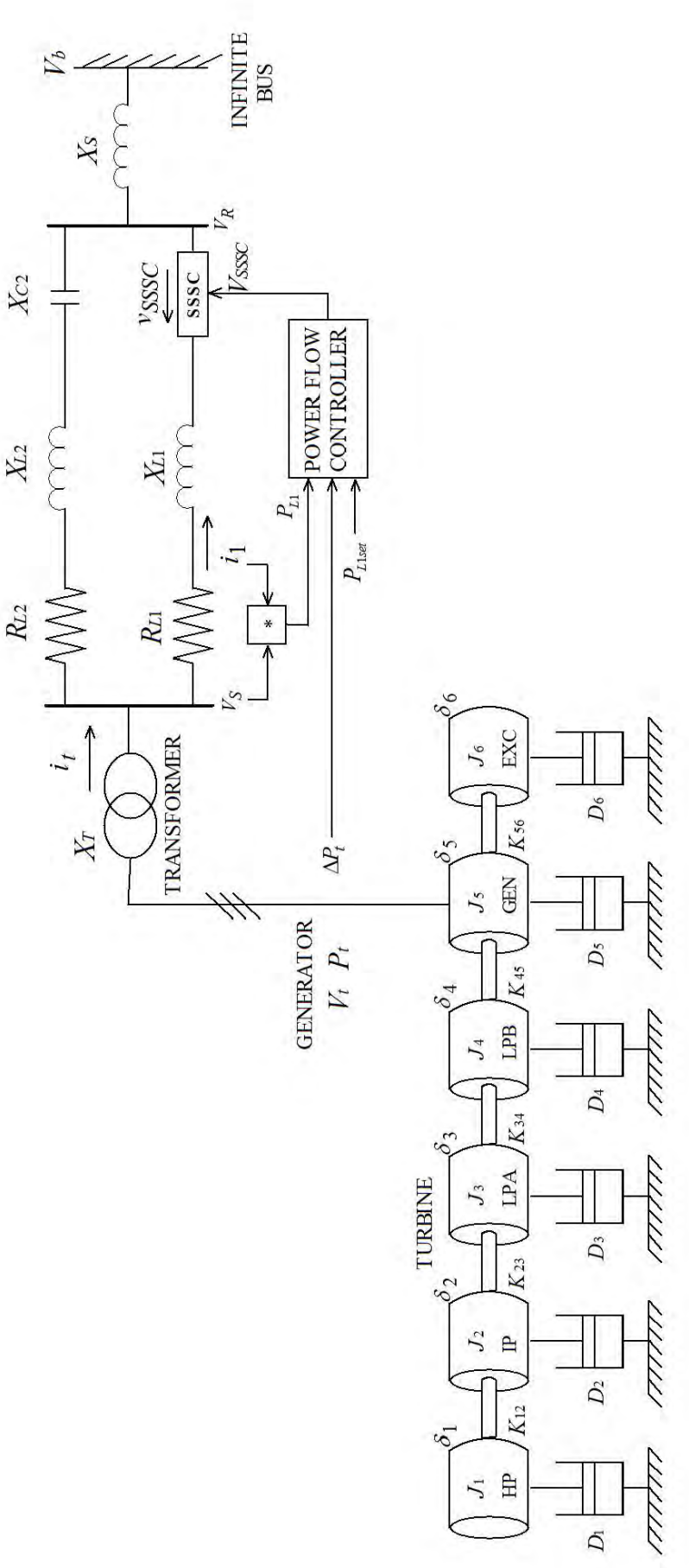

Fig. 6.7 Single line diagram of the study system with conventional series compensation in Line 2

6.6.1 Locating SSR-stable Ranges of Line 2 Compensation

In order to identify SSR-stable ranges of the series compensation in Line 2, the following study initially considers the SSR characteristics of the study system of Fig. 6.7 at different values of conventional series compensating reactance in Line 2, while the magnitude of the voltage injected by the V_{SSSC}-controlled SSSC in Line 1 is held fixed at V_{SSSC} = 0.03 pu., without the power flow controller enabled. The value of the conventional series compensating reactance in Line 2 is varied from X_{C2} = 0.10 pu. to X_{C2} = 0.95 pu. corresponding to an increase in the percentage compensation of transmission Line 2 from 10% to 95%. Fig. 6.8 shows the real parts of the eigenvalues associated with the torsional modes of this study system at each value of X_{C2} as the compensation in Line 2 is varied in this way.

It can be observed that as the conventional series compensation in Line 2 is increased, there is successive destabilisation of the mechanical torsional modes M4, M3, M2 and M1 as the real parts of the eigenvalues associated with each of these torsional modes moves into the positive plane of Fig. 6.8. It can be observed that there are certain ranges of series capacitive compensation in Line 2 where the real parts of all the torsional mode eigenvalues M1, M2, M3 and M4 are in the negative plane of Fig. 6.8 (that is all four torsional modes are simultaneously SSR-stable). Within these stable ranges, two specific values of series compensating reactance were chosen for further study in the remaining eigenvalue scans, case A: X_{C2} = 0.23 pu. and case B: X_{C2} = 0.36 pu. At each of these values of conventional series compensation in Line 2, the SSR characteristics of the V_{SSSC}-controlled SSSC compensation in Line 1 were then considered for a range of its compensation values.

6.6.2 Locating an SSR-stable Operating Point for the V_{SSSC}-controlled SSSC in Line 1 in the presence of Conventional Series Capacitors for the two Selected Cases in adjacent Line 2

In order to identify the SSR-stable operating ranges of the V_{SSSC}-controlled SSSC in Line 1 for each of the above two values of series capacitive compensation in Line 2, the eigenvalues of the study system were calculated as the magnitude of the voltage V_{SSSC} injected by the V_{SSSC}-controlled SSSC

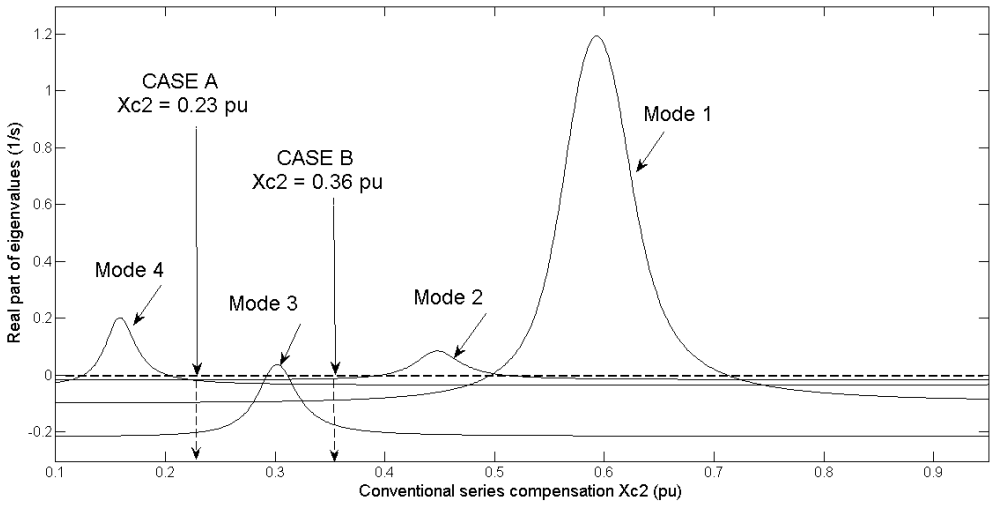

Fig. 6.8 Real parts of the eigenvalues of the study system as the conventional series compensation X_{C2} is varied from 0.1 pu. to 0.95 pu. with V_{SSSC} in Line 1 fixed at 0.03 pu.

is varied from 0.03 pu. to 0.51 pu, without power flow control enabled around the SSSC, with the series compensation X_{C2} in Line 2 fixed, in turn, at each of the values chosen in case A and case B. Fig. 6.9 shows the real parts of the eigenvalues associated with the torsional modes of this study system as the magnitude of the voltage V_{SSSC} injected by the SSSC in Line 1 is varied in this way with the compensation in Line 2 fixed at the value for case A: X_{C2} = 0.23 pu. It can be observed that as the magnitude of the injected voltage V_{SSSC} in Line 1 is increased the mechanical torsional mode M4 eventually becomes unstable as the real part of the eigenvalue associated with this particular torsional mode moves into the positive plane of Fig. 6.9. The results in Fig. 6.9 show that the SSR-stable operating range of the magnitude of the injected voltage in Line 1 is from V_{SSSC} = 0.03 pu. to a maximum value of V_{SSSC} = 0.11 pu. for the case A value of conventional compensation in Line 2, since at all values of V_{SSSC} above 0.11 pu, torsional mode M4 remains unstable.

Fig. 6.10 shows the real parts of the eigenvalues associated with the torsional modes of this study system as the magnitude of the voltage V_{SSSC} injected by the SSSC in Line 1 is again varied from 0.03 pu. to 0.51 pu. with the series compensation X_{C2} in Line 2 fixed at the value for case B: X_{C2} = 0.36 pu. It can be observed that as magnitude of the injected voltage V_{SSSC} in Line 1 is increased all the torsional modes M4, M3, M2 and M1 remain stable as the real parts of the eigenvalues associated with these torsional modes remain in the negative plane of Fig. 6.10. The results in Fig. 6.10 show that the entire operating range considered in this particular study for the magnitude of the voltage injected by the V_{SSSC}-controlled SSSC in Line 1 is SSR stable at the case B value of conventional series compensation in Line 2.

Figs. 6.9 and 6.10 have shown the SSR-stable operating ranges of the magnitude of the voltage injected by the V_{SSSC}-controlled SSSC in Line 1 at the two different values of capacitive reactance in Line 2 (case A and case B). In order to study the effect of the power flow controller on torsional mode damping at the two different values of conventional series compensation in Line 2 in these two cases, a common SSR-stable operating value of V_{SSSC0} = 0.1 pu. was used for the V_{SSSC}-controlled SSSC's set-point value of injected voltage in the eigenvalue studies that are to follow.

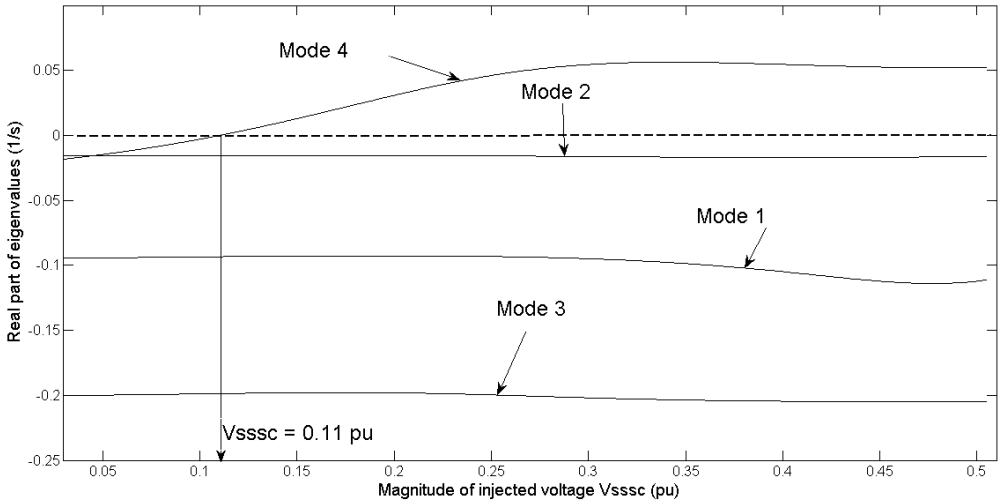

Fig. 6.9 Real parts of the eigenvalues of the study system as the magnitude of the voltage injected by the SSSC, (V_{SSSC} in Line 1) is varied from 0.03 pu. to 0.51 pu. while the conventional series capacitive reactance X_{C2} in Line 2 is fixed at 0.23 pu. (case A)

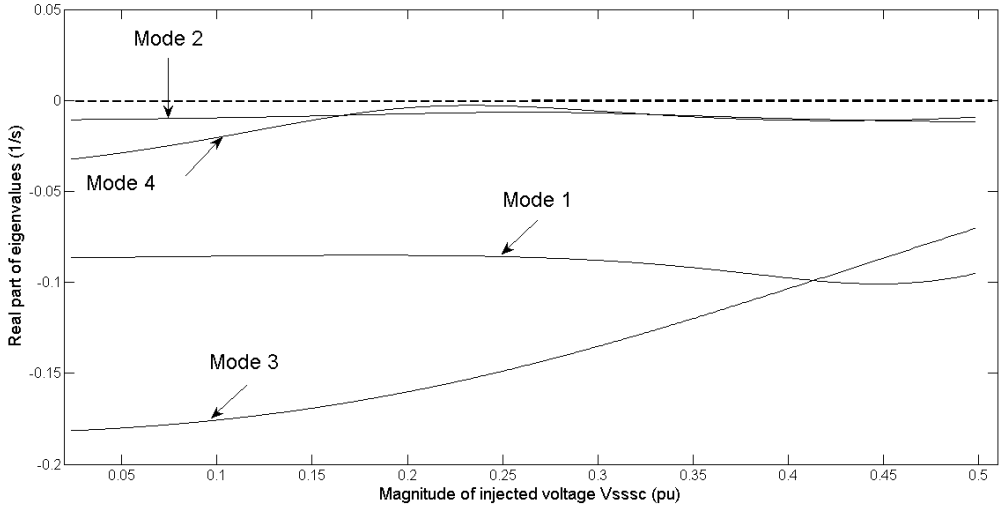

Fig. 6.10 Real parts of the eigenvalues of the study system as the magnitude of the voltage injected by the SSSC, (V_{SSSC} in Line 1) is varied from 0.03 pu. to 0.51 pu. while the conventional series capacitive reactance X_{C2} in Line 2 is fixed at 0.36 pu. (case B)

These studies consider the impact of the design of the power flow controller added around the V_{SSSC}-controlled SSSC on the damping of the electromechanical modes.

6.7 Impact of Quadrature Voltage-Controlled SSSC Power Flow Controller Design on the Damping of the Electromechanical Modes with Conventional Series Capacitors in Line 2

In the previous chapter, the impact on torsional interaction of a reactance-controlled SSSC power flow controller design in the presence of conventional series capacitors in the adjacent Line 2 was presented. In particular, Figs. 5.10 and 5.12 have demonstrated that even in the presence of conventional series capacitors in an adjacent line, which is an additional source of torsional interaction in the transmission system, the influence of the design of a reactance-controlled SSSC-based power flow controller in the constant power mode is still an increase in the damping of all the torsional modes, and initially in the damping of the inertial mode as well, although there is less positive damping added to the inertial mode beyond a certain critical controller bandwidth. In order to investigate the impact of a quadrature voltage-controlled SSSC-based power flow controller on the damping of the torsional modes of the study system of Fig. 6.7, which incorporates a conventional series capacitor in Line 2, the studies of Figs. 5.10 and 5.12 were repeated with the reactance-controlled SSSC replaced by a quadrature voltage-controlled SSSC. Fig. 6.11 shows the loci of the eigenvalues of the study system as the gains K_P and K_I of the power flow controller are together adjusted to increase the power flow controller bandwidth from 0.13 rad/s to 33.5 rad/s when the power flow controller is set to operate in constant power mode at a nominal value of V_{SSSC0} = 0.1 pu. and with X_{C2} fixed at 0.23 pu. (case A).

From Fig. 6.11 it can be observed that as the bandwidth of the power flow controller is increased, the real eigenvalue P0, corresponding to the closed-loop pole in the power flow controller transfer function, moves further into the left-hand plane. Fig. 6.11 also reveals that increasing the bandwidth of the power flow controller does influence the damping of the torsional modes of the study system. It can be observed that as the response time of the controller is made faster (up to a controller

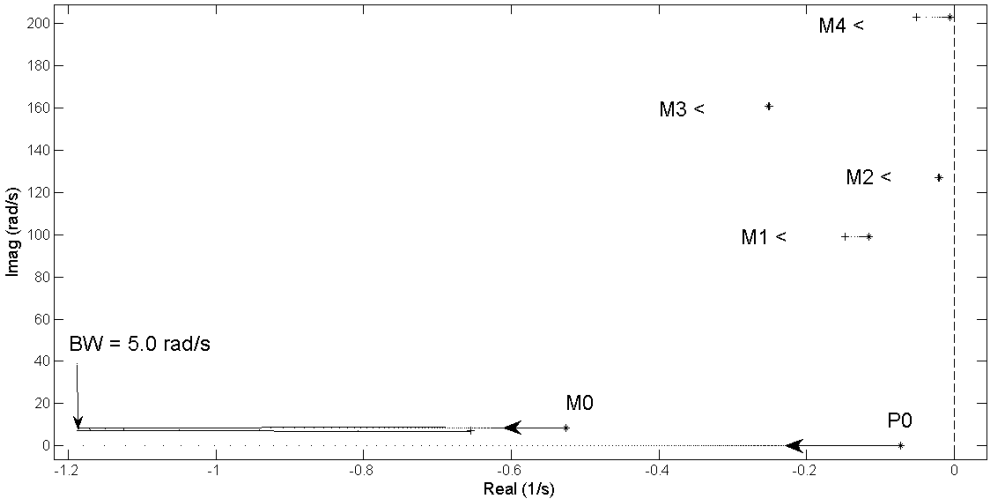

Fig. 6.11 Loci of the eigenvalues of the study system as the V_{SSSC}-controlled SSSC-based power flow controller's bandwidth is varied from 0.13 rad/s to 33.5 rad/s with the controller set in constant power mode, V_{SSSC0} = 0.1 pu. and X_{C2} = 0.23 pu. (case A).

bandwidth of 5.0 rad/s), the eigenvalues M1, M2, M3 and M4 associated with the torsional shaft modes, together with the eigenvalue M0 associated with the generator's inertial swing mode, all move to the left. However, when the controller's bandwidth is increased beyond 5.0 rad/s, all the torsional mode eigenvalues M1, M2, M3 and M4 continue to move towards the left, but the inertial mode eigenvalue M0 starts to move back towards the right hand plane. The result in Fig. 6.11 thus shows that in the constant power mode of operation, even with the presence of a fixed series capacitor in Line 2, the effect of the power flow controller is to increase the damping of the inertial swing mode as well as the damping of all of the torsional modes; furthermore this positive influence on the electromechanical modes increases at increasing bandwidths of the controller up to 5.0 rad/s. However, at controller bandwidths that are higher than 5.0 rad/s, while there is still an increasing positive influence on the damping of the torsional modes, the influence of the power flow controller on the inertial mode damping is less significant than is the case at lower bandwidths (although still net positive).

The above study was repeated for the second, case B value of compensation in Line 2, in which the fixed series capacitive reactance X_{C2} was set at 0.36 pu. with the results shown in Fig. 6.12. As expected, the real eigenvalue P0 associated with the response of the closed-loop pole of the power flow controller moves towards the left as the controller's bandwidth is increased from 0.13 rad/s to 33.5 rad/s. Fig. 6.12 shows that the controller's bandwidth design also affects the damping of the electromechanical modes of the study system at this different value of conventional series compensation in Line 2. It can be observed that as the response time of the controller is made faster (up to a controller bandwidth of 5.4 rad/s), the eigenvalues M1, M2, M3 and M4 associated with the torsional shaft modes, together with the eigenvalue M0 associated with the generator's inertial swing mode, all move to the left. However, when the controller bandwidth is increased beyond 5.4 rad/s, all the torsional mode eigenvalues M1, M2, M3 and M4 continue to move towards the left while the inertial mode eigenvalue M0 starts to move back towards the right.

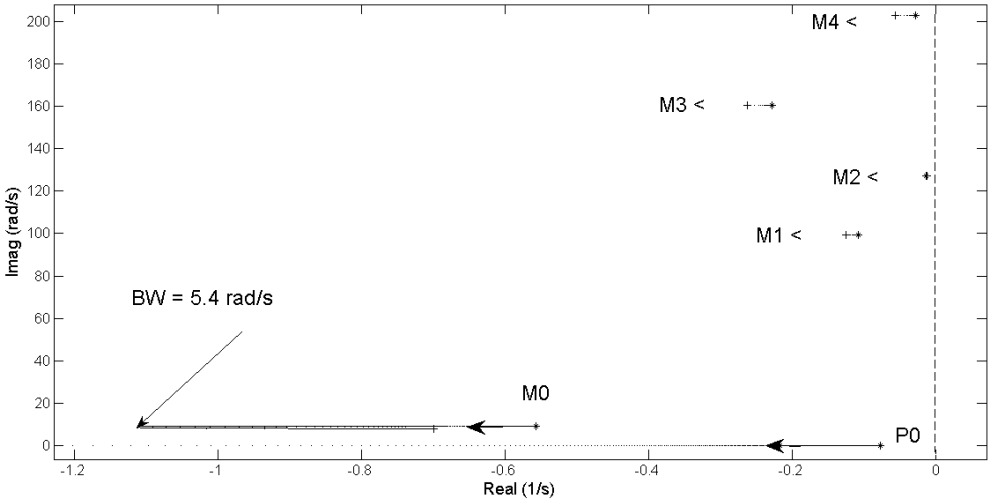

Fig. 6.12 Loci of the eigenvalues of the study system as the V_{SSSC}-controlled SSSC-based power flow controller's bandwidth is varied from 0.13 rad/s to 33.5 rad/s with the controller set in constant power mode, V_{SSSC0} = 0.1 pu. and X_{C2} = 0.36 pu. (case B).

The result in Fig. 6.12 thus shows that in the constant power mode of operation, even with the presence of a fixed series capacitor at a different value of conventional series compensation X_{C2} = 0.36 pu. in Line 2, the effect of the power flow controller is still to increase the damping of the inertial swing mode as well as the damping of all of the torsional modes; furthermore this positive influence on all of the electromechanical modes increases at increasing bandwidths of the controller up to 5.4 rad/s. However, at controller bandwidths that are higher than 5.4 rad/s, there is still a positive influence on the damping of all of the torsional modes, but there is less positive damping added to the inertial mode than at a bandwidth of 5.4 rad/s.

The above results also demonstrate that the influence on torsional interaction of the design of the power flow controller in the constant power mode of operation is of the same nature for both categories of SSSCs even with an additional source of torsional interaction in the adjacent line. Figs. 5.10 and 5.12 for the X_{SSSC}-controlled type of SSSC, and Figs. 6.11 and 6.12 for the V_{SSSC}-controlled type of SSSC, have thus demonstrated that for both types of SSSCs, even in the presence of conventional series capacitors in the adjacent line, the influence of the design of the power flow controller is still an increase in the damping of all the torsional modes, and initially in the damping of the inertial mode as well, although there is less positive damping added to the inertial mode beyond a certain critical controller bandwidth.

As discussed in the previous chapter, the positive impact of fast-responding constant power flow controllers on the damping of the torsional modes of the study system has the further benefit that it allows the SSSC, with its power flow controls, to be operated over a wider range of compensating values without risking SSR as the bandwidth of the controller is increased. The following section of the chapter investigates this issue for the V_{SSSC}-controlled type of SSSC by considering the SSR characteristics of the study system at two different bandwidths of the constant-power mode controller (the highest and lowest bandwidth designs just considered in this section) as the set-point value of the SSSC's injected voltage is varied.

6.8 SSR-stable Ranges of the Study System with V_{SSSC}-controlled SSSC-based Power Flow Controller set to operate in Constant Power Mode at different Controller Bandwidth Designs

In order to further demonstrate the stabilising effect of constant power flow controllers on the SSR characteristics of the study system, the following studies now consider the SSR characteristics of the study system over a range of values of the set-point voltage V_{SSSC0} injected by the SSSC for the lowest and highest controller bandwidth designs (0.13 rad/s and 33.5 rad/s) considered in the previous section. The investigations again start with the simplest case scenario of having the SSSC as the only form of series compensation in the study system (as shown in Fig. 6.1) and then go on to consider the more practical case of adding conventional capacitive compensation in Line 2 (as shown in Fig. 6.7).

6.8.1 Uncompensated Line 2

Fig. 6.13 shows the real parts of the eigenvalues associated with the torsional modes of the study system of Fig 6.1 (no series compensation in Line 2) as the SSSC's set-point value of injected voltage magnitude is increased from V_{SSSC0} = 0.04 pu. to V_{SSSC0} = 0.58 pu. for a fixed controller bandwidth value of 0.13 rad/s. Fig. 6.13 shows that as the set-point value of the SSSC's injected voltage is increased all the mechanical torsional modes M4, M2, M3 and M1 remain stable as the real parts of these torsional mode eigenvalues remain in the negative plane of Fig. 6.13. The results in Fig. 6.13 show that the entire range chosen for the SSSC's voltage magnitude set-point in this study is SSR stable for this particular value of controller bandwidth of 0.13 rad/s.

Fig. 6.14 shows the real parts of the eigenvalues associated with the torsional modes of the study system as the set-point value of the SSSC's injected voltage magnitude is again increased from V_{SSSC0} = 0.04 pu. to V_{SSSC0} = 0.58 pu. for a fixed controller bandwidth value of 33.5 rad/s. It can be observed that as the set-point value of the SSSC's injected voltage is increased the mechanical torsional modes M4, M3, M2 and M1 again all remain stable as the real parts of these torsional mode eigenvalues remain in the negative plane of Fig. 6.14. The results in Fig. 6.14 show that the

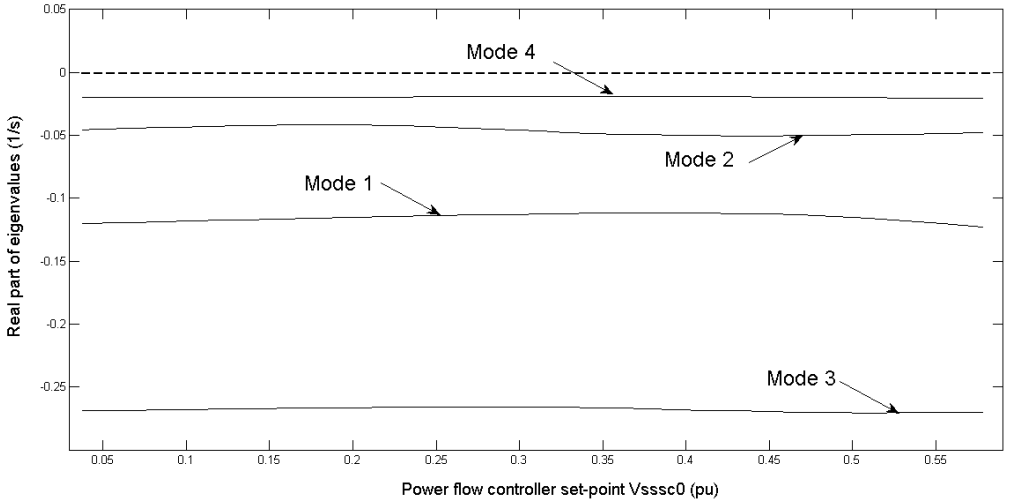

Fig. 6.13 Real parts of the eigenvalues of the study system as the set-point value of the SSSC's injected voltage magnitude V_{SSSC0} is varied from 0.04 pu. to 0.58 pu. at a fixed controller bandwidth of 0.13 rad/s.

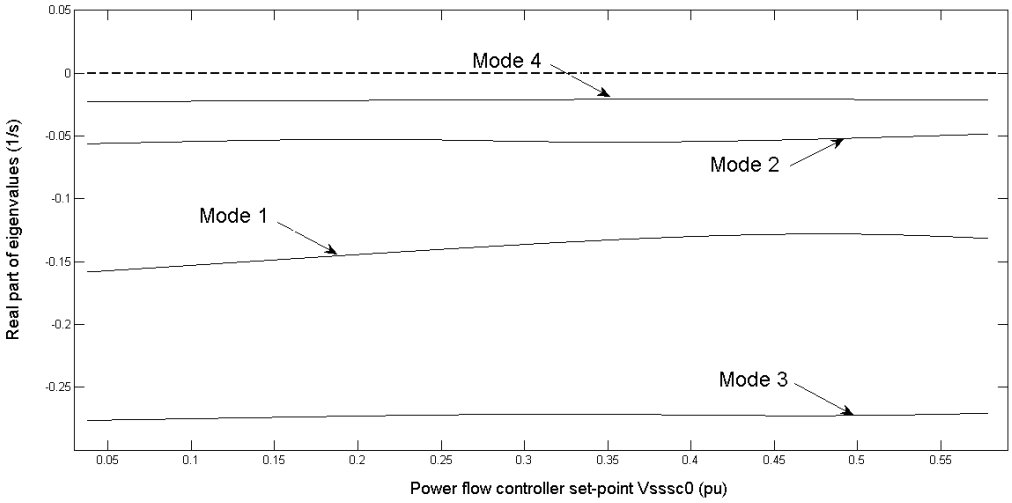

Fig. 6.14 Real parts of the eigenvalues of the study system as the set-point value of the SSSC's injected voltage magnitude V_{SSSC0} is varied from 0.04 pu. to 0.58 pu. at a fixed controller bandwidth of 33.5 rad/s.

entire chosen operating range of the SSSC's voltage magnitude is SSR stable for this particular value of controller bandwidth of 33.5 rad/s.

Figs. 6.13 and 6.14 therefore show that the entire range of selected voltage magnitude set-points for the SSSC can be used at all power flow controller bandwidth designs as the study system remains SSR stable. Furthermore Fig. 6.14 shows that the torsional modes are further stabilised by the action of the faster responding power flow controller as the real parts of all torsional mode eigenvalues are located further away from the positive plane in comparison with the real parts of all the torsional mode eigenvalues in Fig 6.13.

In the previous chapter it was shown that the influence of a faster-operating power flow controller was to permit a wider operating range of SSR-stable values of X_{SSSC0} set-points in the case of a reactance-controlled SSSC (Figs. 5.14 and 5.15) although this widened operating range was nevertheless still relatively limited. However, in this chapter, with the study system incorporating a quadrature voltage-controlled SSSC that is known to have better SSR characteristics, Figs. 6.13 and 6.14 show that the entire studied range of injected voltage magnitude set points V_{SSSC0} can in fact be used without causing SSR. Hence, when considering this simplest case in which the SSSC is the only potential source of SSR in the transmission lines of the study system, quadrature voltage-controlled SSSC-based power flow controllers have been shown to allow a significantly wider range of operating set-points of the SSSC when compared to reactance-controlled SSSC-based power flow controllers. The following subsection now examines the same issue for two different values of conventional series compensation in Line 2.

6.8.2 Conventionally-Compensated Line 2

In section 6.7 the impact of the power flow controller bandwidth on SSR stability was examined for two specific values of fixed, conventional series compensation in Line 2: X_{C2} = 0.23 pu. (case A) and X_{C2} = 0.36 pu. (case B). This section now considers the SSR-stable ranges of the SSSC's magnitude of injected voltage in Line 1 for the lowest and highest bandwidth designs considered for a constant-power controller at each of these values of conventional compensation in Line 2.

Fig. 6.15 shows the real parts of the eigenvalues associated with the torsional modes of the study system as the set-point value of the SSSC's injected voltage magnitude is increased from V_{SSSC0} = 0.04 pu. to V_{SSSC0} = 0.58 pu. for a fixed controller bandwidth value of 0.13 rad/s with the series compensation in Line 2 fixed at a value of X_{C2} = 0.23 pu. Fig. 6.15 shows that as the set-point value of the SSSC's injected voltage magnitude is increased the mechanical torsional mode M4 is destabilised as the real part of the torsional mode eigenvalue M4 moves into the positive plane. Fig. 6.15 shows that the SSR-stable operating range of the SSSC's set-point voltage for this particular value of controller bandwidth of 0.13 rad/s is from V_{SSSC0} = 0.04 pu. to V_{SSSC0} = 0.18 pu. beyond which, torsional mode M4 remains unstable.

Fig. 6.16 shows the real parts of the eigenvalues associated with the torsional modes of the study system as the set-point value of the SSSC's injected voltage magnitude is again increased from V_{SSSC0} = 0.04 pu. to V_{SSSC0} = 0.58 pu. for a controller bandwidth value of 33.5 rad/s with the series compensation in Line 2 fixed at a value of X_{C2} = 0.23 pu. It can be observed that as the set-point value of the SSSC's injected voltage magnitude is increased the mechanical torsional mode M4 is destabilised as the real part of the eigenvalue associated with torsional mode M4 moves into the positive plane of Fig. 6.16. The results in Fig. 6.16 show that the SSR-stable operating range of the SSSC's set-point voltage for this particular value of controller bandwidth of 33.5 rad/s is from V_{SSSC0} = 0.04 pu. to V_{SSSC0} = 0.26 pu. beyond which, torsional mode M4 remains unstable.

Figs. 6.15 and 6.16 show that the SSR-stable operating ranges of SSSC injected voltage set-points are more limited in this more complex case where there is a conventional series capacitor in Line 2 as compared to the unrestricted range of operation when Line 2 is uncompensated (c.f. Figs. 6.13 and 6.14). However, Fig. 6.16 again demonstrates that even in the presence of conventional series compensation in the adjacent line, a fast-operating constant power flow controller permits a wider operating range of SSR-stable values of SSSC injected voltage set-point as compared to the operating range possible at the lower power flow controller bandwidth in Fig. 6.15. Hence, the above studies

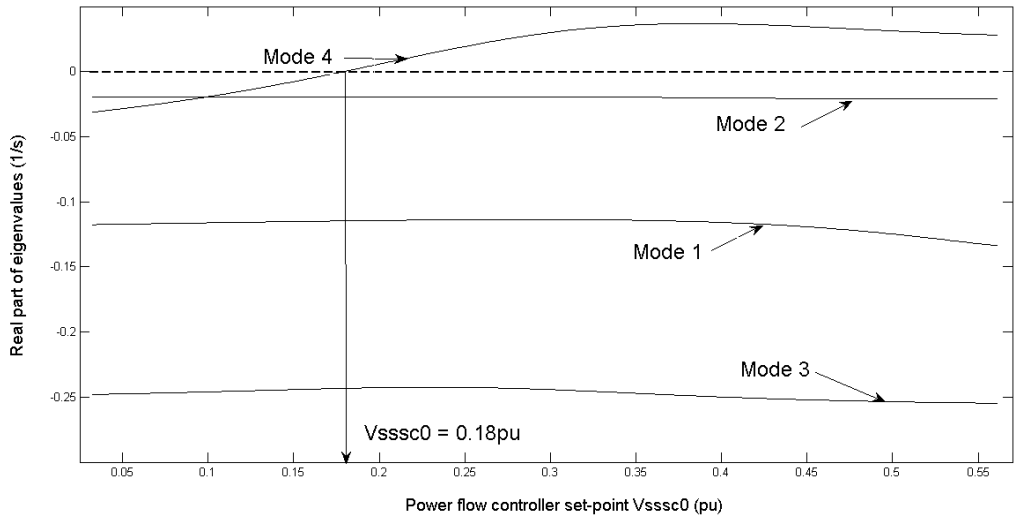

Fig. 6.15 Real parts of the eigenvalues of the study system as the set-point value of the SSSC's injected voltage magnitude V_{SSSC0} is varied from 0.04 pu. to 0.58 pu. at a fixed controller bandwidth of 0.13 rad/s with the series capacitive reactance X_{C2} in Line 2 fixed at 0.23 pu.

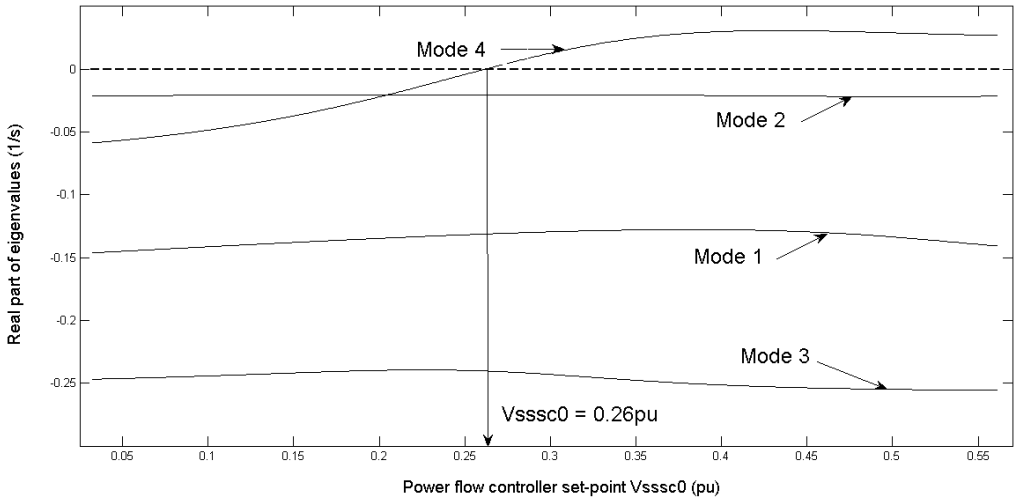

Fig. 6.16 Real parts of the eigenvalues of the study system as the set-point value of the SSSC's injected voltage magnitude V_{SSSC0} is varied from 0.04 pu. to 0.58 pu. at a fixed controller bandwidth of 33.5 rad/s with the series capacitive reactance X_{C2} in Line 2 fixed at 0.23 pu.

clearly demonstrate that even in this more practical case where there are two potential sources of SSR in the transmission system, a much faster power flow controller design has shown further improvement in the SSR characteristics of the study system such that a wider range of operating points of the power flow controller can be employed.

The above study was repeated for the second value of conventional series compensation in Line 2, in which the fixed series capacitive reactance X_{C2} was set at 0.36 pu. Fig. 6.17 shows the real parts of the eigenvalues associated with the torsional modes of the study system as the set-point value of the SSSC's injected voltage magnitude is increased from V_{SSSC0} = 0.04 pu. to V_{SSSC0} = 0.58 pu. for a fixed controller bandwidth value of 0.13 rad/s with the series compensation in Line 2 fixed at a value of X_{C2} = 0.36 pu. Fig. 6.17 shows that as the set-point value of the SSSC's injected voltage magnitude

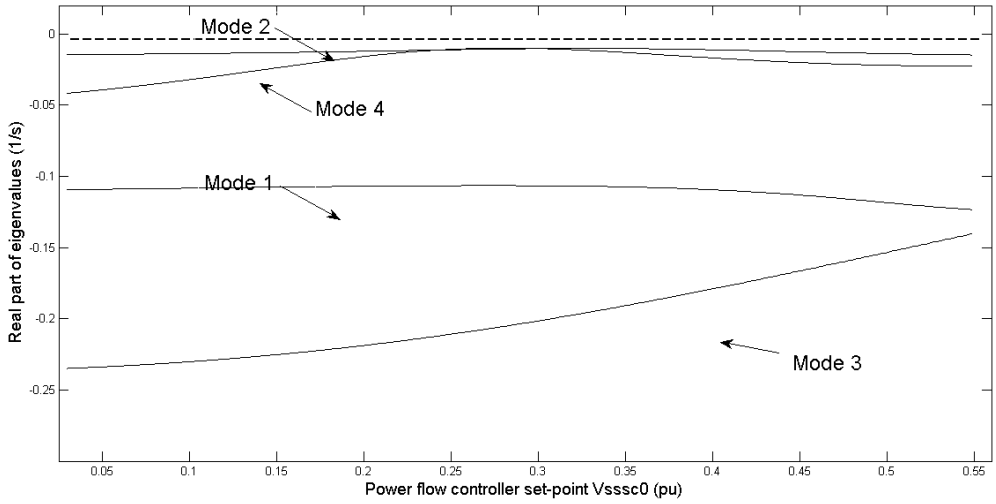

Fig. 6.17 Real parts of the eigenvalues of the study system as the set-point value of the SSSC's injected voltage magnitude V_{SSSC0} is varied from 0.04 pu. to 0.58 pu. at a fixed controller bandwidth of 0.13 rad/s with the series capacitive reactance X_{C2} in Line 2 fixed at 0.36 pu.

is increased, all the mechanical torsional modes M4, M2, M3 and M1 remain stable as the real parts of these torsional mode eigenvalues remain in the negative plane. Fig. 6.17 shows that the entire range chosen for the SSSC's voltage magnitude set-point in this case is SSR-stable for this particular value of controller bandwidth of 0.13 rad/s.

Fig. 6.18 shows the real part of the eigenvalues associated with the torsional modes of the study system as the set-point value of the SSSC's injected voltage magnitude is again increased from V_{SSSC0} = 0.04 pu. to V_{SSSC0} = 0.58 pu. for a fixed controller bandwidth value of 33.5 rad/s with the series compensation in Line 2 fixed at a value of X_{C2} = 0.36 pu. It can be observed that as the set-point value of the SSSC's injected voltage magnitude is increased, all the mechanical torsional modes M4, M2, M3 and M1 remain stable as the real parts of these torsional mode eigenvalues remain in the negative plane of Fig. 6.18. The results in Fig. 6.18 thus show that not only is the entire range of chosen SSSC set-point values also SSR-stable for this highest value of power flow controller bandwidth, but also, in comparison with Fig. 6.17, the results show that this faster-responding power flow controller further stabilises all the torsional modes as the real parts of the eigenvalues are located further into the negative plane of Fig. 6.18.

Hence, firstly the results of this section provide further confirmation that the influence of a constant-power mode power flow controller (in this case based on a quadrature voltage type SSSC) is to add stabilising damping to all the torsional modes and that this stabilising effect on the modes increases as the controller bandwidth is made higher. This has been shown to be the case when the V_{SSSC}-type SSSC on which the power flow controller in this chapter is based is the only source of series compensation in the study system, or for the more practical case where other conventional series capacitor compensation is present in an adjacent line, and for different values of such conventional compensation.

Secondly, the results show that in some cases, the stabilising impact on torsional modes of adding a fast-acting power flow controller around a V_{SSSC}-type of SSSC is sufficient to allow unrestricted variation in the SSSC's controllable compensation without the risk of SSR, even in the presence of

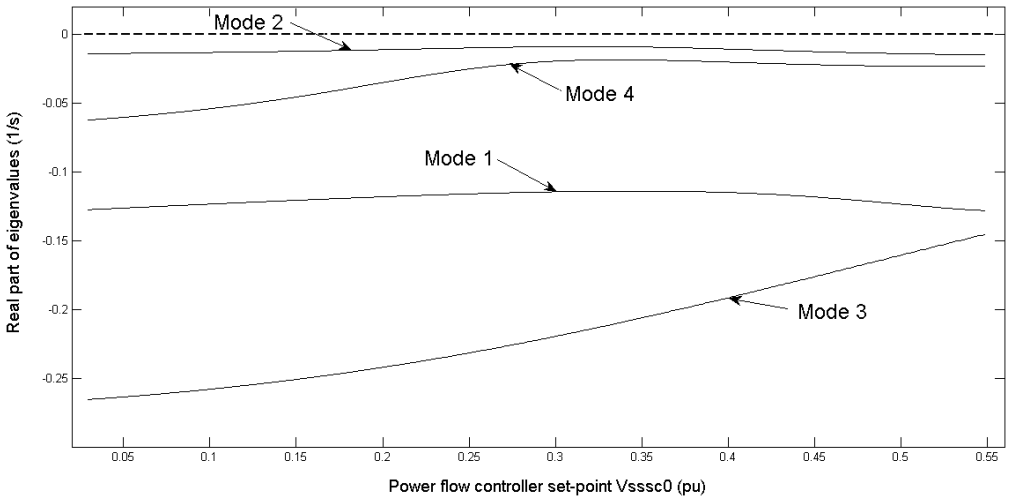

Fig. 6.18 Real parts of the eigenvalues of the study system as the set-point value of the SSSC's injected voltage magnitude V_{SSSC0} is varied from 0.04 pu. to 0.58 pu. at a fixed controller bandwidth of 33.5 rad/s with the series capacitive reactance X_{C2} in Line 2 fixed at 0.36 pu.

conventional compensation elsewhere in the system, whilst in other cases a wider, but not complete range of SSSC operation is made possible by the power flow controls. Similar findings were made in Chapter Five in respect of the stabilising impact of constant power controls applied around a X_{SSSC}-type of SSSC, but because that type of SSSC is itself inherently more prone to torsional interaction, the degree to which the operating range of the SSSC could be extended without risk to SSR was shown to be more modest, both with and without conventional series compensation elsewhere in the system.

The results in this chapter have thus demonstrated that in the constant power mode of operation, quadrature voltage-controlled SSSC-based power flow controllers in fact enable much wider SSR-stable operating ranges of the SSSC, and hence in the power flow controller itself, as compared to reactance-controlled SSSC-based power flow controllers. Furthermore, this advantage of using quadrature voltage-controlled SSSC-based power flow controllers is also present in transmission systems that incorporate conventional series capacitors in the adjacent lines. However in such practical environments, only certain specific conventional series compensation levels in the adjacent line will enable such wide operating ranges of the power flow controller to be realised without risk of SSR.

6.9 Conclusion

Chapter Six has initially verified the correctness of the mathematical model of the power flow controller that has been implemented around the quadrature voltage-controlled SSSC in the study system used in this thesis. The initial eigenvalue results of this chapter also confirmed the findings made by others [18,19] in showing the important differences in the SSR characteristics of the quadrature voltage-controlled SSSC in comparison to the reactance-controlled SSSC when each are used as stand-alone devices, further verifying the models used. The results also extend the findings of [18] to demonstrate that the V_{SSSC}-controlled SSSC is also more SSR-stable than the X_{SSSC}-controlled SSSC as a stand-alone device in a more complex transmission system that incorporates an additional transmission line in parallel. In fact, for the study system used in this thesis, the results show that the V_{SSSC}-controlled SSSC as a stand-alone device, and with no other source of SSR in the transmission system, does itself cause torsional interaction but the destabilising effect of this torsional interaction is however not sufficient to cause SSR.

The results in this chapter also demonstrate that just as is the case for X_{SSSC}-controlled, SSSC-based constant-power controllers, the design of V_{SSSC}-controlled SSSC-based constant-power flow controllers also influences the damping of generator electromechanical modes (torsional and inertial): the influence of increased controller bandwidth is once again an increase in the damping of all the torsional modes, and initially in the damping of the inertial mode as well, although there is less positive damping added to the inertial mode beyond a certain critical controller bandwidth. This positive influence of the power flow controller design on torsional interaction has also been observed for the more practical case of having conventional series capacitors included in the adjacent transmission line of the study system.

The results further show that in some cases, this stabilising impact on torsional modes of adding a fast-acting power flow controller around a V_{SSSC}-type of SSSC is sufficient to allow unrestricted variation in the SSSC's controllable compensation without the risk of SSR, even in the presence of

conventional compensation elsewhere in the system, whilst in other cases a wider, but not completely unrestricted range of SSSC operation is made possible by the power flow controls. Similar findings were made in Chapter Five in respect of the stabilising impact of constant power controls applied around a X_{SSSC}-type of SSSC, but because that type of SSSC is itself inherently more prone to torsional interaction, the degree to which the operating range of the SSSC could be extended without the risk to SSR was shown to be more modest, both with and without conventional series compensation elsewhere in the system.

Hence, in SSR-susceptible systems, V_{SSSC}-controlled SSSC-based power flow controllers are clearly preferable because of the much wider SSR-stable operating range that is possible. However, in more practical environments even if V_{SSSC}-controlled SSSC-based power flow controllers were to be employed, careful SSR analysis would still be required to fully understand the impact on stability of actual compensators in the system.

CHAPTER SEVEN

CONCLUSION

7.1 Introduction

The initial part of this thesis has dealt with the development of mathematical models of a representative study system which is an adaptation of the IEEE First Benchmark system for the study of SSR to allow it to be used to analyse the effect of closed-loop power flow control on SSR stability. Although there are various FACTS series compensators that can be used for power flow control applications, the thesis has considered the use of one of the family of FACTS series compensators in particular, namely the Static Synchronous Series Compensator (SSSC), to carry out closed loop control of AC power flow in a transmission system.

The thesis has then used the detailed mathematical models of the studied power system to investigate the impact on torsional interaction of SSSC-based power flow controllers with and without the presence of conventional series capacitors in an adjacent line of the transmission system. Furthermore, two main types of SSSC implementation, namely the reactance-controlled and the quadrature voltage-controlled types (also referred to in this thesis as X_{SSSC}-controlled and V_{SSSC}-controlled devices) have been considered since both of these types of SSSC have the potential to excite SSR and there are important differences in their SSR characteristics as stand-alone devices [18,19].

This chapter now summarises and reviews the main findings and conclusions drawn from the previous chapters. The chapter also suggests further research work that may be undertaken in this area.

7.2 Detailed Mathematical Model

The mathematical models of the study system developed in Matlab for the simulation studies and analyses in this thesis have been presented in Chapter Three. The dynamics of each element of the chosen study system have been represented in detail in order to predict SSR in an affected machine and its interaction with the system components. The mathematical model of the study system, which is an adaptation of the IEEE First Benchmark Model for SSR studies, provides the flexibility of allowing FACTS series compensation or conventional series capacitors in either of the transmission lines of the system. This Matlab-coded model of the study system provides the functionality to conduct both non-linear time domain simulations as well as numerical linearisation of the model equations required for eigenvalue and transfer function analysis. However, prior to the use of the mathematical models for analyses in the subsequent chapters of this thesis, such user-written models were validated against known and proven dynamic models to the full extent possible.

For this reason, comparisons of the dynamic models of the generator electrical system, torsional spring mass model, and conventionally compensated parallel line transmission system developed for this thesis have been validated by direct comparison against PSCAD simulations (The dynamic

models of the SSSC used in this thesis, have already been extensively validated against measured results by others [92]; the validation of the power flow controller models derived for this thesis are validated using specific tests on the simulation model of the study system in Chapter Four and Chapter Six of the thesis).

7.3 Reactance-Controlled SSSC-based Power Flow Controls

The first part of this thesis examined the impact of adding a closed-loop power flow controller around a reactance-controlled SSSC. The eigenvalue results confirmed that a closed-loop power flow controller can affect the small-signal damping characteristics of the inertial swing modes of generators feeding a power system, and in particular that the nature and extent of these effects on the system's stability depend on both the mode in which the power flow controller is operated and its controller response time. The eigenvalue results have therefore reinforced the findings previously reported in [17] which considered only the issue of generator inertial swing mode characteristics and which relied solely on time-domain simulation results. However, based on the findings in [17,65,87,88] that were initially discussed in the literature review, a logical concern was raised as to whether a closed-loop power flow controller could also impact on the SSR stability of any generators with multi-inertia turbines that are susceptible to torsional interaction. Hence Chapter Four of this thesis has presented the results of studies aimed at initially confirming whether one particular form of controllable series compensation, the reactance-controlled SSSC, as well as various forms of high-level system controls implemented around an X_{SSSC}-controlled SSSC, can influence the subsynchronous oscillations in neighbouring turbine-generators. In particular, the results have been able to show, using detailed mathematical models of the chosen study system, that the addition of a closed-loop power flow controller around an X_{SSSC}-controlled SSSC has a significant effect on the damping of generator torsional modes, and, in particular how this effect on torsional mode damping is influenced by the speed at which the power flow controls are designed to respond and, importantly, by the mode of operation selected for the power flow controller.

In particular, the results have shown that in the constant power mode, a fast-responding power flow controller adds damping to both the generator inertial swing mode as well as to all of the turbine's torsional modes. Furthermore, it has been confirmed that this positive impact on torsional mode damping occurs over a range of different operating conditions, and not just at a single operating point; this is an important consideration because by its very nature a power flow controller is intended, in practice, to vary the degree of compensation provided by the X_{SSSC}-controlled SSSC over a range of values in response to the normal variations in transmission system loading levels. By contrast, in the constant angle mode, a fast-responding power flow controller design has been shown to significantly reduce the damping of the inertial swing mode. However, for this mode of operation, the influence of the power flow controls on torsional mode damping has been shown in this thesis to be operating point dependent: at certain operating points the influence of a fast-responding constant angle controller adds damping to a particular torsional mode, while it acts to reduce the damping of the same mode at other operating points.

Thus, not only have the results of these studies shown that a power flow controller influences the damping of shaft torsional modes but, importantly, as a result of these studies it can be concluded that when using X_{SSSC}-controlled SSSC-based power flow controllers in the presence of SSR-susceptible generators, it is clearly preferable to use such controls only in the constant power mode

and not in the constant angle mode of control, so as to avoid destabilising either the inertial swing mode or any turbine shaft torsional modes. Furthermore, even though the studies have shown that the constant power mode of operation is preferable in SSR-susceptible systems because of its positive impact on torsional mode damping over a range of operating conditions, the results nevertheless show that careful SSR analysis is required when designing such controls so as to ensure torsional stability is maintained over the full range of compensation values envisaged for the particular torsional mode frequencies that are present in each particular system in which such schemes are to be deployed.

The designs of the reactance-controlled, SSSC-based power flow controller initially considered for study in Chapter Four of the thesis are relatively slow-responding when compared to the response times of power flow controllers reported in other work, such as [65,95]. Indeed, the results in [65,95] have shown that very fast-response power flow controllers not only can be achieved, but also have been seriously considered in the literature. Furthermore, the discussions reported in [65] in particular also appear, at first glance, to suggest different conclusions to those that were reached in Chapter Four regarding the influence of a constant power flow controller on the damping of the electromechanical modes. Specifically, it had been reported in [65] that a fast-responding constant power flow controller had a detrimental impact on the damping of both inertial and torsional modes, whereas with the initial design method considered in Chapter Four of this thesis it was observed that the constant power flow controller had a beneficial impact on the damping of both the inertial and torsional modes over a range of operating points.

7.4 An Improved Design of Reactance-Controlled SSSC-based Power Flow Controls

Chapter Five of the thesis therefore presented an improved design of the gains of the power flow controller in this study system that allows much higher-bandwidth controllers to be achieved that are comparable to other fast-responding power flow controllers reported in the literature [65,95]. Chapter Five then considered whether the findings reported using the initial controller design approach of Chapter Four, also hold true for fast-responding controllers, particularly in light of the different observations described in [65]. In the process, it has been shown that the alternative approach to pole-zero placement used in this improved design method not only allows greater controller bandwidths to be attained, but, in the case of constant-power type controllers, allows significantly improved stabilisation of all generator electromechanical modes (torsional and inertial) to be achieved.

Detailed studies were presented in Chapter Five to confirm not only that a constant power mode controller adds stabilising damping to all torsional modes, and is able to do so even in the presence of conventional series compensation in an adjacent line, but that this stabilisation can be increased by a faster acting power flow controller. However, the results also showed that although the design of the power flow controller's bandwidth can be made very fast, the mode of operation chosen for the power flow controller does impose some limitations on its controller bandwidth design. For the different operating conditions of the transmission network considered in this thesis, it was observed that in the constant power mode of operation, for controller bandwidths beyond certain critical values, damping does begin to be removed from the inertial mode as the bandwidth increases, although the net impact of the power flow controller on damping remained positive at all bandwidths considered. Hence, by considering a wider range of controller bandwidths for study,

compared to the range of controller bandwidths considered in [65], the results in this thesis are of wider scope than those in [65] and arguably extend the findings of that study, by demonstrating the change in the influence of the controller response times on damping beyond a critical value of bandwidth.

In other words, in light of the findings in this thesis, the apparently different observations reported in [65] may well in fact be consistent with those of this thesis, and simply be valid over a narrower range of conditions than those considered here: that is, if the range of controller bandwidths considered for study in [65] lay above the critical controller bandwidth identified here, then within that narrower range of controller bandwidths considered in [65] the damping of the inertial mode would appear only to decrease at increasing controller bandwidths. By contrast, by also considering lower bandwidth designs, the results in this thesis also demonstrate that the influence of increasing controller bandwidth in a range that lies below the critical bandwidth value is to add damping to the inertial mode.

As a result of considering a wider range of controller bandwidths for study, the results in this thesis have also shown that if the aim is to optimise the damping of all the electromechanical modes, a bandwidth equal to this critical value will be the best design of the controller for the constant power mode. However, if the aim is to achieve the fastest possible power flow controller response, the maximum achievable bandwidth can be used since all the electromechanical modes are still stable at this highest controller bandwidth. The observations described in [65], where a much higher upper limit was used in the range of controller bandwidths considered, further suggested that at very fast controller bandwidths, the effect of increasing controller bandwidths may also be to destabilise the torsional modes. However, it is difficult to comment in depth on the likely reasons for this conclusion since the studies in [65] employed a TCSC, which has distinct SSR characteristics to those of the SSSC.

The investigations using the improved controller design approach in Chapter Five added further weight to the conclusions, reached in Chapter Four, that the alternative mode of operation of a power flow controller that has been proposed in the literature (constant angle mode) is not suitable for environments where SSR is a concern. In particular, this mode of control has been shown to destabilise a number of generator torsional modes in the study system, with the extent of the destabilisation of torsional mode 4 and the inertial swing mode being very sensitive to the system operating conditions and power flow controller design.

7.5 Quadrature Voltage-Controlled SSSC-based Power Flow Controls

Chapter Six of the thesis presented the results of the studies into the influence of power flow controllers implemented around a quadrature voltage-controlled SSSC. The initial eigenvalue results of Chapter Six have confirmed the findings made by others [18,19] in showing the important differences in the SSR characteristics of the quadrature voltage-controlled SSSC in comparison to the reactance-controlled SSSC when each are used as stand-alone devices, further verifying the mathematical models of these devices used in this thesis. This thesis also extends the findings of [18] to demonstrate that the V_{SSSC}-controlled SSSC is also more SSR-stable than the X_{SSSC}-controlled SSSC as a stand-alone device in a more complex transmission system that incorporates an additional transmission line in parallel. In fact, for the study system used in this thesis, the results show that the V_{SSSC}-controlled SSSC as a stand-alone device, and with no other source of SSR in the transmission

system, does itself cause torsional interaction but the destabilising effect of this torsional interaction is however not sufficient to cause SSR.

This thesis has further demonstrated that just as is the case for X_{SSSC}-controlled, SSSC-based constant-power controllers, the design of V_{SSSC}-controlled SSSC-based constant-power flow controllers also influences the damping of generator electromechanical modes (torsional and inertial): the influence of increased controller bandwidth is once again an increase in the damping of all the torsional modes, and initially in the damping of the inertial mode as well, although there is, again, less positive damping added to the inertial mode beyond a certain critical controller bandwidth. This positive influence of the power flow controller design on torsional interaction has also been observed for the more practical case of having conventional series capacitors included in the adjacent transmission line of the study system.

The results further show that in some cases, this stabilising impact on torsional modes of adding a fast-acting power flow controller around a V_{SSSC}-type of SSSC is sufficient to allow unrestricted variation in the SSSC's controllable compensation without the risk of SSR, even in the presence of conventional compensation elsewhere in the system, whilst in other cases a wider, but not completely unrestricted range of SSSC operation is made possible by the power flow controls. Similar findings were made in Chapter Five in respect of the stabilising impact of constant power controls applied around a X_{SSSC}-type of SSSC, but because that type of SSSC is itself inherently more prone to torsional interaction, the degree to which the operating range of the SSSC could be extended without the risk to SSR was shown to be more modest, both with and without conventional series compensation elsewhere in the system.

Hence, in SSR-susceptible systems, V_{SSSC}-controlled SSSC-based power flow controllers are clearly preferable because of the much wider SSR-stable operating range that is possible. However, in more practical environments even if V_{SSSC}-controlled SSSC-based power flow controllers were to be employed, careful SSR analysis would still be required to fully understand the impact on stability of actual compensators in the system.

7.6 Suggestions for Further Work

This thesis has presented an investigation into the impact of closed-loop SSSC-based power flow controllers on torsional interaction. However, there are further areas in this field of FACTS-based power flow controllers that still need to be investigated. Some suggestions for further work are as follows.

(a) This thesis has focused on only the SSSC which is one member of the family FACTS series compensators. The study system developed in this thesis has initially been used to investigate the SSR characteristics of the SSSC as a standalone device in more complex transmission system that incorporates an additional transmission line in parallel which has the flexibility of including series compensation. This study can also be extended to consider other FACTS devices such as the TCSC or the UPFC in order to investigate the SSR characteristics of these compensators as stand-alone FACTS devices in a more complex transmission system.

(b) As discussed in Chapter Five, some of the findings made by others in [65] with regards to the impact of a fast-responding TCSC-based power flow controller on the damping of certain particular torsional modes are different to the conclusions drawn from the results obtained this thesis with respect to the SSSC. Hence, the other FACTS compensators such as the TCSC or the UPFC which have different SSR characteristics as compared to the SSSC, can also be considered in this research study to investigate their impact on torsional interaction when closed-loop power flow controls are implemented around them.

(c) Practical confirmation of the findings of this thesis could be considered by the implementation of a scaled-down laboratory test system. Prior to a full practical investigation, the hardware implementation of the firing control system and the voltage source inverter can be initially considered in a hardware-in-loop test using the Real Time Digital Simulator which was recently purchased by the University to confirm the findings made in this thesis. Finally, the full practical investigation can also be considered by using the Micro-alternators in the Machines Research Laboratory which are multi-inertia turbine-generators.

APPENDIX A

DERIVATION OF SYSTEM MODELS

A.1 Mechanical Shaft Model

The equations describing the dynamic behaviour of the spring-mass model of Fig. 3.7 is as follows

$$[J]p^2\underline{\delta} + [D]p\underline{\delta} + [K]\underline{\delta} + \underline{T_e} + \underline{T_m} = \underline{0} \tag{A.1}$$

where

$$[J] = diag.[J_1 \quad J_2 \quad J_3 \quad J_4 \quad J_5 \quad J_6] \tag{A.2}$$

$$[D] = diag.[D_1 \quad D_2 \quad D_3 \quad D_4 \quad D_5 \quad D_6] \tag{A.3}$$

$$[K] = \begin{bmatrix} K_{12} & -K_{12} & 0 & 0 & 0 & 0 \\ -K_{12} & K_{12}+K_{23} & -K_{23} & 0 & 0 & 0 \\ 0 & -K_{23} & K_{23}+K_{34} & -K_{34} & 0 & 0 \\ 0 & 0 & -K_{34} & K_{34}+K_{45} & -K_{45} & 0 \\ 0 & 0 & 0 & -K_{45} & K_{45}+K_{56} & -K_{56} \\ 0 & 0 & 0 & 0 & -K_{56} & K_{56} \end{bmatrix} \tag{A.4}$$

$\underline{\delta} = [\delta_1 \quad \delta_2 \quad \delta_3 \quad \delta_4 \quad \delta_5 \quad \delta_6]$ is the rotor position vector and $\underline{T_e} = [0 \quad 0 \quad 0 \quad 0 \quad T_e \quad 0]^T$.

The matrix Eqn. A.1 consists of six, second order differential equations; each of these second order differential equations is decomposed into two, first order differential equations by change of variable $p\delta_i = \Delta\omega_i$ where $\Delta\omega_i$ is the speed deviation of the i_{th} inertial mass of the spring-mass model of the turbine-shaft of Fig. 3.7, and can be written as follows

$$J_1 p\Delta\omega_1 + D_1\Delta\omega_1 + K_{12}(\delta_1 - \delta_2) + T_{m1} = 0 \tag{A.5}$$

$$p\delta_1 = \Delta\omega_1 \tag{A.6}$$

$$J_2 p\Delta\omega_2 + D_2\Delta\omega_2 + K_{12}(\delta_2 - \delta_1) + K_{23}(\delta_2 - \delta_3) + T_{m2} = 0 \tag{A.7}$$

$$p\delta_2 = \Delta\omega_2 \tag{A.8}$$

$$J_3 p\Delta\omega_3 + D_3\Delta\omega_3 + K_{23}(\delta_3 - \delta_2) + K_{34}(\delta_3 - \delta_4) + T_{m3} = 0 \tag{A.9}$$

$$p\delta_3 = \Delta\omega_3 \tag{A.10}$$

$$J_4 p\Delta\omega_4 + D_4\Delta\omega_4 + K_{34}(\delta_4 - \delta_3) + K_{45}(\delta_4 - \delta_5) + T_{m4} = 0 \tag{A.11}$$

$$p\delta_4 = \Delta\omega_4 \tag{A.12}$$

$$J_5 p\Delta\omega_5 + D_5\Delta\omega_5 + K_{45}(\delta_5 - \delta_4) + K_{56}(\delta_5 - \delta_6) + T_e + T_{m5} = 0 \tag{A.13}$$

$$p\delta_5 = \Delta\omega_5 \tag{A.14}$$

$$J_6 p\Delta\omega_6 + D_6\Delta\omega_6 + K_{56}(\delta_5 - \delta_6) + T_{m6} = 0 \quad \text{(A.15)}$$

$$p\delta_6 = \Delta\omega_6 \quad \text{(A.16)}$$

where

$$T_{m1} = \frac{a_1\omega_0}{\omega_1}P_m; \quad \omega_1 = \omega_0 + \Delta\omega_1 \quad \text{(A.17)}$$

$$T_{m2} = \frac{a_2\omega_0}{\omega_2}P_m; \quad \omega_2 = \omega_0 + \Delta\omega_2 \quad \text{(A.18)}$$

$$T_{m3} = \frac{a_3\omega_0}{\omega_3}P_m; \quad \omega_3 = \omega_0 + \Delta\omega_3 \quad \text{(A.19)}$$

$$T_{m4} = \frac{a_4\omega_0}{\omega_4}P_m; \quad \omega_4 = \omega_0 + \Delta\omega_4 \quad \text{(A.20)}$$

$$T_{m5} = \frac{a_5\omega_0}{\omega_5}P_m; \quad \omega_5 = \omega_0 + \Delta\omega_5 \quad \text{(A.21)}$$

$$T_{m6} = \frac{a_6\omega_0}{\omega_6}P_m; \quad \omega_6 = \omega_0 + \Delta\omega_6 \quad \text{(A.22)}$$

P_m = total ouput power to the shaft from all turbine stages

a_i is the fraction of the input power coming from location 'i'

ω_0 is the system synchronous frequency.

A.2 Parallel Transmission Line Models

The equations describing the dynamic behaviour of two three-phase RLC transmission lines can be written by inspection of Fig. A1 as

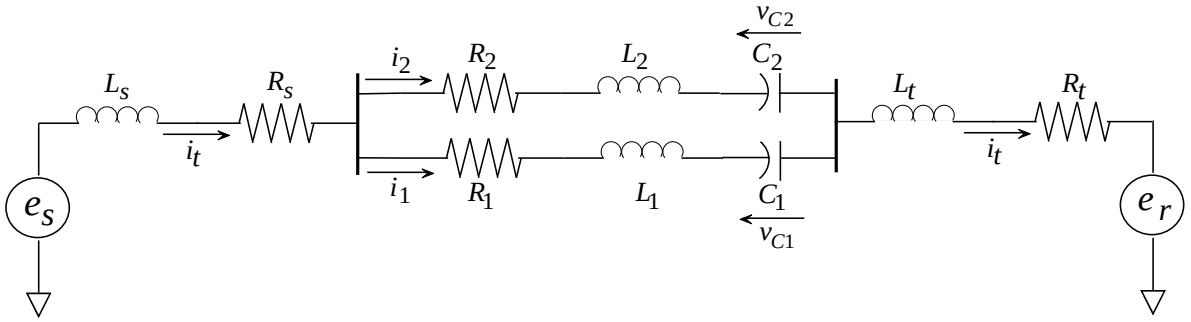

Fig. A1 Single line diagram of a parallel RLC transmission line system.

$$e_s - e_r = e_{sr} = (L_s + L_t)pi_t + (R_s + R_t)i_t + R_1 i_1 + L_1 pi_1 + v_{C1} \quad \text{(A.23)}$$

$$e_{sr} = (L_s + L_t)pi_t + (R_s + R_t)i_t + R_2 i_2 + L_2 pi_2 + v_{C2} \quad \text{(A.24)}$$

$$i_2 = i_t - i_1 \quad \text{(A.25)}$$

$$pv_{C1} = \frac{1}{C_1}i_1 = \omega_0 X_{C1} i_1 \quad \text{(A.26)}$$

$$pv_{C2} = \frac{1}{C_2} i_2 = \omega_0 X_{C2} i_2 \tag{A.27}$$

By substituting Eqn. A.25 into Eqn. A.23

$$e_{sr} = (L_s + L_t)pi_t + (R_s + R_t)i_t + R_2(i_t - i_1) + L_2 p(i_t - i_1) + v_{C2} \tag{A.28}$$

Equation A.23 can be written as

$$pi_t = \frac{1}{(L_s + L_t)}\{e_{sr} - (R_s + R_t)i_t - R_1 i_1 - L_1 pi_1 - v_{C1}\} \tag{A.29}$$

By substituting Eqn. A.29 into Eqn. A.28, the resulting Eqn. can be written as

$$pi_1 = \left\{\frac{R_2 - \frac{L_2(R_s + R_t)}{L_s + L_t}}{L_1 + L_2 + \frac{L_1 L_2}{L_s + L_t}}\right\} i_t + \left\{\frac{-R_1 - R_2 - \frac{R_1 L_2}{L_s + L_t}}{L_1 + L_2 + \frac{L_1 L_2}{L_s + L_t}}\right\} i_1 + \left\{\frac{-1 - \frac{L_2}{L_s + L_t}}{L_1 + L_2 + \frac{L_1 L_2}{L_s + L_t}}\right\} v_{C1} + \left\{\frac{1}{L_1 + L_2 + \frac{L_1 L_2}{L_s + L_t}}\right\} v_{C2} + \left\{\frac{\frac{L_2}{L_s + L_t}}{L_1 + L_2 + \frac{L_1 L_2}{L_s + L_t}}\right\} e_{sr} \tag{A.30}$$

Equation A.28 can be written as

$$pi_1 = \frac{1}{L_2}\{-e_{sr} + (L_s + L_t)pi_t + (R_s + R_t)i_t + R_2(i_t - i_1) + L_2 pi_t + v_{C2}\} \tag{A.31}$$

Substituting Eqn. A.31 into Eqn. A.23, the resulting Eqn. can be written as

$$pi_t = \left\{\frac{-(R_s + R_t) - \frac{L_1}{L_2}(R_s + R_t) - \frac{L_1 R_2}{L_2}}{L_s + L_t + \frac{L_1}{L_2}(L_s + L_t) + L_1}\right\} i_t + \left\{\frac{-R_1 - \frac{L_1}{L_2} R_2}{L_s + L_t + \frac{L_1}{L_2}(L_s + L_t) + L_1}\right\} i_1 + \left\{\frac{-1}{L_s + L_t + \frac{L_1}{L_2}(L_s + L_t) + L_1}\right\} v_{C1} + \left\{\frac{-\frac{L_1}{L_2}}{L_s + L_t + \frac{L_1}{L_2}(L_s + L_t) + L_1}\right\} v_{C2} + \left\{\frac{1 + \frac{L_1}{L_2}}{L_s + L_t + \frac{L_1}{L_2}(L_s + L_t) + L_1}\right\} e_{sr} \tag{A.32}$$

Equations A.32, A.30, A.26 and A.27, describing the dynamics of the transmission network may be written in shorthand notation as

APPENDIX A

$$p[i_t]_{abc} = a_{11}[i_t]_{abc} + a_{12}[i_1]_{abc} + a_{13}[v_{C1}]_{abc} + a_{14}[v_{C2}]_{abc} + a_{15}[e_{sr}]_{abc} \quad \text{(A.33)}$$

$$p[i_1]_{abc} = a_{21}[i_t]_{abc} + a_{22}[i_1]_{abc} + a_{23}[v_{C1}]_{abc} + a_{24}[v_{C2}]_{abc} + a_{25}[e_{sr}]_{abc} \quad \text{(A.34)}$$

$$p[v_{C1}]_{abc} = \omega_0 X_{C1}[i_1]_{abc} \quad \text{(A.35)}$$

$$p[v_{C2}]_{abc} = \omega_0 X_{C2}[i_t]_{abc} - \omega_0 X_{C2}[i_1]_{abc} \quad \text{(A.36)}$$

where

$$a_{11} = \frac{-(R_s + R_t) - \frac{L_1}{L_2}(R_s + R_t) - \frac{L_1 R_2}{L_2}}{L_s + L_t + \frac{L_1}{L_2}(L_s + L_t) + L_1}; \qquad a_{12} = \frac{-R_1 - \frac{L_1}{L_2}R_2}{L_s + L_t + \frac{L_1}{L_2}(L_s + L_t) + L_1};$$

$$a_{13} = \frac{-1}{L_s + L_t + \frac{L_1}{L_2}(L_s + L_t) + L_1}; \qquad a_{14} = \frac{-\frac{L_1}{L_2}}{L_s + L_t + \frac{L_1}{L_2}(L_s + L_t) + L_1};$$

$$a_{15} = \frac{1 + \frac{L_1}{L_2}}{L_s + L_t + \frac{L_1}{L_2}(L_s + L_t) + L_1}; \qquad a_{21} = \frac{R_2 - \frac{L_2(R_s + R_t)}{L_s + L_t}}{L_1 + L_2 + \frac{L_1 L_2}{L_s + L_t}};$$

$$a_{22} = \frac{-R_1 - R_2 - \frac{R_1 L_2}{L_s + L_t}}{L_1 + L_2 + \frac{L_1 L_2}{L_s + L_t}}; \qquad a_{23} = \frac{-1 - \frac{L_2}{L_s + L_t}}{L_1 + L_2 + \frac{L_1 L_2}{L_s + L_t}};$$

$$a_{24} = \frac{1}{L_1 + L_2 + \frac{L_1 L_2}{L_s + L_t}}; \qquad a_{25} = \frac{\frac{L_2}{L_s + L_t}}{L_1 + L_2 + \frac{L_1 L_2}{L_s + L_t}};$$

Equations A.33 to A.36 describing the dynamics of the transmission network in the stationary (abc) reference frame may be transformed into the synchronously rotating (dq) reference frame and written in shorthand notation as

$$p[i_t]_{dq} = a_{11}[i_t]_{dq} - \begin{bmatrix} 0 & \omega_0 \\ -\omega_0 & 0 \end{bmatrix}[i_t]_{dq} + a_{12}[i_1]_{dq} + a_{13}[v_{C1}]_{dq} + a_{14}[v_{C2}]_{dq} + a_{15}[e_{sr}]_{dq} \quad \text{(A.37)}$$

$$p[i_1]_{dq} = a_{21}[i_t]_{dq} + a_{22}[i_1]_{dq} - \begin{bmatrix} 0 & \omega_0 \\ -\omega_0 & 0 \end{bmatrix}[i_1]_{dq} + a_{23}[v_{C1}]_{dq} + a_{24}[v_{C2}]_{dq} + a_{25}[e_{sr}]_{dq} \quad \text{(A.38)}$$

$$p[v_{C1}]_{dq} = \omega_0 X_{C1}[i_1]_{dq} - \begin{bmatrix} 0 & \omega_0 \\ -\omega_0 & 0 \end{bmatrix}[v_{C1}]_{dq} \quad \text{(A.39)}$$

$$p[v_{C2}]_{dq} = \omega_0 X_{C2}[i_t]_{dq} - \omega_0 X_{C2}[i_1]_{dq} - \begin{bmatrix} 0 & \omega_0 \\ -\omega_0 & 0 \end{bmatrix}[v_{C2}]_{dq} \quad \text{(A.40)}$$

APPENDIX B
PSCAD MODEL OF THE MODIFIED IEEE FBM FOR SSR ANALYSIS

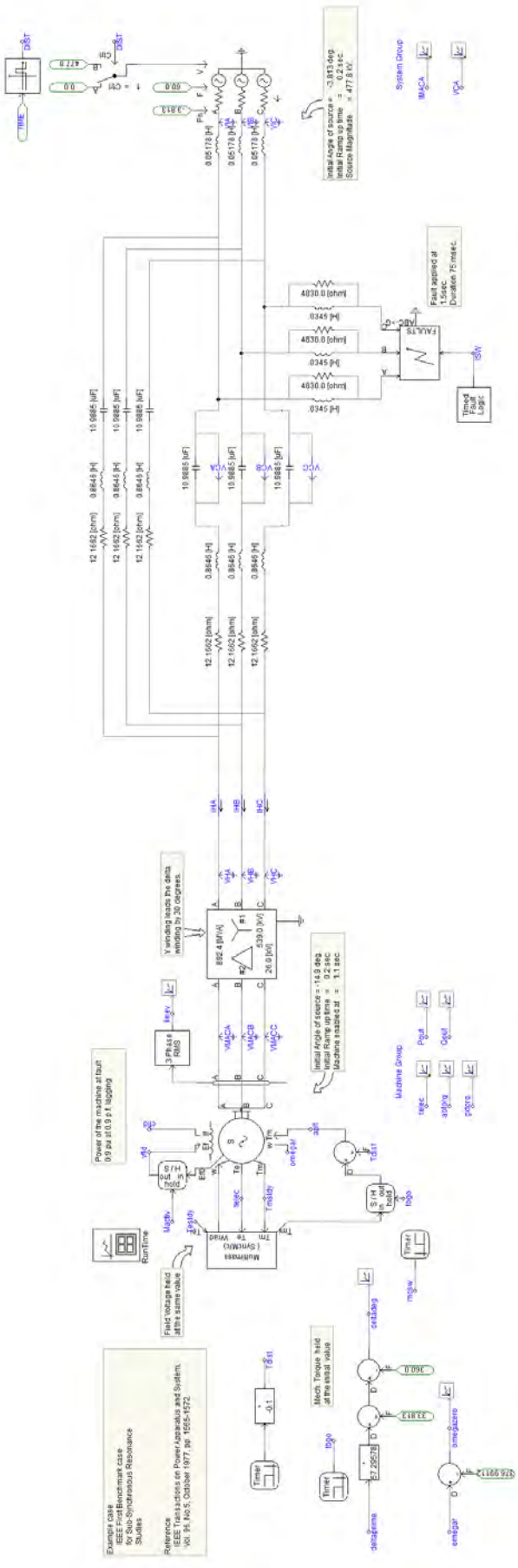

Fig. B1 PSCAD Simulation Model of the IEEE FBM for SSR.

APPENDIX C

PARAMETERS OF IEEE FIRST BENCHMARK MODEL

This appendix contains the parameters and set points (input variables) of the study system in per unit, referred to the common base of 892.4 MVA, 500 kV used in [20].

C.1 Generator & Transformer Electrical Parameters

V_{b_0} = 1.0	V_{t_0} = 1.0	P_{t_0} = 0.5	
X_T = 0.14			
X_{md} = 1.66	X_{ad} = 0.13	X_{kd} = 0.0055	X_{fd} = 0.062
R_a = 0.0	R_{kd} = 0.0041	R_{fd} = 0.0014	
X_{mq} = 1.58	X_{aq} = 0.13	X_{kq1} = 0.095	X_{kq2} = 0.326
R_{kq1} = 0.0082	R_{kq2} = 0.014		

C.2 Generator Mechanical Parameters

$J_1 = 4.93 \times 10^{-4}$	$J_2 = 8.25 \times 10^{-4}$	J_3 = 0.00456	J_4 = 0.00469
J_5 = 0.00461	$J_6 = 1.82 \times 10^{-4}$		
K_{12} = 19.303	K_{23} = 34.929	K_{34} = 52.038	K_{45} = 70.858
K_{56} = 2.822			
D_1 = 0.0	D_2 = 0.0	D_3 = 0.0	D_4 = 0.0
D_5 = 0.0	D_6 = 0.0		

C.3 Turbine Torque Share

HP = 30 %	IP = 26 %	LPA = 22 %	LPB = 22 %
GEN= 0 %	EXC = 0 %		

APPENDIX C

C.4 Transmission System Parameters

X_s = 0.06 R_{L1} = 0.04 X_{L1} = 1.0

R_{L2} = 0.04 X_{L2} = 1.0

X_{SSSC0} or V_{SSSC0} and X_{C2} depends on case study

C.5 SSSC and Power Flow Controller Parameters

X_{SSSC}-controlled type

C = 0.01613

K_{VP} = 10.159 H_V = 0.1 V_{dc}^{*} = 0.01613 K_{AI} = 3.9 * $_o$

H_p = 0.3

V_{SSSC}-controlled type

C = 0.01613

K_{VP} = 13.5 H_V = 0.1 V_{dc}^{*} = 0.01613 K_{AI} = 5.0 * $_o$

H_p = 0.3

where H_V and H_p are defined in [89]; K_P and K_I depends on case study.

APPENDIX D

SOURCE CODE FOR ANALYTICAL STUDIES

D.1 Matlab Programs for Analytical Studies

The new models developed and programmed in Matlab that form part of the original work of this thesis are, as outlined in the main body of the document: the transmission system equations for the modified IEEE FBM for SSR containing two lines, one with conventional series compensation, the other with SSSC compensation; the power flow controller model dynamic equations; and the code needed to determine the initial condition of this modified IEEE FBM system's state variables by means of a load flow. These original models and Matlab code were integrated by the author into an existing Matlab/Simulink framework that included a dynamic model of a multi-inertia turbine generator, made available from previous work in [33]. All code in this appendix shown in green is the existing framework developed in [33]. All code in blue in this appendix has been developed and added by the author if this thesis.

D.1.1 Reactance-Controlled SSSC-based Power Flow Controller in the Modified IEEE FBM for SSR

```
%Simulation program for modified IEEE SSR FBM with 2 transmission lines with SSSC and power flow controls

%requires accompanying files ssinitial_FBM2tx_sssc1_pfc.m and
%plt_FBM2tx_sssc1_pfc.m and blk_FBM2tx_sssc1_pfc



%Flag to select type of study to be carried out from the following options:
%StudyType=0 -- time domain simulation
%StudyType=1 -- calculate system eigenvalues using numerically linearised model
%StudyType=2 -- calculate transfer functions (mag + phase) using numerically linearised model
%StudyType=3 -- calculate transfer functions (poles + zeros) using numerically linearised model

StudyType=1;

clc
%clear
st=clock;

global R1 Xl1 Xsssc0 R2 Xl2 Xc2 Rs Rtrans Xs Xtrans Tsssc Kp Ki Pt pfc_mode

global M1 M2 M3 M4 Wo Ly MWO Ldstr Lqstr
global MdtransLdrinv MqtransLqrinv a1 a2 a3 a4 a5 a6 JinvDK Jinv Tevec Tmvec
global Xmd Xmq Xad Xaq Xfd Rfd Ra K12 K23 K34 K45 K56

global a11 a12 a13 a14 a15 a21 a22 a23 a24 a25
global intvars

global scmax Vref hv kvp hp kpp kai dccap

global Vbus

%Mode of operation of power flow controller
%pfc_mode=0 -- constant power mode
%pfc_mode=1 -- constant angle mode

 pfc_mode=0;

Wo = 2*pi*50;
r120 = 2*pi/3;

%Inputs
Vt = 1.00;
Vb = 1.00;
```

APPENDIX D

```
Pt = 0.5; %inductive SSSC use 0.2 and capacitive SSSC nominal 0.4 pu (0.5 pu for PSCC results)
Ts = 0.13; %settling time of power flow controller (0.13s for 33.5rad/s and 30s for 0.13rad/s)

%Transmission system parameters
%system impedance
Xs = 0.06;
Rs = 0.0;
%Line 1 impedances
R1  = 0.04;
Xl1 = 1.0; %inductive use 0.5 and capacitive use 1.0
%SSSC paramaters
Xsssc0 = 0.36; % change sign to negative if inductive
Tsssc  = 0.001; % Time constant of block linking PFC controller and Xsssc input of SSSC
%Line 2 impedances
R2  = 0.04;
Xl2 = 1.0;
Xc2 = 0.36;
%Generator transformer impedances
Xtrans = 0.14;
Rtrans = 0.00;

%SSSC parameters and inputs
Vbase = 220/sqrt(3);
Zbase = 16.13;
scmax = sqrt(2);
dccap = 1000.0e-6*Zbase;
hv = 1/10.0;
Vref = (300.0/Vbase)*hv;
kvp = 80.0*(Zbase/Vbase); % inductive value = 12.5 and capacitive use 80.0*(Zbase/Vbase)
kpp = 2/3; % inductive sign -ve and capactive sign +ve
hp = 0.3;
kai = 3.9*2*pi*50;

%Generator electrical system parameters
Xmd=1.66;
Xad=0.13;
Xkd=0.0055;
Xfd=0.062;
Rfd=0.0014;
Rkd=0.0041;
Ra=0.0;
Xmq=1.58;
Xaq=0.13;
Xkq1=0.095;
Xkq2=0.326;
Rkq1=0.0082;
Rkq2=0.014;

%Turbine mechanical system parameters
J1=2*0.092897/377;
J2=2*0.155589/377;
J3=2*0.858670/377;
J4=2*0.884215/377;
J5=2*0.868495/377;
J6=2*0.0342165/377;

D1=0.0;
D2=0.0;
D3=0.0;
D4=0.0;
D5=0.0;
D6=0.0;

K12=19.303;
K23=34.929;
K34=52.038;
K45=70.858;
K56=2.822;

a1=0.30;
a2=0.26;
a3=0.22;
a4=0.22;
a5=0.0;
```

APPENDIX D

```
a6=0.0;

%Conversion of line reactances to inductances
Ls = Xs/Wo;
L1 = X11/Wo;
L2 = X12/Wo;

%Calculate vectors and matrices with multi-machine form of generator parameters (synch rotating frame)

function ConvPars2MMform

Lt = Lg + (Xtrans/Wo);
Rt = Ra + Rtrans;

Jinv = inv(diag([-J1 -J2 -J3 -J4 -J5 -J6 1 1 1 1 1 1]));
DK = diag([D1 D2 D3 D4 D5 D6 0 0 0 0 0 0])...
+ diag([0 -K12 -K23 -K34 -K45 -K56 0],5)...
+ diag([K12 (K12+K23) (K23+K34) (K34+K45) (K45+K56) K56],6)...
+ diag([-K12 -K23 -K34 -K45 -K56],7)...
+ diag([1 1 1 1 1 1],-6);
JinvDK = Jinv*DK;
Tevec = zeros(12,1);
Tmvec = zeros(12,1);

%Coefficients for transmission line equations
a11 = -((Rs + Rt) + (Rs + Rt)*L1/L2 + R2*L1/L2)/(Lt + Ls + (L1*(Lt +Ls)/L2) + L1);
a12 = (-R1 + (L1*R2/L2))/(Lt + Ls + (L1*(Lt + Ls)/L2) + L1);
a13 = -1/(Lt + Ls + (L1*(Lt + Ls)/L2) + L1);
a14 = (-L1/L2)/(Lt + Ls + (L1*(Lt + Ls)/L2) + L1);
a15 = (1 + (L1/L2))/(Lt + Ls + (L1*(Lt +Ls)/L2) + L1);

a21 = (R2-(Rs + Rt)*L1/(Ls + Lt))/(L1 + L2 + (L1*L2)/(Lt + Ls));
a22 = (-R1 - R2 - (R1*L2)/(Lt + Ls))/(L1 + L2 + (L1*L2)/(Lt + Ls));
a23 = (-1 - L2/(Lt + Ls))/(L1 + L2 + (L1*L2)/(Lt + Ls));
a24 = 1/(L1 + L2 + (L1*L2)/(Lt + Ls));
a25 = (L2/(Lt + Ls))/(L1 + L2 + (L1*L2)/(Lt + Ls));


switch StudyType,

%-------------------------------------------------------------------------------------------------------%
%-------------------------------------Non-linear time domain simulation---------------------------------%
%-------------------------------------------------------------------------------------------------------%

case 0,

disp('')
disp('               Time domain simulation in progress... ')
%Simulation directives
delt   = 0.5e-3;
dover3 = delt/3;

tfault = 1.5;
tlift  = 35.0;
tfin   = 35.0;

nn   = 1;
ll   = nn-1;
kk   = 0;
np   = fix(tfin/delt/nn);

t=0;

xdot=zeros(26,1);
x=zeros(26,1);

%%Subroutine to calculate initial values of state variables
[x,Vbus,Vfd,Pmech,P1set] = ssinitial_FBM2tx_sssc1_pfc(Vt,Vb,Ts);

%Input vector in sfunc format
u(1,1) = Vbus(1,1);
u(2,1) = Vbus(2,1);
u(3,1) = Vfd;
u(4,1) = Pmech;
u(5,1) = P1set;

%Set up matrices for output of numerical integration
```

APPENDIX D

```
z = zeros(np,1);
xo = zeros(np,30);
intvars = zeros(1);


Pmech_o = Pmech;        %save initial value of input

%-------------------------Integration loop-------------------------%

while t < tfin
if ((t >= tfault)&(t < tlift))
%system disturbance if required

%New input voltage
u(4,1) = Pmech - 0.01;

elseif (t>=tlift)
%Lift system disturbance
u(4,1) = Pmech_o;

end

  [xdot] = plt_FBM2tx_sssc1_pfc(0,x,u,1);
  fk1 = xdot*dover3;
  [ydot] = plt_FBM2tx_sssc1_pfc(0,x+fk1,u,1);
  fk2 = ydot*dover3;
  [ydot] = plt_FBM2tx_sssc1_pfc(0,x+0.5*(fk1+fk2),u,1);
  fk3 = ydot*dover3;
  [ydot] = plt_FBM2tx_sssc1_pfc(0,x+(1/8)*(3*fk1+9*fk3),u,1);
  fk4 = ydot*dover3;
  [ydot] = plt_FBM2tx_sssc1_pfc(0,x+0.5*(3*fk1-9*fk2+12*fk4),u,1);
  fk5 = ydot*dover3;

  x = x + 0.5*fk1 + 2*fk4 + 0.5*fk5;

%time vector and output vectors for plotting

  ll=ll+1;
  if ll == nn
     ll=0;
     kk=kk+1;
     z(kk) = t;
     %transfomer variables
     xo(kk,1) = x(1);        %instantaneous d-axis current
     xo(kk,2) = x(2);        %instantaneous q-axis current
     xo(kk,3) = sqrt((x(1)^2 + x(2)^2)); %Ipk1
     inv_prk = [cos(Wo*t) sin(Wo*t) 1;cos(Wo*t-r120) sin(Wo*t-r120) 1;cos(Wo*t+r120) sin(Wo*t+r120) 1];
     i_abc1 = inv_prk*[x(1); x(2); 0];
     xo(kk,4) = i_abc1(1);
     xo(kk,5) = i_abc1(2);
     xo(kk,6) = i_abc1(3);
     %line #1 variables
     xo(kk,7) = x(3);        %instantaneous d-axis current
     xo(kk,8) = x(4);        %instantaneous q-axis current
     xo(kk,9) = sqrt((x(3)^2 + x(4)^2)); %Ipk2
     i_abc2 = inv_prk*[x(3); x(4); 0];
     xo(kk,10) = i_abc2(1);
     xo(kk,11) = i_abc2(2);
     xo(kk,12) = i_abc2(3);
     xo(kk,13) = x(5);
     xo(kk,14) = x(6);
     xo(kk,15) = sqrt((x(5)^2 + x(6)^2)); %Vc1pk
     Vc1_abc = inv_prk*[x(5); x(6); 0];
     xo(kk,16) = Vc1_abc(1);
     xo(kk,17) = Vc1_abc(2);
     xo(kk,18) = Vc1_abc(3);
     xo(kk,19) = x(23);
     xo(kk,20) = x(17);
     xo(kk,21) = intvars(4)*K56; %GEN-EXC Torque
     xo(kk,22) = intvars(5)*K34; %LPA-LPB Torque
     xo(kk,23) = intvars(12); % Pmech
     xo(kk,24) = intvars(13); % Xsssc
     xo(kk,25) = intvars(8);  % P1
     xo(kk,26) = intvars(14); % Actual Pt
     xo(kk,27) = intvars(20); % P2
     xo(kk,28) = intvars(22)*K12;  %HP-IP Torque
     xo(kk,29) = intvars(23)*K23;  %IP-LPA Torque
```

```
     xo(kk,30) = intvars(24)*K45;  %LPB-GEN Torque
 end
 t = t+delt;

end

elt=etime(clock,st);
disp('Total simulation time taken was '),elt
disp('seconds')

%-----------------------------------------------------------------------------------------------------%
%-----------------Calculate system eigenvalues using numerically linearised model---------------------%
%-----------------------------------------------------------------------------------------------------%

case 1,

disp('')
disp('               Eigenvalues scan in progress... ')
%Analysis directives
% No. of points over the range of scanned parameter (must be >= 1)
nsc = 600;

% No. of roots
nrts = 26;

%Start and end values of parameter to be scanned
start = 0.1;
stop  = 0.9;

if nsc > 1
   delt=(stop-start)/(nsc-1);
elseif nsc == 1
   delt=0;
else
   error('invalid no. of points in scan range');
end

%Loop to calculate eigenvalues for each value of scanned parameter
for scan=1:nsc

%parameter to be scanned
  Xsssc0=start+(scan-1)*delt;
  %Xc2=Xc1;

  Xsssc0save(scan)=Xsssc0;


%%Subroutine to calculate initial values of state variables
[x,Vbus,Vfd,Pmech,P1set] = ssinitial_FBM2tx_sssc1_pfc(Vt,Vb,Ts);

%Input vector in sfunc format
u(1,1) = Vbus(1,1);
u(2,1) = Vbus(2,1);
u(3,1) = Vfd;
u(4,1) = Pmech;
u(5,1) = P1set;

  XX0 = x;

  %Test for correctness of steady state vector if necessary
  %[xdots]=plt_2txFBM_sssc1(0,XX0,u,1);
  %xdots
  %pause

  [AA,BB,CC,DD]=linmod('blk_FBM2tx_sssc1_pfc',XX0,u,1e-8);

  eval=eig(AA);

  x=real(eval);
  y=imag(eval);
  idx=(scan-1)*nrts;
  for en=1:nrts
      out(1,idx+en)=x(en);
      out(2,idx+en)=y(en);
  end

end
```

APPENDIX D

```
lst = (nsc-1)*nrts;

plot(out(1,[1:nrts]),out(2,[1:nrts]),'*',out(1,:),out(2,:),'.',...
out(1,[lst+1:lst+nrts]),out(2,[lst+1:lst+nrts]),'o')
grid;

elt=etime(clock,st);
disp('Total simulation time taken was '),elt
disp('seconds')

%-------------------------------------------------------------------------------------------------------%
%-----------Calculate mag + phase of transfer functions using numerically linearised model-------------%
%-------------------------------------------------------------------------------------------------------%

case 2,

%Analysis directives
% No. of points over the range of scanned parameter (must be >= 1)
nsc = 4;
% No. of roots
nrts = 26;

%Start and end values of parameter to be scanned
start = 1.2;
stop  = 0.45;

%Define vector of frequencies at which to calculate transfer functions
wvec=logspace(-2,3,500);

if nsc > 1
   delt=(stop-start)/(nsc-1);
elseif nsc == 1
   delt=0;
else
   error('invalid no. of points in scan range');
end

%Loop to calculate eigenvalues for each value of scanned parameter
for scan=1:nsc

%parameter to be scanned
  Ts=start+(scan-1)*delt;
  %Xc2=Xc1;

  Tssave(scan)=Ts;


%%Subroutine to calculate initial values of state variables
[x,Vbus,Vfd,Pmech,P1set] = ssinitial_FBM2tx_sssc1_pfc(Vt,Vb,Ts);

%Input vector in sfunc format
u(1,1) = Vbus(1,1);
u(2,1) = Vbus(2,1);
u(3,1) = Vfd;
u(4,1) = Pmech;
u(5,1) = P1set;

  XX0 = x;

  %Test for correctness of steady state vector if necessary
  %[xdots]=plt_2txFBM_sssc1(0,XX0,u,1);
  %xdots
  %pause

  [AA,BB,CC,DD]=linmod('blk_FBM2tx_sssc1_pfc',XX0,u,1e-8);

  [mag,phase]=bode(AA,BB,CC,DD,5,wvec);

  for ii=1:500
     mtf(scan,ii)=20*log10(mag(ii,5));
     ptf(scan,ii)=phase(ii,5);
  end

end

lst = (nsc-1)*nrts;
```

APPENDIX D

```
subplot(211),semilogx(wvec,mtf(1,:),wvec,mtf(2,:),wvec,mtf(3,:),wvec,mtf(4,:))
grid
subplot(212),semilogx(wvec,ptf(1,:),wvec,ptf(2,:),wvec,ptf(3,:),wvec,ptf(4,:))
grid


%-------------------------------------------------------------------------------------------------------%
%-----------Calculate poles + zeros of transfer functions using numerically linearised model-----------%
%-------------------------------------------------------------------------------------------------------%

case 3,

%Analysis directives
% No. of points over the range of scanned parameter (must be >= 1)
nsc = 4;
% No. of roots
nrts = 26;

%Start and end values of parameter to be scanned
start = 25.0;
stop  = 5.0;

if nsc > 1
   delt=(stop-start)/(nsc-1);
elseif nsc == 1
   delt=0;
else
   error('invalid no. of points in scan range');
end

%Loop to calculate eigenvalues for each value of scanned parameter
for scan=1:nsc

%parameter to be scanned
  Ts=start+(scan-1)*delt;
  %Xc2=Xc1;

  Tssave(scan)=Ts;


%%Subroutine to calculate initial values of state variables
[x,Vbus,Vfd,Pmech,P1set] = ssinitial_FBM2tx_sssc1_pfc(Vt,Vb,Ts);

%Input vector in sfunc format
u(1,1) = Vbus(1,1);
u(2,1) = Vbus(2,1);
u(3,1) = Vfd;
u(4,1) = Pmech;
u(5,1) = P1set;

  XX0 = x;

  %Test for correctness of steady state vector if necessary
  %[xdots]=plt_2txFBM_sssc1(0,XX0,u,1);
  %xdots
  %pause

  [AA,BB,CC,DD]=linmod('blk_FBM2tx_sssc1_pfc',XX0,u,1e-8);

  [zero,pole,Kay]=ss2zp(AA,BB,CC,DD,5);

  xp(:,scan)=real(pole);
  yp(:,scan)=imag(pole);

  %Caution here: if there are no zeros in the transfer function then the variable zero will be an
  %empty matrix and the plotting below will need to be adjusted.

  for ii=1:length(zero(:,1))
    xz(ii,scan)=real(zero(ii,5));
    yz(ii,scan)=imag(zero(ii,5));
  end

end

  lst = (nsc-1)*nrts;
```

```
  plot(xp(:,1),yp(:,1),'+',xp(:,:),yp(:,:),'.'...
  ,xz(:,1),yz(:,1),'o',xz(:,:),yz(:,:),'o')

grid;

% Unexpected StudyType
  otherwise
    error(['Undefined StudyType = ',num2str(StudyType)]);

end
```

```
function [x,Vbus,Vfd,Pmech,P1set] = ssinitial_FBM2tx_sssc1_pfc(Vt,Vb,Ts)

%routine to carry out steady state initialisation of system for numerical linearisation
global R1 Xl1 Xsssc0 R2 Xl2 Xc2 Rs Rtrans Xs Xtrans Tsssc Kp Ki Pt pfc_mode

global M1 M2 M3 M4 Wo Ly MWO Ldstr Lqstr
global MdtransLdrinv MqtransLqrinv a1 a2 a3 a4 a5 a6 JinvDK Jinv Tevec Tmvec
global Xmd Xmq Xad Xaq Xfd Rfd Ra K12 K23 K34 K45 K56

global a11 a12 a13 a14 a15 a21 a22 a23 a24 a25
global intvars

global scmax Vref hv kvp hp kpp kai dccap

x=zeros(26,1);

Xsssc = Xsssc0;
%set up admittances for load flow

Z1 = R1 + j*(Xl1-Xsssc);
Z2 = R2 + j*(Xl2-Xc2);
Z3 = (Z1*Z2)/(Z1 + Z2);
R3 = real(Z3);
X3 = imag(Z3);

Y21 = -1/((R3 + Rs + Rtrans) + j*(X3 + Xs + Xtrans));
Y12 = Y21;
Y22 = -Y21;
Y11 = -Y12;

V1 = Vb +j*0;
P2 = Pt;
%load flow on modified IEEE FBM network
%assumed value of reactive power at generator terminals
Q2=0;
%approximate initial value for angle of Vt
angV2 = asin(Pt*(X3 + Xtrans + Xs)/(Vt*Vb));
V2 = Vt*cos(angV2) + j*Vt*sin(angV2);

delQ = 1;
count = 0;
while delQ > (1e-6)
    count=count+1;
    if count>100
       disp('Load flow has not converged in 100 iterations')
       break
    end
    Q2temp = Q2;
    Q2 = -imag(conj(V2)*(Y22*V2 + Y21*V1));
    V2temp = (1/Y22)*((P2-j*Q2)/conj(V2) - Y21*V1);
    V2 = abs(V2)*cos(angle(V2temp)) + j*abs(V2)*sin(angle(V2temp));
    delQ = abs(Q2 - Q2temp);
end

%Solve generator phasor diagram from load flow
I2 = Y21*V1 + Y22*V2;
P2 = real(V2*conj(I2));
Q2 = imag(V2*conj(I2));
Ig = (sqrt(P2^2 + Q2^2))/Vt;
phi = atan2(Q2,P2);

num = Ig*((Xmq+Xaq)*cos(phi) - Ra*sin(phi));
den = Vt + Ig*(Ra*cos(phi) + (Xmq+Xaq)*sin(phi));
delpri = atan2(num,den);
alpha = (pi/2)-delpri-phi;
```

APPENDIX D

```
Igd = -Ig*cos(alpha);
Igq = -Ig*sin(alpha);
Vtd = Vt*sin(delpri);
Vtq = Vt*cos(delpri);

Eod = Vtd + Igq*(Xmq+Xaq) - Igd*Ra;
Eoq = Vtq - Igd*(Xmd+Xad) - Igq*Ra;

Eo = sqrt(Eod^2 + Eoq^2);
If = sqrt(2)*Eo/Xmd;
Vfd = If*Rfd;
Vbus(1,1) = 0;
Vbus(2,1) = -sqrt(2)*Vb;


id = sqrt(2)*Igd;
iq = -sqrt(2)*Igq;
psid = (1/Wo)*( (Xmd+Xad)*id + Xmd*If );
psiq = (1/Wo)*( (Xmq+Xaq)*iq );
Te = (Wo/2)*(psid*iq - psiq*id);
Pmech = -Te;

%Populate state vector with solved steady state values
delta = delpri + angle(V2);
x(1) = id*cos(delta) + iq*sin(delta);
x(2) = -id*sin(delta) + iq*cos(delta);

x(9) = (1/Wo)*( Xmd*id + (Xfd+Xmd)*If );
x(10) = (1/Wo)*( Xmd*id + Xmd*If );
x(11) = (1/Wo)*( Xmq*iq );
x(12) = (1/Wo)*( Xmq*iq );

Tevec(5) = Te;

Tmvec(1) = a1*Pmech;
Tmvec(2) = a2*Pmech;
Tmvec(3) = a3*Pmech;
Tmvec(4) = a4*Pmech;
Tmvec(5) = a5*Pmech;
Tmvec(6) = a6*Pmech;

x(23) = delta;
x(24) = ( K56*x(23)-Tmvec(6) )/K56;
x(22) = ( K45*x(23) + K56*(x(23)-x(24)) + Tevec(5) + Tmvec(5) )/K45;
x(21) = ( K34*x(22) + K45*(x(22)-x(23)) + Tmvec(4) )/K34;
x(20) = ( K23*x(21) + K34*(x(21)-x(22)) + Tmvec(3) )/K23;
x(19) = ( K12*x(20) + K23*(x(20)-x(21)) + Tmvec(2) )/K12;


% using matrix method to find the state variables for the remaining transmission line branches

c11 = a22/a25 - a12/a15;
c12 = -Wo/a25;
c13 = a23/a25 - a13/a15;
c14 = a24/a25 - a14/a15;
c15 = a11/a15 - a21/a25;
c16 = -Wo/a15;

dd(1,1) = c15*x(1) + c16*x(2);
dd(2,1) = -c16*x(1) + c15*x(2);
dd(3,1) = 0.0;
dd(4,1) = 0.0;
dd(5,1) = -Wo*Xc2*x(1);
dd(6,1) = -Wo*Xc2*x(2);

cc = zeros(6,6);

cc(1,1) = c11;
cc(2,1) = -c12;
cc(3,1) = Wo*Xsssc;
cc(5,1) = -Wo*Xc2;

cc(1,2) = c12;
cc(2,2) = c11;
cc(4,2) = Wo*Xsssc;
cc(6,2) = -Wo*Xc2;
```

```
cc(1,3) = c13;
cc(4,3) = Wo;

cc(2,4) = c13;
cc(3,4) = -Wo;

cc(1,5) = c14;
cc(6,5) = Wo;

cc(2,6) = c14;
cc(5,6) = -Wo;


x_zero38 = inv(cc)*dd;

x(3) = x_zero38(1);
x(4) = x_zero38(2);
vc1D = x_zero38(3);
vc1Q = x_zero38(4);
x(7) = x_zero38(5);
x(8) = x_zero38(6);

%States of SSSC
x(5) =  Vref/hv;
x(6) = atan2(vc1D,vc1Q);

%Power flow controller variables and inputs

Ls = Xs/Wo;
L1 = Xl1/Wo;
Vsd = Vbus(1,1) - Rs*x(1) - Wo*Ls*x(2);
Vsq = Vbus(2,1) - Rs*x(2) + Wo*Ls*x(1);
P1 = (1/2)*(Vsd*x(3) + Vsq*x(4));
Q1 = (1/2)*(Vsd*x(4) - Vsq*x(3));
Vrd = Vsd - R1*x(3) - Wo*L1*x(4) - vc1D;
Vrq = Vsq - R1*x(4) + Wo*L1*x(3) - vc1Q;
Vs_pk = sqrt((Vsd^2 + Vsq^2));
Vr_pk = sqrt((Vrd^2 + Vrq^2));
Vs = Vs_pk/sqrt(2);
Vr = Vr_pk/sqrt(2);
delta_sr = asin((P1*(Xl1 - Xsssc))/(Vs*Vr));
Kplant_pri = (Vs*Vr*sin(delta_sr))/(Xl1 - Xsssc)^2;
P1set = P1;
Tz     = 0.0033; % Tz = 0.1 or 0.0033 for original/improved zero position
Tp     = Ts/5.0;
Ki = 1/(Kplant_pri*(Tp - Tz));
Kp = Tz/(Kplant_pri*(Tp - Tz));

x(25) = Xsssc; %Power flow controller operates SSSC equivalent to Xsssc0
x(26) = 0.0;  %P1star = P1set and delPt is zero at steady state
```

```
%Plant equations in sfunction format

function [sys,x0,str,ts] = plt_FBM2tx_sssc1_pfc(t,x,u,flag)

global R1 Xl1 Xsssc0 R2 Xl2 Xc2 Rs Rtrans Xs Xtrans Tsssc Kp Ki Pt pfc_mode

global M1 M2 M3 M4 Wo Ly MWO Ldstr Lqstr
global MdtransLdrinv MqtransLqrinv a1 a2 a3 a4 a5 a6 JinvDK Jinv Tevec Tmvec
global Xmd Xmq Xad Xaq Xfd Rfd Ra K12 K23 K34 K45 K56

global a11 a12 a13 a14 a15 a21 a22 a23 a24 a25
global intvars

global scmax Vref hv kvp hp kpp kai dccap

switch flag,

  % Initialization

  case 0,
    [sys,x0,str,ts]=mdlInitializeSizes;

  % Derivatives
  case 1,
    sys=mdlDerivatives(t,x,u);
```

```
  % Outputs %
  case 3,
    sys=mdlOutputs(t,x,u);

  % Unused Flags %
  case { 2, 4, 9 }
    sys=[];

  % Unexpected flags %
  otherwise
    error(['Unhandled flag = ',num2str(flag)]);

end

% end sfuntmpl

%=============================================================================
% mdlInitializeSizes
% Return the sizes, initial conditions, and sample times for the S-function.
%=============================================================================
function [sys,x0,str,ts]=mdlInitializeSizes

sizes = simsizes;

sizes.NumContStates  = 26;
sizes.NumDiscStates  = 0;
sizes.NumOutputs     = 5;
sizes.NumInputs      = 5;
sizes.DirFeedthrough = 0;
sizes.NumSampleTimes = 1;   % at least one sample time is needed

sys = simsizes(sizes);

% initialize the initial conditions

x0 = zeros(26,1);

% str is always an empty matrix
str = [];

% initialize the array of sample times
ts  = [0 0];

% end mdlInitializeSizes

%=============================================================================
% mdlDerivatives
% Return the derivatives for the continuous states.
%=============================================================================
function sys=mdlDerivatives(t,x,u)

global R1 Xl1 Xsssc0 R2 Xl2 Xc2 Rs Rtrans Xs Xtrans Tsssc Kp Ki Pt pfc_mode

global M1 M2 M3 M4 Wo Ly MWO Ldstr Lqstr
global MdtransLdrinv MqtransLqrinv a1 a2 a3 a4 a5 a6 JinvDK Jinv Tevec Tmvec
global Xmd Xmq Xad Xaq Xfd Rfd Ra K12 K23 K34 K45 K56

global a11 a12 a13 a14 a15 a21 a22 a23 a24 a25
global intvars

global scmax Vref hv kvp hp kpp kai dccap

%Inputs
vb(1,1) = u(1,1);          %Esd
vb(2,1) = u(2,1);          %Esq   Infinite bus voltages
vr(1,1) = u(3,1);          %field voltage
vr(2,1) = 0;
vr(3,1) = 0;
vr(4,1) = 0;               %damper winding input voltages (zero)
Pm      = u(4,1);          %Pmech
P1set   = u(5,1);          %Commanded P1 value

%SSSC equations
Isq = x(3)^2+x(4)^2;
M = abs(x(25))*sqrt(Isq);
vc1D = M*sin( x(6) );
vc1Q = M*cos( x(6) );
```

APPENDIX D

```
Pi = (3/2)*(vc1D*x(3) + vc1Q*x(4));
ev = Vref - hv*x(5);
Pstar = kvp*ev;

ep = Pstar - hp*Pi;
etheta = ( kpp/(abs(x(25))*Isq) ) * ep;

%DC storage capacitor dynamic equations
sys(5,1) = Pi / ( dccap*x(5) );

%Feedback regulator dynamic equations
sys(6,1) = kai*etheta;

%Generator electrical equations
%rotor equations
sys(9:12,1) = vr - M3*x(9:12) + M4*[cos(x(23)) -sin(x(23)); sin(x(23)) cos(x(23))]*x(1:2);

%Transmission line equations
%variables for lumping stator equations into line equations
V1 = [cos(x(23)) sin(x(23)); -sin(x(23)) cos(x(23))] * (...
     M1*sys(9:12,1) + (Wo+x(17))*M2*x(9:12) );

V2 = Ly*(Wo+2*x(17))*[sin(2*x(23)) cos(2*x(23)); cos(2*x(23)) -sin(2*x(23))]*x(1:2);

Linv = inv( [1 0; 0 1] + (a15*Ly)*...
       [cos(2*x(23)) -sin(2*x(23)); -sin(2*x(23)) -cos(2*x(23))] );

%stator dq equations
sys(1:2,1) = Linv*( a11*x(1:2) - MWO*x(1:2) + a12*x(3:4) + a13*[vc1D; vc1Q] + a14*x(7:8)...
    + a15*vb - a15*V1 + a15*V2 );

%line 1 current equations
C1 = a25*Ly*[cos(2*x(23)) -sin(2*x(23)); -sin(2*x(23)) -cos(2*x(23))]*Linv;

sys(3:4,1) = a21*x(1:2) - a11*C1*x(1:2) + C1*MWO*x(1:2) + a22*x(3:4) - MWO*x(3:4)...
    - a12*C1*x(3:4) + a23*[vc1D; vc1Q] - a13*C1*[vc1D; vc1Q] + a24*x(7:8) - a14*C1*x(7:8)...
    + a25*vb - a15*C1*vb  - a25*V1 + a15*C1*V1 + a25*V2 - a15*C1*V2 ;

%line 2 capacitor voltage equations
sys(7:8,1) = Wo*Xc2*x(1:2) - Wo*Xc2*x(3:4) - MWO*x(7:8);

%Generator mechanical equations

Te = (Wo/2)*(...
(Ldstr-Lqstr)*( x(1)*x(2)*cos(2*x(23)) + (x(1)^2 - x(2)^2)*0.5*sin(2*x(23)) )...
+ MdtransLdrinv*x(9:10)*(x(1)*sin(x(23)) + x(2)*cos(x(23)))...
- MqtransLqrinv*x(11:12)*(x(1)*cos(x(23)) - x(2)*sin(x(23)))    );

Tevec(5) = Te;
Tmvec(1) = (a1/(Wo+x(13)))*Wo*Pm;
Tmvec(2) = (a2/(Wo+x(14)))*Wo*Pm;
Tmvec(3) = (a3/(Wo+x(15)))*Wo*Pm;
Tmvec(4) = (a4/(Wo+x(16)))*Wo*Pm;
Tmvec(5) = (a5/(Wo+x(17)))*Wo*Pm;
Tmvec(6) = (a6/(Wo+x(18)))*Wo*Pm;

sys(13:24,1) = JinvDK*x(13:24) + Jinv*( Tevec + Tmvec );

intvars(1) = Te;
intvars(2) = sqrt(x(3)^2 + x(4)^2);
intvars(3) = sqrt(x(5)^2 + x(6)^2);
intvars(4) = x(23)-x(24);
intvars(5) = x(21)-x(22);
intvars(22)= x(19)-x(20);
intvars(23)= x(20)-x(21);
intvars(24)= x(22)-x(23);

%intermediate outputs variables from plant equations

Ls = Xs/Wo;
intvars(6) = vb(1,1) - Rs*x(1) - Wo*Ls*x(2) - Ls*sys(1,1); %Vsd
intvars(7) = vb(2,1) - Rs*x(2) + Wo*Ls*x(1) - Ls*sys(2,1); %Vsq
L1 = Xl1/Wo;
intvars(9)  = intvars(6) - R1*x(3) - Wo*L1*x(4) - vc1D - L1*sys(3,1); %Vrd
intvars(10) = intvars(7) - R1*x(4) + Wo*L1*x(3) - vc1Q - L1*sys(4,1); %Vrq
Ltrans = Xtrans/Wo;
```

APPENDIX D

```
intvars(16) = intvars(9) - Rtrans*x(1) - Wo*Ltrans*x(2) - Ltrans*sys(1,1); %Erd
intvars(17) = intvars(10) - Rtrans*x(2) + Wo*Ltrans*x(1) - Ltrans*sys(2,1); %Erq

intvars(8) = (1/2)*(intvars(6)*x(3) + intvars(7)*x(4));   % Actual P1
intvars(14) = (1/2)*(intvars(16)*x(1) + intvars(17)*x(2));  %Actual Pt
intvars(15) = intvars(14) - (-Pt);   %delPt
P1star = P1set + intvars(15)*pfc_mode; % input of pfc

%plant equ for power flow controller

sys(25,1) = 1/Tsssc*(Xsssc0 + Kp*(P1star - intvars(8)) + x(26) - x(25));
sys(26,1)= Ki*(P1star - intvars(8) + 0*x(26));


intvars(11) = (1/2)*(intvars(6)*x(4) - intvars(7)*x(3));   %Q1
intvars(12) = Pm;
intvars(13) = x(25);
intvars(18) = x(1) - x(3); %I2d
intvars(19) = x(2) - x(4); %I2q
intvars(20)= (1/2)*(intvars(6)*intvars(18) + intvars(7)*intvars(19));   %P2
intvars(21)= (1/2)*(intvars(6)*intvars(19) - intvars(7)*intvars(18));   %Q2

% end mdlDerivatives

%=============================================================================
% mdlOutputs
% Return the block outputs.
%=============================================================================
function sys=mdlOutputs(t,x,u)

global R1 Xl1 Xsssc0 R2 Xl2 Xc2 Rs Rtrans Xs Xtrans Tsssc Kp Ki Pt

global M1 M2 M3 M4 Wo Ly MWO Ldstr Lqstr
global MdtransLdrinv MqtransLqrinv a1 a2 a3 a4 a5 a6 JinvDK Jinv Tevec Tmvec
global Xmd Xmq Xad Xaq Xfd Rfd Ra K12 K23 K34 K45 K56

global a11 a12 a13 a14 a15 a21 a22 a23 a24 a25
global intvars

global scmax Vref hv kvp hp kpp kai dccap

global Vbus

Ls = Xs/Wo;

sys(1,1) = x(1);
sys(2,1) = x(3);
sys(3,1) = Vbus(1,1) - Rs*x(1) - Wo*Ls*x(2); %Vsd
sys(4,1) = Vbus(2,1) - Rs*x(2) + Wo*Ls*x(1); %Vsq
sys(5,1) = (1/2)*(sys(3,1)*x(3) + sys(4,1)*x(4)); %P1

% end mdlOutputs
```

REFERENCES

[1] UN Report, “The World at Six Billion”, Oct. 1999. [http://www.un.org/esa/population/publications/sixbillion/sixbillion.htm]

[2] US Energy Information Administration, “World Electricity Data: International Energy Annual”, 2006. [http://www.eia.doe.gov/iea/elec.html]

[3] Sinomach Industry News Magazine, “Installed Electric Power Capacity in China Breaks Through 900 GW”, Vol. 13, No. 3, Oct. 2010.

[4] Y. H. Song, *Flexible AC Transmission Systems*, The IEE, London, ISBN 0-85296-771-3, 1999.

[5] V. Madani and D. Novosel, “Getting a grip on the grid”, IEEE Spectrum, Vol. 42, No. 12, Dec. 2005, pp. 42-47.

[6] N. G. Hingorani and L. Gyugyi, *Understanding FACTS: Concepts and Technology of Flexible AC Transmission System*, IEEE Press, ISBN 0-7803-3455-8, 2000.

[7] E. W. Kimbark, “Improvement of System Stability by Switched Series Capacitors”, *IEEE Trans. on PAS.*, Vol. PAS-85, No. 2, Feb. 1966, pp. 157-188.

[8] J. W. Ballance and S. Goldberg, “Subsynchronous Resonance in Series Compensated Transmission lines”, *IEEE Trans. on PAS.*, Vol. PAS-92, No. 5, Sep. 1973, pp. 1649-1658.

[9] C. E. J. Bowler, “Understanding Subsynchronous Resonance”, Proc. of IEEE PES Winter Meeting and Tesla Symposium, New York, USA, Jan. 1976, pp. 66-73.

[10] N. G. Hingorani, “Power Electronics in Electric Utilities: Role of Power Electronics in Future Power System”, *Proc. of the IEEE*, Vol. 76, No. 4, Apr. 1988, pp. 481-482.

[11] J. J. Paserba, “How FACTS Controllers Benefit AC Transmission Systems”, Proc. of IEEE PES Conf. on Transmission and Distribution, Dallas, TX, USA, Sep. 2003.

[12] P. Pourbeik, M. Bahrman, E. John and W. Wong, “Modern Countermeasures to Blackouts”, IEEE Power and Energy Magazine, Vol. 4, No. 5, Sep. 2006, pp. 36-45.

[13] P. Kundur, *Power System Stability and Control*, McGraw-Hill Inc., New York, ISBN 0-07-035958-X, 1994.

[14] IEEE Subsynchronous Resonance Working Group, “Proposed Terms and Definitions for Subsynchronous Oscillations”, *IEEE Trans. on PAS.*, Vol. PAS-99, No. 2, Mar. 1980, pp. 506-511.

[15] E. V. Larsen, C. E. J. Bowler, B. Damsky and S. Nilsson, “Benefits of Thyristor Controlled Series Compensation”, CIGRE Annual Meeting, Paper No. 14/37/38-04, Paris, 1992.

[16] N. Martins, J. J. Paserba, J. C. P. Pinto, “Using a TCSC for Line Power Scheduling and System Oscillation Damping – Small Signal and Transient Stability Studies”, Proc. of IEEE PES Winter Meeting, Singapore, Vol. 2, Jan. 2000, pp. 1455-1461.

REFERENCES

[17] A. Ally, B. S. Rigby, "The Impact of Closed-Loop Power Flow Control Strategies on the Power System Stability Characteristics in a Single Generator System", *SAIEE Africa Research Journal*, Vol. 97, No.1, Mar. 2006, pp.34-42.

[18] B. S. Rigby, R. G. Harley, "Resonant Characteristics of Inverter-Based Transmission Line Series Compensators", Proc. of IEEE Power Electronics Specialists Conf., Charleston, USA, Jun. 1999, pp. 412-417.

[19] A. C. Pradhan and P. W. Lehn, "Frequency-Domain Analysis of the Static Synchronous Series Compensator", *IEEE Trans. on PD.*, Vol. 21, No. 1, Jan. 2006, pp. 440-449.

[20] IEEE Dynamic System Performance Working Group, "First Benchmark Model for Computer Simulation of Subsynchronous Resonance", *IEEE Trans. on PAS.*, Vol. PAS-96, No. 5, Sep. 1977, pp.1565-72.

[21] MathWorks, "Using MATLAB Version 7.9, Computation, Visualisation and Programming", The MathWorks Inc., 2009.

[22] Manitoba HVDC Research Centre, "PSCAD Version 4.2 User's Guide", Manitoba HVDC Research Centre Inc., 2006.

[23] R. Pillay Carpanen, B. S. Rigby, "SSR Characteristics of A Transmission Network with Multiple Series Compensated Lines", Proc. of Southern African Universities Power Engineering Conf. (SAUPEC), Cape Town, South Africa, Jan. 2007, CD-ROM index.

[24] R. Pillay Carpanen, B. S. Rigby, "Isolating the Influences of An SSSC and its Power Flow Controller on Torsional Interaction", Proc. of Southern African Universities Power Engineering Conf. (SAUPEC), Durban, South Africa, Jan. 2008, pp. 88-95.

[25] B. S. Rigby, R. Pillay Carpanen, "The Impact of FACTS-Based Power Flow Control on System Stability", Proc. of International Conf. on Advanced Power System Automation and Protection (APAP), Jeju, Korea, Mar. 2007.

[26] R. Pillay Carpanen, B. S. Rigby, "A FACTS-Based Power Flow Controller Model for The IEEE SSR First Benchmark Model", Proc. of IEEE PES PowerAfrica Conf., Johannesburg, South Africa, Jul. 2007, ISBN 1-4244-1478-4.

[27] R. Pillay Carpanen, B. S. Rigby, "Impact of a SSSC-based Power Flow Controller on SSR", Proc. of the 16th Power Systems Computation Conf., Glasgow, UK, 2008, ISBN 978-0-947649-28-9.

[28] R. Pillay Carpanen, B. S. Rigby, "A Contribution to Modelling and Analysis of SSSC-Based Power Flow Controls and their Impact on SSR", *Electric Power Systems Research (EPSR)*, Vol. 88, 2012, pp. 98-111.

[29] R. Pillay Carpanen, B. S. Rigby, "An Improved SSSC-Based Power Flow Controller Design Method and its Impact on Torsional Interaction", *International Journal of Electrical Power and Energy Systems*, Vol. 43, 2012, pp. 194-209.

REFERENCES

[30] R. Pillay Carpanen, B. S. Rigby, "Analytical Study of the Impacts of an SSSC and its Power Flow Controller on Torsional Interaction" (manuscript accepted subject to minor corrections in *Electrical Engineering Journal - Springer*).

[31] IEEE Subsynchronous Resonance Working Group, "Second Benchmark Model for Computer Simulation of Subsynchronous Resonance", IEEE Trans. on PAS., Vol. PAS-104, No. 5, May. 1985, pp. 1057-1066.

[32] P. M. Anderson, B. L. Agrawal and J. E. Van Ness, *Subsynchronous Resonance in Power Systems, IEEE Press*, New York, ISBN 0-87942-258-0, 1990.

[33] B. S. Rigby, "Analysis and Implementation of a FACTS Series Compensator based on a Single Voltage-Source Inverter", PhD Thesis, University of Natal, South Africa, 1997.

[34] IEEE Subsynchronous Resonance Working Group, "Reader's Guide to Subsynchronous Resonance", *IEEE Trans. on PS.*, Vol. 7, No. 1, Feb. 1992, pp. 150-157.

[35] IEEE Subsynchronous Resonance Working Group, "Terms, Definitions and Symbols for Subsynchronous Oscillations", *IEEE Trans. on PAS.*, Vol. PAS-104, No. 6, Jun. 1985, pp. 1326-1334.

[36] IEEE Dynamic Systems Performance Working Group, "Proposed Terms and Definitions for Subsynchronous Resonance in Series Compensated Transmission Systems", Proc. of IEEE PES Winter Meeting and Tesla Symposium, New York, USA, Jan. 1976, pp. 55-58.

[37] IEEE Dynamic Systems Performance Working Group, "A Bibliography for the Study of Subsynchronous Resonance between Rotating Machines and Power Systems", *IEEE Trans. on PAS.*, Vol. PAS-95, No. 1, Jan. 1976, pp. 216-218.

[38] IEEE Dynamic System Performance Working Group, "First Supplement to A Bibliography for the Study of Subsynchronous Resonance between Rotating Machines and Power Systems", *IEEE Trans. on PAS.*, Vol. PAS-98, No. 6, Nov. 1979, pp. 1872-1875.

[39] IEEE Subsynchronous Resonance Working Group, "Second Supplement to A Bibliography for the Study of Subsynchronous Resonance between Rotating Machines and Power Systems", *IEEE Trans. on PAS.*, Vol. PAS-104, No. 2, Feb. 1985, pp. 321-327.

[40] IEEE Subsynchronous Resonance Working Group, "Third Supplement to A Bibliography for the Study of Subsynchronous Resonance between Rotating Machines and Power Systems", *IEEE Trans. on PS.*, Vol. 6, No. 2, May. 1991, pp. 830-834.

[41] IEEE Torsional Issues Working Group, "Fourth Supplement to A Bibliography for the Study of Subsynchronous Resonance between Rotating Machines and Power Systems", *IEEE Trans. on PS.*, Vol. 6, No. 2, May. 1991, pp. 830-834.

[42] O. L. Elgerd, *Electric Energy Systems Theory*, McGraw-Hill Inc., New York, 2nd Ed., ISBN 0-07019-230-8 1982.

REFERENCES

[43] R. G. Harley, B. S. Rigby, G. D. Jennings, "Design of A Controlled Converter which Emulates A Series Capacitive Compensator for Long Power Lines", Proc. of International Conf. on Power Electronics and Motion Control, Warsaw, Poland, Sep. 1994,pp. 213-218.

[44] K. R. Padiyar, *Power System Dynamics*, John Wiley & Sons (Asia) Pte Ltd, Singapore, ISBN 0-471-19002-0, 1996.

[45] B. L. Aggrawal, R. G. Farmer, "Use of Frequency Scanning Techniques for Subsynchronous Resonance Analysis", *IEEE Trans. on PAS.*, Vol. PAS-98, No. 2, Mar. 1979, pp. 341-349.

[46] IEEE FACTS Working Group, "Proposed Terms and Definitions for Flexible AC Transmission Systems (FACTS)", *IEEE Trans. on PD.*, Vol. 12, No. 4, Oct. 1997, pp. 1848-1853.

[47] L. Gyugyi, "Solid-State Control of Electric Power in AC Transmission", International Symposium on Electric Energy Converters in Power Systems, Invited Paper T-IP. 4, Capri, Italy, 1989.

[48] F. AL. Jowder, "Influence of Mode of Operation of the SSSC on the Small Disturbance and Transient Stability of a Radial Power System", *IEEE Trans. on PS.*, Vol. 20, No. 2, May. 2005, pp. 935-942.

[49] L. Gyugyi, "Solid State Control of AC Power Transmission", Proc. of EPRI FACTS Conf. 1, Cincinnati, USA, 1990, pp.1.7-1 – 1.7-44.

[50] L. Gyugyi, "Dynamic Compensation of AC Transmission Lines by Solid State Synchronous Voltage Sources", *IEEE Trans. on PD.*, Vol. 9, No. 2, Apr. 1994, pp. 904-911.

[51] L. Gyugyi, C. D. Schauder, K.K. Sen, "Static Synchronous Series Compensator: A Solid-State Approach to the Series Compensation of Transmission Lines", *IEEE Trans. on PD.*, Vol. 12, No. 1, Jan. 1997, pp. 406-417.

[52] J. F. Hauer, D. C. Erickson, T. Wilkinson, J. D. Eden, M. K. Donnelly, D. J. Trudnowski, R. J. Piwko, C. Bowler, "Tests Results And Initial Operating Experience for the BPA 500 kV Thyristor Controlled Series Capacitor Unit at the Slatt Substation – Part 2 – Modulation, SSR, and Performance Monitoring", Proc. of EPRI FACTS Conf. 3, Baltimore, Maryland, USA, Oct. 1994, pp. (4-1)-(4-15).

[53] A. T. Hill, E. V. Larsen, E. Hyman, "Thyristor Control for SSR Suppression – A Case Study", Proc. of EPRI FACTS Conf. 3, Baltimore, Maryland, USA, Oct. 1994, pp. (20-1)-(20-17).

[54] S. G. Jalali, R. H. Lasseter, I. Dobson, "Dynamic Response of a Thyristor Controlled Switched Capacitor", *IEEE Trans. on PD.*, Vol. 9, No. 3, Jul. 1994, pp. 1609-1615.

[55] W. Zhu, R. Spee, R. R. Mohler, G. C. Alexander, W. A. Mittelstadt, D. Maratukulam, "An EMTP Study of SSR Mitigation Using the Thyristor Controlled Series Capacitor", *IEEE Trans. on PD.*, Vol. 10, No. 3, Jul. 1995, pp. 1479-1485.

[56] H. A. Othman, L. Angquist, "Analytical Modeling of Thyristor Controlled Series Capacitors for SSR Studies", *IEEE Trans. on PS.*, Vol. 11, No. 1, Feb. 1996, pp. 119-127.

REFERENCES

[57] R. J. Piwko, C.A. Wegner, S. J. Kinney, J. D. Eden, "Subsynchronous Resonance Performance Tests of the Slatt Thyristor Controlled Series Capacitor", *IEEE Trans. on PD.*, Vol. 11, No. 2, Apr. 1996, pp. 1112-1119.

[58] R. Rajaraman, I. Dobson, R. H. Lasseter, Y. Shern, "Computing the Damping of Subsynchronous Oscillations due to a Thyristor Controlled Series Capacitor", *IEEE Trans. on PD.*, Vol. 11, No. 2, Apr. 1996, pp. 1120-1127.

[59] J. F. Hauer, W. A. Mittelstadt, R. J. Piwko, B. L. Damsky, J. D. Eden, "Modulation and SSR Tests Performed on the BPA 500 kV Thyristor Controlled Series Capacitor Unit at the Slatt Substation", *IEEE Trans. on PS.*, Vol. 11, No. 2, May. 1996, pp. 801-806.

[60] B. P. Perkins, M. R. Iravani, "Dynamic Modeling of a TCSC with Application to SSR Analysis", *IEEE Trans. on PS.*, Vol. 12, No. 4, Nov. 1997, pp. 1619-1625.

[61] P. Mattaveli, A. M. Stanković, G. C. Verghese, " SSR Analysis with Dynamic Phasor Model of Thyristor Controlled Series Capacitor", *IEEE Trans. on PS.*, Vol. 14, No. 1, Feb. 1999, pp. 200-208.

[62] P. C. Srivastava, A. Ghosh, S. V. Jayaram Kumar, "Model-based control design of a TCSC-compensated power system", *International Journal of Electical Power and Energy Systems*, Vol. 21, 1999, pp. 299-307.

[63] A. Ghosh, S, V. Jayaram Kumar, S. Sachchidanand, "Subsynchronous Resonance Analysis using a Discrete Time Model of a Thyristor Controlled Series Capacitor", *International Journal of Electical Power and Energy Systems*, Vol. 21, 1999, pp. 571-578.

[64] S. V. Jayaram Kumar, A. Ghosh, S. Sachchidanand, "Damping of Subsynchronous Resonance Oscillations with a TCSC and a PSS and their Control Interaction", *Electric Power Systems Research (EPSR)*, Vol. 54, 2000, pp. 29-36.

[65] L. A. S. Pilotto, A. Bianco, W. F. Long, A. Edris, "Impact of TCSC Control Methodologies on Subsynchronous Oscillations", *IEEE Trans. on PD.*, Vol. 18, No. 1, Jan. 2003, pp. 243-252.

[66] D. Jovcic, G. N. Pillai, "Analytical Modeling of TCSC Dynamics", *IEEE Trans. on PD.*, Vol. 20, No. 2, Apr. 2005, pp. 1097-1104.

[67] G. N. Pillai, D. Jovcic, "SSR Analysis with a New Analytical Model of Thyristor Controlled Series Capacitor", Proc. of 15th Power Systems Computation Conf. (PSCC), Liege, Belgium, Aug. 2005, Session 34-3, pp 1-6.

[68] K. R. Padiyar, N. Prabhu, "A Comparative Study of SSR Characteristics of TCSC and SSSC", Proc. of 15th Power Systems Computation Conf. (PSCC), Liege, Belgium, Aug. 2005, Session 34-2, pp 1-7.

[69] S. R. Joshi, A. M. Kulkarni, "Analysis of SSR Performance of TCSC Control Schemes Using a Modular High Bandwidth Discrete-Time Dynamic Model", *IEEE Trans. on PS.*, Vol. 24, No. 2, May. 2009, pp. 840-848.

REFERENCES

[70] S. R. Joshi, E. P. Cheriyan, A. M. Kulkarni, "Output feedback SSR damping controller design based on modular discrete-time dynamic model of TCSC", *Proc. of IET on Generation, Transmission and Distribution*, Vol. 3, No. 6, 2009, pp. 561-573.

[71] D. Rai, S. O. Faried, G. Ramakrishna, A. Edris, "Hybrid series compensation scheme capable of damping subsynchronous resonance", *Proc. of IET on Generation, Transmission and Distribution*, Vol. 4, No. 3, 2010, pp. 456-466.

[72] D. N. Kosterev, W. A. Mittelstadt, R. R. Mohler, W. J. Kolodziej, "An Application Study for Rating and Sizing Controlled and Conventional Series Compensation", *IEEE Trans. PD.*, Vol. 11, No, 2, Apr. 1996, pp. 1105-1111.

[73] K. B. Stump, R. A. Hedin, W. A. Mittelstadt, D. N. Kosterev, "Preliminary Analysis of Subsynchronous Resonance in the Colstrip West 500 kV Transmission System", Proc. of EPRI Future of Power Delivery Conf., Washington D.C., USA, April, 1996.

[74] L. S. Kumar, A. Ghosh, "Static Synchronous Series Compensator – Design, Control and Application", *Electric Power Systems Research (EPSR)*, Vol. 49, 1999, pp. 139-148.

[75] K. R. Padiyar, N. Prabhu, "Analysis of Subsynchronous Resonance with Three Level Twelve-Pulse VSC based SSSC", Proc. of IEEE Conf. on Convergent Technologies (TENCON), Oct. 2003, Vol. 1, pp. 76-80.

[76] H. Barati, A. Lashkar Ara, M. Ehsan, M. Fotuhi-Firuzabad, S. M. T. Bathaee, " Application of Static Synchronous Series Compensator to Damp Subsynchronous Resonance", Proc. of IEEE Conf. on Power Electronics, Drives and Energy Systems", New Delhi, India, Dec. 2006, pp. 1-6.

[77] K. R. Padiyar and N. Prabhu, "Analysis of SSR with Three-Level Twelve pulse VSC-Based Interline Power-Flow Controller", *IEEE Trans. on PD.*, Vol 22, No. 3, Jul. 2007, pp. 1688-1695.

[78] G. N. Pillai, A. Ghosh, A. Joshi, "Torsional Oscillation Studies in an SSSC Compensated Power System", *Electric Power Systems Research (EPSR)*, Vol. 55, 2000, pp. 57-64.

[79] G. N. Pillai, A. Ghosh, A. Joshi, "Robust Control of SSSC to Improve Torsional Damping", Proc. of IEEE PES Winter Meeting, Vol. 3, Feb. 2001, pp. 1115 – 1120.

[80] J-C. Seo, S-I. Moon, J-K. Park, J-W. Choe, "Design of a Robust SSSC Supplementary Controller to Supress the SSR in the Series Compensated System", Proc. of IEEE PES Winter Meeting, Vol. 3, Feb. 2001, pp. 1283 – 1288.

[81] G. N. Pillai, A. Ghosh, A. Joshi, "Torsional Interaction Studies on a Power System Compensated by SSSC and Fixed Capacitor", *IEEE Trans. on PD.*, Vol. 18, No. 3, Jul. 2003, pp. 988-993.

[82] F.-W. Huang, B. S. Rigby, R. G. Harley, "Static Synchronous Series Compensator Control for Active Damping of Generator Torsional Oscillations": Proc. of the International Conf. on Advanced Power System Automation and Protection APAP2004, Jeju, South Korea, Oct. 2004, pp. 610-615.

REFERENCES

[83] F. A. R. Al Jowder, B-T. Ooi, "Series Compensation of a Radial Power System by a Combination of SSSC and Dielectric Capacitors", *IEEE Trans. on PD.*, Vol. 20, No. 1, Jan. 2005, pp. 458-465.

[84] M. Bongiorno, L. Angquist, J. Svesson, "A Novel Control Strategy for Subsynchronous Resonance Mitigation Using SSSC", *IEEE Trans. on PD.*, Vol. 23, No. 2, Apr. 2008, pp. 1033-1041.

[85] M. Bongiorno, J. Svesson, L. Angquist, "Single-Phase VSC Based SSSC for Subsynchronous Resonance", *IEEE Trans. on PD.*, Vol. 23, No. 3, Jul. 2008, pp. 1544-1552.

[86] S. O. Faried, G. Tang, A. Edris, "Supplemental Control of Voltage Sourced Converter-Based Back-to-Back for Damping Subsynchronous Resonance", Proc. of IEEE PES General Meeting, Calgary, Canada, Jul. 2009, pp. 1-6.

[87] R. G. Harley and J.C. Balda, "Subsynchronous resonance damping by specially controlling a parallel HVDC link", *Proc. of IEE on Generation, Transmission and Distribution*, Vol. 132, No. 3, 1985, pp. 154-160.

[88] K. R. Padiyar and N. Prabhu, "Investigation of Subsynchronous Resonance with VSC-Based HVDC Transmission Systems", *IEEE Trans. on PD.*, Vol. 24, No. 1, Jan. 2009, pp. 433-440.

[89] B. S. Rigby, R. G. Harley, "An Improved Control Scheme for a Series-Capacitive Reactance Compensator Based on a Voltage-Source Inverter", *IEEE Trans. on IAS.*, Vol. 34, No. 2, Mar. 1998, pp. 355-363.

[90] B. Adkins and R. G. Harley, *The General Theory of Alternating Current Machines: Applications to Practical Problems*, Chapman and Hall, London, ISBN 0-412-15560-5, 1975.

[91] G. D. Jennings, "Modelling and Analysis of Turbogenerators in Single and Multi-Machine Subsynchronous Resonance Studies", PhD Thesis, University of Natal, Durban, South Africa, 1987.

[92] B. S. Rigby, N. S. Chonco, R. G. Harley, "Analysis of a Power Oscillation Damping Scheme Using a Voltage-Source Inverter", *IEEE Trans. on IAS.*, Vol. 38, No. 4, Jul. 2002, pp. 1105-1113.

[93] K. Ogata, *Modern Control Engineering*, Prentice-Hall of India Pvt Ltd, New Delhi, ISBN 81-203-1237-6, 1997.

[94] B. S. Rigby, "An AC Transmission Line Power Flow Controller Using a Thyristor Controlled Series Capacitor", Proc. of IEEE Africon Conf. George, South Africa, 2002, pp. 773-778.

[95] R. Mihalic, I. Papic, "Static Synchronous Series Compensator – a mean for dynamic power flow control in electric power systems", *Electric Power Systems Research (EPSR)*, Vol. 45, 1998, pp. 65-72.